A Bio-inspired Distributed Control Architecture: Coupled Artificial Signalling Networks

Luis Alberto Fuente Fernández

Ph.D.

University of York
Electronics

September 2014

A Bio-inspired Distributed Control Architecture: Coupled Artificial Signalling Networks

Luis Alberto Fuente Fernández

September 2014

Intelligent Systems Research Group
Electronics
University of York

Abstract

This thesis studies the applicability of computational models inspired by the structure and dynamics of signalling networks to the control of complex control problems. In particular, this thesis presents two different abstractions that aim to capture the signal processing abilities of biological cells: a stand-alone signalling network and a coupled signalling network. While the former mimics the interacting relationships amongst the components in a signalling pathway, the latter replicates the connectionism amongst signalling pathways. After initially investigating the feasibility of these models for controlling two complex numerical dynamical systems, Chirikov's standard map and the Lorenz system, this thesis explores their applicability to a difficult real world control problem, the generation of adaptive rhythmic locomotion patterns within a legged robotic system. The results highlight that the locomotive movements of a six-legged robot could be controlled in order to adapt the robot's trajectory in a range of challenging environments. In this sense, signalling networks are responsible for the robot adaptability and inter limb coordination as they self-adjust their dynamics according to the terrain's irregularities. More generally, the results of this thesis highlight the capacity of coupled signalling networks to decompose non-linear problems into smaller sub-tasks, which can then be independently solved.

Contents

List of Figures

List of Tables

Acknowledgments

Apart form my own efforts, the success of this thesis mostly depends on the encouragement and guidance of many others. I would like to take this opportunity to express my gratitude to people who have been instrumental in the successful completion of this study.

I would like to express my deepest appreciation to my main supervisors **Professor Andy M. Tyrrell** and **Dr. Michael A. Lones**, whose constant guidance and support helped me in completing this study, from the very first day up to this manuscript. Without their support, effortless advice and persistent help, this thesis will not have been possible. Thank you for this opportunity! I am particularly grateful to Dr. Michael A. Lones whose friendship, infinite patience, pastoral care and beer knowledge have played a truly important role in the positive completion of this thesis. Although I disagreed at first, he gave me the best possible advise "*No worries, it will work*". You were 100% right!

I would like to extend my gratitude to the additional members of the AlBiNo project, **Professor Susan Stepney**, **Dr. Leo S. Caves** and **Alex P. Turner** for sharing their knowledge and constructive comments which helped a lot in improving this study.

I am specially thankful to my beloved family **Toribio**, **María del Carmen**, **Carmen María** and beloved partner, **Julia**. Although you have not been literally beside me, I would like you to know that your altruistic enthusiasm and priceless support are my motivation and inspiration for everything, as I dedicate this thesis manuscript to all of you. Thank you for supporting me and allowing me to follow my ambitions. Without your enduring love, constant guidance, care, motivation and encouragement, I could not have made it this far. Muchas Gracias!

Last but not least, I would like to thank all my university colleagues, **Antonio**, **Luis P.**, **Stuart**, **Lachie**, **Piti**, **James A.**, **Carlos** and **Michael G.**. Thank you for all the fun,

inside jokes, brainstorms and memories we have shared together and for making my PhD life extra enjoyable and unforgettable. I am particularly grateful to the Spanish team and my Mexican friends for all productive conversations, advice, late discussions, house events and nights out we had together while discovering the vast majority of the great pubs of York. These pub sessions were the best possible way to improve my Mexican-Spanish, relax from the PhD and make me feel like being at home. I will also like to personally thank my lunch mates whose subreal and imaginative conversations, and jokes were a breath of fresh air every day. I cannot forget the 6-a-side Electronic football team, which accepted me from the first game and eased my integration into the Electronic department. Wednesdays at 5 o'clock were the best gateway to evade myself from the frustrations of the PhD. Finally, I would like to thank all the people, that although not explicitly mentioned here, have contributed to make this dream come true. It was amazing having all these years spent with all of you!

Thank you very much from the outputs of my Signalling Networks!

Declaration

All work in this thesis is entirely original to the best knowledge and belief of the author. It contains no material perviously published by other authors, except where due reference has been made in the text. This research is supported by the EPSRC grant (ref: EP/F060041/1), *Artificial Biochemical Networks: Computational Models and Architectures*. Some of the research presented in this thesis has previously been published by the author:

- Luis A. Fuente, Michael A. Lones, Alexander P. Turner, Susan Stepney, Leo S. Caves, Andy M. Tyrrell. *Evolved Artificial Signalling Networks for the Control of a Conservative Complex Dynamical System.* 9th International Conference on Information Processing in Cells and Tissues (IPCAT 2012) Cambridge, UK, April 2012. LNCS, Volume 7223, Springer 2012

- Luis A. Fuente, Michael A. Lones, Alexander P. Turner, Susan Stepney, Leo S. D. Caves, Andy M. Tyrrell. *Computational Models of Signalling Networks for Non-linear Control*, Biosystems, Volume 112, Issue 2, May 2013

- Luis A. Fuente, Michael A. Lones, Alexander P. Turner, Susan Stepney, Leo S. D. Caves, Andy M. Tyrrell. *Adaptive Robotic Gait Control using coupled Artificial Signalling Networks, Hopf Oscillators and Inverse Kinematics*, IEEE Congress on Evolutionary Computation 2013, Cancun, Mexico, June 2013. IEEE, 2013

- Michael A. Lones, Alexander P. Turner, Luis A. Fuente, Susan Stepney, Leo S. D. Caves, Andy M. Tyrrell. *Biochemical Connectionism*, Natural Computing, Volume 12, Issue 2, pages 453-472, December 2013.

Hypothesis

This thesis hypothesises that **evolvable computational abstractions of signalling networks can be used to create bio-inspired control architectures for multi-legged robotic systems**. This hypothesis is supported by the following arguments:

- Signalling networks are the biological mechanisms responsible for the transformation of extracellular stimuli into cellular regulatory control commands.
- Signalling pathways have the ability to collaborate together and develop complex processing units able to simultaneously process several stimuli and increase the robustness of the cellular response.
- The structure, function and behaviour of signalling networks are the result of an evolutionary process.
- Biochemical networks can be used to perform control tasks in environments whose complexity resembles the dynamical properties of cellular environments.
- Sensory information is essential to induce adaptive locomotive rhythms. Although biological CPGs can produce periodic motion without sensory feedback, control signals are essential to achieve coordination amongst legs and locomotive movements.
- Locomotion in multi-legged systems results from the local influences amongst leg controllers in a similar way crosstalk and compartmentalisation produce coordinated cellular responses.

Chapter 1

Introduction

Contents

1.1 Biological Motivation

Cells are the basic biological units of life of all known biological organisms. They coexist in complex environments where they adaptively interact with each other and with their surrounding. These interactions are typically governed by a collection of protein-mediated networks of biochemical reactions which regulate the behaviour of biological cells. Nevertheless, there are the control properties of biochemical networks within biochemical organisms which makes them computationally interesting.

Amongst the different biochemical networks, this thesis draws its attention to signalling networks. They represent the main communication mechanism connecting cells with their environment (Krauss, 2001). Signalling networks grant cells the ability to perceive stimuli, produce understandable cellular signals and adapt to constantly fluctuating environments. In multi-cellular organisms, the role of cellular signalling is especially significant. This is also responsible for the coordination of complex intercellular relationships and the production of

collective responses. Computational models representing the structure and function of the cellular signal transduction process are called *Artificial Signalling networks* (ASN).

A signalling network is the sequence of catalytic reactions that allows cells to precisely respond to their surrounding. This process, generally known as signal transduction, translates extracellular stimuli into meaningful cellular signals. Signalling pathways are its simplest transduction units (Bray, 1990). Signal transduction begins at the membrane domain, where a receptor protein translates and diffuses extracellular signals inside the cell. These signals are then broadcast across the cytoplasm by means of a chain of catalytic reactions, which lead to changes in gene expressions and bring about alterations in the cellular activity (Danos et al., 2008; Silverthorn, 2009). The group of all alterations in the cell behaviour associated to the sensing of an extracellular stimulus define the cellular response. Although signalling pathways are able to work in isolation, responding simultaneously to several stimuli normally requires cooperation between them. This results in the formation of extended signalling networks and the generation of cooperative cellular responses. Cells offer mainly two mechanisms to increase their signalling capacity: crosstalk and compartmentalisation. Both define spatiality within cellular signalling by determining as and where catalytic reactions occur (McCarthy, 2010).

This thesis aims to introduce a computational model whose topology and dynamics imitates the processing properties of cellular signalling networks. This model, named Coupled Artificial Signalling Network (CASN), explores the benefits of crosstalk and compartmentalisation in order to develop a connectionist architecture, which can be applied to solve complex control problems.

1.2 Evolvability

Signalling networks allows cells to produce reliable and specific response upon the transduction of extracellular stimuli. This robustness is the result of a long-term evolutionary process where genetic alterations incorporate new functions and increase their adaptability to the surrounding environment (Marijuán et al., 2013).

The work reported in this thesis rests on the assumption that connectivity-based constraints associated with signalling models can be overcome using evolutionary strategies. Hence, evolutionary algorithms are used to redefine the spatial topology of the proposed

signalling models so that it exclusively depend on their interaction with the environment. Additionally, this study also investigate the applicability of a multi-chromosomal representation (Mayer & Spitzlinger, 2003) to encode individual signalling networks and preserve its dynamical properties during the evolution process. This type of encoding is a natural mechanism to represent interactions amongst biochemical networks and also promotes the evolvability of large computational architectures (Pierrot & Hinterding, 1997).

1.3 Dynamical Systems

Dynamical systems are related to the mathematical recipe that describes how a complex system changes over time. This definition suggests the existence of a rule which relates past states of the system with its current state and also enables the prediction of future states (Stepney, 2012). Traditionally, dynamical systems are mathematically described by either difference or differential equations to represent a behaviour occurring in discrete or continuous time. They also involve a collection of variables and control parameters whose interactions and numerical values define their behaviour. Perhaps, the most appealing dynamical systems are those exhibiting a complex, unstable and unpredictable behaviour, which is known as *chaos* (Ott, 2002). Common to these system is also their capacity to migrate from an ordered state to a chaotic state, and vice verse. This phenomenon is conventionally termed as *edge of chaos* (Langton, 1990).

This thesis evaluates the capacity of artificial signalling models to generate complex dynamics and robust control directives when carrying out charging in two dynamical systems: the Lorenz system and Chirikov's standard map (Fuente et al., 2012, 2013*b*). Despite these systems sitting at opposite end of the dynamical system spectrum, their dynamics represent the complexity found in cellular environments. These dynamical systems has also been considered in Lones et al. (2014) to investigate the control capabilities of computational models whose structure and function are motivated by the organisation of biochemical networks. Thus, they represent an appropriate test bed to evaluate the advantages and disadvantages of the proposed ASN models upon various kinds of complex problems. The Lorenz map is a continuous time dissipative dynamical system, whose behaviour can be either ordered or chaotic depending on the values of its governing parameters. Opposite the Chirikov's standard map is a discrete-time conservative dynamical system. Its state space embraces ordered and chaotic regions which coexist together. Nevertheless, characteristics to both systems is

that behavioural diversity can be controlled by their governing parameters. This property is explored in this thesis to control chaos using the proposed signalling representations. The objective is to evolve ASN and CASN controllers able to carry out chaos targeting in these two dynamical systems via the control of their governing parameters.

1.4 Bio-inspired Robotics

Bio-inspired robotics is the area of research arisen at the intersection of biology and robotics. Its main focus is the use of robots as a tool to evaluate biological ideas (Guillot, 2008; Floreano & Mattiussi, 2008). Within this context, this thesis aims to evaluate whether the dynamical characteristics of the proposed ASN models can be applied to solve solve complex physical problems. Locomotion in multi-legged robotic systems is an example of this kind of problem as legs should synchronously move in a particular manner to engage locomotive movements.

Although consideration of environmental information is not essential in the generation of synchronised and rhythmic locomotion patterns, it increases the adaptability of control system in real environments (Frasca et al., 2004). However, integrating environmental information in a robotic control system is a hard problem, particularly when these environmental signal come from diverse and potentially noisy sources. Nevertheless, this is a task at which signalling networks are evidently good at solving within a biological context. In this respect, this thesis focuses on bio-inspired locomotion control in a hexapod robot and aims to develop a bio-inspired decentralised locomotion controller for a multi-legged robotic system (Fuente et al., 2013*a*). This includes high-level control to integrate sensory information and low-level control to determine the robot's posture and gait. Three different biological concepts are considered to achieve high-level locomotion: *cellular signalling*, *decentralised control* and *central pattern generators*. Their combination with the inverse kinematics technique for low-level control results in a layered decentralised architecture for bio-inspired legged locomotion. The core of this approach is that a system of nonlinear Hopf oscillators is efficiently optimised by an evolved CASN, which, in turns is coupled with the mechanical body of the robot. The proposed topology comprises three hierarchical layers: a top layer of sensory integration and behaviour modulation, an intermediate layer of gait generation and a bottom layer of posture formation.

1.5 Thesis Contributions

This work makes the following specific contributions to knowledge:

- The development and understanding of a new computational model for intracellular signalling networks, whose topology and function are the result of an evolutionary process rather than predefined connections.
- The demonstration that the processing capabilities of signalling networks can be used to solve complex control problems.
- The usage of crosstalk and compartmentalisation to solve problems where there is a strong dependence amongst its interrelated elements.
- The development of a layered and decentralised bio-inspired controller for a hexapod robot where sensory inputs can be translated into meaningful oscillatory patterns using signalling networks.
- The complete kinematic analysis, including forwards and inverse kinematic solutions, of a six-legged robot with 24-DOF.
- The development of a trajectory planning algorithm to translate two-dimensional oscillatory wave gaits into locomotive movements so that step's length and height can be independently modulated.

1.6 Thesis Organisation

This thesis is divided into seven chapters which are organised in two main sections. Chapters 2 and 3 introduce the underlying biological concepts, review related work in signalling networks and present the proposed computational models. Chapters 4 to 6 evaluate the validity of the proposed models and describe the novel contributions of this thesis. Specifically:

Chapter 1 is the introduction to this thesis.

Chapter 2 presents the biological fundamentals of intracellular signal transduction, placing particular emphasis upon higher-level cellular organisations.

Chapter 3 reviews related work in signalling networks, discusses the usage of evolutionary computation within the cellular signalling context and presents the computational models considered in the scope of the thesis.

Chapter 4 describes the concept of dynamical systems and analyses the applicability of the proposed signalling models for the control of two complex numerical dynamical systems.

Chapter 5 presents the legged robotic system, describes its 3-D simulator and provides an analysis of the kinematics of the robotic platform; highlighting the peculiarities associated with its kinematic configuration.

Chapter 6 introduces the hierarchical decentralised architecture used to achieve robotic control using signalling networks, discusses the motivation behind the approach and examines the experimental results.

Chapter 7 concludes with final considerations and presents some speculative suggestions about the future guidelines of the research documented in this thesis.

Chapter 2

Biological Inspiration: Cellular Signalling

Contents

Cells need to engage in many forms of communication to enable them to sense and respond to their environment. This capability is essential for cells to survive and adapt to their constantly fluctuating surroundings. In multicellular organisms, the role of cellular communication is especially significant as it is also responsible for the coordination of multicellular interactions and the production of collective responses. Cellular signalling is a biological communication mechanism that regulates the activity of cells, in which signalling pathways are its main highways guiding the flux of information between the cell surface and its nucleus. In order

to do so, catalytic reactions diffuse extracellular signals amongst proteins, which may either be clustered in the same pathway or belong to another pathway.

One of the main goals of this thesis is to capture the advantages of intracellular signalling and apply them to the development of a computational architecture that can be used in real world applications. This chapter sheds light into the biological fundamentals underlying the research presented in this manuscript. Thus, the main aspects of cellular signalling are considered, paying close attention to intracellular signalling and its regulatory capacity. Of special interest is the ability of crosstalk to enlarge cells' signalling capacity and elicit robust and adaptive responses. In addition, this chapter also reviews mathematically the major chemical reactions amongst proteins and analyses their implications in the signal transduction context. Finally, this chapter ends with last thoughts about cellular signalling and its tools to regulate the specificity and intensity of the cellular response.

2.1 Cellular Signalling

In biological organisms, cells are exposed to wide range of incoming chemical signals. It is within the cell's capacity to sense specific signals, transduce them and generate accurate responses. The main task is to guarantee the survival of the living organisms. Cellular signalling is the communication process whereby cells interact with each other and their external environment (Rhee, 2006). The result of these interactions is a biochemical reaction in the cell. The nature of the response mostly depends on the type of molecules, the strength of the signal, and the regulatory mechanisms involved in its generation (Krauss, 2001). Some responses may occur locally inside the receiving cell, for example the creation of ion channels in the plasma membrane or the modification of the cytoskeleton[1]. Other types of response, although internally launched, show their effect externally and promote the interaction amongst cells and their environment. Cellular signalling consists of two stages: intracellular and intercellular signalling. While the former constitutes the biological inspiration of this research, the latter provides its future guidance.

[1]The cytoskeleton is an internal cellular component responsible for the control of the cell shape, movement and localisation of reactions.

2.1.1 Stages of Cellular Signalling

Cellular signalling is the sequence of biochemical events that, triggered by an extracellular chemical signal, induces an adaptive cellular response. These signals are known as *first messengers*. They are produced by *signalling glands* in response to certain stimuli and travel through the vascular system until they arrive at specific *target cells*, where they dock to receptor proteins and initiate the intracellular activity. The group of processes by which chemical signals attain their corresponding target cells in known as *intercellular signalling*. In contrast, the chain of processes occurring locally inside the target cells is called *intracellular signalling*. It begins with the binding of first messengers and their diffusion inside the cell in the form of *secondary messengers*. Such messengers spread across the cell using *signalling pathways* until they reach the cellular nucleus. Pathways then regulate genes expression, which brings about a change in the cellular activity. Chemical signals are removed once they produce the desired effect. Any disorder during cellular signaling may provoke uncontrolled behaviours and disease. A schematic representation of the cellular signalling process can be seen below in Figure 2.1.

The cellular signalling process described here is widely accepted and can be decomposed in seven different stages :

1. *Creaction* of a chemical signal in the signalling gland.

2. *Secretion* of the signal to the extracellular space.

3. *Transportation* of the signal to the target cell.

4. *Recognition* of the signal by a receptor protein in the target cell.

5. *Transmission* of the signal downstream of the target cell.

6. *Transformation* of the signal into a biochemical reaction in the target cell.

7. *Termination* of the signal.

Having introduced the concept of cellular signalling and its different stages, the rest of this chapter focuses on intracellular signalling, especially on its regulatory mechanisms.

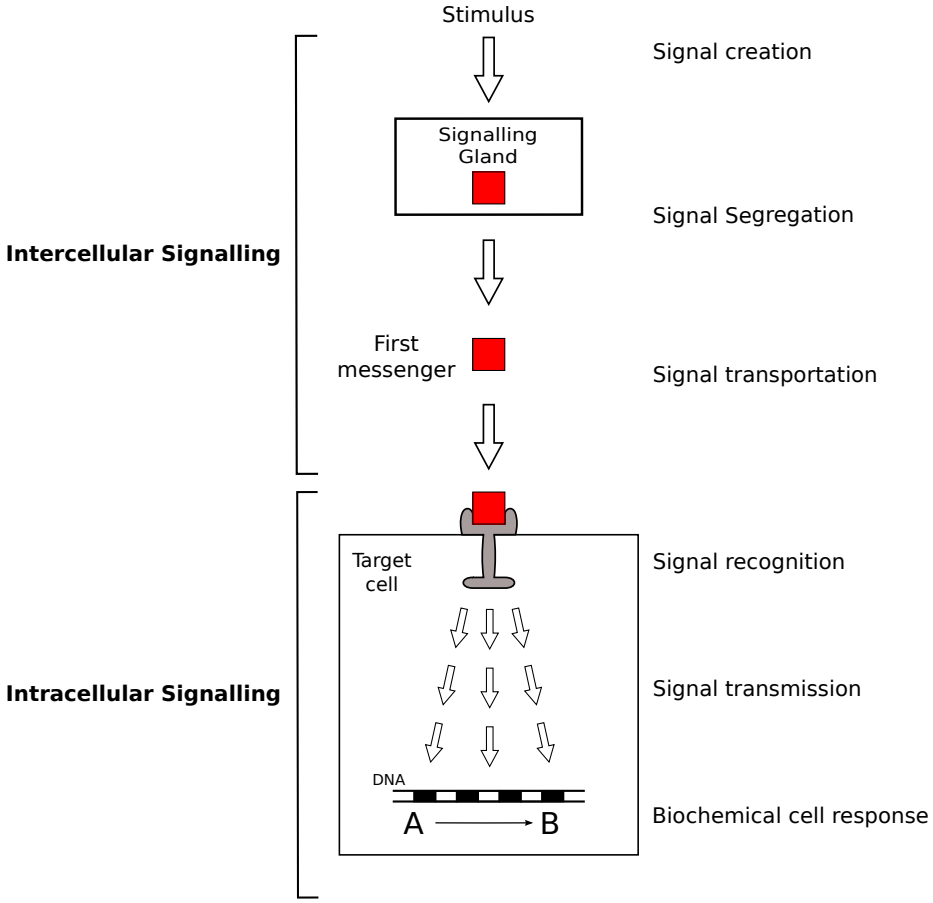

Figure 2.1: Steps in cellular signalling. Initially, the signal is segregated by a triggering stimulus. Upon reception, the signal is recorded and transformed into chemical messengers, which travel throughout the cell. Finally, a biochemical reaction occurs instigating a cellular response. Adapted from Figure 3.2 in Krauss (2001) Chapter 3.

.

2.2 Intracellular Signalling

Intracellular signalling is the collection of events that transfers incoming chemical signals into the cell and elicits a physiological response (Silverthorn, 2009). Specialised proteins, known as receptors, are utilised for the reception of these signals. When a receptor becomes active, it transmits the signals further to the effector proteins, which transform them into secondary messengers. Adaptor proteins may also contribute to the formation of these messengers. A chain of spatially and temporary ordered signal transduction reactions transport secondary messengers further in the signalling pathway. Finally, a distinctive biochemical reaction occurs in the cell and enables the cellular response. This represents the end-point of intracellular signalling.

Intracellular signalling is highly variable. It depends on the type of the reception mechanism, the manner signals are transmitted and the nature of the biochemical reaction (Krauss, 2001). Likewise, the sort of molecular components and their spatial location also inspire different intracellular signal transduction models. The main components of intracellular signalling are illustrated in Figure 2.2.

2.2.1 Components of Intracellular Signalling

The main components of intracellular signalling are proteins. They can be either enzymes or regulatory molecules linking enzymes in signalling pathways. The interaction amongst proteins usually releases diffusible messengers and allows the transmission of the signal.

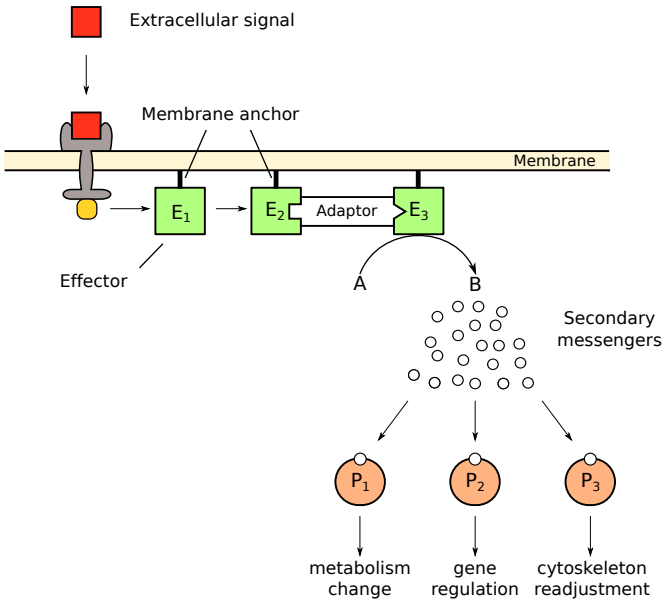

Figure 2.2: Components of intracellular signalling. Intracellular signaling begins when receptor proteins recognise and transport extracellular chemical signals inside cells. In doing so, effector proteins transform these signals into secondary messengers, which unleashes the activation of a sequence of diffusive chemical reactions throughout the cell. When secondary messengers reach the cell genes, a concrete biochemical reaction occurs, representing the cellular response. Adapted from Figure 3.3 in Krauss (2001) Chapter 3.

.

Plasma Membrane

The plasma membrane is the cell's outer layer and surrounds the protoplasm. It acts as a barrier preventing the entrance of inappropriate extracellular molecules as well as anchoring the cell cytoplasm. Additionally, the plasma membrane permits direct-contact cellular

interactions through its surface receptors. An example of this behaviour is the single-pass transmembrane receptor protein of the Notch pathway (Bray, 2006).

The plasma membrane is a two-dimensional impermeable barrier that separates two watery environments. It is composed of phospholipids, each consists of one hydrophilic head and two hydrophobic tails. The phospholipid barrier has two phospholipid rows, each with the hydrophilic head at the opposite end of the membrane. Figure 2.3 depicts a horizontal section of the cell plasma membrane.

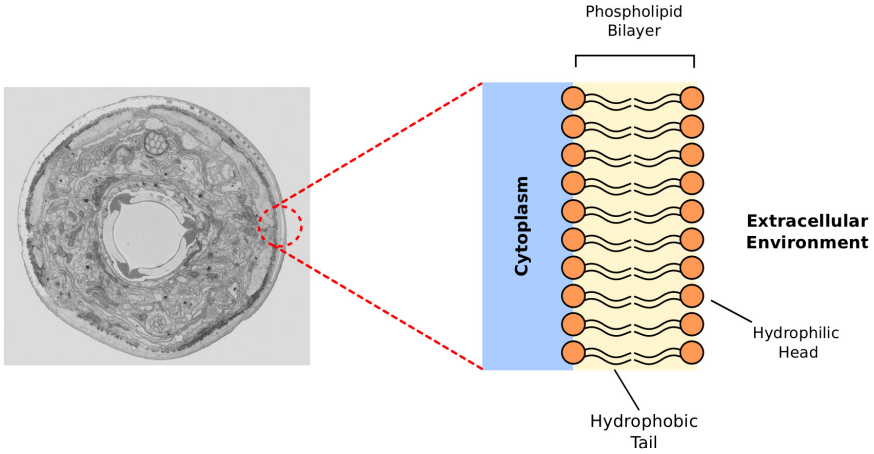

Figure 2.3: Cellular plasmatic membrane. It protects cells from the entrance of undesired molecules as well as grouping all cellular components together. Left-hand side image reproduced from Shaham (2005).

.

Receptors

Receptors are specialised proteins that connect cells with their outside world. During signal transduction, extracellular chemical signals bind to the receptors leading to changes in their structure which allow the transmission of extracellular signals inside the cell. This binding process is highly selective. Ehrlich suggested that binding specificity is the consequence of the existence of sensing chemicals (side-chains) on the surface of the receptors with only react with certain molecules (Ehrlich, 1897). Although theorised more than 100 years ago, this principle is still commonly accepted. The lock-and-key mechanism represents yet a more accurate analogy to exemplify the signal-receptor binding process (see Section 2.3.2).

Decisive for the initiation of intracellular singalling is the concentration of the freely circulating chemical signal. An increment in the concentration of the signal usually unleashes

signal transduction. The intensity of the secondary messengers is the main intracellular regulatory element and closely depends on the concentration of the extracellular signal, the signal-receptor binding affinity and the amount of receptor proteins. These three parameters constitute the hallmarks of intracellular signal transduction (Krauss, 2001).

Depending on their location in cells, there exists two types of receptor proteins: cell-surface and cytoplasmic receptors. A cell-surface receptor (see Figure 2.4a) is a transmembrane protein. It has an extracellular domain, where signals are detected, connected with an intracellular domain through a transmembrane domain. Therefore, signals do not actually need to enter into the cell. Characteristic for cytoplasmic receptors (see Figure 2.4b) is that chemical signals should penetrate the cytoplasm in order to activate them. Cytoplasmic receptors are usually located at the nucleus or cytosol[2].

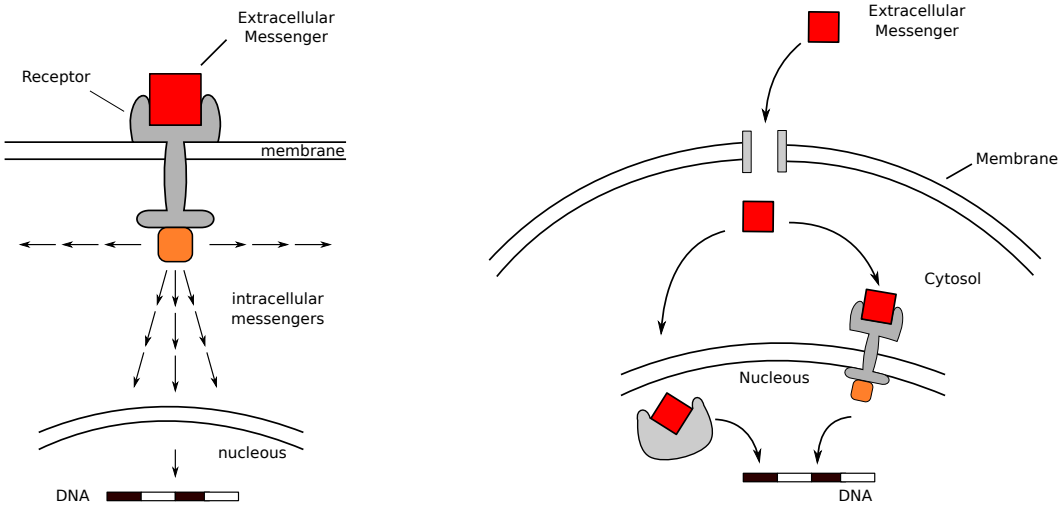

(a) Cell-membrane receptor (b) Cytoplasmic receptor

Figure 2.4: Types of receptor proteins in cells signalling. (a) Illustrates a cell-surface receptor. It recognises signals at the cell membrane and transforms them into intracellular signals. As exemplified in (b), cytoplasmic receptors are located inside the cell in either the cytosol or nucleus. In both locations, signals must enter into the cell to bind the receptor. Adapted from Figure 3.8 in Krauss (2001) Chapter 3.

Intracellular Messengers

Intracellular messengers are the molecules that propagate extracellular chemical signals downstream in the target cell. After binding cellular receptors, these signals arrive at the effector proteins, which in turn transform them into diffusible messengers and disperse them throughout the cytoplasm. Such messengers are termed secondary messengers.

[2] The cytosol is the part of the cytoplasm surrounding organelles.

Secondary messengers are the active components of signalling pathways (Bhalla & Iyengar, 1999). They mobilise proteins for subsequent signal transductions. The transmission of a signal inside a cell involves two steps: the binding of the secondary messenger(s) to a protein and the segregation of new messenger(s) as a result of a chemical reaction in the protein. In addition to this, secondary messengers have the capacity to react with proteins within different signalling pathways. This phenomenon, called *crosstalk*, favours the combination of multiple extracellular signals and increases the messengers' diversity inside the target cell.

Regulatory GTPases

A GTPase (guanosine triphosphate, GTP) is a class of receptor-domain protein that switches the state of a signalling pathway. While its active state enables signal transduction, its inactive state represses extracellular signalling (Sprinzl, 1994).

Effector Proteins

Effector proteins are small molecules that bind to enzymes and allosterically[3] regulate their activity (Bishop & Hall, 2000). By doing so, they modulate the affinity between secondary messengers and enzymes, increasing or decreasing the enzymatic activity. When coupled to receptor proteins, effectors also collaborate in the transformation of extracellular signals into secondary messengers.

Adaptor Proteins

Adaptor proteins are the protein-binding molecules that organise signal transduction. In particular, adaptors group proteins together and enhance the production of secondary messengers, which amplify the transduced signal and generate a more robust and concrete cellular response. Specificity in cellular signalling is closely related to the the chemical composition of the binding molecules in adaptor proteins (Flynn, 2001).

Despite their protein nature, adaptors do not show any catalytic activity. They are the spatial and temporal coordinators of signal transduction (Hepler & Gilman, 1992). As

[3]In a biological context, allosteric refers to an alteration in the structure or activity of an enzyme by the binding of a metabolic molecule at an enzymatic site different to the active sites.

temporal coordinators, they promote the formation of signalling pathways by determining as and when catalytic reactions take place. As spatial coordinators, they define the area of action of secondary messengers. In practice, this capacity defines how cells sense their environment and respond to its fluctuations.

Scaffold Proteins

Scaffold proteins also regulate intracellular signalling. Although they lack specific functions, scaffold proteins collaborate mainly in the formation of signalling pathways and the clustering of signalling components into protein complexes[4]. Additionally, scaffold proteins also contribute to the coordination of feedback loops in signalling pathways (Uhlik et al., 2004; Locasale et al., 2007). As a consequence of their ambiguity in function, some authors consider scaffolds as a subclass of adaptor proteins (Fisher et al., 2000). Nevertheless, scaffold proteins are the main regulatory components in some signalling pathways, such as MAPK, calcium signalling or innate immune signalling.

2.3 Signalling Pathway Regulation

As previously mentioned, the principal objective of intracellular signalling is to stimulate a cellular response from extracellular stimuli. In order to do that, cellular components group together and form a signalling pathway where they transmit extracellular signals downstream of the cell. Such components, described in Section 2.2, can be divided into proteins and messengers molecules. Likewise, proteins can be either enzymes or regulatory proteins. While the former promote the formation of new diffusive messengers, the latter governs their diffusion. The rest of this chapter focuses on how the extracellular information is regulated in signalling pathways and their major intracellular mechanisms to elicit adaptive cellular responses. It also review the main enzymatic reactions found in living eukaryotic organisms.

Signalling pathway regulation is inherently complex (Siso-Nadal et al., 2009). Pathways can work either in isolation or in collaboration with other pathways. In addition to this, cells do not usually respond individually to stimuli; instead they simultaneously receive multiple signals. To overcome these situations cellular signalling offers two solutions: signal amplifica-

[4] A protein complex is a polypeptide structure that increases the reaction rate and the binding affinity between enzymes and its substrates.

tion by crosstalk and compartmentalisation. Whereas crosstalk between signalling pathways characterises signal transduction and enables cells to compute different and multiple inputs in parallel, compartmentalisation increases the specificity of the cellular response. A clear example of the importance of both mechanisms becomes evident when a cell inputs two antagonist signals [5], each triggering a mutually exclusive response. Upon this situation, the cell must resolve which signal to transduce. In a biological context, this implies that either one pathway transduces the signal and suppresses the activity of the other or signals are enclosed into separate compartments and transduced in parallel.

2.3.1 Signalling Pathways

The capacity to manage the functional capabilities of biological systems depends on the ability to orchestrate the biochemical reactions that occur inside their cells. Signalling pathways are the simplest cellular structures connecting the extracellular environment with the genes they regulate. They are composed of interacting proteins whose main objective is the broadcasting of chemical signals to the cellular nucleus. At this stage, the regulation of gene expression lead to a change in the synthesis of new proteins, which represents the cellular response to the extracellular stimulus. Enzymes are the main components of signalling pathways.

Amplification

The transmission of a signal to the cellular nucleus requires a sequence of enzymatic and diffusive transformations, each usually amplify the strength of the signal. An initial level of amplification occurs at the membrane level, and it is associated with the transformation of signals into intracellular messengers and their consequent diffusion. An active receptor is able to initiate signal transduction upon minimal concentrations of chemical signals. At this point, receptors can also crosstalk (see Figure 2.5c) and release new messengers inside the cell to stimulate cellular activity (Katz et al., 2000).

A second level of amplification takes place internally in the cell. Signalling pathways are non-linear successions of events (Taniguchi et al., 2006). On one hand, pathways may display spatial arrangements, called *feedback loops*, to modulate the flux of messengers (see Figure 2.5a). On the other hand, one or more components of a pathway may alter the activity

[5] Antagonist are molecules that perturb the activity of other chemical entities.

of another pathway. In this case, a common component crosstalks with both pathways (see Figure 2.5d). An example of this inter-pathway interaction is the crosstalk between the salicylic acid and jasmonic acid pathways (Kunkel & Brooks, 2002). Another form of crosstalk can be observed in the interactions between the cAMP and MAPK pathway, which occur at the gene level (see Figure 2.5b). Components of cAMP pathways activate the MAPK genes responsible for the production of lymphocytes (Sengupta et al., 2007). In any of the above situations, crosstalk acts as a cellular amplification mechanism. It contributes to the formation of larger processing regions inside the cell, increases the diversity and variability of signalling components and eases the generation of collaborative responses.

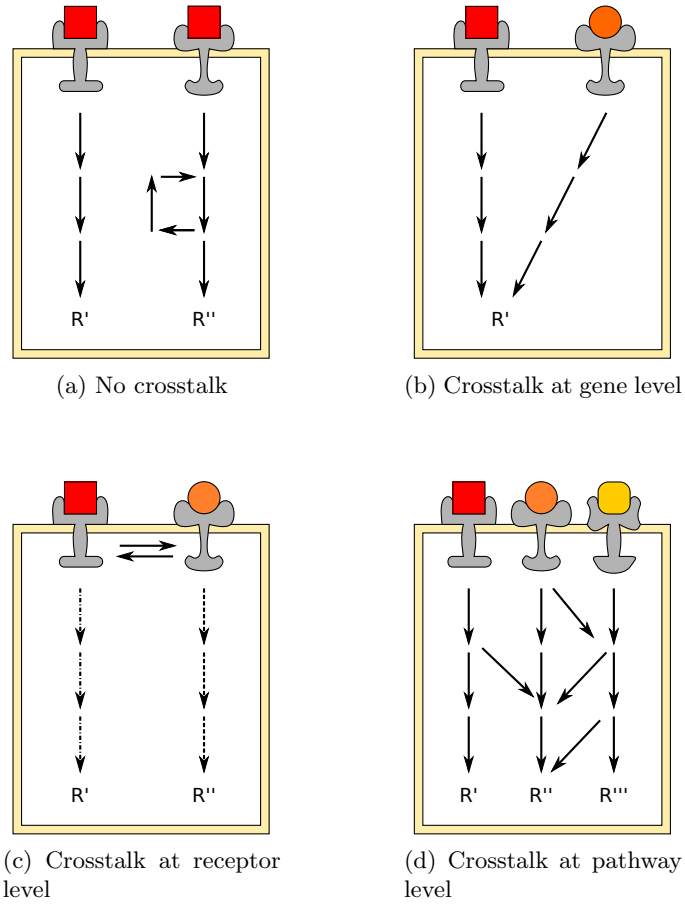

(a) No crosstalk

(b) Crosstalk at gene level

(c) Crosstalk at receptor level

(d) Crosstalk at pathway level

Figure 2.5: Amplification of external signals using crosstalk. (a) Different types of receptor proteins bind the same extracellular signal and induce different reactions. Signalling pathways may contain motifs to modulate signal transduction. (b) The binding of two different signals activates two pathways which promote identical biochemical reactions. (c) Upon the binding of two different chemical signals, receptors crosstalk at the plasma membrane and activate two complementary pathways (Widgerow, 2011). (d) Different pathways crosstalk each other and lead to different biochemical reactions. Likewise, the same receptor can activate several pathways at once.

Some signalling pathways also show a third level of amplification, as in the case of the calcium pathway through ion channels. Although calcium ion are the main secondary messengers, the reception process may also diffuse phospholipase C messengers. These activate internal organelles wherein calcium ions are also produced (Morgan, 1989).

Compartmentalisation

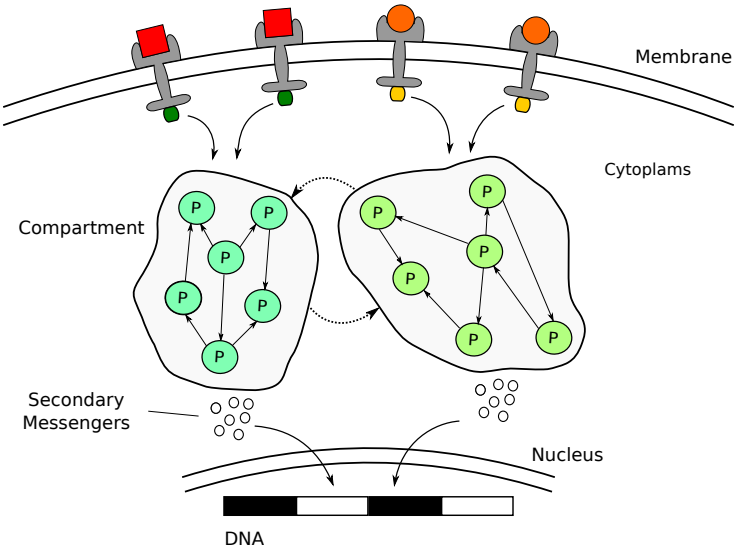

Figure 2.6: Signal transduction under the effect of compartments. The reception of two different extracellular signals may force the cell to process them separately. Compartments are the cellular organelles which group cellular components together allowing them to work as independent units and produce opposite responses. Likewise, compartments can interact with each other.

Cells are constantly exposed to a wide variety of signals. Receptor proteins constitute an initial filter specifying which extracellular signals can penetrate into the cell. However, there are situations where this is not sufficient to elicit adequate responses. Compartmentalisation is the cellular mechanism that allows cells to increase the efficiency of the response (Weng et al., 1999). It becomes essential in situations where simultaneous responses to opposite events requires the sharing of intracellular messengers (Mor & Philips, 2006). In order to cope with these, the cytoplasm is divided into compartments, which embrace different cellular components and surround them by a lipid-like membrane (see Figure 2.6). The most well known compartment is the cellular nucleus.

In a cellular signalling context, compartments are multi-pathway structures which work in isolation. Thereby, it is possible to delimit the diffusion of cellular messengers and separately transduce chemical signals which may generate opposite responses. Although compartments

are structurally and functionally independent, they may interact with each other. These interactions are not fixed, but they are deployed by specific messengers, when a drastic response is required. The type of connectivity between compartments is related with which genes are transcribed. The formation of compartments occurs during the early stages of cell development favoured by the clustering capacity of scaffold proteins (Marijuán, 1995).

2.3.2 Enzymes

Enzymes are the molecules responsible for most of the chemical reactions in living organisms. They act as efficient catalysts, controlling the speed of specific chemical reactions (Cooper, 2000). During the enzymatic process, reactant molecules, the *substrates*, are transformed into another type of molecules, the *products*. Active sites are the regions in the enzymes where substrates bind and undergo a catalytic reaction. Such a reaction also provokes the formation of successive intermediate transition-states, the enzyme-substrate complexes. After the reaction occurs, the final product is released (see Figure 2.7). In the case multiple substrates dock the active sites, the binding order prior to the reaction clearly define they type of reaction.

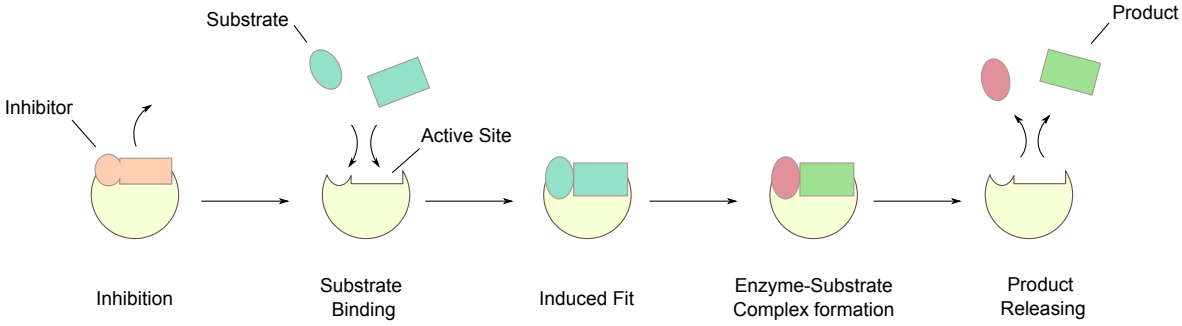

Figure 2.7: Example of enzyme catalytic reaction. Upon their activation, enzymes are able to receive substrate molecules. Since enzyme are very selective, they only react with few substrates amongst many possible. When a substrate is affine enough it binds the enzyme's active sites and catalyse it, initiating the reaction. The substrate binding carry alter the cell surface (induce fit) upon which the reaction rate achieves its equilibrium state. During the catalysis enzyme-substrate complexes are formed prior to the transformation of the substrate into one or more products. Finally, the product molecules are released, enabling new reactions.

.

Enzymes are highly specific as to their catalytic reaction and the type of the reactants. They have the ability to interact and react uniquely with certain substrates. The differentiation criteria is the affinity between substrates and active sites. This is called the *lock-and-key*

mechanism and rests on the assumption that substrates and active sites have complementary shapes, which fit together (Koshland, 1995). However, this binding also implies a conformation change on the cell surface, *induced fit*, increasing the strength of the enzymatic binding and stabilising it.

Enzymes, as many catalysts, require certain activation energy to occur. However, this energy level is only achievable at high temperatures. In living organisms, the body temperature is considered low, suppressing the catalytic capacities of the enzymes (Agarwal, 2005). To make these reactions energetically viable, the enzyme-substrate affinity minimises the thermal energy, which lowers the activation energy. Under these conditions, enzymes reach their equilibrium state, increasing their reaction rates. At the equilibrium state, the concentrations of the reactant and the product is always identical after the catalysis.

There also exists additional classes of molecules able to alter the activity of enzymes by deciding when and how catalysis occurs (Fersht, 1999). Enzyme inhibitors are molecules that bind to an enzyme and decrease or neutralise its activity. In contrast, enzyme activators are molecules that, in combination with the enzymes, increase their catalytic capacity. Alternatively, some enzymes also require cofactors, non-protein chemical compounds, to initiate their activity. The regulation of the enzymatic activity is the principal mechanism to ensure that the output of signalling and metabolic pathways meets the biological requirements and the kinetic energy of catalytic reactions is efficiently used.

2.4 Enzyme Kinetics

Enzyme kinetics is the study of the catalytic reactions in enzymes. These reactions are characterised by two properties: the speed at which products are generated and the maximum achievable reaction rate under ideal conditions. The combination of these two elements defines how enzymes chemically interact with their environment.

2.4.1 Michaelis-Menten Kinetics

Michaelis-Menten kinetics (Michaelis & Menten, 1913) is a mathematical model of single-substrate and irreversible enzymatic reactions. It divides the kinetic reaction (2.1) into two steps: the binding of a substrate S to the active site of an enzyme E, which generates an

enzyme-substrate complex ES, and the decomposition of this complex to release the new product molecule P and reestablish the enzyme E.

$$\underbrace{\mathrm{E} + \mathrm{S} \underset{K_{-1}}{\overset{K_1}{\rightleftharpoons}} \mathrm{ES}}_{\text{binding}} \overbrace{\xrightarrow{K_2} \mathrm{E} + \mathrm{P}}^{\text{catalysis}} \tag{2.1}$$

K_1, K_{-1} and K_2 are the reaction rates. In particular, K_2 determines the maximum number of substrates S an enzyme is able to catalyse per active site and unit of time. The Michelis-Menten equation describes the biochemical reaction (2.1) as the catalytic rate needed to transform a substrate into a product and depends on the enzyme and substrate concentrations prior to the reaction. The Michaelis-Menten equation is as follows,

$$\nu = \frac{V_{max}[\mathrm{S}]}{K_m + [\mathrm{S}]} \tag{2.2}$$

where ν is the production rate, V_{max} is the maximum production rate, K_m is the Michaelis constant and [S] is the substrate concentration. A plot of the Michaelis-Menten equation can be seen in Figure 2.8.

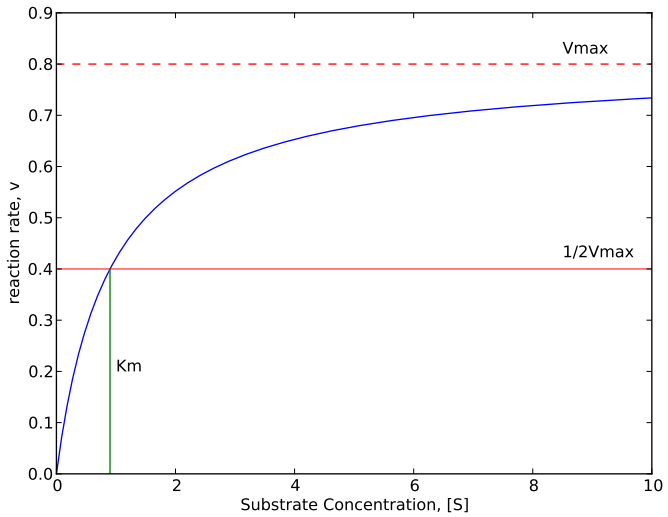

Figure 2.8: Plot of the Michaelis-Menten equation. It represents the predicted reaction rate as a function of the substrate concentration. The equation also models the enzyme saturation level. The correct determination of V_{max} and K_m is of great importance in the accuracy of the model prediction. An example curve with $V_{max} = 0.8$ and $K_m = 0.9$.

.

Typically, the Michaelis-Menten equation shows two behaviours with regard to the Michaelis constant K_m (Berg et al., 2002). K_m determines the strength of the enzyme-substrate binding and is defined as the enzyme concentration at 50% of the reaction rate. In mathematical terms, it means that K_m is a switching point, where substrate concentration values below K_m, ($[S] \ll K_m$), display a linear type growth, and values above K_m, ($[S] \gg K_m$), show an asymptotic growth towards V_{max}. Of particular importance is the capacity of K_m to catalyse enzymatic reactions. The higher the K_m value, the weaker the enzyme binds to its substrate and the lower the production rate; likewise, the smaller the value, the higher the substrate affinity is (see Figure 2.9). The value of V_{max} is the enzymatic saturation limit and matches the maximum reaction velocity. The slower the V_{max}, the lesser the product concentration, which inhibits the transmission of signals across the cell, whereas the higher V_{max}, the stronger the intensity of the signal.

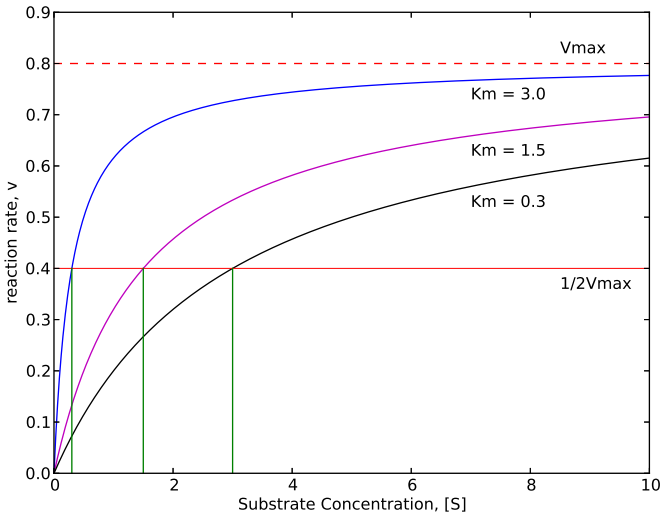

Figure 2.9: Effect of K_m in the concentration of an enzyme. The changes in the reaction are given by different values of K_m, $K_m = 0.3$, $K_m = 1.5$ and $K_m = 3.5$. The initial enzyme concentration values and V_{max} remain constant.

.

2.4.2 Cooperativity

When multiple substrate molecules bind to the same enzyme with identical affinity, there is a possibility that the binding of the initial substrate alters the ability of subsequent active sites to bind other substrate molecules. This action is commonly termed *cooperativity*. Enzymes exhibit four different types of cooperativity:

- *Positive Cooperativity*: the initial binding enhances the capacity of the enzyme to dock with additional substrate molecules.

- *Negative Cooperativity*: the initial binding acts upon the occupation of the subsequent active site by decreasing its binding affinity.

- *Homotropic Cooperativity*: the substrate causing the cooperativity is affected by it.

- *Heterotropic Cooperativity*: a third molecule, which might not be a substrate, modifies the enzyme-substrate affinity.

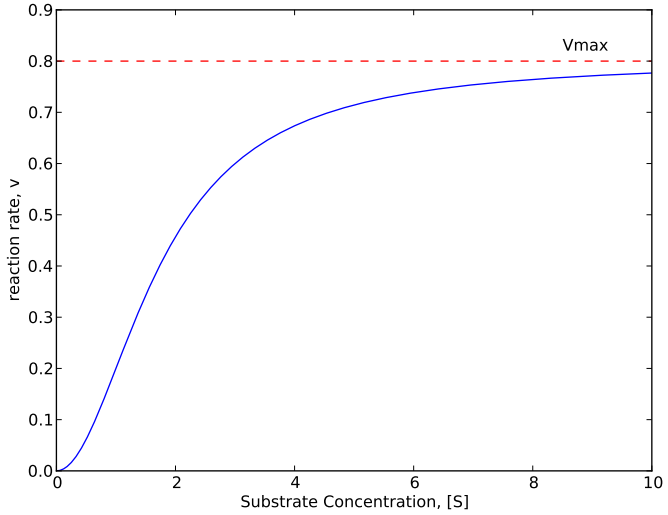

Figure 2.10: Representation of the Hill equation indicating positive cooperativity between the substrate molecule and its active site. An example curve with $h = 2$, $V_{max} = 0.8$ and $K_D = 0.2$.

Cooperativity amongst active sites is described by the following chemical reaction,

$$\mathrm{E} + n\mathrm{S} \overset{K_D}{\longleftrightarrow} \mathrm{ES} \tag{2.3}$$

where E is the free enzyme, S is the substrate molecule, n is the number of active sites, K_D is the dissociation constant and ES is the resulting enzyme-substrate complex. The Hill equation (Hill, 1910) describes the biochemical reaction (2.3) as the saturation level of an enzyme. It quantifies the number of substrate molecules that must bind to an active site to accomplish a functional effect (Weiss, 1997),

$$\nu = \frac{V_{max}[\mathrm{S}]^h}{K_D + [\mathrm{S}]^h} \tag{2.4}$$

where V_{max} is the maximum reaction rate, h is the Hill coefficient, K_D is the dissociation constant and [S] is the substrate concentration. It is important to highlight that the fundamentals of this formula are no longer accepted in the research community (Weiss, 1997), but the equation is still used to measure the degree of cooperativity amongst active sites. A plot of the Hill equation can be seen in Figure 2.10.

The Hill equation is characterised by an exponential sensitivity prior to saturation. Small changes in the substrate concentration promptly increase the reaction rate. Unlike the hyperbolic shape of the Michealis-Menten equation (see Figure 2.8), the Hill equation shows a sigmoidal shape, whose steepness is governed by the Hill coefficient. Such a coefficient reflects the degree of the enzymatic cooperativity: the greater the value, the higher the level of cooperativity and, therefore, the more steep the transition is.

An alternatively function of the Hill coefficient is to discriminate amongst the different types of cooperativity (see Figure 2.11). Hence, Hill coefficient values larger than 1 entail positive cooperativity (plot 3), negative cooperativity (plot 1) leads to Hill coefficient values smaller than 1, and Hill coefficient values equal to 1 entail no cooperativity (plot 2); in this case the Hill function turns into the Michaelis-Menten equation. Finally, absolute cooperativity is achieved when every active site is occupied (plot 4). Further, it is important to notice that the Hill coefficient cannot exceed the number of active sites.

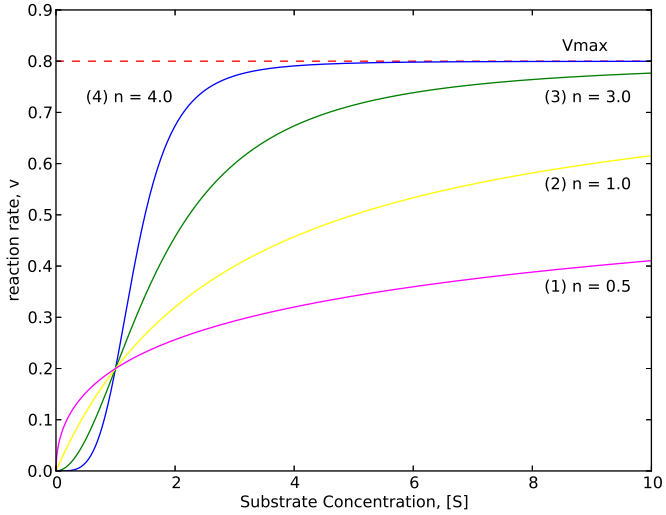

Figure 2.11: Hill example curves with Hill coefficient values of $n = 0.5, 1, 2$ and 4 respectively. Since the simulated enzyme has a maximum of four active sites, absolute cooperativity is reached with $n = 4$. The intersection between all curves occurs at $[ES]n/[S]_{tot}$.

2.4.3 Phosphorylation

Protein kinase phosphorylation is a common mechanism in the coordination of multiple cellular processes. It regulates most of the cellular pathways, especially those involving signalling proteins. In a chemical context, phosphorylation is an enzymatic reaction (2.5), in which an enzyme catalyses another enzyme by providing its substrate molecules in the form of phosphatase groups PO_4,

$$\text{Enzyme} \xrightarrow[\text{ATP}\longrightarrow\text{ADP}]{} \text{Enzyme} \tag{2.5}$$

where ATP are phosphorylated nucleotides (substrate molecules) and ADP are the nucleotides (product molecules) released during a hydrolytic reaction. A signalling pathway regulated by phosphorylation is a signal transduction network called *protein kinase cascade*. Such networks depict a cyclical regulatory sequence, in which kinases are initially phosphorylated and then dephosphorylated. This entails a conformational change in the enzyme structure which lead to it continuous activation and deactivation. A kinase can also be doubly phosphorylated on two different active sites, causing it to become fully active. There does not exist a standard

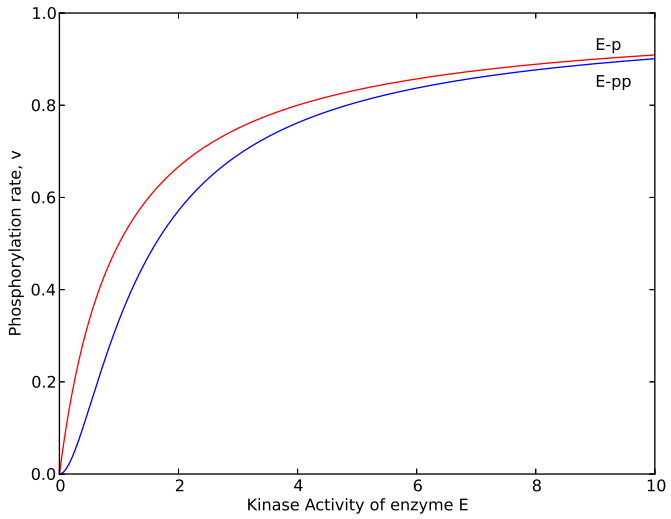

Figure 2.12: Activation kinase curves for a single (E-p) or double (E-pp) phosphorylation of the enzyme E.

mathematical model to describe this regulatory process. This is a consequence of the large variety of participants in protein kinase cascades. The work presented here relies on the steady-state of first-order kinetics to model protein kinase phosphorylation, which suffices to illustrate the regulatory principles and avoids the development of detailed computational models of signalling networks (Alon, 2007). In this context, the phosphorylation rate is the

concentration of the phosphorylated enzymes given by:

$$\nu = \frac{w[\mathrm{S}]}{1 + [\mathrm{S}]} \tag{2.6}$$

where [S] is the concentration of each participating enzyme and w is the rate at which phosphatase groups are transferred. However, this formula is only applicable when the kinase is phosphorylated on one active site. The effect of phosphorylation on two sites is modeled by a steeper saturation function (Alon, 2007):

$$\nu = \frac{w[\mathrm{S}]^2}{1 + [\mathrm{S}] + [\mathrm{S}]^2} \tag{2.7}$$

Figure 2.12 illustrates an example cuve of the phosphorylation rate for a single and double phosphorylated enzyme. More sophisticated mathematical models offering a more realistic description of protein kinase cascades can be found in Bray & Lay (1994); Prehoda & Lim (2002) and Salazar & Hofer (2003).

2.4.4 Multisubstrate Reactions

The majority of the enzymatic reactions are not single-substrate. The formation of products usually requires the participation of multiple substrates. Examples of these reactions includes ordered substrate binding (Hickman et al., 1999), random substrate binding (Graham et al., 1993) and the ping-pong mechanism (Rogers & Gibon, 2009). When more than one substrate molecule binds a enzyme, the order of the intermediate reactions characterises the entire reaction. Nevertheless, the necessity to deal with many intermediate stages frequently limits the applicability of mathematical models to reactions with a maximum of two substrates (Bisswanger, 2002). Probabilistic techniques handle this limitation by modeling the reaction rate as the probability for a substrate molecule to be bound on an active site. In this context, the Michaelis-Menten kinetics can also be applied to multi-substrate reactions (Alon, 2007).

Considering multiple substrate-enzyme bindings as independent events, the reaction rate of an enzyme with multiple-occupied active sites is given by the activation rate times the probability of a substrate to be bound on an active site:

$$\nu([\mathrm{S}_1], \ldots, [\mathrm{S}]_m) = \frac{\sum_i \beta_i ([\mathrm{S}]_i / K_{m_i})^{n_i}}{1 + \sum_i ([\mathrm{S}]_i / K_{m_i})^{m_i}} \tag{2.8}$$

where K_m is the Michaelis constant, [S] is the substrate concentration, β is the activation rate and represents the maximal contribution of each binding in the final production rate and, n and m are the Hill coefficients. $n = 0$ and $m > 0$ express inhibition and $n = m$ represents activation. A plot of the probabilistic Michaelis-Menten equation for multiple-substrate reactions can be seen in Figure 2.13.

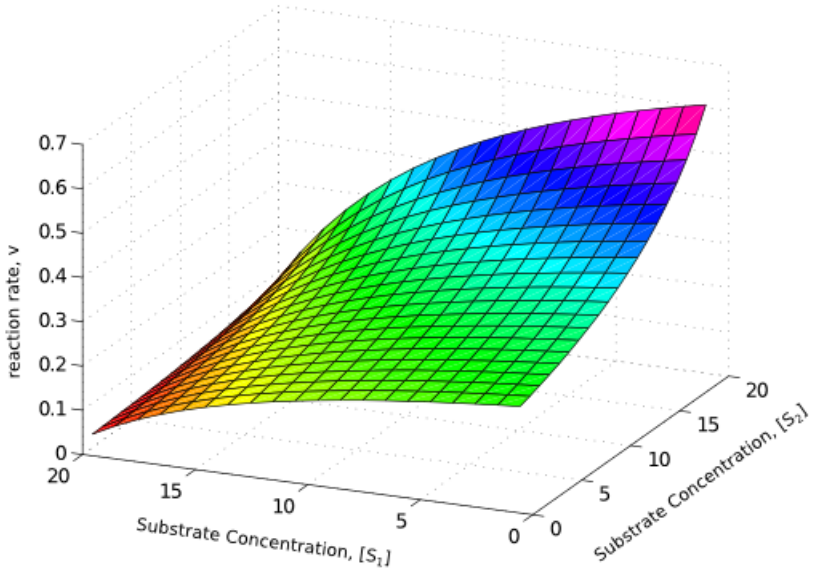

Figure 2.13: The probabilistic Michaelis-Menten equation for multiple-substrate reactions equation. It represents the predicted reaction rate as a function of two substrate concentrations. An example curve with $w_1 = 0.25$, $w_2 = 0.7$ and $K_{m_1} = K_{m_2} = 0.9$.

.

2.5 Summary

Cellular signalling is one of the main regulatory mechanisms within cells. It gives them the capacity to interact with their outside environment in order to assure their survival. The process starts when a signalling gland reacts to an extracellular stimulus and ends with a chemical response in the form of a biochemical reaction within a target cell. Meanwhile, a chain of events extracellularly transports the stimulus from the signalling gland to the target cell and intracellularly diffuses it across the target cell.

Broadly speaking, intracellular signalling is the sequence of biochemical reactions which transduce chemical signals from the plasma membrane to the cellular nucleus. Signalling pathways are the simplest cellular structures connecting the outside environment with the

genes they regulate. A closer inspection reveals that intracellular signalling starts when a receptor protein binds an extracellular signal and disseminates an initial messenger to the effector proteins inside the cell. These in turn release secondary messengers, which guide the flux of information further downstream of the cell along signalling pathways. Spatially and temporally variable catalytic reactions lead to changes in gene expression and bring about an alteration in the cellular activity. Enzymes are the main components of signalling pathways as they spread secondary messengers across the cytoplasm. Intracellular signalling shows a complex organisation which enables cells to deal with all the variety of incoming signals and mainly generate adaptive cellular responses. Cells offers two main mechanisms to increase their signalling capacity: crosstalk and compartmentalisation. While the former promotes the interaction amongst pathways, the exchange of extracellular information, and the formation of extended processing structures, the latter limits the spreading of intracellular messengers, giving rise to highly specialised processing units. Of special interest in this research is the role crosstalk plays in the transduction process. It defines the interaction amongst signalling pathways, lead to the formation of large signalling networks and engages colligated responses. These biological control mechanisms constitute the biological inspiration of this thesis. The importance they manifest in biological organisms when reacting to nonlinear cellular environments makes them computationally interesting.

Taking as a reference point intracellular signalling, this thesis introduces a novel enzyme-mediated network called *Coupled Artificial Signalling Network* (CASN). It is coupled in the sense that individual *Artificial Signalling Networks* (ASN) are linked using crosstalk connections. It is enzyme-mediated in the sense that the simplest units in an ASN are enzymes and are regulated using a catalytic reaction. This architecture takes advantage of crosstalk and compartmentalisation to model the structural and temporal topologies found in signalling networks when an extracellular stimulus is transduced and, to capture their complex dynamics. The underlaying objective is the development of a computational structure able to process several inputs in parallel and also in total or partial isolation, which can then be then combined to produce cooperative control directives. Having exposed the biological basis of this thesis, the next chapter introduces the computational aspects of the ASN models considered in this thesis and describes how crosstalk connections can be used to produce extended processing architectures whose activities and functions mirror biological signalling networks.

Chapter 3

Artificial Signalling Networks

Contents

Computational techniques are increasingly used to analyse and represent the properties of complex biochemical networks, including those involved in cell signalling. This chapter examines the concept of *Artificial Signalling Network* (ASN) as an approach to capture the signalling processes inside cells, which decode outside environmental information and generate robust and adaptive responses. The majority of the existing models are to a great extent sensitive to the amount of biological information about concrete facets of the signalling process. This foments either granular representations which involve complex simulations or simplified approaches which constrain the dynamics of the modelled processes. Taking advantage of the self-organising capacity of signalling networks, this chapter explores the use of evolutionary

algorithms to produce functional signalling models able to express rich dynamics and whose topology is uniquely the result of the interactions with the environment.

Although early molecular biologists perceived signalling networks as a linear succession of events (one stimulus - one response), there is sufficient biological evidence to demonstrate that cells show a more sophisticated internal organisation. With this in mind, this chapter presents two ASN representations: a stand-alone ASN and a coupled ASN (CASN). While the former models the interacting molecules inside pathways, the latter extends the previous model by means of the use of crosstalk, which mimics cooperation amongst signalling pathways and allows the formation of larger signalling structures (Fuente et al., 2012, 2013*b*). Finally, the chapter concludes with a discussion about the computational benefits of the proposed models and their applicability in the control of complex behaviours.

3.1 Artificial Biochemical Networks

Activities and dynamics of biological systems emerge from non-linear molecular interactions taking place inside cells. These complex interactions underlie a set of biochemical networks whose properties determine both the structure and function of biological organisms. This work considers three kinds of biochemical network: genetic, metabolic and signalling.

A *genetic network* results from the regulatory interactions between genes. It captures how genes regulate each other's expression levels over time by means of transcription factors. A *metabolic network* emerges from the enzyme-mediated reactions that occur within cells. It favours the preservation of the physiological equilibrium inside a cell. A *signalling network* comprises the protein-protein interactions that translate external inputs into meaningful biological signals. It emerges when the products of biochemical reactions become the substrates of others, forming chains of reactions known as signalling pathways. This product-substrate sharing can also be observed between different pathways. The genetic, metabolic and signalling networks have been described as the self-modifying, self-organising and self-reshaping components of a cell's biochemical network (Marijuán, 1995). Computational models of these three biochemical structures have been collectively termed *Artificial Biochemical Networks* (ABNs) (Fuente et al., 2012; Turner et al., 2012; Lones et al., 2014).

Despite their emergent dynamics when individually considered, these networks do not work in isolation. Coupling between these three networks can be found in the regulation of a

protein production, where the genetic network modifies the behaviour of both the signalling and metabolic networks, in the delivering of inner/outer chemical signals, where signalling networks alter the dynamics of the metabolic and genetic networks; and in the absorption of nutrients, where a metabolic network regulates a genetic network. Commonly, the transduction of extracellular stimuli also requires the participation of various signalling pathways, which collaboratively generate cellular responses. Figure 3.1 illustrates the main interactions between these three types of biochemical networks.

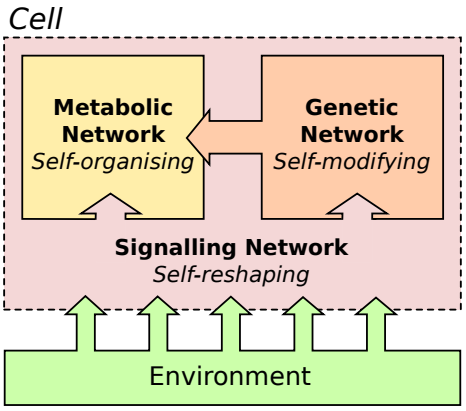

Figure 3.1: Interactions between the three different types of biochemical networks inside a biological cell. Adapted from Figure 2 in Lones et al. (2014).

The ability of biochemical networks to encapsulate cellular interactions has led to a growing interest in the integration of biological networks into computational models, which represent and modulate their dynamics. A number of authors have investigated the use of computational architectures based on models of interacting biochemical pathways. In Lones et al. (2010), the authors introduce a metabolic and genetic network representation and explore how its emergent dynamics can be used in the control of complex dynamical problems. The same authors also explore the coupling between the metabolic pathway and the genetic pathway in the context of robotics (Lones et al., 2011). Turner et al. (2012) presents a computational model of a genetic network with an epigenetic layer of numerical identifiers applied over the genes: one identifier per objective confronted by the system. For a given task, the subset of identified genes are used to build the model. In their latest work, Turner et al. (2013) suggests a self-shaping genetic network able to alter its structure and self-emergent dynamics upon the activation of concrete epigenetic molecules, which only become functional when its expression level is above a certain threshold. This type of emergent behaviour is well suited to solve problems exhibiting switching dynamics. Taking these models as computational inspiration, the work in thesis focuses on the interactions of signalling pathways with

other pathways and how their cooperation leads to colligated cellular responses. This form of connectionism is the principal route through which biological organisms handle the complexity of environmental interactions. In particular, this thesis explores the computational properties of a representative model inspired by the organisation and processes of signalling networks.

3.2 Signalling Networks

A signalling network is a sequence of events triggered by a biochemical signal that requires an adaptive cellular response. It comprises the set of protein-mediated reactions enabling cells to sense, transduce and understand extracellular signals. Cellular signalling commences with the detection of concrete classes of extracellular signals, and their posterior binding by receptor molecules. Following the absorption of such signals inside the cell, a set of interacting proteins spread them across the cytosol by means of either secondary messenger or protein kinase cascades. When the transduced signals reach the genes located in the nucleus, they modify their expression level, which brings about changes in the cellular activity. The set of alterations in the cell's behaviour represents the cellular response to the received stimulus (stimuli). A schematic illustration of a prototypical signalling pathway emphasising its signal processing components is shown in Figure 3.2.

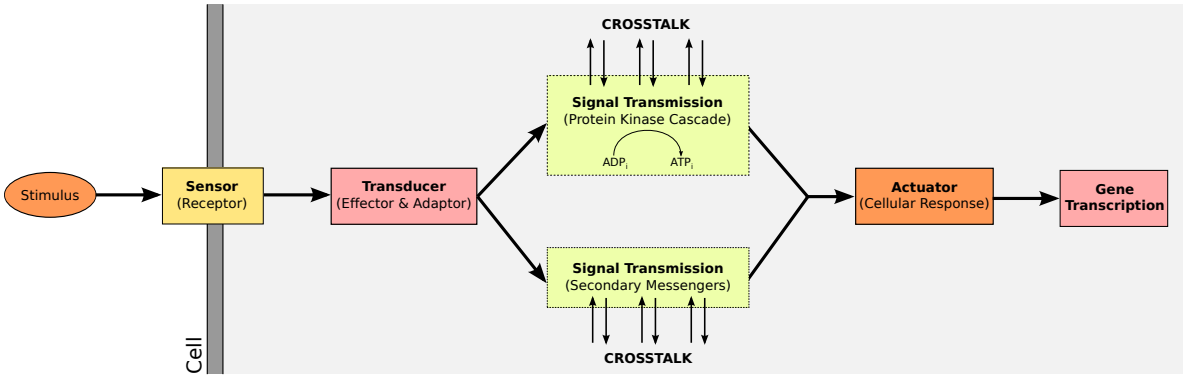

Figure 3.2: Prototypical stand-alone signalling pathway in eukaryotic cells. The binding of a stimulus to a receptor in the extracellular domain triggers a set of transient modifications in the intracellular domain. These include the transformation of the extracellular signal into understandable cellular molecules and their subsequent processing by means of protein-motivated biochemical reactions. Located at the end of the signal transduction process, actuators provoke the cellular response mainly via the transcription of certain genes. Adapted from Figure 1 in Marijuán et al. (2013).

From a biological perspective, there has been an extensive interest in unravelling the catalytic interactions underlying intracellular signal transduction. However the complexity and internal organisation of these interactions is only now beginning to be understood. In terms of numbers, as many as 10% of the proteins in mammalian cells are involved in the intracellular signalling process, which, although organised in a relatively small number of standard pathways [1], orginate a large diversity of signalling structures in each cell. Each represent an isolated or colligated fully functional processing pipe for the entrance of extracellular information into the cell. In case the reader is further interested in specific aspects of the signalling process in eukaryotic cells, CST (1999) (Cell Signalling Technology) is a biological database containing detailed information about particular signalling pathways, their components and their functionality.

In a computational context, intracellular signal transduction is a relatively unknown process. One of the main reasons for this is related to the existence of a large amount of detailed information about concrete aspects of the signalling process. Although this provides considerable understanding of certain functional characteristics of signal transduction, it also lacks in presenting an overall picture of their interacting components and their intrinsic dynamics. Signalling networks are computationally interesting for a number of reasons. This includes the capacity to express complex and robust behaviours with respect to multiple and independent stimuli, the ability to function as independent working units which can also collaborate and develop large signalling structures, the ability to adapt to fluctuating environments and —from the perspective of evolutionary algorithms— their evolvability. In this sense, this thesis interprets the concept of *Artificial Signalling Network* (ASN) as an abstraction of the interacting molecules within signalling pathways whose shape emerges uniquely from the interaction with the environment. This closely models the self-organised dynamics[2] that enable cells to receive chemical signals as inputs and generate some adaptive response.

The existence of concrete biological knowledge has lead to a large diversity of ASN representations which attempt to accurately reproduce the behaviour of particular signalling pathways by analysing the temporal and spatial dynamics of each participant in isolation. Conversely, ASN modelling is highly dependent on the type of experimental data, the amount

[1] There exist 24 major signalling pathways in eukaryotic cells attending to their roles in development and physiology (Marijuán et al., 2013).

[2] Self-organised dynamics refers to the ordered dynamics spontaneously arisen out of the local interactions between the basic elements (enzymes in the scope of this thesis) of an initially unordered system.

of *a priori* knowledge available about a concrete pathway and the modelling context. The number of the participant molecules and their types may also discriminate different ASN models. Although a precise classification of the vast amount of ASN models becomes ambitious, this work considers the amount of *a priori* information related to particular signalling processes as the primary form of classification (Kestler et al., 2008). Thus, ASN models are said to be either quantitative or qualitative. While the former requires a considerable amount of information to produce models able to quantify the concentration of the modelled elements, the latter generates computationally complex abstractions, which are commonly simplifications of the signalling process. The rest of this section presents a representative sample of the work undertaken in capturing complexity of signalling networks.

3.2.1 Quantitative Models

The quantitative description of signalling networks is the main approach to model ASN. Commonly, these models rely on experimental and mathematical representations for the identification of the functional elements as well as their interactions in concrete pathways. Initial steps in such models conceived signalling pathways as linear processing cascades of proteins interactions. Cellular responses were typically quantified as fluctuations in proteins' activity (Kholodenko et al., 1997). An unidirectional, linear view of a signalling pathway is illustrated in Figure 3.3. Linear ASN models have been extensively developed for the Wnt pathway (Lee et al., 2003) and the JAK/STAT pathway (Yamada et al., 2003).

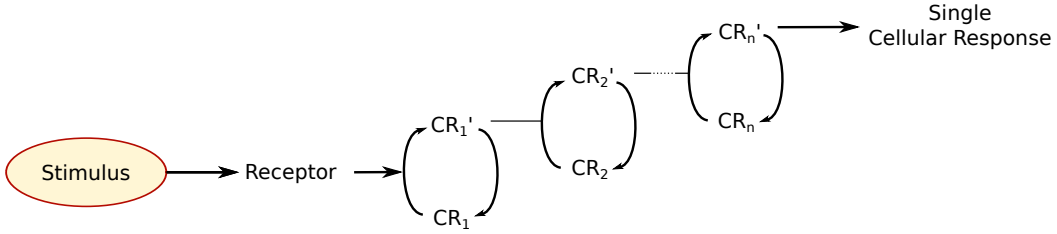

Figure 3.3: Simplest linear representation of a signalling pathway, where CR_i represents either a catalytic or phosphorylation reaction.

.

The consideration of feedback loops has helped to integrate dynamical behaviours and control mechanisms leading to a new generation of computational models. Feedback loops can be either negative or positive. The former generally decrements the intensity or duration of the propagated signal, while the latter amplifies it, increasing also the sensitivity of the model to external fluctuations (Neves & Iyengar, 2002). This means that even subtle

variations in the stimulus concentration are sufficient to activate a signalling pathway. The topological characteristics of signalling networks in terms of feedback loops is principally analysed through boolean networks (Kwon & Cho, 2008; Morris et al., 2010). Feedback loops not only enhance the robustness of a signalling network against its state perturbation, but they are the main biological tool for the transduction of extracellular stimuli. More recently, the consideration of probabilistic feedback loops to increase the expressiveness of the emergent dynamics in ASN and modulate the information control flow has been explored in Kampmann (1996). However, the enzymes participating in catalytic reactions does not always behave as ideal or probabilistic switches, instead they act as fuzzy logic elements with variable responses. In this respect, the fuzzy model suggested in Huang & Hahn (2009) computes the dynamics of the IL-6 pathway based on the state of its components, the initial inputs and a set of fuzzy rules.

Perhaps the most interesting computational property of feedback loops is its complex and parametrisable behaviour, which eases the formation of large non-linear signalling structures. Therefore, ASNs can be modelled as an organised network comprising multiple signalling pathways. This higher organisation provides an alternative signalling regulatory mechanism on top of the linear pathways and offers better channels to redirect and amplify extracellular signals across the cell. The dynamics of these representations emerge for the multiple ways in which these pathways interact, cross-regulate and collaborate. The biological inspiration of the initial ASN models dealing with inter-pathway interactions comes from the Wnt signalling pathway (Tu et al., 2007) and consider the stochastic modelling of mediator proteins to govern the information flow and quantify information exchanged in crosstalk interactions (Asthagiri & Lauffenburger, 2000). Similarly, Shea et al. (1997) considers mathematical models based on the standard Michaelis-Mentel kinetics to model crosstalk connections and modulate logic functions. More advanced qualitative ASN representations include higher-organised spatial distributions to restrict the stimulus' spreading scope within biological eukaryotic cells (Inagaki et al., 1994; Hartwell et al., 1999). In this sense, the effect of compartmentalisation in signalling transduction is analysed in Fisher et al. (1999), where each compartment is implemented as an agent-based network consisting of a set of molecules interacting internally with relative isolation regardless of the external interactions. In fact, the combination of feedback loops with predefined spacial topologies exhibits self-emergent properties and lead to stable behaviours upon fluctuating stimuli.

Despite the large diversity of quantitative models and the immense amount of information they encapsulate, the reconstruction of signalling pathways is insufficiently accurate to capture the complexity of their signalling components. Quantitative models provide a good substrate for the biochemical representation of cellular signalling, but they lack in the incorporation of the temporal and mechanical properties of signalling pathways. Additional abstractions of quantitative models also include Petri Nets (Sackmann et al., 2006) and Markov chains (Said et al., 2003).

3.2.2 Qualitative Models

Qualitative approaches describe ASNs as protein-protein interaction networks, where nodes are molecules and edges are undirected reactions (Bray, 1995). Such models constitute graph-based approaches aiming to capture the spatial and temporal properties of signalling pathways. It is common to classify qualitative ASN models as being either discrete-time or continuous-time approaches.

Discrete ASN models focus on the importance of the network's topology upon the model dynamics. An exponent of this category is the architecture described in Klamt et al. (2006). The authors introduce a multi-layered network in order to address the existence of different sub-processing areas within signalling pathways. Although the model also implements crosstalk mechanisms, the connectivity of the approach is constrained to a set of predefined interactions which do not suffice to capture the inherent complexity of enzyme relationships. Another example of this limitation can be found in the use of Bayesian Network representations, which are intrinsically acyclic (Sachs et al., 2002; Tulupyev & Nikolenko, 2005). Extensions of discrete-time models rely on the sigmoid function to approximate the regulatory switching behaviour of non-linear biological systems (Gazi & Ghassemlooy, 2004), directed graphs to capture the directionality of enzymatic reactions (Sachs et al., 2005) and network motif representations to define concrete functionalities of signalling pathways (Milo et al., 2002)

Although discrete models are able to produce an accurate spatial description of the signal transduction process, they are unable to incorporate the temporal dynamics in enzyme reactions. Continuous ASN approaches counteract this problem by describing how the network behaviour changes over the course of time with regard to fluctuations in enzyme concentrations. Most of the continuous ASN models require the numerical integration of a set of

interconnected differential equations. In this sense, each variable denotes an enzymatic concentration, which in turn, is the diffusive kinase generated during the signalling period. Since enzyme and signalling pathways are intrinsically dynamical phenomena, numerical simulations provide an ideal platform for the verification of whether a conceptual model of a signalling pathway can replicate biological signalling processes and therefore, the implicit analysis of which elements need to be modified to meet biological plausibility. Crosstalk between signalling pathways in continuous ASN models has been explored in the context of how a signalling pathway regulates the activity of a component of another pathway (Heinrich et al., 2002) and how two different pathways have a common component for the exchanging information (Somsen et al., 2002). Despite their capacity to accurately model signalling networks, continuous ASN models still require a precise description of biological processes and the computational complexity of the models exponentially increase in relation to the number of components. The modelling of phosphorylated protein kinase cascades is the most common example of continuous qualitative ASN models (Arkin & Ross, 1994; Heinrich et al., 2002).

The work presented in this thesis considers the usage of evolutionary algorithms (EAs) as an alternative methodology to design ASNs. EAs can induce complex behaviours in a concise and evolvable way (Lones et al., 2010) and similarly, some specific functionalities are achievable only through evolutionary proceses (Decraene et al., 2007). Evolved ASNs have been successfully used to compute simple forms of biological signal processing (Bray & Lay, 1994; Deckard & Sauro, 2004). In contrast to these approaches, this work takes advantage of EAs to model ASNs in a manner where *a priori* knowledge of either the participating elements or their interactions is not necessary. By doing this, connectivity-based constraints are avoided which encourages the creation of a topology resulting uniquely from the interaction of the ASN model with its environment. This process, known as *self-organisation*, is a spontaneous phenomenon resulting from the coordination arisen out of the local interactions between enzymes. It not only resembles the evolutionary transformations experimented by cellular signalling systems themselves to incorporate the complex processing capabilities that living cells have to maintain with their environment, but also overcomes the limitations found in enzyme connectivity and the existing proximity between biological structures and computation models.

3.3 Biological Evolution

In 1859 Charles Darwin presented his *theory of evolution* by means of natural selection (Darwin & Bynum, 1859). The idea that biological populations are completely formed by a selection process governed by random variations caused an explosion of controversy. When members of a population of living organisms die, they are replaced by the progeny of parents, which are better adapted to survive within the environment where the natural selection takes place. This selection process contributes to the preservation of the genetic inheritances that fit better with the functional roles they perform, but it also introduces small variations which increments their adaptability.

Evolution is a process that leads to changes in the distinctive characteristics of a population of organisms over successive generations. There are three main elements in an evolutionary system: the entity being evolved, its representation and the mechanism of variations (Lones, 2004). In the case of a pack of living organisms, the entity being evolved is the organism's genotype, its representation is its phenotype and the mechanisms of variation are the meiosis and genomic mutations. These three elements define the structure and behaviour of biological organisms.

Associated with the process of evolution is the term *Evolvability*, a measure to determine capacity of an evolutionary system to evolve into a diversity of adaptive solutions. This means that two individuals with an identical phenotype and fitness may differ in their evolvability within the same environment. A similar definition of evolvability is also provided in Conrad (1990). For a biological organism to adaptively evolve, the selection process provides individuals with the capacity to express new variants, which also need to be suited to their environment. Although beneficial variations are rare, without them adaptation cannot occur. Analogously, the evolvability of evolutionary systems is a function of the evolvability of the mechanisms of variation and the evolvability of the entity's representation (Lones, 2004).

3.3.1 Evolutionary Computation

Evolutionary computation (EC) is a stochastic approach consisting of search, optimisation and design algorithms based on the Darwinian principles of evolution by natural selection. The subset of evolutionary computation that exclusively considers mechanisms inspired by biological evolution is known as evolutionary algorithms (EAs). They are a population-based

metaheuristic approach that uses iterative progress to achieve a desired end.

The manner in which an evolutionary algorithm proceeds is significantly standardised (see Procedure 3.1). The algorithm starts with the generation of a certain number of individuals. Each individual represents a potential solution to some problem. The set of all individuals is known as the *population* and it is the data structure which holds the evolving entities. Typically, these individuals are randomly initialised and constitute the initial population (step 1). Then, the entire population is evaluated using some fitness function which is a measure to determine the quality of an individual and its capacity to solve a problem. The fitness function scores each potential solution with a fitness value. Following evaluation, there are numerous iterative stages until the population contains an optimal solution, or until it converges to a sub-optimal solution. The objective of these stages is the optimisation of the candidate solutions and therefore, the increment of the fitness of the population. The first stage is a selection process in which some of the best candidates (parents) are chosen to seed the next generation (step 3). After this, a mating process endorses the incomplete population with the new candidate solutions (children) which are derived from the selected individuals (step 4). Finally, the new population is again evaluated to determine whether a candidate with sufficient quality is found (step 6). This candidate represents the solution of the problem.

Procedure 3.1 Evolutionary algorithm (EC)

1: Generation and initialisation of the initial population
2: **repeat**
3: Selection of a number of candidate solutions as parents based on quality
4: Generation of the new candidate solutions in a mating process
5: Promote a number of unaltered parents to the new population (Optional)
6: Evaluate each candidate solution to calculate its fitness
7: **until** number of generation required **OR** optimal solution found

In contrast to the previous procedure which defines the general outline of an evolutionary algorithm, there exist different variations of evolutionary computing with respect to the representation used to characterise candidate solutions, and the recombination mechanisms involved in the generation of new solutions from the existing solutions. Likewise, the number of individuals in the population, the manner by which individuals are selected and the number of individuals replaced during the breeding process are differentiating elements in individual algorithms. Examples of these variations include generic algorithms (Holland, 1975), evolution strategies (Rosemberg, 1967), evolutionary programming (Fogel et al., 1966) and genetic programming (Koza, 1992) amongst others. The work in this thesis is concerned mainly with

genetic algorithms and, particularly, with the use of a multi-chromosomal representation to encode each candidate solution.

3.3.2 Genetic Algorithms

A genetic algorithm (GA) is an evolutionary algorithm that mimics the processes of natural selection and sexual reproduction of evolution in nature. GA candidates are typically described by a linear string over a certain type of alphabet. Although these strings are traditionally represented using a binary alphabet, higher-cardinality alphabets can also be considered. Each GA candidate is commonly referred to as a *chromosome* and historically has a fixed length. Each position within the chromosome is known as a *gene* and its value as an *allele*. New solutions derive from existing solutions by applying the crossover and mutation operators, whose effects resemble the mating process of biological chromosomes. While mutation only modifies the allele of a particular gene, crossover recombines the genetic material from two existing chromosomes.

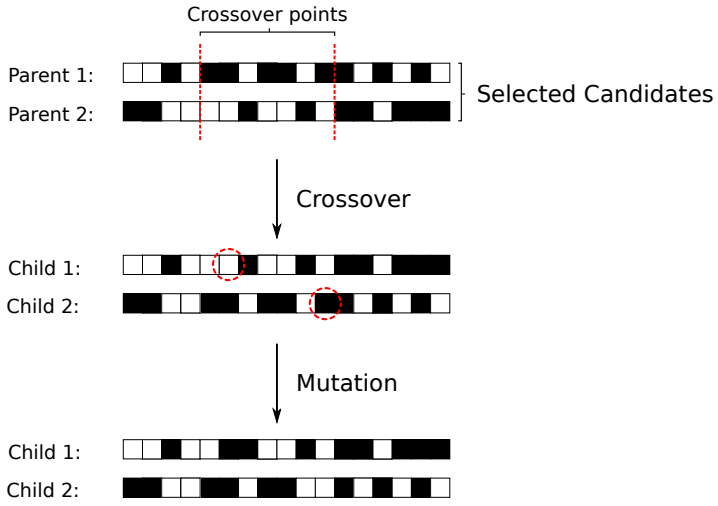

Figure 3.4: Mating process in genetic algorithms. New solutions derive from existing solutions by applying the crossover and mutation operators. Crossover (2-point crossover) is implemented over the selected parents and leads to the exchange of genetic information at the crossover points. Mutation is applied over the generated children by altering an allele in the chromosome of each child. In this example, the mutation operator inverts a white box to a black box (child 1) and a back box to a white box (child 2).

.

From an evolvability perspective, crossover is the dominant operator as it has the ability to combine strings containing partial solutions in order to generate more promising candidate solutions, which advances the search for optimal solutions. The process of crossover is as

follows: the two string candidate solutions are lined up and single or multiple crossover point(s) are randomly selected along the chromosome length. Finally, the portion of the two chromosomes between two consecutive crossover points are exchanged. This produce two offsprings: one containing the symbols of the first string and those swapped up to the crossover points, and the other containing the complementary swap. Mutation is a local search operator that prevents the generation of a uniform population unable to improve the quality of new candidate solutions. For example, if genes are encoded using a binary alphabet, the mutation operator inverts a 0 to a 1, or complementary, a 1 to a 0. A mutation is considered neutral if the gene's modification does not have any effect in the phenotype (Galván-López et al., 2011). This usually derives into the existence of plateaus in the fitness landscape, regions in the search space which fitness remains constant. Neutrality during the evolution process does not necessarily means that the population is stuck in a local minima[3]. Instead, this lack of improvements denotes either transient periods where the population navigates amongst neutral landscapes before reaching higher-fit areas (Barnett, 2001; Katada et al., 2004) or equilibrium periods where the population shows similar behaviours (Katada et al., 2004). An illustration of the breeding process in genetic algorithms is depicted in Figure 3.4. Most GAs are considered to be *generational*, which implies the replacing of either the entire population or the majority of the population at each iteration.

3.3.3 Multi-Chromosomal Representation

A multi-chromosomal representation is an evolutionary strategy that allows the overcoming of the problem of growing complexity in genotype landscapes by means of partitioning the search space (Mayer & Spitzlinger, 2003). The use of multiple chromosomes is biologically motived by the *Meiosis* process in natural evolution, in which the formation of new offspring requires the collaboration of all parental chromosomes. In addition to the genetic crossover, meiosis exhibits an additional mechanism of exchanging genetic information at the chromosome domain.

Chromosome exchanging between two candidate solutions selected as parents entails the addition of an extra genetic operator called *chromosome shuffling*. It determines the probability at which each parental chromosome pair is exchanged. Chromosome shuffling is as follows: the chromosomes of the two candidate solutions are aligned in phase and then, homologous

[3] From an evolutionary perspective, a local minima are the smallest values that the fitness landscape take at a point within a given neighbourhood.

chromosomes are swapped. An example of the recombination process in multi-chromosomal candidate solutions is illustrated in Figure 3.5. The usage of a genotype representation based

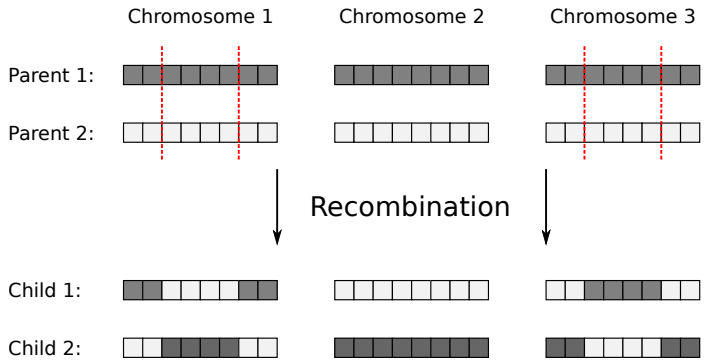

Figure 3.5: Recombination of two candidate solutions with three chromosomes. The first chromosome is recombined using only the crossover operation (2-point crossover), the second chromosome is recombined using uniquely the chromosome shuffling operator and the recombination process of the third chromosome combines the crossover (2-point crossover) and the chromosome shuffling operators. Chromosome shuffling differs from standard 2-points crossover when only one of the two children is considered as part of the next generation. The effect of chromosome shuffling becomes noticeable when uniquely one of the children is considered to be part of the next generation. Adapted from Figure 1 in Mayer & Spitzlinger (2003).

.

on multiple chromosomes presents three prominent advantages. First, it allows the decomposition of complex problems into simpler sub-problems, each encoded in a single chromosome. In consequence, the inputs and outputs of such complex problems can also be redistributed amongst the different chromosomes, easing its solvability (Pierrot & Hinterding, 1997) and increasing its evolvability (Cavill et al., 2005). Second, each chromosome can be independently encoded using a representation adapted to the sub-problem, which is beneficial to evolve complex structures. Third, it enhances the evolvability of evolutionary systems and induces the formation of more robust candidate solutions. This is because entire chromosomes of quality candidates can be transferred to the new candidate solutions increasing their chances of survival.

In an attempt to develop larger interconnected cellular signalling networks, multiple recombined chromosomes offer a natural possibility to encode the interaction between multiple pathways. Each individual pathways and its crosstalk connections are encoded in the same chromosome and therefore, the effect of the numerous inputs is restricted to the nodes and outputs encoded in the chromosomes. Although this reduces the interconnectivity between the sub-problems represented in each chromosome, it also originates a form of comparmentalisation which imitates the regulatory mechanisms found in cellular signalling. The amount

of crosstalk connections in a signalling network provides a measure of the frequency of participation of each signalling pathway in the formation of the problem's outputs.

3.4 Computational Models of Biological Signalling Networks

One of the main objectives of this thesis is to highlight the computational properties of signalling networks, particularly when used within the context of evolutionary algorithms. In this respect, this work exposes how representative models of signalling networks can be applied to a range of idealised computational tasks (see Chapter 4) and real world complex problems (see Chapter 6). This section presents the two ASN models considered in the scope of this thesis.

3.4.1 Stand-Alone Artificial Signalling Network (ASN)

Intracellular signalling in cells results from the enzymatic dynamics inside signalling pathways. Although there exists a high variability in the number of participants, their dynamics are essential in the generation of adequate cellular responses. In addition, enzymes only become functional when they are assembled together within a biochemical structure, wherein they can be catalysed in a specific manner. For this reason, the models exposed in this thesis are represented as directed interaction graphs. This eases the capturing of the intrinsic topological and temporal relationships of intracellular signalling pathways. An ASN consists of an indexed set of enzyme-based nodes and set of directed connections representing the participants in a biochemical reaction and the type of reaction: enhancing or inhibitory. Each reaction relates the substrates of a set of indexed enzymes in order to calculate the continuous-valued product concentration. Taking as reference the Artificial Metabolic Network (AMN) proposed in Lones et al. (2010), the proposed stand-alone ASN considers a layered internal representation to deal with the spatial representation of a signalling pathway. Therefore, it is possible to distinguish between receptor and regulatory enzymes. While the former are the inputs nodes of the ASN and can only catalise biochemical reactions, the latter represents the inner and outputs nodes of the ASN and can act either as substrates or products within enzymatic reactions. An abstract representation of a stand-alone ASN is illustrated in Figure 3.6.

Formally: ASN $= \langle C, E, R, I_E, O_E, t_S \rangle$, where:

C is the set of chemical concentrations $\{c_0, c_1, \ldots, c_{n_C} : \mathbb{R}\}$.

E is the set of enzymes $\{e_0, e_1, \ldots, e_{c_E} : e_i = \langle S_i, P_i, m_i \rangle\}$, where:

S_i is the set of chemicals used by the enzyme as *substrates*.

P_i is the set of chemicals used by the enzyme as *products*.

$m_i : \mathbb{R}^n \to \mathbb{R}^n$ is the enzyme's substrate-product mapping function.

R is the set of reaction rates $\{r_0, r_1, \ldots, r_{n_E} :\in \{+, -\}\}$.

$I_E \in E$ is the set of enzymes used as external inputs.

$O_E \in E$ is the set of enzymes used as external outputs.

t_S is the number of time steps per execution.

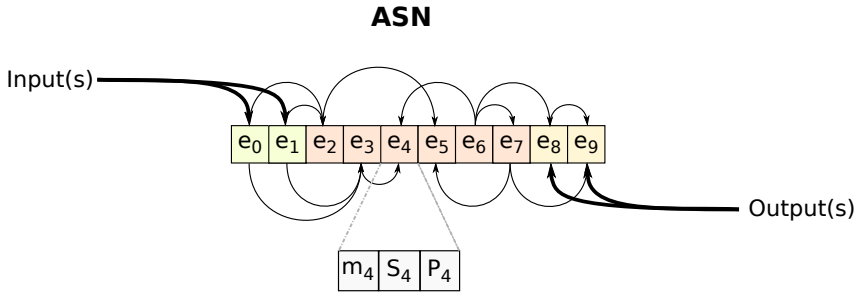

Figure 3.6: Stand-alone artificial signalling network, where $I_E = \{e_0, e_1\}$ and $O_E = \{e_8, e_9\}$. Black thin arrows represent the catalytic reactions between enzymes.

.

The execution of the stand-alone ASN starts with the random initialisation of its enzymatic concentrations (S_i and P_i) and its reaction rates R_i, if not previously executed. The concentrations of the external inputs are explicitly delivered to the network by setting the substrate concentrations of the nominated enzymes in I_E. At each time step, each enzyme e_i applies its mapping function m_i to the current concentration of its substrate S_i to determine the current concentration of its product P_i according with its reaction rate r_i. This new concentration is the mean output of all different contributing enzymes:

$$p_i = \sum_{e_j \in E_{c_i}} \frac{m(E_{c_i^{e_j}})}{|E_{c_i}|} \tag{3.1}$$

where E_{c_i} is the set of enzymes for which $c_i^{e_j}$ is the output value of $e_j \in E$ for c_i. After iterating the network a specific number of times t_S, the outputs are extracted from the final

product concentrations of the enzymes whose indices are in O_E. The execution of a stand-alone ASN is summarised in Algorithm 3.2.

Algorithm 3.2 Execution of a stand-alone ASN

```
if first execution then
  initialise e_i ∈ E
end if
Set I_E concentrations from external inputs
for i = 0 to time steps do
  for j = 0 to network size do
    S_j = mean(e_j ∈ E)
    P_j = m_j(S_j)
  end for
end for
External outputs = P(e ∈ O_E)
```

3.4.2 Coupled Artificial Signalling Network (CASN)

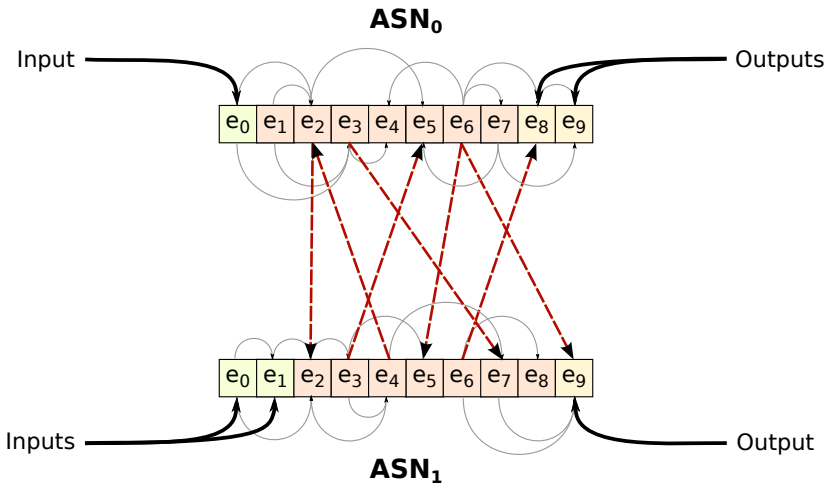

Figure 3.7: Coupled artificial signalling network consisting of two different ASNs, where $I_E = \{e_0\} \in \text{ASN}_0$ and $I_E = \{e_0, e_1\} \in \text{ASN}_1$ are its inputs, and $O_E = \{e_8, e_9\} \in \text{ASN}_0$ and $O_E = \{e_9\} \in \text{ASN}_1$ its outputs. The gray arrows represent catalytic reactions between enzymes and the red dotted arrows connecting neighbouring ASNs denote crosstalk connections.

The previously described ASN model is a representation of a single signalling pathway and its dynamics. In biological cells, responses are often the result of the collaboration between multiple pathways. Crosstalk connections are the biological mechanisms capturing the interaction between signalling that leads to the formation of complex signalling networks. Based on this principle, this work introduces the concept of coupled artificial signalling net-

works (CASN) to model these interactions. In this model, each ASN represents a signalling pathway and crosstalk interactions are graphically represented as directed edges connecting two neighboring ASNs. This simulates the exiting two-level spatial signalling organisation inside living cells. Typically, large signalling regions are a collection of individual signalling pathways plus their underlying molecular interactions which interconnect such pathways. An abstract representation of a CASN is illustrated in Figure 3.7.

Formally: CASN $= \langle ASN, C_P \rangle$, where $C_P \in [0, 1]$ is the enzyme's probability of crosstalk. Therefore, each enzyme have a maximum of one outputting crosstalk connection but may also be involved in multiple crosstalk reactions. Although crosstalk at a receptor level can be also found during the intracellular signalling process, the proposed model restricts crosstalk interactions to regulatory enzymes. Crosstalk is represented as a catalytic reaction in which the enzymes involved have their product concentrations asymptotically reduced to half of their maximum value. This limitation attempts to imitate the low production rates associated with the high-energy consumption in crosstalk reactions. Similarly, CASN also accounts for

Algorithm 3.3 Execution of a CASN

```
if first execution then
  Initialize ASN → e ∈ E
  for each e_i ∈ coupled-ASN do
    Add crosstalk connection based on C_P probability
  end for
end if
Set I_E concentrations from external inputs
for i = 0 to |ASN| do
  for j = 0 to time steps do
    for k = 0 to network size do
      S_k = mean(e_ik ∈ r_k)
      P_k = m_k(S_k)
    end for
  end for
end for
External outputs = mean(O_E)
```

signalling transduction models with multiple-bound enzymes. In particular, this work takes a closer look at the effect of having two types of enzymes depending on the number of times they are phosphorylated: single or double. This more accurately represents the different phosphorylation levels in cascades of protein kinase. For more detail, see Chapter 2. The execution of a CASN is summarised in Algorithm 3.3.

3.4.3 Enzyme Mappings

Four types of parametrisable mapping functions are selected to model enzyme interactions (see Table 3.1). They are the most common representations of the catalytic reactions within biological systems (see Chapter 2). The mapping functions are described as follows:

- *The Michaelis Menten equation* characterises enzyme kinematic reactions. It is a hyperbolic function, where $\nu \in [0, 1]$ is the asymptotic threshold and $k \in [0, 1]$ determines its gradient.

- *The Hill equation* quantifies the substrate-enzyme cooperativity. It is a quasi-sigmoidal function in which $\nu \in [0, 1]$ is its asymptotic threshold, $k \in [0, 1]$ establishes its gradient and $h \in [1, 10]$ is the Hill coefficient. Note there is always cooperativity between enzymes. In addition, this equation is complemented by adding the binding probability $\beta \in [0, 1]$ to stimulate the reaction speed at high substrate concentrations.

- *The first-order kinetics equation* describes the enzymatic rate of phosphorylation, where $\nu \in [0, 1]$ is its asymptotic threshold.

- *The Multi-Dimensional Michaelis-Menten equation* describes multi-substrate reactions based on a binding $\beta \in [0, 1]$, where $\nu \in [0, 1]$ is the asymptotic threshold and $k \in [0, 1]$ determines its gradient and $m, n \in [1, 10]$ are the Hill coefficients.

For multiple inputs $c = \sum_{j=0}^{n}(i_i w_i)/n$, where $i_0, i_1, \ldots, i_n$ and $w_0, w_1, \ldots, w_n \in [-1, 1]$ are corresponding input weights. Negative values indicate inhibition, with the concentration determined by $m^{-}(c) = 1 - m(c)$.

Table 3.1: Mapping functions representing the interactions among enzymes in the ASN and CASN

Hill equation: $m(x) = vx^h(k^h x^h)^{-1}$
Michaelis-Menten equation: $m(x) = vx(k - x)^{-1}$
Multi-Dimension Michaelis Menten equation: $m(x) = \sum_{i=0}^{k} \beta_i (x_i/k_i)^{n_i}(1 + \sum_{i=0}^{n}(x_i/k_i)^{m_i})^{-1}$
First-order kinematic equation: $m(x) = vx^2(1 + x + x^2)^{-1}$

3.4.4 Evolutionary Algorithm

Both ASN models are evolved using a standard evolutionary algorithm with elitism (rate = 0.2) and tournament selection (size = 4). Child solutions are generated via uniform crossover (rate = 0.3), point mutation (rate = 0.015/element) and chromosome shuffling (rate = 0.1). A multi-chromosomal representation is used to evolve CASN. The evolution process for both ASNs models starts with the generation of a random initial population.

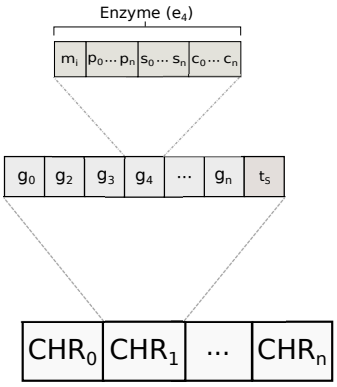

Figure 3.8: Encoding of the CASNs used by the evolutionary algorithm.

.

Each CASN is linearly encoded as an indexed array of chromosomes. Each chromosome represents an individual ASN as an indexed array of genes (see Figure 3.8). Crosstalk interactions are encoded locally in the ASN and its crosstalk rate remains constant during the entire evolution process. In an attempt to reduce the complexity of the network and avoid unexpected solution size pathologies, the number of enzymes of each individual ASN is fixed. Based on the initial experimentation, a pathway length of 10 enzymes is sufficient to express valid solutions. Changing the size of the network has essentially no effect on their performance. The timing variable t_S is inside the interval $[0, 100]$. Again, the upper limit is more than sufficient to express valid solutions. There is no evolutionary pressure toward time-efficient solutions.

For both representations, input and output enzymes are determined according to their relative index (i.e. low- and high-numbered genes). Chemical values, mapping values and connection weights are represented using a floating-point notation and mutated using a Gaussian function with its centre at the current value. Crossover points lie between the enzymes' boundaries. Mutation is restricted to one of the following operations in order to meet biolog-

ical plausibility in graph-based representations (Ziegler & Banzhaf, 2001):

- Increasing or decreasing chemical concentrations (S_i and P_i).
- Changing mapping function parameters.
- Changing reaction rates by modifying connection weights.
- Adding or removing a reaction's reactants.
- Changing the execution time.

The usage of continuous values to represent enzymatic concentrations shows two prominent benefits. First, they ease the coupling with external environments, such that inputs and outputs do not require a binary encoding. Second, continuous values provide an infinite state space (within the limits of representation), which can lead to more complexity in both the network's dynamics and its expression capacity. This contrasts with the limited space observed in alternative representations of biochemical networks. In Boolean Networks, for instance, the set of possible states is constrained to 2^N, where N is the number of nodes. Table 3.2 summarises the parameters used to represent the proposed ASN architectures.

Table 3.2: Parameters of the proposed stand-alone and coupled ASN architectures.

Variable	Type	Range
Substrate S_i	Double	[0 – 1]
Product P_i	Double	[0 – 1]
Input Weights	Double	[-1 – 1]
Crosstalk Rate	Double	[0 – 1]
Num. Iterations	Integer	[0 – 100]
Enzymes per ASN	–	10
Mich-Men. ν	Double	[0 - 1]
Mich-Men. k	Double	[0 - 1]
Hill ν	Double	[0 - 1]
Hill k	Double	[0 - 1]
Hill h	Integer	[1 - 10]
Phospo. ν	Double	[0 - 1]
P. Mich-Men. β	Double	[0 - 1]
P. Mich-Men. ν	Double	[0 - 1]
P. Mich-Men. k	Double	[0 - 1]
P. Mich-Men. m	Integer	[0 - 10]
P. Mich-Men. n	Integer	[0 - 10]
Crossover rate	–	0.3
Mutation rate	–	0.015
Chro. Shuffling	–	0.1
Elitism rate	–	0.2
Tournament size	–	4

3.5 Summary

This chapter has presented two computational models of signalling networks, whose main aim is to capture the interacting relationships amongst the participating elements in the intracellular signalling process. The first of these models is called a stand-alone artificial signalling network and it is an abstraction of a signalling pathway, the simplest communication units within cells. The proposed approach is represented using a directed graph, as it eases the structural and function analysis of signalling networks. Each node defines an enzyme and each directed arc codifies a catalytic biochemical reaction. Likewise, each enzyme is described by a substrate concentration, a product concentration, a mapping function and a set of inhibitory or enhancing catalytic reactions. During the execution of the network, the mapping function relates the substrate concentration of all participating enzymes with the product concentration based on the type of the catalytic reactions. External signal inputs are directly delivered to the substate concentrations of the low-numbered enzymes in the ASN, while the outputs are extracted from the product concentration of high-numbered enzymes in the ASN. The number of inputs and outputs in the ASN is configurable depending on the application problem.

The second model, called a coupled artificial signalling network, is biologically motivated by the interaction between multiple pathways. These interactions produce a higher cellular organisation enabling cells to response simultaneously to multiple external stimuli. In addition, the cooperation amongst pathways brings about more robust and specialised responses. Signalling pathways biologically interact with each other by means of crosstalk reactions, which force the exchanging of signalling material. In this work, the level of crosstalk of an ASN is modelled as the number of enzymes involved in crosstalk catalytic reactions. Crosstalk connections are randomly established at the beginning of the execution of the network. Likewise, crosstalk is limited to the non-receptor enzymes of neighbouring ASNs. The number of crosstalked ASNs and also the level of crosstalk can be modulated according to the problem.

One of the main disadvantages of the current computational approaches to modelling signalling networks are their high dependence on the amount of existing information about the signalling aspect to be modelled. This gives rise to either computationally complex or considerably constrains signalling models. In order to overcome these difficulties, this chapter has considered the used of evolutionary algorithms to obtain signalling representations whose form do not rely on the amount of *a priori* knowledge, but solely results from the direct

interaction of the model with its environment. A multi-chromosomal representation is used to encode CASNs. In an attempt to develop larger signalling networks, multiple recombined chromosomes offer a natural possibility to encode separate cellular regions.

With this in mind, the next chapter explores the capacity of the proposed ASN models to exhibit complex dynamics and produce robust control commands to controlling the chaotic dynamics of two dynamical system: the Lorenz system and Chirikov's standard map. Although these system sit at opposite ends of the dynamical system spectrum, the variety of its dynamics are representative of the complexity found in cellular environments. Particularly, the Lorenz map is a continuous-time dissipative dynamical system, whose behaviour can be either ordered or chaotic depending on the value of its governing parameters. On the other hand, Chirikov's standard map is a discrete-time conservative dynamical system. Its space state embraces ordered and chaotic regions, which coexist together. Common to both systems that this diversity of behaviours is commanded by their governing parameters. This property is explored by CASN and stand-alone ASN to controlling chaos using the governing parameter rather than interacting directly with their trajectories. The aim is to evolve ASN-based controllers able to carry out chaos targeting in the system's state space via control of its governing parameters.

Chapter 4

Controlling Dynamical Systems using Artificial Signalling Networks

Contents

Artificial Signalling Networks (ASNs) are computational models inspired by the function and structure of cellular signalling pathways. The principal role of such pathways is to guarantee the correct interaction amongst cells and their external environment. Thus, signalling pathways have to sense, process and decode biological stimuli in a determined manner so cells can produce appropriate reactive responses to extracellular events. This chapter aims to explore whether this feature – a key property of signalling networks– can be used to carry out chaos control using both stand-alone ASNs and coupled ASNs (CASNs) in two behaviorally different dynamical systems: the Lorenz system and Chirikov's standard map. Although they lie at opposite ends of the dynamical system spectrum, their dynamics are representative of the complexity found in cellular environments. The main goal of this chapter is to

demonstrate that the properties allowing signalling networks to interact with cells' surrounding can be computationally inferred through an evolutionary process and, consequently used to achieve chaos targeting. In order to do so, both ASN-based models alter the dynamical system's status via the modulation of the system's governing parameter. Additionally, this chapter also aims to evaluate the importance of crosstalk as a signalling tool to produce concrete control directives and sophisticated controllers mirroring the spatial distributions of cellular signalling networks. Different crosstalk rates are considered in order to explore how the information exchanged amongst signalling networks affects the control solution. With this in mind, this chapter firstly introduces the concept of a dynamical system, describes the problem of chaos control and presents an overview of the principal approaches to address it. The second section introduces Chirikov's standard map, discusses the control strategy and presents the results. Likewise, the third section presents the Lorenz system, justifies the control strategy and analyses the results. Finally, a discussion about the relevance of the results concludes the chapter.

4.1 Dynamical Systems

4.1.1 Definition

A dynamical system is any mathematical representation consisting of an abstract state space and an evolutionary function defining both the system's current state and its evolution in time through the space state (Stepney, 2012). Dynamical systems can be initially classified as *autonomous*, *non-autonomous* or *constructive*. In autonomous systems, dynamics are not perturbed by the outside work. In non-autonomous systems, dynamics are altered by the inputs received from an external environment. In constructive systems, the system's structure changes during computation time. Likewise, dynamical systems can also be *discrete*, *continuous* or *hybrid*, depending on whether the evolution function is a difference equation, a differential equation or a combination of both respectively.

In particular, a dynamical system is defined by its state space, a state vector indicating the system's state at any given time, and an evolutionary function that establishes how the state vector changes over time. If this function produces a unique evolutionary direction, then it is termed *deterministic*. Otherwise, it is termed *stochastic* and generates a state vector with a

finite number of consequents [1]. Given a set of initial conditions, a dynamical system follows a sequence of states, which constitutes its *trajectory*. Trajectories are generally outlined by initial nonlinear exploratory periods known as *transients*, after which trajectories may converge to a subregion in the state space called an *attractor*. The set of trajectories evolving towards the same attractor represents the *basin of attraction*. A dynamical system in which all its trajectories contract to concrete subregions of the state space is termed *dissipative*. Those showing divergent trajectories are *conservative*. Dynamical systems display four different types of attractors:

- *Point attractor*, trajectories converge to a single point in the system's state space, as in the damped harmonically driven pendulum (see Figure 4.1(a)).

- *Limit cycle attractor*, trajectories describe closed orbits around the attractor in the system's state space, as in the Van der Pol oscillator (see Figure 4.1(b)).

- *Torodial attractor*, trajectories attain to a surface in the system's state space with a toroidal structure, as in the Li system (see Figure 4.1(c)).

- *Strange attractor*, trajectories within the basin of the attractor converge to non-linear regions in the system's state space whist nearby trajectories diverge exponentially, as in the Rössler system (see Figure 4.1(d)).

Dynamical systems also show ordered and chaotic behaviours within their state space. Unlike ordered behaviours in which trajectories are predictable, chaotic behaviours are denoted by aperiodic and unpredictable trajectories. Despite their deterministic nature, chaotic dynamical systems are characterised by an exponential sensitivity to initial conditions and the existence of strange attractors in their state space (Ott, 2002). Whereas the former suggests that small changes in the initial conditions produce different trajectories which will exponentially move apart (a phenomenon popularly known as *butterfly effect*), the latter defines fractal and non-linear regions where trajectories may converge.

[1] Within this context, the term consequent refers to each possible state the evolutionary function generates: i.e the odds and evens game. In the case time is discrete and the state vector corresponds to the result of the evaluation of the number of fingers, the state space is finite and consists of two consequents, odds and evens.

4.1.2 Controlling chaos

Amongst the range of behaviours a dynamical system is able to dispense, *chaos* is perhaps the most appealing. Although pioneers in control theory perceived chaos as an inconvenience and tried to avoid it (Bollt, 1995), chaotic dynamics occur in a wide range of manufactured and biological systems. For this reason, there is a growing interest in capturing chaotic dynamics and bringing them into order. *Chaos control* refers to the process in which chaotic dynamics can be controlled using time dependent perturbations. This means that chaotic systems are forced to transit to another dynamical state amongst all their possibilities, which is generally stable and predictable. The extent of such perturbations is typically small in order to preserve the system's natural dynamics. Several methods have been postulated for chaos control, but they are generally divided into three main categories: parametric variation, time-delay feedback and intelligent approaches (Chen & Dong, 1998).

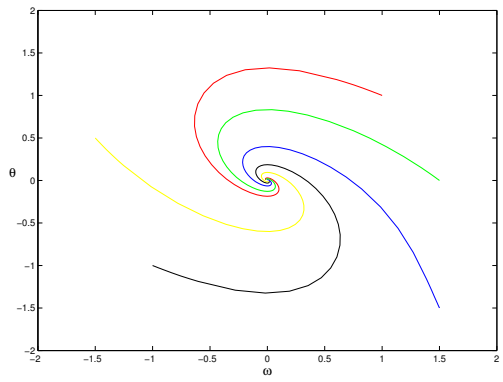

(a) Driven Pendulum

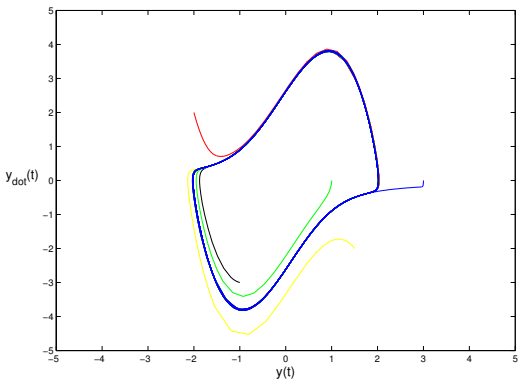

(b) Van der Pol

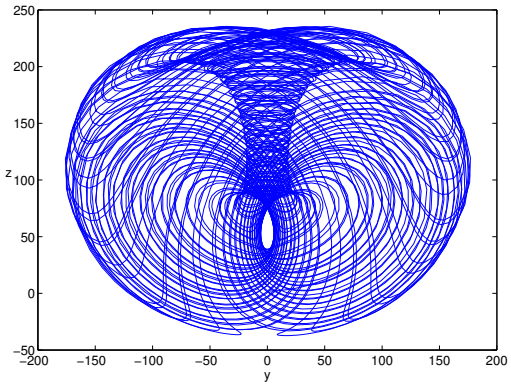

(c) Li System

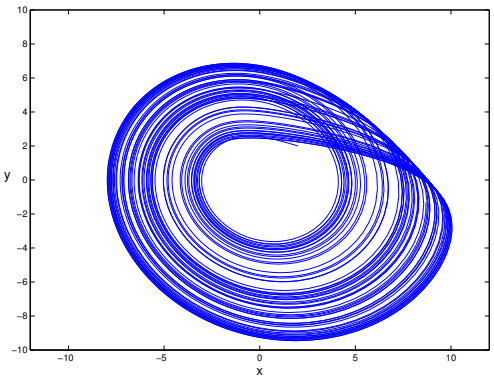

(d) Rössler system

Figure 4.1: Examples of the different types of attractors in the state space of a dynamical system: (a) point attractor in the driven pendulum, (b) limit cycle attractor in the Hopf oscillator, (c) toroidal attractor in Li System and (d) strange attractor in the Lorenz system

Parametric variation approaches attempt to reduce or extinguish chaos by altering the system's governing parameters. Of these, the Ott-Grebogi-Yorke (OGY) method (Ott et al., 1990) is the highest exponent. It applies time dependent perturbations to one of the parameters in oder to stabilise an unstable periodic orbit. The method waits until the system approaches to the surface of the unstable periodic orbit before exerting the perturbation in the stable direction of the orbit. Examples of the application of the OGY method in chaos control are the double rod pendulum (Cammack, 2003) and Chirikov's standard map (Lai et al., 1993). Variations of this method consider time-dependent coordinates to increase the effectiveness of the control (Dressler & Nitsche, 1992), multiple control points to minimize the stabilisation time (de Paula & Savi, 2011) and additional intermediate control terms to handle high-dimensional chaotic systems (Celso & Lai, 1997).

Time-delay feedback approaches look for the stabilisation of periodic orbits using control signals. This category is typified by Pyragas' method (Pyragas, 1992). Unstable orbits are stabilised via the join application of a feedback and a periodic external force, which is equal to the difference between the dynamical system's current state and a previous state. Nevertheless, its applicability is limited to continuous-time dynamical systems with a scalar variable which can be periodically monitorised. Pyragas' method does not require concrete knowledge about the system's dynamics, but it demands a mathematical analysis of the system's governing parameters. Extended versions of Pyragas' method deal with the inclusion of the system's previous states to increase the dimensionality of the parameter space (Bleich & Socolar, 1996).

Intelligent approaches group computational techniques that use artificial intelligence to control chaos. Examples of these includes adaptive fuzzy controllers (Calvo & Cartwright, 1998), multi-agent systems in distributed systems (Roozemond, 1996) and probabilistic models (Setti et al., 2003). Amongst these approaches, it is possible to distinguish a subset of techniques that does not rely on the concrete state-based standard computing and whose structure and function arises from the processes taking place in biological systems. These, called *computational dynamical systems*, are characterised by their capacity to elicit rich behaviours similar to the ones found in dynamical systems. This feature is highly appealing from a computational perspective as it favours the encapsulation of complex behaviours into modular and evolvable architectures which mirror the spatial properties of biological structures and can be used to solve computational tasks. Examples of these are recurrent neural networks (Weeks & Burgess, 1997), reaction-diffusion networks (Eungdamrong & Iyengar,

2004) and Artificial Biochemical Networks (Lones et al., 2014).

4.1.3 Chaos Targeting

An extension of chaos control is *chaos targeting*. This refers to the problem of finding the shortest path between two subregions in the dynamical system's state space. Chaos targeting takes advantage of the high sensitivity to external perturbations of chaotic systems to deliver small alterations to one of the system's governing parameters. This brings about a change on the system's dynamics and makes it possible to guide a trajectory across its state space. The solution path is the trajectory resulting from the sequence of transformations undergone by the system's state space. Examples of chaos targeting include the guiding of a trajectory to a fixed point in the double rotor map (Kostelich & Barreto, 1996) and the stabilisation of ship oscillations (Mitsubori & Aihara, 2002). In both examples, explicit knowledge about the state space of the dynamical system is required.

With this in mind, this chapter explores the capacity of stand-alone ASNs and CASNs to carry out chaos targeting when concrete knowledge of the dynamical system's state space is unknown. This is examined in two behaviorally different dynamical systems: the Lorenz system and Chirikov's standard map. The former is a continuous-time dissipative dynamical system whose dynamics can be either ordered or chaotic. The latter is a discrete-time conservative dynamical system and its space state contains ordered and chaotic regions, which coexist together. Common to both system is that variations in their governing parameters alter their dynamics. This feature is exploited to perform chaos targeting in the system's state space and to demonstrate the applicability of the proposed ASN models as a control paradigm. Despite the complexities of robotic locomotion, chaos targeting cannot be considered as a control algorithm to generate adaptive locomotive patterns of motion since the evolutionary objective in the case of the multi-legged robot is the opposite, perturbing in a non-time depend manner an stable dynamical system in order to cope with existing environmental irregularities.

There have been previous attempts to use evolutionary algorithms in chaos targeting. These were mainly focused on the optimisation of the system's parameters to achieve a faster stabilisation of periodic orbits at a fixed point. Although, this considerably reduces the computational cost of chaos targeting in the OGY method (Soong et al., 2004; Senkerik et al., 2007), explicit knowledge about the system's dynamics is often required. Unlike these

approaches, the work in this thesis considers evolutionary algorithms in a different manner. Although the objective is still finding of the shortest trajectory connecting two regions of the system's state space, the controller does not input any information about either the structure or dynamical characteristics of the system's state space. Only positional information of the trajectory with respect to its final destination is provided. This resembles the normal running of cellular signalling networks, which do not have any explicit information about their surrounding or extracellular messengers.

4.2 Chirikov's Standard Map

Chirikov's standard map (Chirikov, 1962) is a conservative and discrete-time dynamical system which iteratively models the interaction between two canonical variables within the unit square (see Equation 4.1). It describes the dynamical properties of a kicked rotor: a mass constrained into a circular orbit in which periodic kicks are enforced with a force corresponding to k. The dynamics observed in the standard map also occur in a range of other physical models, for example ionic systems, particle accelerators and gravitational systems amongst others.

$$\begin{aligned} x_{n+1} &= (x_n + y_{n+1}) \bmod 1 \\ y_{n+1} &= y_n - \frac{k}{2\pi}\sin(2\pi x_n) \end{aligned} \tag{4.1}$$

where x and y are two dynamical variables, x_{n+1} and x_{n+1} indicate the new values of x and y after one map iteration and k is a dimensionless parameter governing the degree of chaos.

One of the map's main properties is its capacity to capture different dynamics as its non-linearity changes. While low k values preserve an ordered state with trajectories converging to cyclic orbits bounded on the y-axis (see Figure 4.2a), chaos starts to emerge in the form of islands of chaotic dynamics along the y-axis as k progressively increases (see Figures 4.2(b) - (c)). The standard map shows a behavioural inflection point, k_c at $k \approx 0.972$ (see Figure 4.2d). For $k > k_c$ the initial permeability begins to disappear, meaning that chaotic islands are partially connected, which theoretically enables trajectories to vertically cross the map (see Figures 4.2(e) - (i)). As an example of this, only 32.5% of the trajectories are able to move from the bottom to the top of the map with an average length of 34200 iterations when $k = 1.0$, using 1000 randomly chosen points and an upper limit of 10^6 iterations, while 55.7%

of the trajectories reached the top of the map with an average length of 13600 iterations using similar measuring conditions and $k = 1.05$.

4.2.1 State Space Targeting

As previously mentioned, an increment in the permeability of the standard map is only achievable as $k >> k_c$. This makes it possible to follow a chaotic trajectory from $y = 0$ to $y = 1$. Following the examples in Lones et al. (2010, 2014), the objective is to find a controller able to tranverse Chirikov's standard map from a bottom area to a top area in the shortest number of steps (chaos targeting). In order to achieve this, both coupled and uncoupled ASNs are allowed to modulate the governing parameter k in the interval $[1.0, 1.1]$. This range is sufficient to ensure the presence of chaotic islands in the middle region of the standard map, but k is also sufficiently high to partially restrict the ordered regions[2] and allow trajectories to traverse vertically the map.

Table 4.1: Parameters used to carry out chaos targeting in Chirikov's map.

Variable	Type	Range
k	Double	[1.0 – 1.1]
Population	–	50
Generations	–	200

Each guided trajectory starts in a predefined region at the bottom of the map ($[0.45 - 0.0] \longrightarrow [0.55 - 0.05]$) and ends at specific region at the top ($[0.45 - 0.95] \longrightarrow [0.55 - 1.0]$). Similar regions are initially considered in Schroer & Ott (1997) and later used in Lones et al. (2014). Inputs for stand-alone ASNs and CASNs are the current position in the map (x, y) and the Euclidean distance between the current position and the top-center of the map. Both ASN representations have a single output which corresponds to the value of k. For CASNs, the output is the standard mean of all contributing ASNs. Evolved controllers are evaluated on 20 trajectories from random points within the starting region. Fitness is the mean number of steps required for these trajectories to reach the top. Trajectories unable to navigate across the standard map within an upper limit of 1000 steps are penalised with an constant fitness of 2000 steps. Both coupled and uncoupled ASN representations are evolved using a population of 200 individuals and a generation limit of 50. Initial results have shown

[2] Ordered regions in Chirikov's map capture passing trajectories and prevent them from progressing across the map.

this configuration is sufficient to obtain valid solutions (Fuente et al., 2012, 2013*b*). This evolutionary configuration has been selected to enable direct comparison to the performance of the ABNs in Lones et al. (2011, 2014) in terms of the number of the steps needed to carry out chaos targeting in Chirkiov's map. Table 4.1 summarises the parameters used to carry out chaos targeting in Chirikov's map.

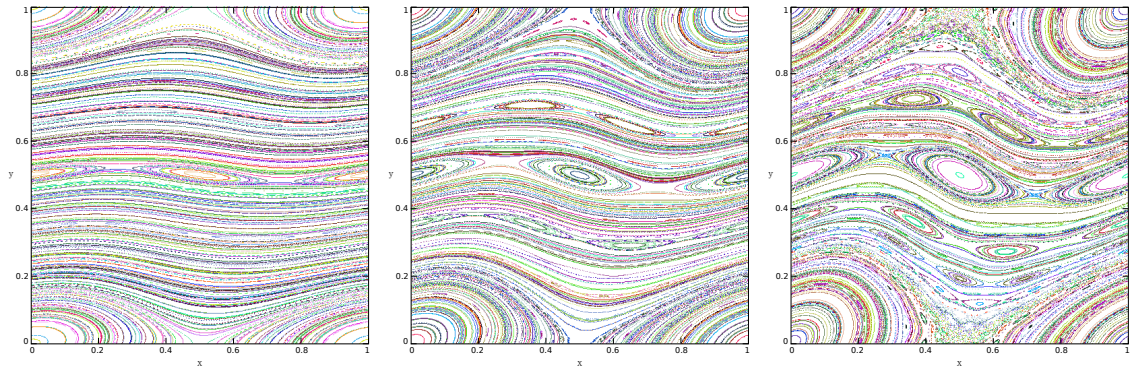

(a) $k = 0.25$ (b) $k = 0.5$ (c) $k = 0.75$

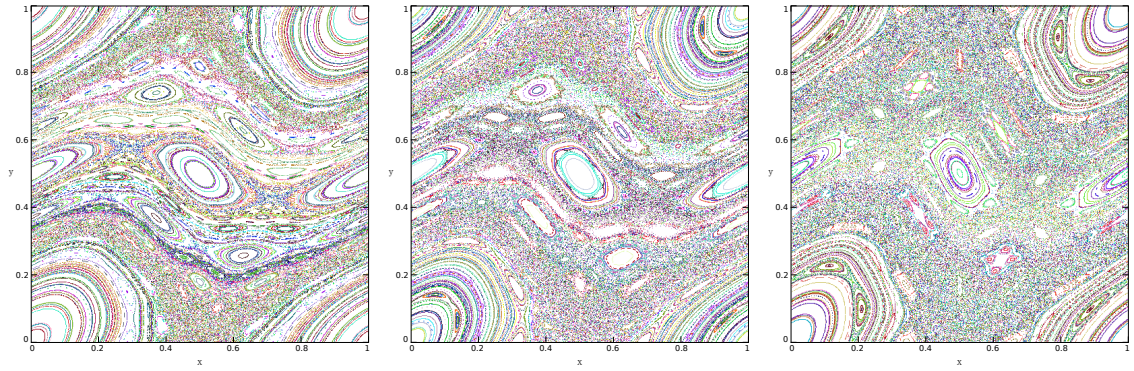

(d) $k = 0.975$ (e) $k = 1.1$ (f) $k = 1.25$

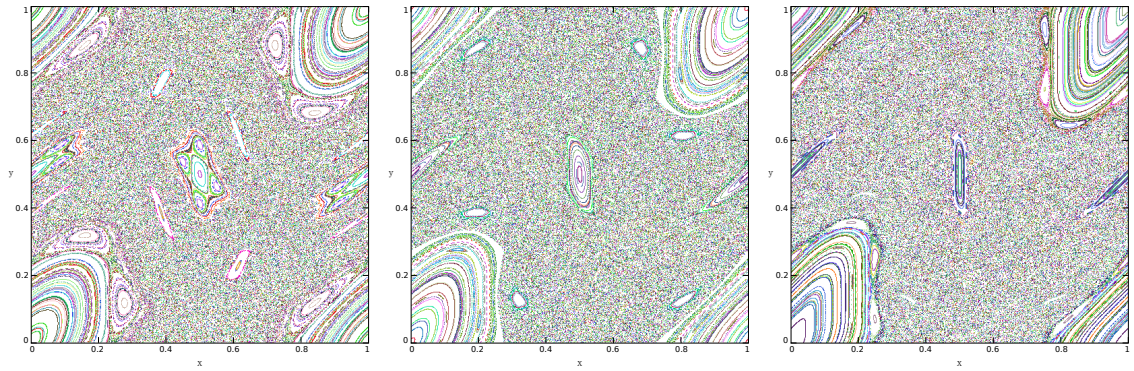

(g) $k = 1.5$ (h) $k = 1.75$ (i) $k = 2.0$

Figure 4.2: Sampled trajectories of Chirikov's standard map for several values of k, showing the transition from the ordered to the chaotic state. Each plot shows 300 random trajectories of length 500 across the unit interval.

4.2.2 Controlling Chirikov's Standard Map

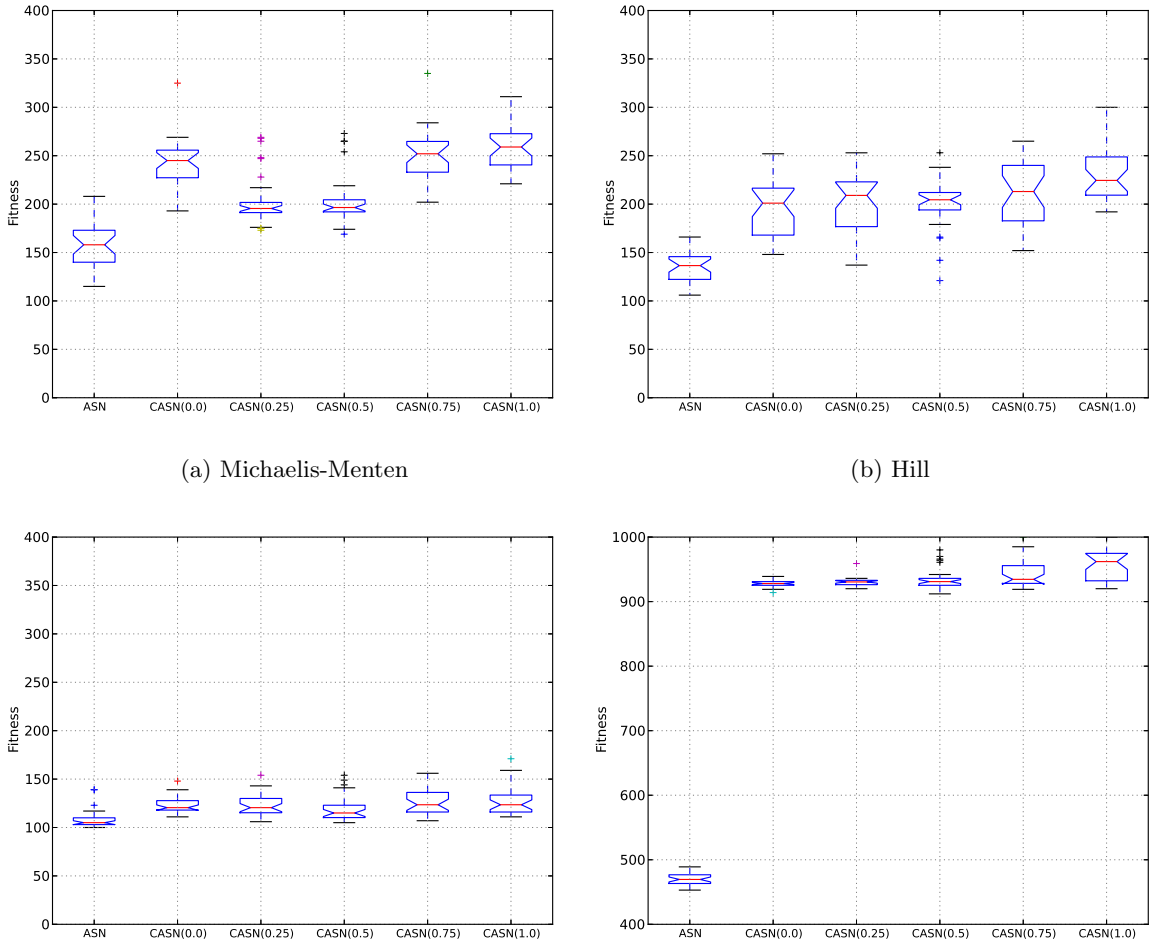

(a) Michaelis-Menten

(b) Hill

(c) Probabilistic Michaelis-Menten

(d) Phosphorylation

Figure 4.3: Fitness distributions for the stand-alone ASN and CASN, carrying out state space targeting in the Chrikov's standard map using the principal regulatory functions found in enzymatic systems: (a) Hill, (b) Michaelis-Menten, (c) Probabilistic Michaelis-Menten and (d) Phosphorylation equations. All ASN networks are of length 10. Distributions toward the bottom part of the figures are better. [3]

Figure 4.3 summarises the fitness distributions in terms of the number of steps required to successfully transverse Chirikov's standard map for the stand-alone ASN and CASN using the major regulatory functions found in enzymatic systems. Results demonstrate that both representations produced evolved controllers able to find valid solutions. These show scores ranging between 100 and 300 steps for most of the configurations with the notable exception of the phosphorylation equation. Figure 4.3 also illustrates the effect the ASN representation has upon the fitness distributions. Although stand-alone ASNs steadily lead to solutions

[3] The change in the vertical scale of Figure4.3(d) is required to ease the visualisation of the fitness distributions of CASN controllers evolved using the Phosphorylation equation.

with lower fitness on average, good solutions can still be found using CASNs. The fact that CASNs are able to guide a trajectory across the standard map is indicative of their capacity to solve problems where there is a strong dependence amongst their variables. Thus, these problems can be decomposed into several small tasks (one per sub-ASN), which are solved semi-independently. In Chirikov's standard map, the value of x_{n+1} is calculated from the value of y_{n+1}. This property becomes more evident when there are not crosstalk connections between each sub-ASN, meaning that each correlated sub-task is solved totally in isolation (see box plot denoted by CASN(0.0) in Figures 4.3(a)-(d)).

The best stand-alone ASN controllers have a median path length of $\sim$ 100 steps while the best CASN controllers require an average of $\sim$ 115 steps to transverse Chirikov's map. Example paths and their associated evolved controllers are shown in Figures 4.4 and 4.5 for the stand-alone ASN and CASN respectively. Quantitatively, these solutions bear a resemblance to the trajectories obtained in Lones et al. (2010), where the authors evolve ABN controllers which traverse the standard map in $\sim$ 110 steps when $k \in [1.0, 1.1]$, to the mapping method exposed in Schroer & Ott (1997), where derived orbits require an average of $\sim$ 125 steps when $k = 1.25$ and to the targeting paths described in Turner et al. (2012), where trajectories are able to cross the standard map in both directions in $\sim$ 250 steps when $k \in [1.0, 1.1]$.

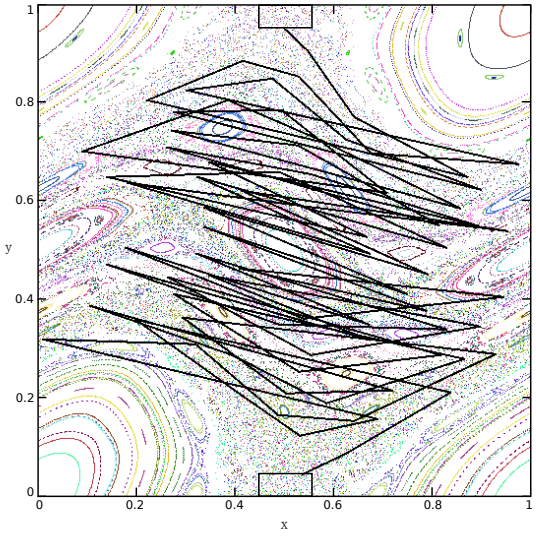

(a) State space targeting trajectory

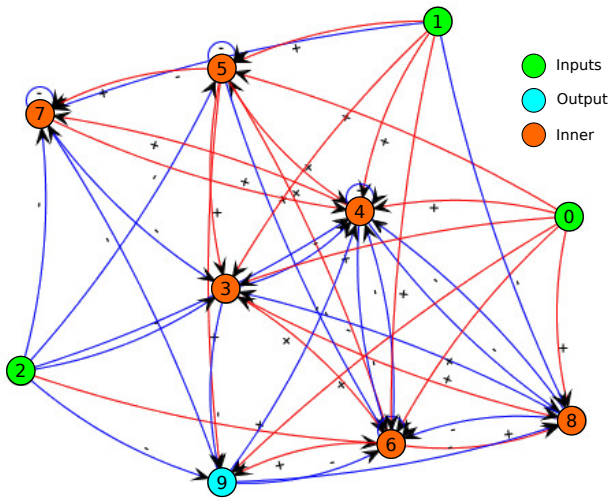

(b) Stand-alone ASN

Figure 4.4: Example solution (a) and its associated stand-alone ASN using the probabilistic Michaelis-Menten equation (b) carrying out space state targeting in Chirikov's standard map in 76 steps. The standard map is plotted with $k = 1.08$ (the last value output by the controller).

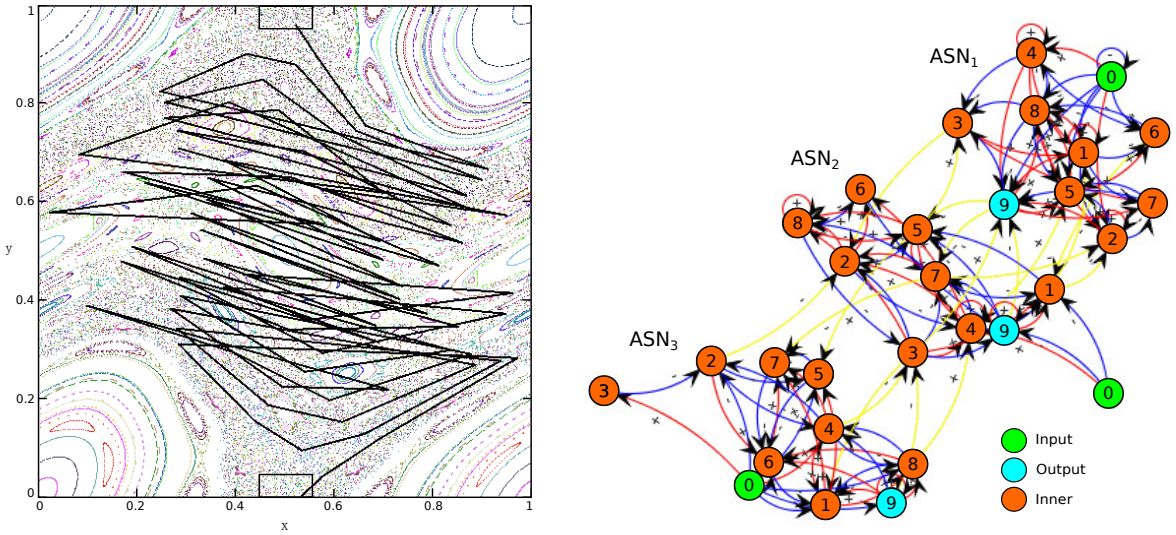

(a) State Space targeting trajectory

(b) Coupled ASN

Figure 4.5: Example solution (a) and its associated CASN using the probabilistic Michaelis-Menten equation and a crosstalk rate of 0.25 (b) carrying out state space targeting in Chirikov's standard map in 79 steps. The standard map is plotted with $k = 1.057$ (the last value output by the controller).

The choice of regulatory function also has a notable impact over the fitness distributions (see Figure 4.3). However, it is perhaps no surprise that the probabilistic Michealis-Menten and Hill equations produce controllers with better fitness for both ASN representations while the single Michaelis-Menten and the Phosphorylation equations perform poorly. From a biological perspective, this loss in performance can be explained attending to the rate of the chemical reaction being modelled. Thus, high-ordered reactions, such as the probabilistic Michaelis-Menten and Hill equation, allow the description of multi-substrate catalytic reactions and favour the complete expression of enzymatic affinities, which has a remarkable importance as a biological regulatory mechanism (Somogyi et al., 1997). Affinity is expressed in the Hill equation by means of the Hill coefficient and the binding probability in the probabilistic Michaelis-Menten equation. On the other side, low-ordered reactions exclusively model reactions with a maximum of one binding site. Therefore, the reaction rate either depends linearly on the concentration of its only bound substrate (Michaelis-Menten) or is independent of the substrate (Phosphorylation), in which case it is constant. Although this work has attempted to emulate the effect of multiple binding sites in the Michaelis-Menten and Phosphorylation equations via the computation of the enzyme's substrate as the mean of all participating enzymes, results show that low-ordered regulatory functions lack capacity to accurately represent the complex relationships taking place within biological cellular signalling.

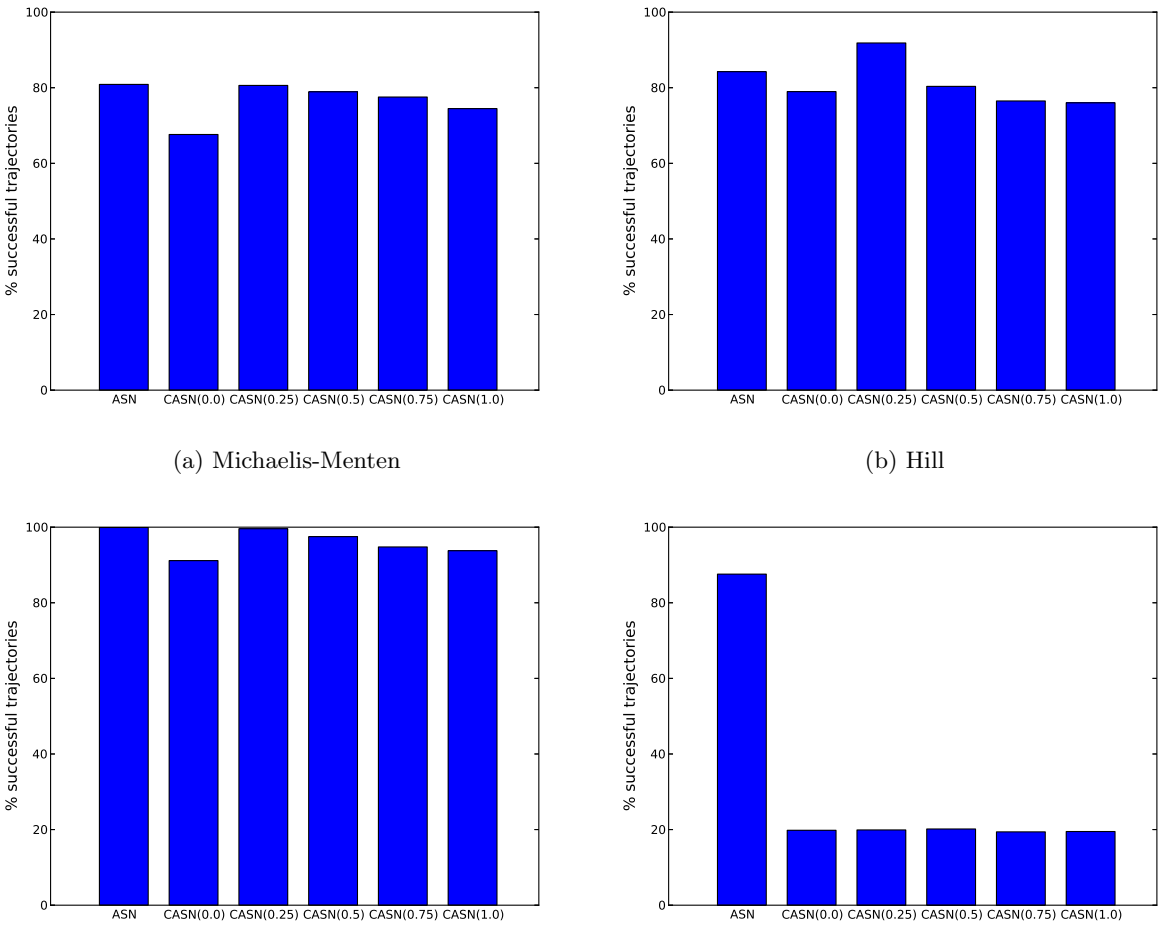

(a) Michaelis-Menten

(b) Hill

(c) Probabilistic Michaelis-Menten

(d) Phosphorylation

Figure 4.6: Effect of the crosstalk rate upon the capacity of CASNs to find effective solutions. Evolved controllers are evaluated on 10,000 different trajectories. Averages over the top part of the figures are better.

With the exception of stand-alone ASNs, the evolved controllers showing the lowest fitness correspond to CASNs with a crosstalk rate of 0.5 independently of the regulatory function used. This highlights the effect the crosstalk rate has upon the capacity of controllers to perform state space targeting within Chirikov's standard map. Figure 4.6 compares the ability of the proposed ASN representations to guide a trajectory across the map by showing the average number of trajectories that successfully reached the top targeting region. The best evolved controllers per regulatory function and crosstalk rate were reevaluated on 10,000 trajectories starting at random points within the bottom region. The results not only reinforce the previous assumption that high-ordered regulatory functions are beneficial to model the dynamical complexity of biological signalling networks, but also indicate that low levels of crosstalk increase the capacity of evolved controllers to find good and effective solutions. On

the other hand, high levels of crosstalk seems to induce some sort of uncorrelated noise which overlap the dynamics of each crosstalked subnetwork decreasing the overall performance of the controller. An example of the incidence of crosstalk can be seen when the rate of crosstalk is equal to 1. Upon this configuration, all enzymes in the CASN are involved in crosstalk and, therefore, inputs are broadcast throughout the entire network which has a negative impact on the ability to obtain effective solutions. Similar observation regarding the effect of crosstalk are noted in Arias & Hayward (2006).

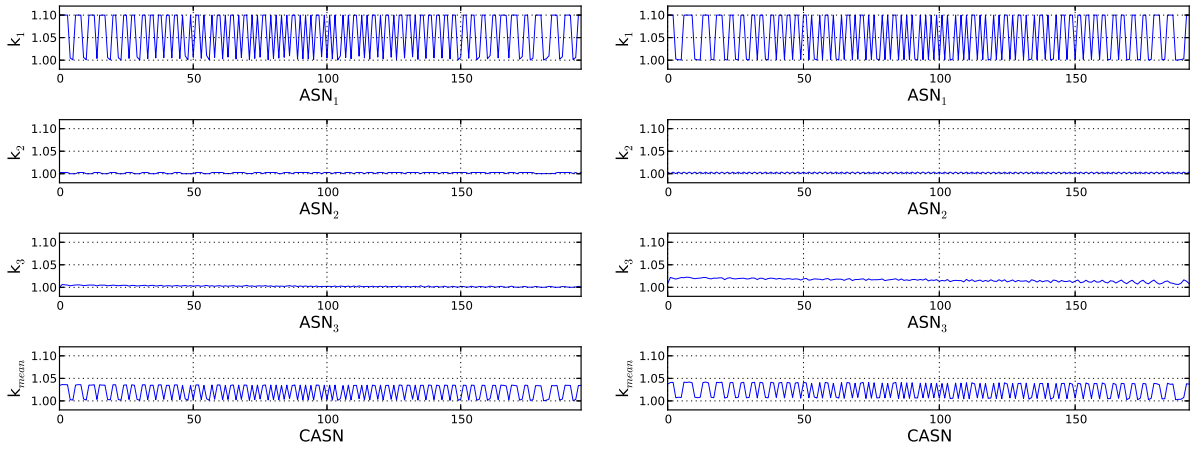

(a) Michaelis-Menten

(b) Hill

(c) Probabilistic Michaelis-Menten

(d) Phosphorylation

Figure 4.7: Example of several CASNs showing the values of their partial outputs and the effect these have on the global output, k_{mean}. CASNs use a crosstalk rate of 0.5.

The analysis of each sub-output in CASNs indicates that not all inputs are relevant in order to find valid solutions. This can be noted in Figure 4.7 when comparing the outputs of the ASN_1, ASN_2 and ASN_3, which are responsible for inputing and processing of the x and y coordinates of the guided trajectory, and the Euclidean distance from the current

position to the top-centre of the map d respectively. While ASN_1 shows an oscillatory output maximised within the limits of the modulation interval, ASN_2 depicts an almost constant output attached to the lower limit interval. Likewise, ASN_3 exhibits an scaled down output depending linearly on d, which means that the value of k_3 approaches to the bottom part of the modulation interval as long as the guided trajectory reaches the top region of the standard map. This generates an output with a descending slope corresponding to the vertical displacement of the trajectory in the standard map (see third plot in Figures 4.7(a) - (d)). Further, the oscillations in the values of k_3 are a consequence of the horizontal displacements of the trajectory. The uniformity shown by the values of k_2 suggests that the y-coordinate is not sufficient to produce the required dynamics in ASN_2 required to find good solutions. This indicates that k_1 is main responsible for tailoring the governing parameter of Chirikov's map and, consequently, pulling up the trajectory. Similar conclusions were drawn in Fuente et al. (2013*b*).

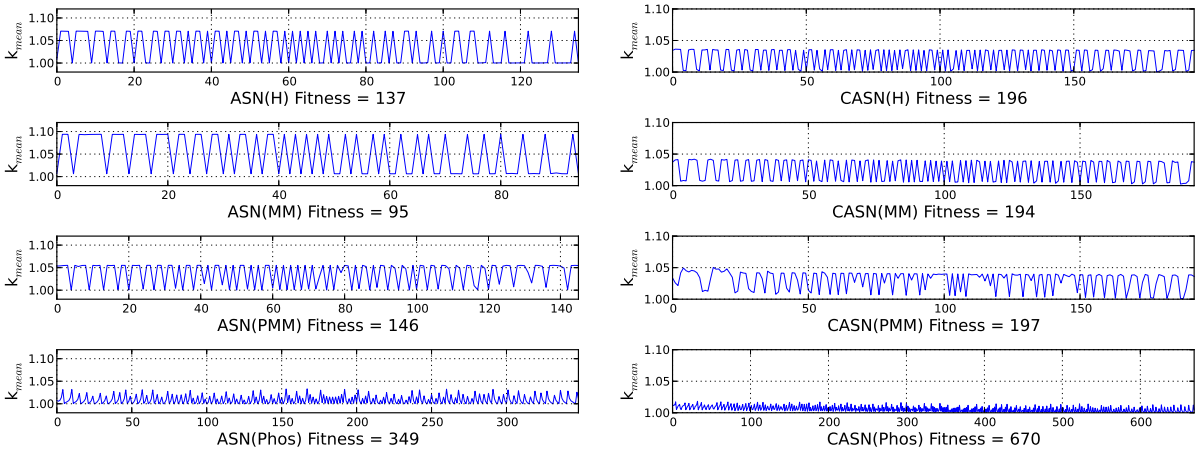

(a) Stand-Alone ASN

(b) Coupled ASN

Figure 4.8: Outputs generated by four stand-alone ASNs (a) and four CASNs (b) when carrying out state space targeting in Chirikov's standard map. CASNs use a crosstalk of 0.5.

Figure 4.8 compares the output of four ASNs with another four CASNs, one per regulatory function. Overall, it can be observed that the outputs of the ASNs are slightly shifted towards the upper region of the modulation interval, which favours the evolution of controllers with better fitness distributions. One explanation for this is that the calculation of the CASN's output as the mean of all contributing sub-ASNs does not promote the capacity of CASNs to obtain good solutions. The poor dynamism exhibited by ASN_2 and ASN_3 steadily scales down the value of k_{mean} (and consequently, the value of k_1), meaning the middle part of

the standard map becomes more ordered which decreases its permeability and reduces the capacity of the evolved controllers to obtain good solutions. The searching of alternative methodologies to determinate the output of a CASN when it depends on all sub-ASNs is one of the future research directions of the work presented in this thesis (see Chapter 7).

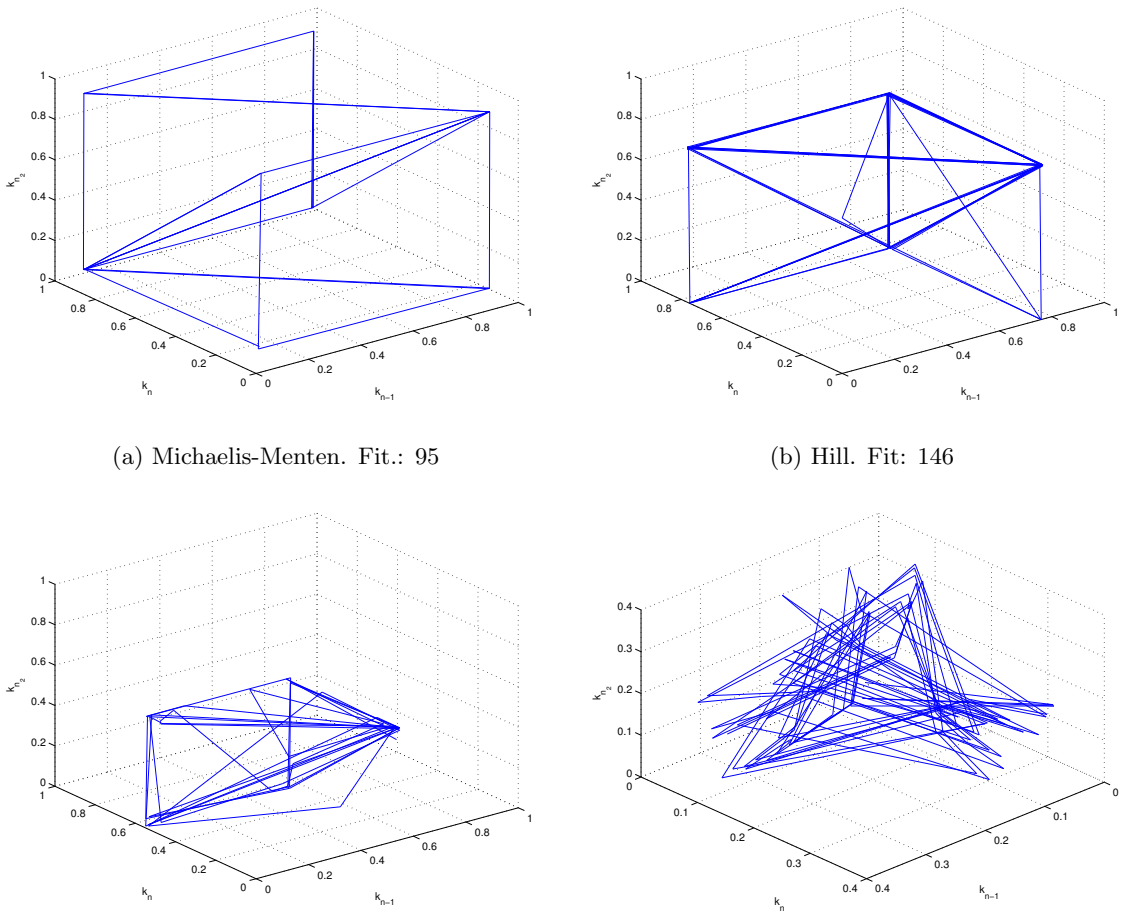

(a) Michaelis-Menten. Fit.: 95

(b) Hill. Fit: 146

(c) Prob. Michaelis-Menten. Fit.: 197

(d) Phosphorylation. Fit.: 346

Figure 4.9: Phase portrait representations produced from the output k, showing four different evolved ASNs controlling a trajectory in Chirikov's standard map for: (a) Michaelis-Menten, (b) Hill, (c) Probabilistic Michaelis-Menten and (d) Phosphorylation equations.

Coupled and uncoupled ASN controllers for Chirikov's standard map show a large diversity of control strategies, which vary depending mostly on the regulatory function and the solution's performance. This makes them intrinsically difficult to analyse. A phase portrait is a non-linear technique used to visualise how solutions of a given system evolve over time and explore their different dynamical behaviours. This representation uses time delay embedding to preserve the intrinsic properties of a given system in order to make observations based on the fluctuation of a variable over time (Kantz & Schreiber, 2004). The delay embedding is

represented by a state vector S_n (observable variable over time) and its embedding dimension m with a delay τ as follows:

$$S_n = (S_{n-(m-1)\tau}, S_{n-(m-2)\tau}, \cdots, S_{n-\tau}, S_n). \tag{4.2}$$

Time delay embedding increases the dimensionality of the phase data in order to reconstruct phase state. This is done by observing a variable during a certain period and introducing a fixed delay to generate additional dimensional points. The linear fluctuation of the observed variable can be then analyses using multi-dimensional representations. The governing parameter k is utilised to visualised the structure of the control strategies obtained while carrying out chaos targeting in Chirikov's map.

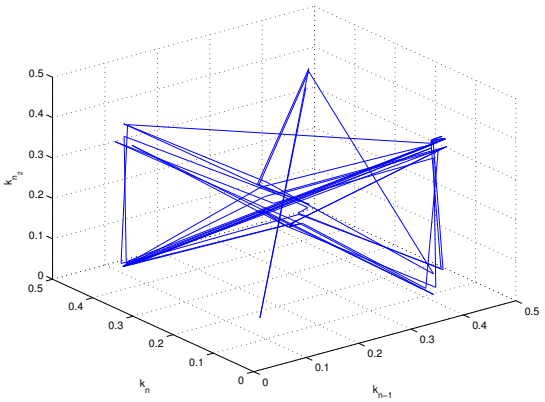

(a) Michaelis-Menten. Fit.: 194

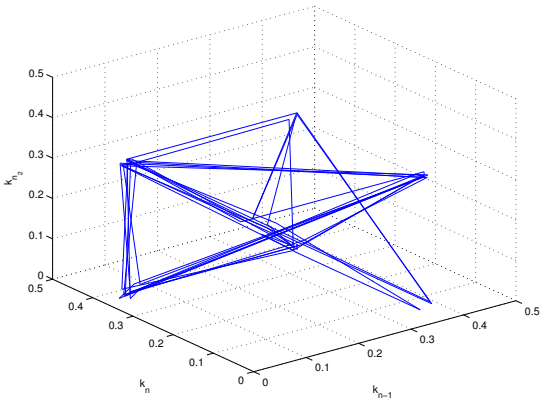

(b) Hill. Fit.: 196

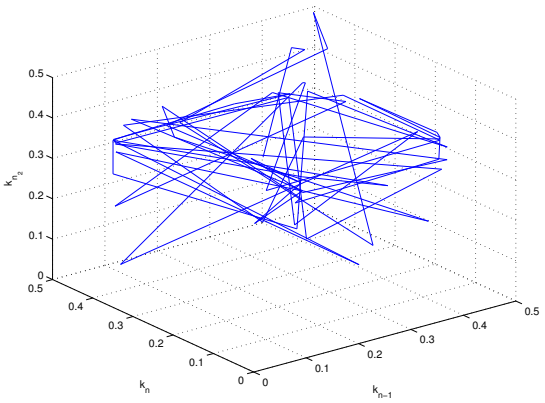

(c) Prob. Michaelis-Menten. Fit.: 146

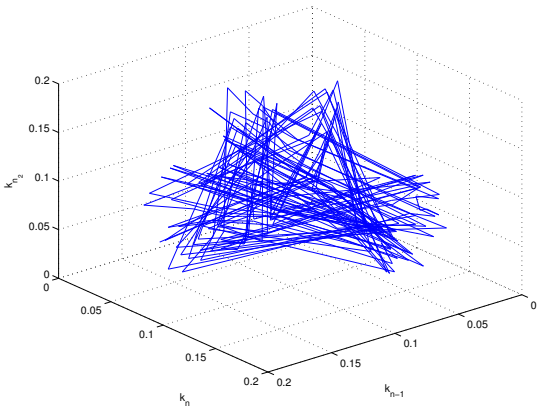

(d) Phosphorylation. Fit.: 670

Figure 4.10: Phase portrait representations produced from the output k, showing four different evolved CASNs controlling a trajectory in Chirikov's standard map for: (a) Michaelis-Menten, (b) Hill, (c) Probabilistic Michaelis-Menten and (d) Phosphorylation equations. CASNs use a crosstalk rate of 0.5.

Figures 4.9 and 4.10 shows the reconstructed phase portraits of four representative controllers for the stand-alone ASN and coupled ASN respectively while carrying out chaos targeting in Chrikov's standard map. A comparison of the phase portraits for ASN and CASN with each other highlights that ASN solutions show a rather organised attractor structure. This validates the previous findings and explains why ASN controllers steadily lead to better solution on average. Although crosstalk eases the cohesion of functionally independent sub-ASNs preserving unaltered their intrinsic dynamics, the structure of the constantly-oscillatory control strategy prevents sub-ASNs for a notable reaction to external perturbations, which increases the complexity of the obtained solutions.

Additionally, it can be noted that the Probabilistic Michaelis-Menten equation produces a rather chaotic phase portrait in both cases despite delivering the fittest controllers (see Figures 4.9 and 4.10). This can also be observed in Figure 4.10 when comparing the global outputs for the CASN controllers. Despite being symmetrical, the output generated by the Proabilistic Michaelis-Menten equation shows aperiodic oscillations before and after the guided trajectory crosses the islands of chaotic dynamics located in the center of Chirikov's map. This may indicate the existence of an *edge of chaos*[4] (Langton, 1990) between overly constrained transitions of k prior to the central chaotic islands and the rather unconstrained transitions that take place while the trajectory navigates through the islands. This phenomenon can be highlighted using Lyapunov exponents, which estimate the rate of divergence of nearby trajectories and measure the level of chaocity of a dynamical system. This sensitivity to the initial conditions is computed as follows:

$$\| \delta x(t) \| \approx e^{\lambda t} \| \delta x(0) \| \tag{4.3}$$

where λ is the rate of divergence of trajectories in the system and is called *Lyapunov exponent*. The presence of a positive exponent indicates the existence of chaos. In this work, Rosenstein's algorithm is used to determine the largest Lyapunov exponent of a time series (Rosenstein et al., 1993). A main conclusion is that the existence of an edge of chaos cannot be generalised to all CASN(PMM[5]) global outputs, this property is only inherent to a certain number of networks.

An example of edge of chaos can be seen in Figure 4.11, which plots a time series with a $\lambda = 2.03$ of a CASN(PMM, 0.5) and its associated Lyapunov exponents. In order to simplify

[4] Edge of chaos is the term normally used to name the boundary between an ordered and a chaotic state.
[5] PMM refers to Probabilistic Michaelis Menten

the visualisation of the edge of chaos only the exponents corresponding to the trajectory crossing the island of chaotic dynamics are displayed. As can be seen there are two points where the largest Lyapunov exponent is negative. These correspond to the critical points where the CASN controller changes its state from chaotic to ordered and vice versa. This suggests certain controllers are able to prominently change the nature of their dynamics according to external changes.

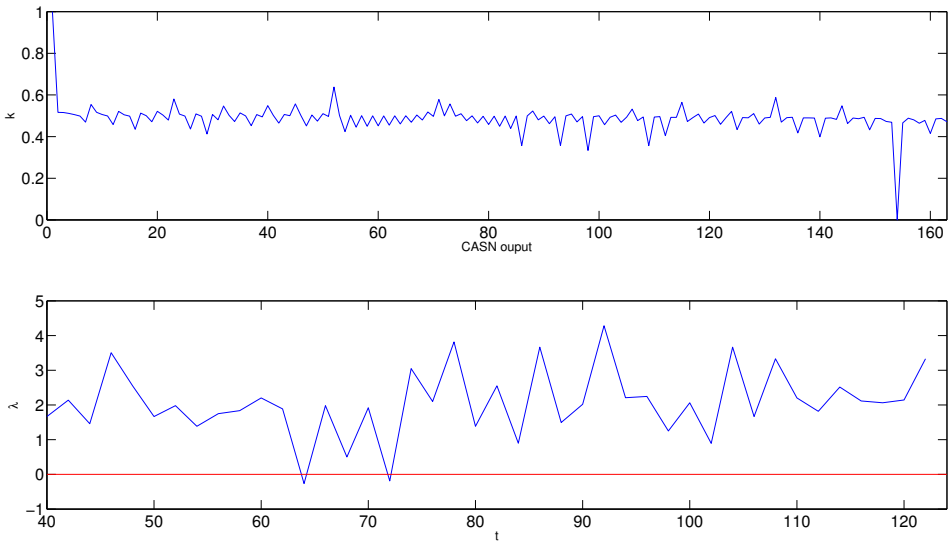

Figure 4.11: Outputs generated by a CASN while carrying out chaos targeting in Chrikov's standard map and the corresponding Lyapunov exponents. The CASN is regulated by the Probabilistic Michaelis-Menten equation and has a crosstalk rate of 0.5.

Reconstructed phase portraits and time series analysis of the output support the assumption that uncoupled controllers display different dynamical structures as they traverse Chrikov's map (see Figure 4.12). Thus, the topological structure of the evolved solution changes as long as it firstly moves from the lower chaotic region to the middle region with mixed dynamics, and latterly from the middle region to the upper chaotic region. The characteristics of the problem being solved suggests that evolved controllers show a degree of symmetry in the sequence of movements they need to guide a trajectory between the initial and final targeting regions. In particular, movements across different chaotic regions in the standard map are governed by different parts of the evolved controllers (see Figure 4.12). This example illustrates the capacity of both ASN representations to generate adaptive behaviours upon external fluctuations without modifying the existing topology of the controller, and highlights the ability of CASNs to cope with nonlinear environments despite each variable

being independently processed.

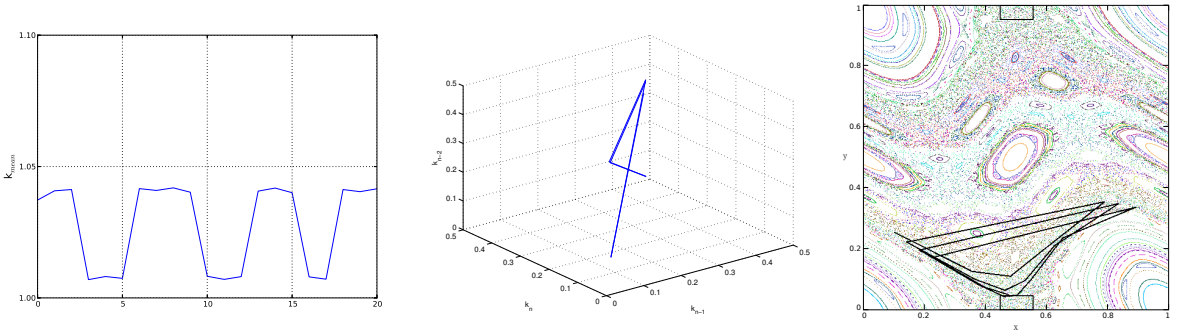

(a) Steps 0-21

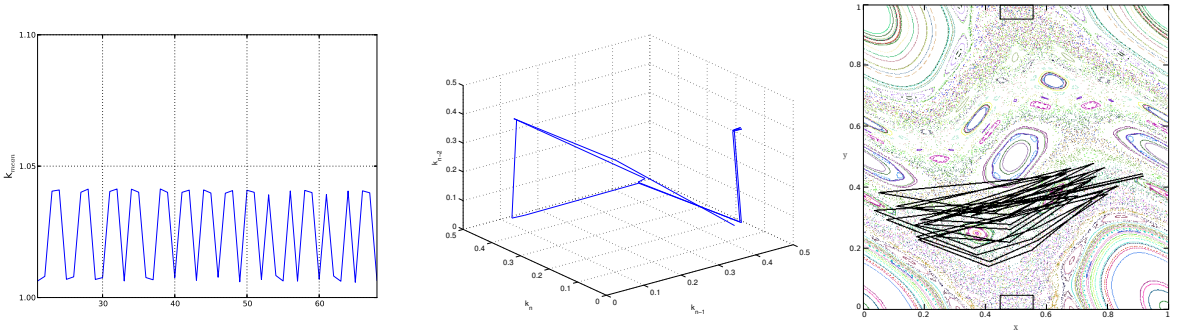

(b) Steps 21-69

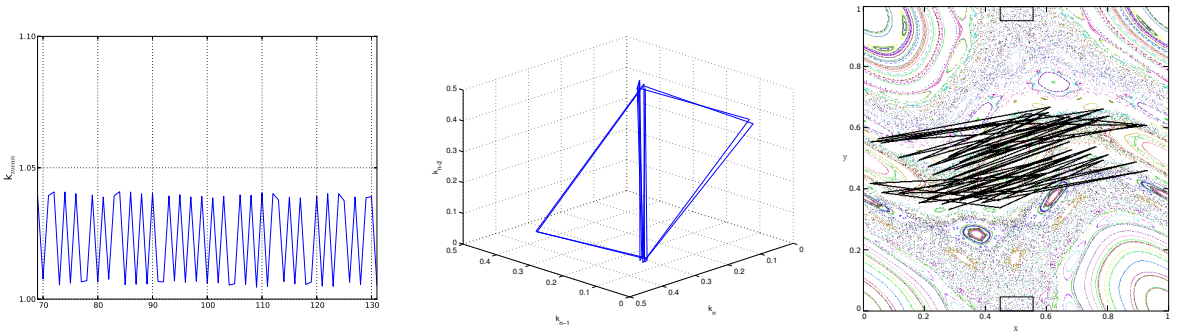

(c) Steps 69-132

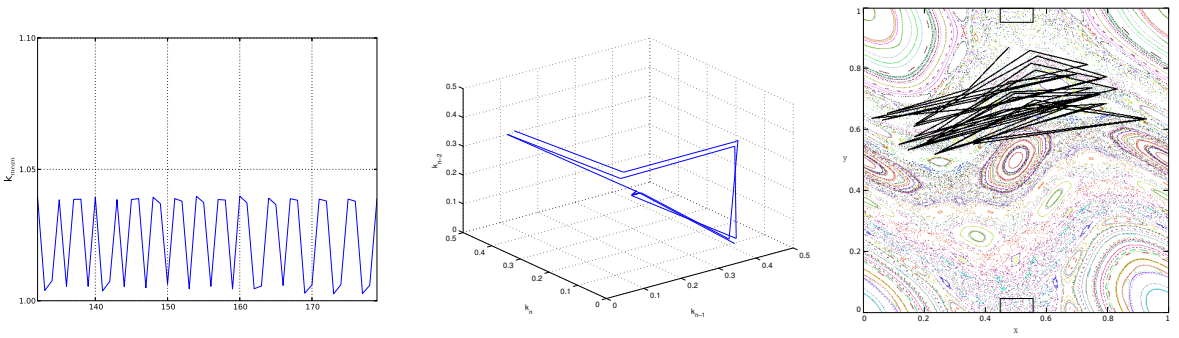

(d) Steps 132-179

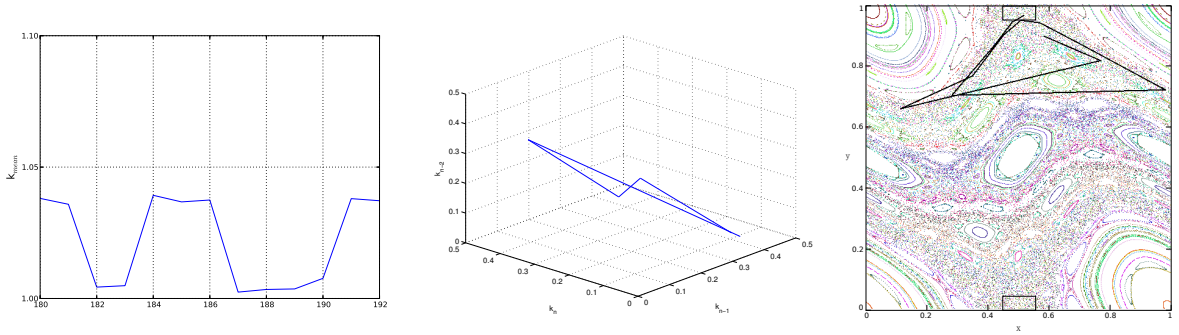

(e) Steps 179-193

Figure 4.12: Correspondence between the trajectory followed in Chirikov's standard map, the reconstructed phase space and the output of the CASN, showing three dynamical areas: (a)-(b) bottom region, (c) middle chaotic region and (d)-(e) top region

4.3 Lorenz System

The Lorenz system (Lorenz, 1963) is a dissipative and continuous-time dynamical system that describes the oscillatory behaviours occurring in planetary atmospheres. It is defined by a set of three ordinary differential equations:

$$\begin{aligned} \dot{x} &= \sigma(y - x) \\ \dot{y} &= x(\rho - z) - y \\ \dot{z} &= xy - \beta z \end{aligned} \tag{4.4}$$

where x, y and z define the system state, and σ (the Prandtl number), ρ (Rayleigh number) and β (geometric factor) are the Lorenz variables. Particularly, this work takes $\sigma = 10$ and $\beta = 8/3$.

For $\rho \gtrsim 24.74$ the Lorenz system shows a chaotic solution, which is denoted by an initial transient phase followed by an aperiodic oscillatory state (see Figure 4.13(a)). It is aperiodic in the sense that oscillations are irregular and never repeat the same pattern. The visualisation of the Lorenz system as a set of trajectories in the phase space also reveals a structure with all initial points bounding to a single two-lobed strange attractor (see Figure 4.13(b)). Trajectories attached to this attractor steadily orbit two unstable equilibrium points ϵ_+ and ϵ_- located at:

$$\epsilon_+ = (\sqrt{\beta(\rho-1)}, \sqrt{\beta(\rho-1)}, (\rho-1)) \tag{4.5}$$

$$\epsilon_- = (-\sqrt{\beta(\rho-1)}, -\sqrt{\beta(\rho-1)}, (\rho-1)) \tag{4.6}$$

The motion in the Lorenz attractor is defined by an infinite number of unstable periodic orbits. They are unstable in the sense that they swing around the right lobe before quickly heading to the center of the left lobe where they orbit for only a limited period of time before returning approximately to the same position on the right lobe. This sequence of movements repeats indefinitely. The number of trajectories orbiting the equilibrium points varies unpredictably between the two lobes of the attractor.

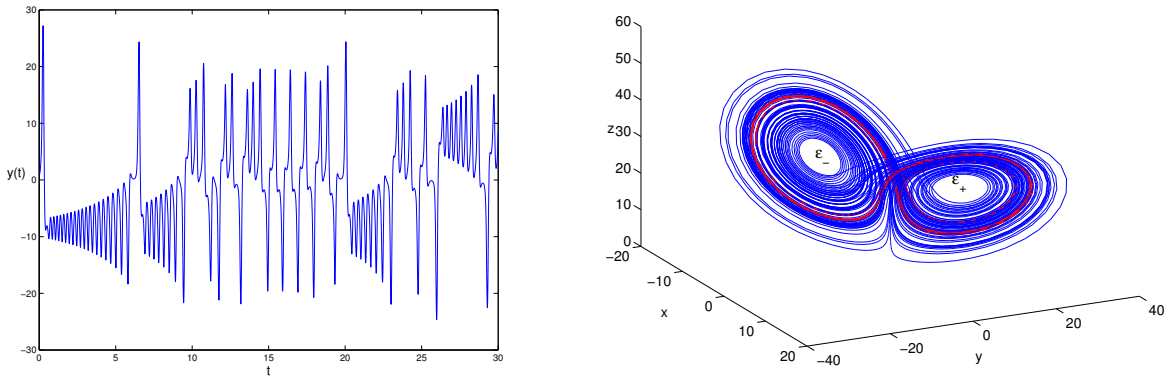

(a) Time series analysis of $\dot{y}$

(b) Phase state visualisation

Figure 4.13: A trajectory within the Lorenz attractor with $\sigma = 10$, $\rho = 28$, $\beta = 8/3$. While (a) depicts the initial transient phase flowed by the aperiodic oscillation of the trajectory generated by $\dot{y}$ when plotted with a step size of $\Delta_t = 0.01$ in the range $[0, 30]$, (b) shows the position of the equilibrium points ϵ_- and ϵ_+. The red line illustrates the instability of one of the periodic orbits followed by the trajectory.

4.3.1 State Space Targeting

Following the example in Lones et al. (2014), the objective is to find an evolved controller able to first guide a trajectory between the two equilibrium points, and second stabilise it at the reached point for a defined period of time. Evolved controllers are evaluated on their ability to navigate from ϵ_- to ϵ_+ remaining there until $t = 50$ and then travel back to ϵ_- and remain there until $t = 100$ (chaos targeting). In order to do this, stand-alone ASNs and CASNs are allowed to modulate ρ in the range $[0 - 100]$, while β and σ remain constant. The Rayleigh

parameter ρ is the governing parameter of the Lorenz system, responsible for the instability of periodic orbits and the velocity of convergence of trajectories to these orbits. Inputs for both ASN representations are the trajectory's current location (x, y, z) with its values scaled from $[-50, 50]$ to $[0, 1]$ and the Euclidean distance d from the trajectory's location to the target also in the unit interval. The real distance value is only provided when the Euclidean distance is smaller than 2.0; otherwise, its value is equal to the maximum input value. Both ASN models generate a single output representing the value of ρ. In particular, CASNs consist of four sub-ASNs, each of which has one input and one output. The global output is the standard mean of all contributing ASNs. Crosstalk is only allowed between neighbouring sub-ASNs.

The Lorenz system is numerically integrated using the fourth-order Runge-Kutta method with a step size of $\Delta = 0.01$. Both ASN representations are executed every 10 steps in order to determine the new value of ρ. The fitness function f_L is the average amount of time guided trajectories remain stable at both equilibrium points. This is defined as follows:

$$f_L = \sum \frac{1 - d}{s} \tag{4.7}$$

where s indicates the number of time steps. Both coupled and uncoupled ASN representations are evolved using a population of 500 individuals and a generation limit of 50. This evolutionary configuration is sufficient to obtain valid solutions and has been selected to enable direct comparison to the performance of the ABNs in Lones et al. (2011, 2014) in terms of the amount of time the controlled trajectory spends at the equilibrium points. Table 4.2 summarises the parameters used to carry out chaos targeting in the Lorenz system.

Table 4.2: Parameters used to carry out chaos targeting in the Lorenz system

Variable	Type	Range
ρ	Double	0 - 100
x	Double	[0 – 1]
y	Double	[0 – 1]
z	Double	]0 – 1]
Population	–	50
Generations	–	500

4.3.2 Controlling the Lorenz System

Figure 4.14 summarises the fitness distributions of the stand-alone ASN and CASN evolved controllers based on their capacity to guide unstable trajectories, and then keep them stable at both equilibrium points using the main enzymatic regulatory functions and different crosstalk rates. Results indicate that both ASN representations are able to find valid solutions with the notable exception of the Phosphorylation equation. As with Chirikov's map, the best evolved controllers on average correspond to low crosstalk rates independently of the regulatory function. Nonetheless, the fittest CASN controller comes from the Probabilistic Michaelis-Menten equation and a crosstalk rate of 0.75 (see Figure 4.14(c)). Unlike Chrikov's map where uncoupled ASN controllers steadily led to better solutions on average, CASNs controllers in the Lorenz system display fitness distributions more shifted toward the optimum solution for most of the parametrisations. Independently of the regulatory function, crosstalk rates of 0.25 generally produce the controllers with better fitness on average (see Figures 4.14(a)-(d)). These results reinforce the capacity of CASNs to solve highly correlated problems (the Lorenz system has two nonlinearities). This also emphatises the importance of crosstalk as a mechanism to develop large computational models which allow the solution of complex problems in a decentralised manner via computing each variable quasi-independently. This closely resembles the signalling mechanism's ability to process both multiple and antagonist stimuli in biological cells.

Figure 4.14 also shows that the choice of regulatory function is relatively important in order to obtain valid ASN-based controllers (even more than in Chirikov's map). For both ASN models, controllers regulated by the Michaelis-Menten and the Phosphorylation equations exhibit both a limited performance and lack capacity to find efficient solutions respectively, while Probabilistic Michaelis-Menten and Hill equations lead to controllers showing reasonably fit solutions on average. Near-optimal solutions are mostly restricted to the Probabilistic Michaelis-Menten equation for both ASN representations. This evidences that high-ordered enzymatic reactions appear to be fundamental in order to mirror the complexity existing in cellular signalling networks. Further, this may suggest that enzymes participating in the signalling process have multiple binding sites and are vasty interconnected. It means that signalling enzymes request multiple substrates to effectively transduce secondary messengers and thus, reactively respond to extracellular events.

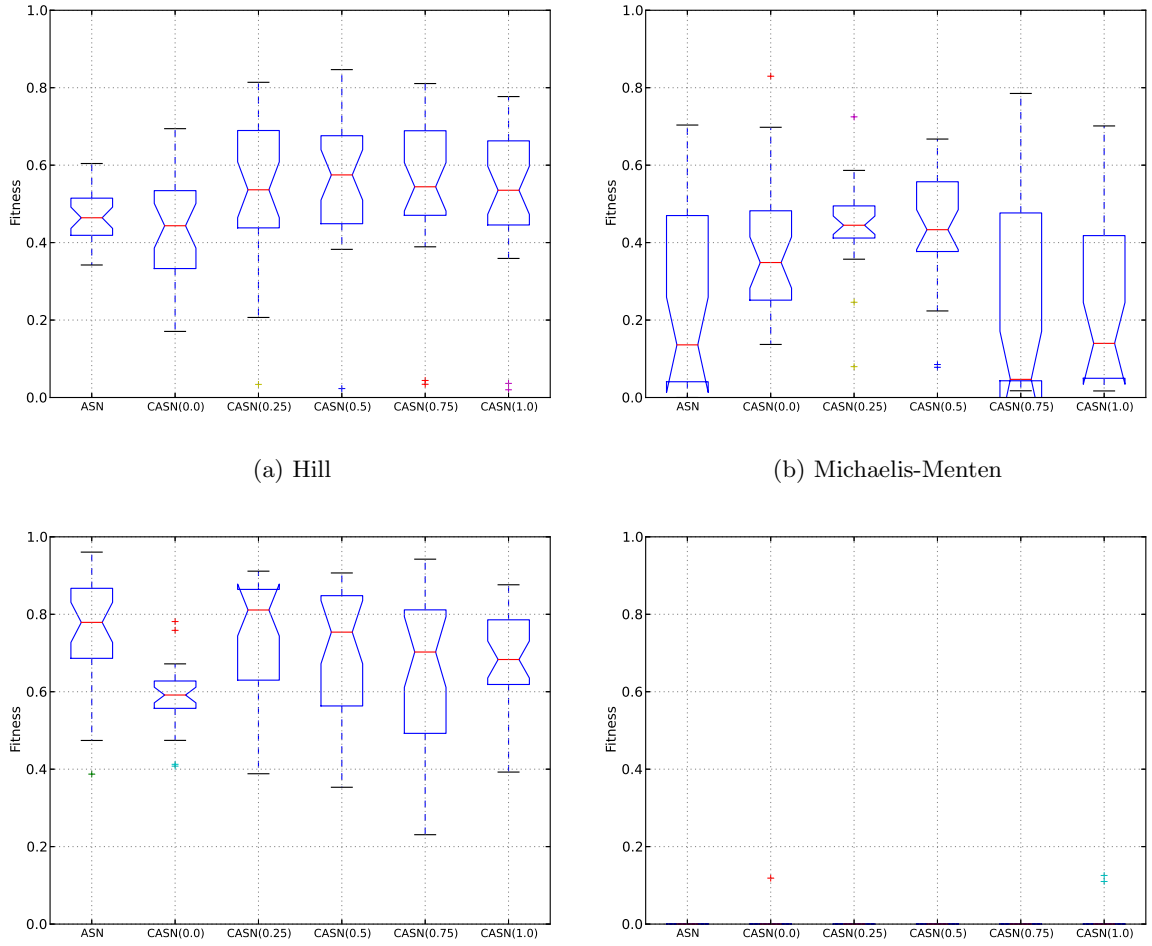

(a) Hill

(b) Michaelis-Menten

(c) Probabilistic Michaelis-Menten

(d) Phosphorylation

Figure 4.14: Fitness distributions for the stand-alone ASNs and CASNs, carrying out chaos targeting in the Lorenz system using the principal regulatory functions found in enzymatic systems: (a) Hill equation, (b) Michaelis-Menten equation, (c) Probabilistic Michaelis-Menten equation and (d) Phosphorylation equation. All ASNs and sub-ASN networks are of length 10. Distributions toward the top part of the figures are better.

The CASN evolved controllers have an average fitness of ~ 0.82 when regulated by the Probabilistic Michaelis-Menten equation and coupled with a crosstalk rate of 0.25. Likewise, the best stand-alone ASN controllers show an averaged fitness of ~ 0.78 using the same regulatory function. Examples of controlled trajectories and their associated stand-alone ASN and CASN evolved controllers are illustrated in Figures 4.15 and 4.16 respectively. Similar fitness distributions were also obtained in Lones et al. (2014) when coupled ABNs ($\text{AGN}^{[6]} \longrightarrow \text{AMN}^{[7]}$) are regulated by the sigmoid function and the Logistic map (Sig $\longrightarrow$ Log). A closer inspection of the CASN controller's structure reveals that the controlled

[6] Artificial Genetic Network
[7] Artificial Metabolic Network

trajectory reaches ϵ_+ at time $t = 2.3$ and stays stable orbiting the equilibrium point at an average distance of 1.23 units. The CASN controller also requires a time interval of $\Delta_t = 2.8$ to guide the trajectory between ϵ_+ and ϵ_- with obits at an averaged distance of 1.64 units. The best stand-alone ASN controller needs a time interval of $\Delta_t = 1.6$ to reach ϵ_+ where stabilises the trajectory at an average distance of 1.0 units and it requires a time interval of $\Delta_t = 3.2$ to guide the trajectory back to ϵ_- and stabilise it at an average distance of 1.4 units.

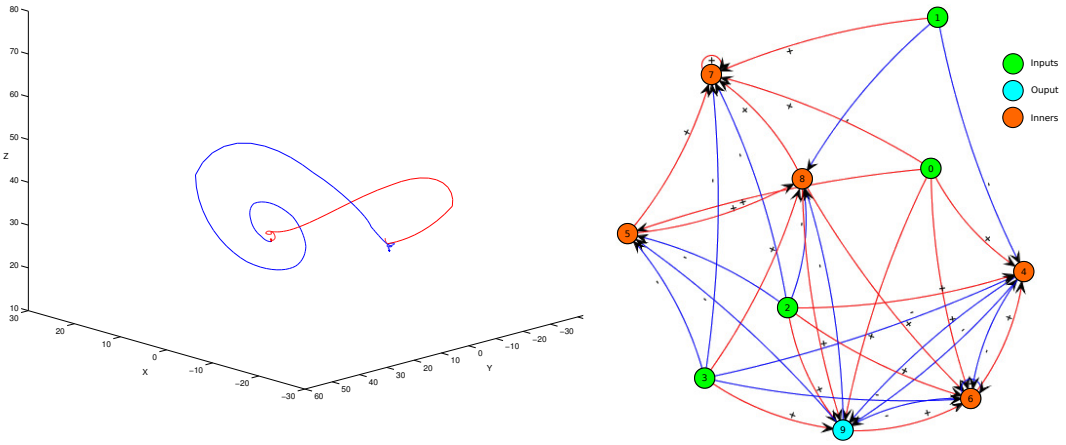

(a) Controlled trajectory (b) Stand-alone ASN

Figure 4.15: Example solution (a) and its associated stand-alone ASN regulated by the probabilistic Michaelis-Menten (b) guiding a trajectory from ϵ_- to ϵ_+ (blue line) and back to ϵ_- (red line). Fitness: 0.97.

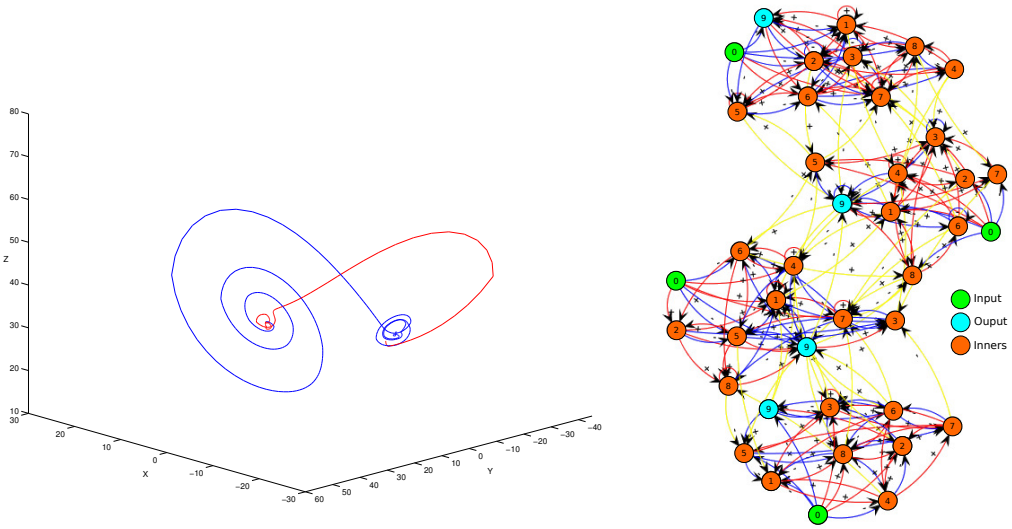

(a) Controlled trajectory (b) Coupled ASN

Figure 4.16: Example solution (a) and its associated CASN(0.75) regulated by the probabilistic Michaelis-Menten (b) guiding a trajectory from ϵ_- to ϵ_+ (blue line) and back to ϵ_- (red line). Fitness: 0.94.

Alternative examples of controlled trajectories and their corresponding control signals are showed in Figure 4.17. Plotted examples are listed in descending order by fitness. A main observation is that control signals exhibit an increasing oscillatory pattern as the fitness decreases. Fittest controllers deploy controlled trajectories and control patterns similar to the examples in Figures 4.17(a)-(b). Both are denoted by an initial transient time followed by a stationary period in which control signals remain unchanging. While the initial variations in the control signal push controlled trajectories away from the attractor, a fixed control signal keeps trajectories stable at the equilibrium point. The transient time typically terminates when the control signal positions the trajectory towards the attractor. This is evidenced by a sudden change of direction in the guided trajectory and can be spotted in the red trace of the controlled trajectory in Figure 4.17. Less efficient solutions show a control pattern characterised by a continuously-varying oscillatory control signal after an also oscillatory transient time (see Figures 4.17(c)-(e)). Therefore, controlled trajectories do not stabilise at the fixed point; instead they describe concentric orbits around it with a diameter proportional to the oscillatory amplitude. Less fit solutions also have longer transient times. For the fittest controllers, it can be noted that the manner uncoupled and coupled controllers have to proceed when trajectories are close to the equilibrium points bear certain resemblance with Pyragras' method (Pyragas, 1992) as the control signal shows a gradually decreasing oscillatory pattern when $\rho = 30$ or $\rho = 50$. A similar observation was also noted in Lones et al. (2014).

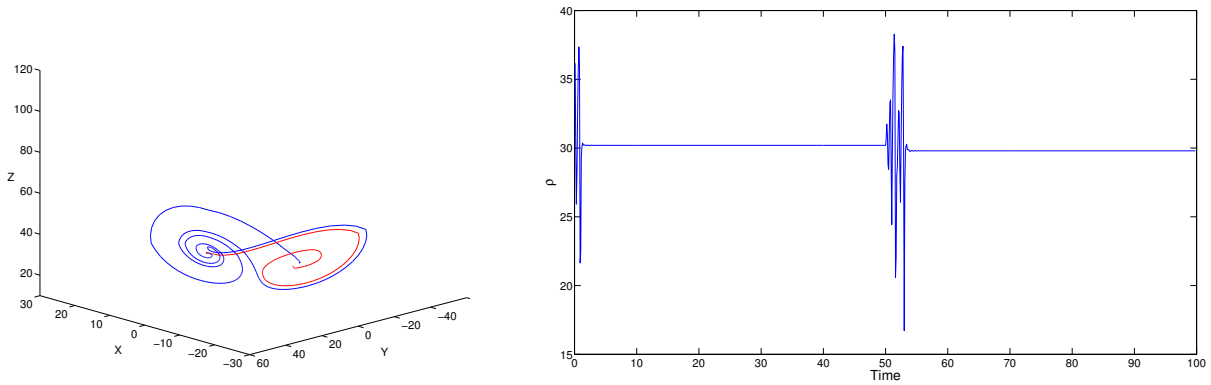

(a) ASN regulated by Probabilistic Michaelis-Menten equation. Fitness: 0.94.

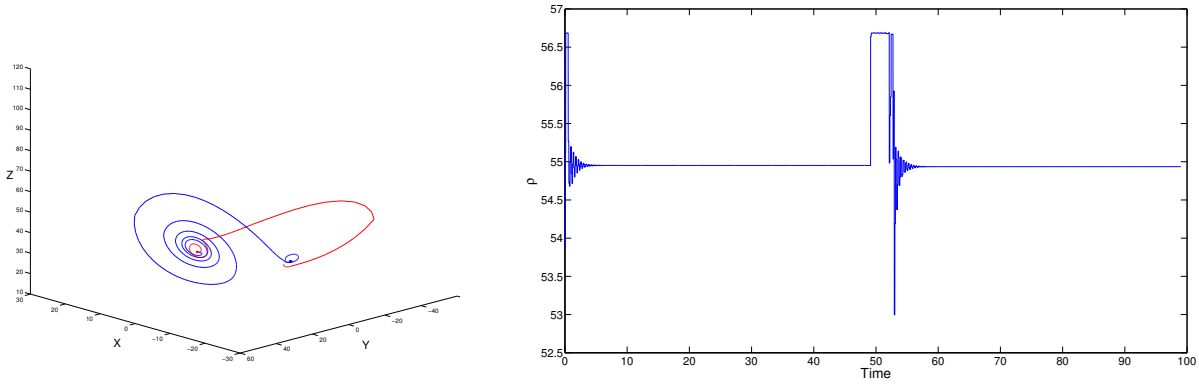

(b) CASN(0.25) regulated by Probabilistic Michaelis-Menten equation. Fitness: 0.82

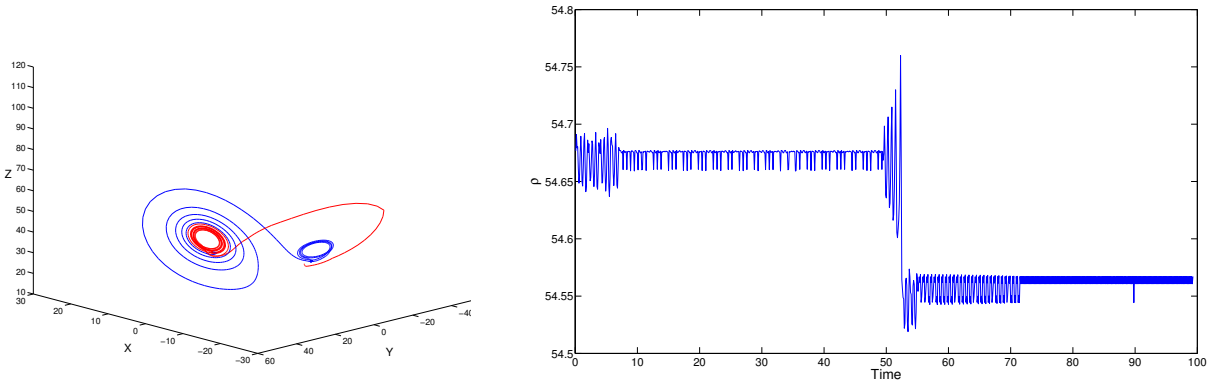

(c) CASN(0.75) regulated by Hill equation. Fitness: 0.71

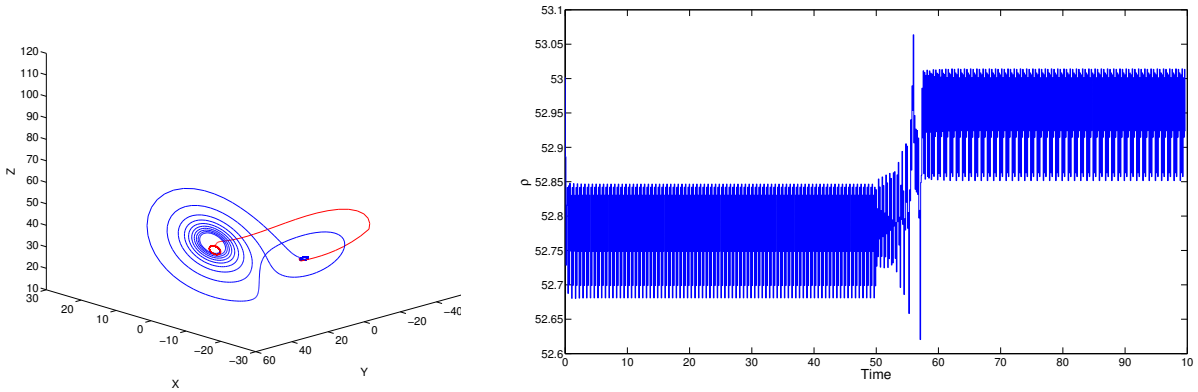

(d) CASN(1.0) regulated by Michaelis-Menten equation. Fitness: 0.51

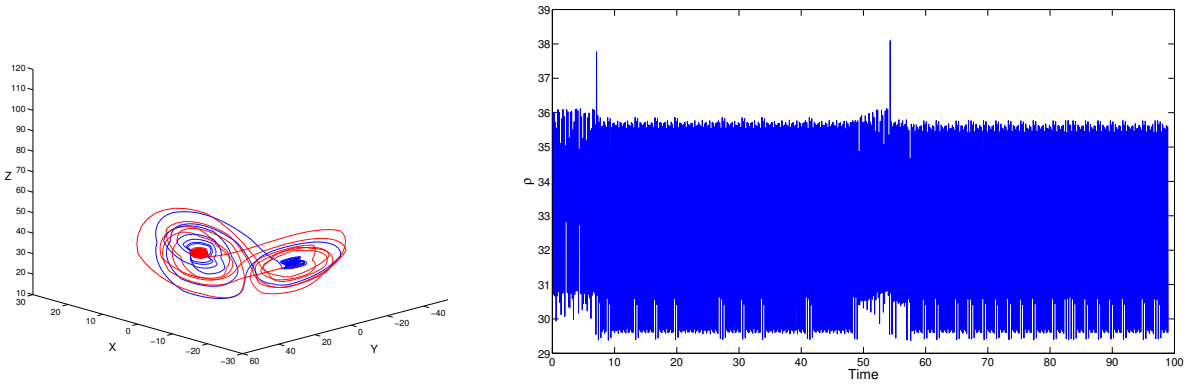

(e) CASN(0.0) regulated by Michaelis-Menten equation. Fitness: 0.23.

Figure 4.17: Example of different ASN and CASN evolved controllers for the Lorenz map, which modulate the Rayleigh parameter ρ using several regulatory functions and different crosstalk rates, showing the controlled trajectory (left) and the modulated Rayleigh parameter (right). Control strategies are shown in descending order.

As in Chirikov's map, CASN evolved controllers in the Lorenz system also lead to some sub-outputs lacking visible dynamics. This feature is observed in Figure 4.18 when comparing the output values of ASN_1, ASN_2, ASN_3 and ASN_4, which are responsible for inputting and processing the x, y and z coordinates of the guided trajectory and the Euclidean distance to the target equilibrium point respectively. Unlike Chirikov's map, these dynamically low sub-outputs are neither constantly delivered by the same pair input/sub-ASN nor attached to equal fixed values. Particularly, CASN controllers show sub-outputs with nearly steady dynamics fixed to ρ values of 0 and 50. As a consequence of the methodology to obtain the global output of CASNs, the effect of this diversity of partial outputs over the global output is twofold. Firstly, it accentuates the small perturbations found in certain partial control patterns and secondly, it reduces the amplitude of oscillation showed in some partial outputs. As a result, CASN evolved controllers produce control strategies that cannot be formed without the collaboration of each participant ASN and favour the emergence of fitter solutions. Nevertheless, it is still arguable whether the calculation of the CASN's output as the mean of all contributing ASN appropriately defines the overall dynamics of coupled ASNs.

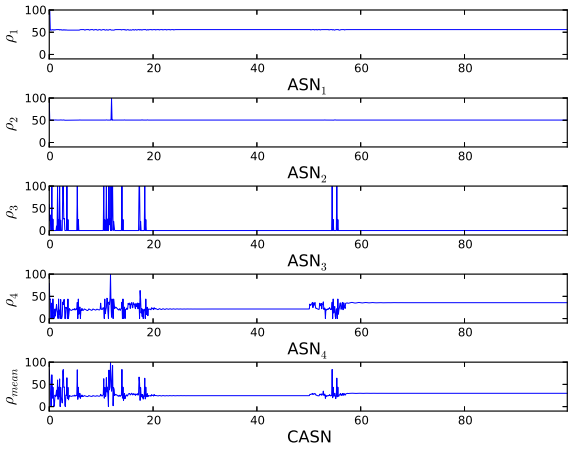

(a) CASN(0.25→Hill). Fitness: 0.47

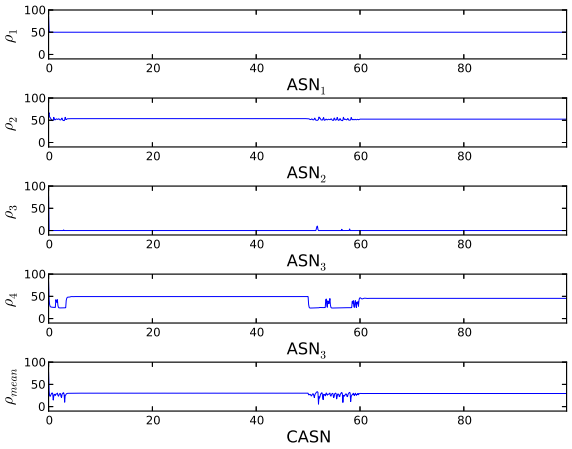

(b) CASN(0.25→Hill). Fitness: 0.77

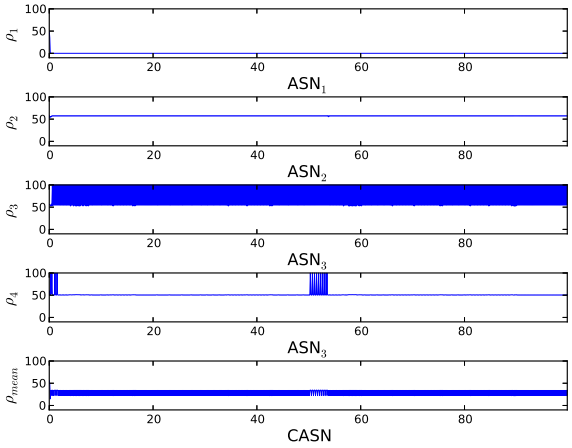

(c) CASN(0.25→MM). Fitness: 0.48

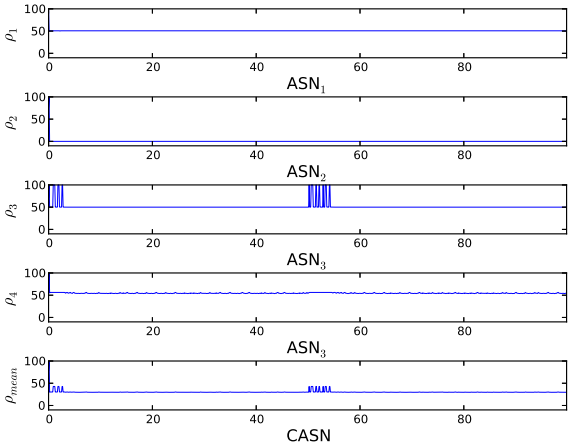

(d) CASN(0.25→MM). Fitness: 0.79

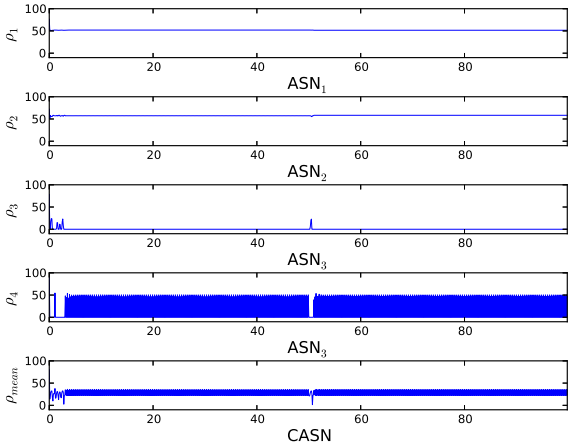

(e) CASN(0.25→PMM). Fitness: 0.48

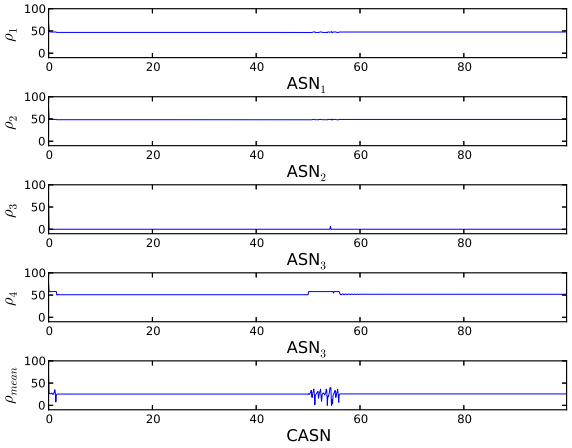

(f) CASN(0.25→PMM). Fitness: 0.82

Figure 4.18: Example of the partial outputs of six different CASN controllers when carrying out the control tasks proposed for the Lorenz Map. Plots illustrate the dynamics of the four sub-ASNs composing a CASN using different regulatory functions and a constant crosstalk of 0.25. It also highlights the evolution in the sub-networks's dynamics as long as the fitness increases. Left-hand side plots ((a), (c) and (e)) show controllers with fitness ≈ 0.50 and right-hand side plots ((b), (d) and (f)) indicate controlles with fitness ≈ 0.80.

Interestingly, crosstalk has a positive effect upon the controllers in the Lorenz system. As can be seen in Figures 4.18 and 4.19, inputting the real distance value into the network when trajectories are nearby the equilibrium points fosters a dynamical change in ASN_4, which gradually affect the network as neighbouring sub-ASNs exchange information amongst each other. This means controllers stop to randomly guide trajectories across the Lorenz map and start to orderly direct them to the equilibrium point. The intensity of the reaction gradually disappears as the change moves toward ASN_1. In this sense, low dynamics suffice to induce a dynamical change in the coupled networks, but also to maintain unaltered the intrinsic dynamics of each sub-ASN. Thus, the enzymatic concentrations remain flat and crosstalk does not affect adjacent sub-ASN's dynamics until an alteration of the distance value perturbs the dynamics of ASN_4. A comparison of the temporal behaviours of a stand-alone ASN and a coupled ASN reveals that CASNs, and specially those with low crosstalk rates, show a rapid switching between dynamical states. This can be observed in Figure 4.19 which shows the evolution of the internal states of a stand-alone ASN and a coupled ASN while controlling a trajectory in the Lorenz system. For both networks, sensing the real Euclidean distance abruptly changes the enzymes' concentration and switches the network's dynamics. It entails that controllers move from a chaotic state to an ordered state. Notably, the effect of crosstalk favours a more discrete switching of the network's dynamics in the coupled ASN than in the stand-alone ASN (see Figure 4.19). As can be noted in Figure 4.19(c), the enzymatic concentrations of the stand-alone ASN show an oscillation with a gradually decreasing magnitude before the concentrations stabilise. In the case of CASNs with high crosstalk rates, inputting the correct value of the distance has a lesser impact over the network dynamics, which prevent them to express reactive behaviours (see Figure 4.19(b)). This may explain why CASN controllers show fitness distribution closer to the optimum. It also prompts that coupled networks and, principally those with low crosstalk have a higher reactive capacity to external changes as they generate more precise control directives. Further, it also highlights that CASN with high crosstalk rates and stand-alone ASNs shows mixed dynamics which disturb each other adding unrelated noise to the control problem.

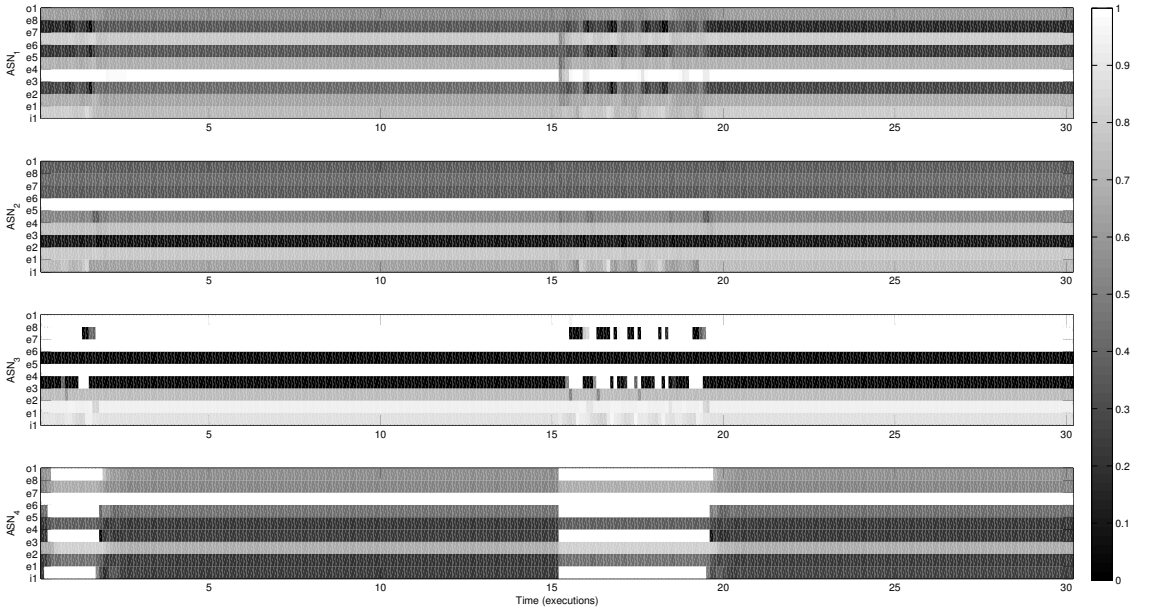

(a) Time Series CASN(PMM, 0.25). Fitness: 0.8906

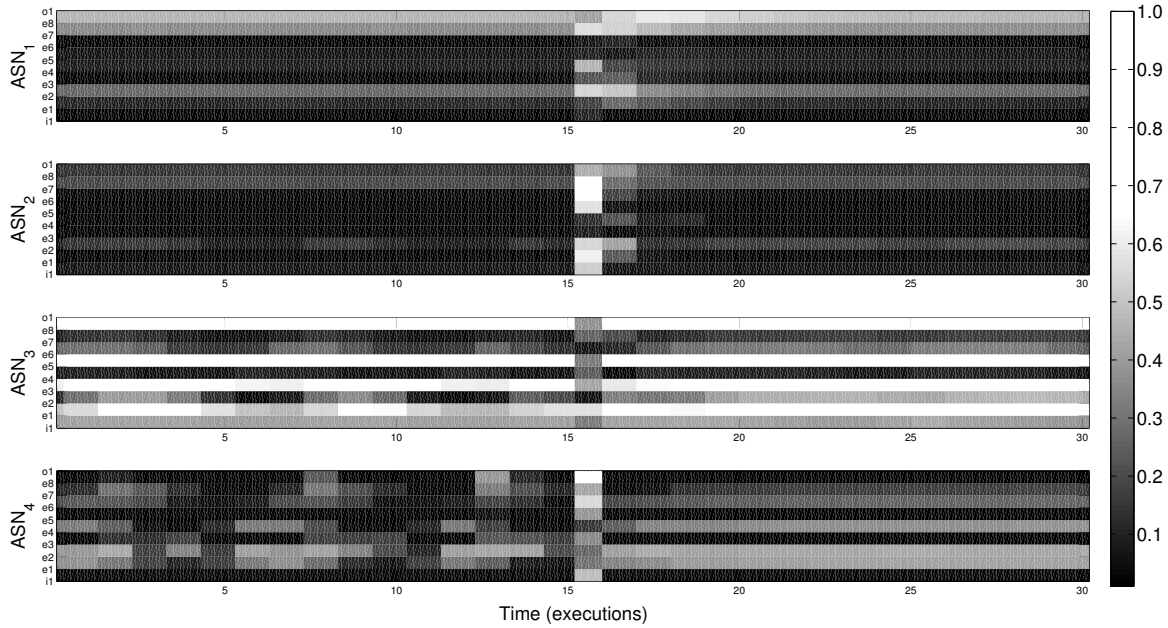

(b) Time Series CASN(PMM, 1.0). Fitness: 0.8407

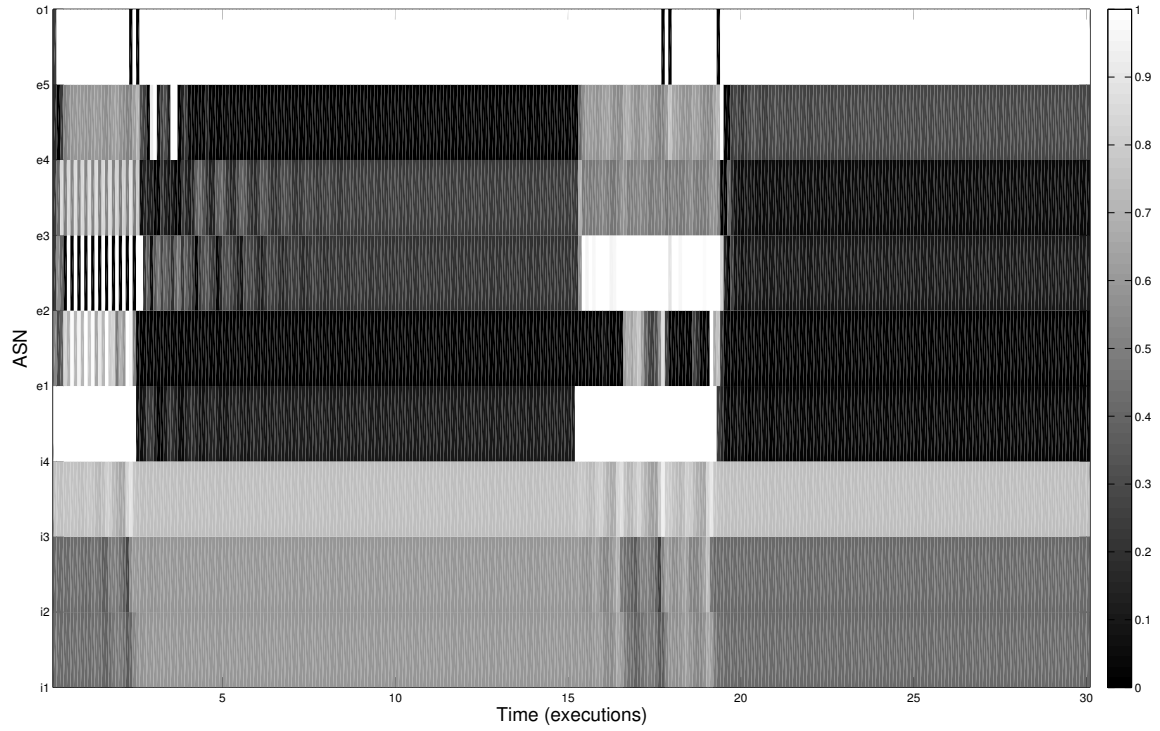

(c) Time Series ASN(PMM). Fitness: 0.8867

Figure 4.19: Examples of the internal state of an evolved CASN and an evolved stand-alone ASN controlling a trajectory in the Lorenz map. As the trajectory approaches ϵ_+ the distance signal, i_0 in ASN_4 and i_4 in the ASN and CASN respectively switches on, which perturbs in the enzymes' concentration and brings on a change in the signalling state and the control output o_0 in ASN_1 and o_1 in the ASN.

As previously seen, CASN evolved controllers in the Lorenz system shows a large diversity of control strategies, which makes the obtained solutions difficult to analyse. Phase state reconstruction is used to gain on understanding about the intrinsic characteristic of the controllers. Figure 4.20 illustrates some representative examples of reconstructed phase spaces. In general, it can be noted that the controller's attractor modifies and simplifies its structure as the fitness increases. The governing parameter ρ is utilised to visualised the structure of the control strategies obtained while carrying out chaos targeting in the Lorenz system. In general, controllers appear to have a largely symmetrical structure, showing similar but opposite behaviours when moving from ϵ_- to ϵ_+ or vice versa. Surprisingly, low fitness controllers also display well-structured attractors, with a structure defined by four wings, two on each side and connected at both ends by a central line (see Figure 4.20(i)). Wings have a triangular shape and never intersect each other. As the fitness increases, the attractor

begins to lose its native structure as new symmetrical arrangements emerge on its top side. These compress the initial attractor structure and reduce its size (see Figures 4.20(f)-(d)). The new attractor exhibits a more unorganised structure in which is still possible to recognise the original frame. Its topology shows two distinctive areas: a stump-like shape in the bottom part and replica of the original attractor structure in the top part. Progressive increments provokes the gradual retraction of the bottom structure until nearly disappearing (see Figure 4.20(c)). Fittest controllers also show a largely symmetrical structure which still resemblers the original attractor structure, but is now characterised by a lesser number of lateral wings (see Figures 4.20(a)-(b)). This evolution corresponds to the transition from a continuously-oscillatory to an ordered control strategy.

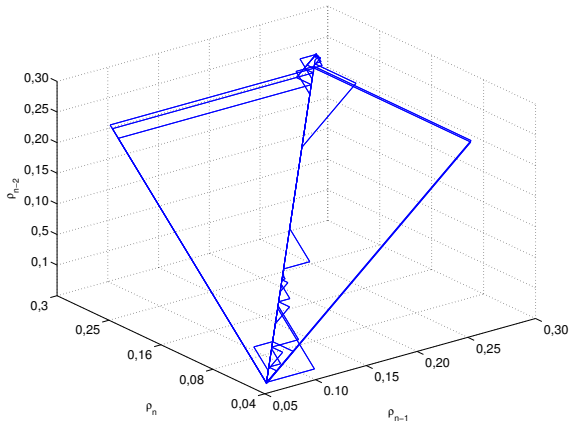

(a) Fitness: 0.94

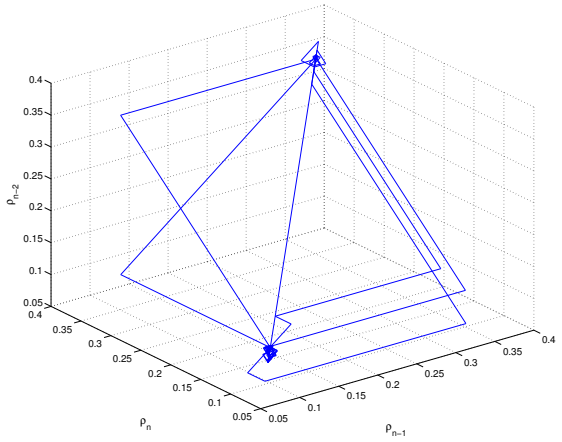

(b) Fitness: 0.86

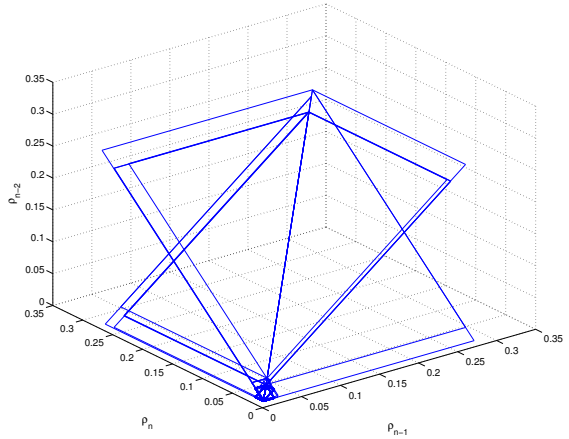

(c) Fitness: 0.75

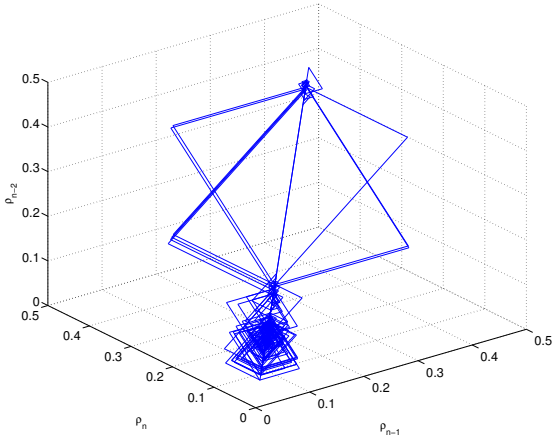

(d) Fitness: 0.68

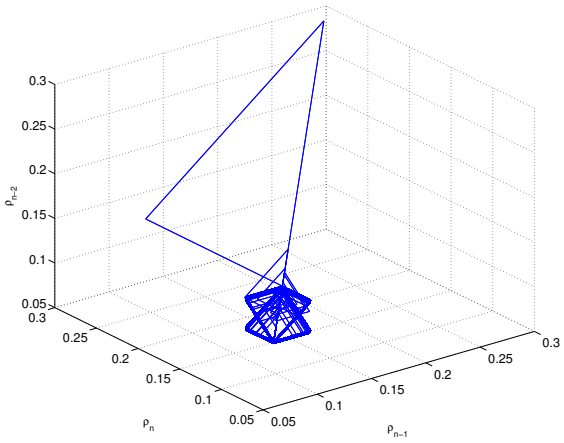

(e) Fitness: 0.60

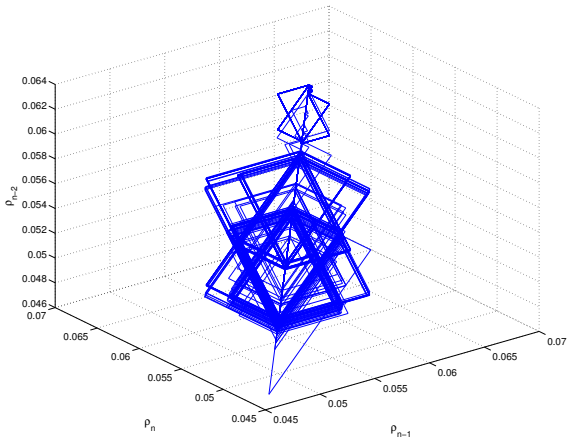

(f) Fitness: 0.55

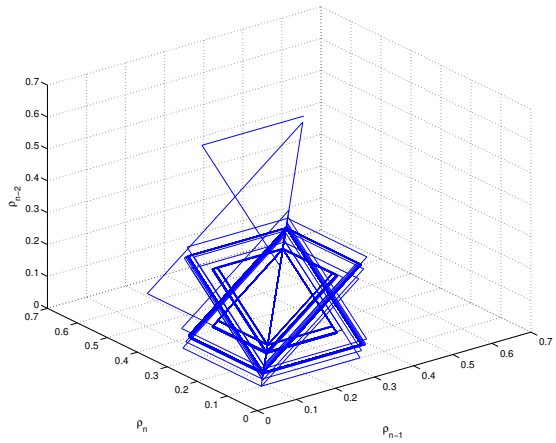

(g) Fitness: 0.43

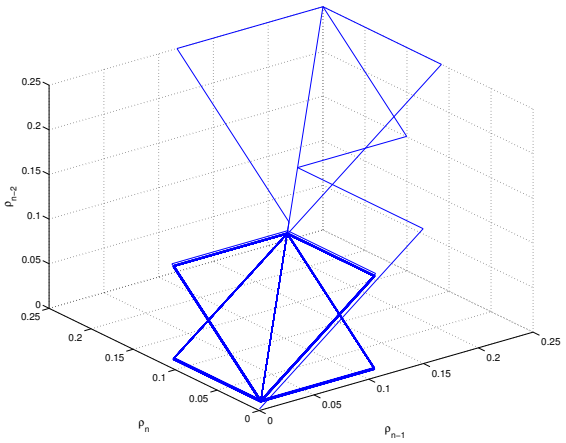

(h) Fitness: 0.35

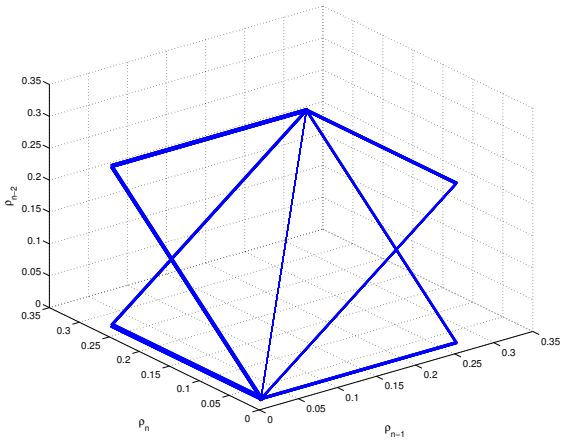

(i) Fitness: 0.27

Figure 4.20: Evolution of CASN-based controllers' attractor structure in the Lorenz map. Controllers alter and simplify its structure as their fitness increases. Low fitness controllers display well-structured attractors, with a structure defined by four wings, two on each side and connected at both ends by a central line. High fitness controllers have symetrical structure characterised by two interconnected wings.

4.4 Summary

This chapter has presented and discussed the application of stand-alone ASNs and coupled ASNs to the control of two behaviorally different dynamical systems: the Lorenz system and Chirikov's standard map. For both systems, evolved ASN-based controllers were required to carry out chaos targeting via the perturbation of the systems' governing parameter using the main enzymatic regulatory functions. In order to simulate the normal running of signalling networks, information about the system structure and dynamics was not provided. Results have indicated that uncoupled and coupled ASNs are able to find valid controllers for both dynamical systems. While CASN controllers lead to the best controllers in the Lorenz system, ASN controllers produce the best controllers in Chirikov's standard map. Further, the best evolved controllers arise from high-ordered regulatory functions, the Probabilistic Michaelis-Menten and Hill equations, in both cases.

Perhaps the most significative observation produced by the previous experiments is the capacity of crosstalk to first conform large computational models that mimic the spatial relationships in biological signalling networks and second solve highly correlated problems in a decentralised manner. For both dynamical systems, low crosstalk rates appear to be more beneficial since they are sufficient to induce a dynamical change in the coupled networks, but also to maintain unaltered the intrinsic dynamics of each sub-ASN. Conversely, high crosstalk rates induce uncorrelated noise in the form of the undesired exchange of information amongst sub-ASNs. This distorts the perceived external event and causes evolved controllers to decrease their performance. A crosstalk rate of 0.5 steadily produces the best CASN controllers in Chrikov's map while a crosstalk rate of 0.25 is sufficient to obtain near optimal CASN controllers in the Lorenz system. The benefits of crosstalk are more prominent in the Lorenz system. The two-step control task promotes the exchange of information between neighboring networks which increases the overall responsiveness of controllers and change the nature of their dynamics.

Having demonstrated the capacity of both ASN representations to successfully solve complex control task and its flexibility to evolve its architecture based on the mere interaction with their environment, the rest of this thesis deals with the development of a decentralised bio-inspired control system which can be applied to solve a physical complex problem. Locomotion in multi-legged robotic systems is an example of this kind of problems. Legs should synchronously move in a particular manner to engage locomotive movements. This thesis

aims to use CASNs to modulate sensory information and reactively alter the governing parameters of a central pattern generator (CPG), whose resulting trajectories are transformed into propelling movements using forwards and inverse kinematics. Thus, the next chapter is about T-Hex, the six legged robotic system used in this research, presents a complete kinematic analysis of such a robot and describes the simulator deployed for this task.

Chapter 5

Kinematic Analysis of the T-Hex Robot

Contents

Previous chapters introduced a novel bio-inspired architecture and its application to two different dynamic systems, located at opposite ends of the dynamic system spectrum. In both situations, the capacity of the proposed architecture to control inherently complex dynamics similar to the ones found in real world environments was illustrated. This chapter focuses on the traditional aspects of robotic control which will be considered in the next chapter as part of a decentralised bio-inspired controller for a multi-legged robotic system. This controller uses CASNs to modulate sensory feedback information and generate adequate perturbations

in a set of oscillatory trajectories. A path planning algorithm translates these trajectories into several positions in the Cartesian space, which in turn, are expressed in the joint space using kinematics.

This chapter aims to present a complete kinematic analysis of the hexapod robotic platform used in this thesis. The objective of this analysis is to describe the positional and orientation relationships underpinning synchronous motion. As part of the analysis, a standard 3R planar manipulator and the commercial PUMA 560 robot are kinematically reviewed. The study of these two robotic systems will not only provide the basis to derivate the kinematic equations describing motion in the hexapod robot, but it will also highlight the characteristics associated with its kinematical configuration. This chapter also presents the robotic platform used in this thesis as well as its 3-D simulator. The chapter concludes with the final considerations about the kinematic problem in the hexapod robotic platform.

5.1 What is "a robot"?

When the first industrial robots appeared in the early 60's, they were conventionally considered as reprogrammable, multifunctional manipulators designed to move objects through various programmed tasks (Robotics-Institute, 1984). Nowadays, the human perception of robots has drastically changed in a way that it is not possible to precisely define them. The author of this thesis understands robots as programmable electro-mechanical devices able to accomplish complex actions and exhibit autonomous behaviours based on environmental information in a reactive manner. A robotic system comprises:

- *Links*, the individual rigid bodies conforming the shape of the robot. Two or more robotic components connected together also define a link if there is no movement amongst them. Robotic systems usually comprise multiple links.

- *Joints*, the locations connecting two consecutive links. Joints allow links to have independent movements. There are two type of joints: revolute or rotatory (R), and prismatic or translatory (P). The number of joints of a manipulator determines its number of degrees of freedom (DOF).

- *Manipulators*, the robot structural elements attached to the robot body. They are made of links and joints. A manipulator is called robot when there is a tool attached to on

of its ends, and there exits a control system.

- *Wrists*, the joints connecting forearms to end-effectors. Manipulator are generally complemented with spherical wrists, which comprise three revolute joints intersecting at a common origin.

- *End-effector*, the last link of a manipulator. It has a tool attached, which performs a specific task.

- *Sensors*, the hardware elements enabling robots the sensing of their internal status and their external environment. They are integrated into the robot.

- *Controller*, the robot processing unit. It collects information from the sensors, processes it and determines the geometrical instructions in a robot.

5.2 The T-Hex Robot

Figure 5.1: T-Hex 4DOF Walking robot combo kit (Lynxmotion, 2010).

The robotic platform chosen for the work reported in this thesis is a commercial six legged robotic kit, the T-Hex 4-DOF Walking robot (see Figure 5.1), manufactured by Lynxmotion (Lynxmotion, 2003). All legs are similar and comprise four joints and four links. Each joint is independently controlled by one servo motor. This grants each leg four degrees of freedom and the robot 24 degrees of freedom. The T-Hex robot includes the following hardware components: a BASIC Atom Pro 28 pin micro controller embedded into Bot Board II, a SSC-32 servo controller and 24 HS-645MG standard servos.

In order to provide the robotic system with the capacity to sense and interact with its environment, the original T-Hex robot is extended with the following range of sensors:

- Six **Sharp GP2D12** infrared sensors: these sensors are lengthways located above each leg in a spherical base on top of the robot body. The three sensors on each side have an orientation of 45^o, 0^o and -45^o about its z-axis from the front to the rear of the robot. Each sensor provides effective distance measurements in the range of 10 to 80 cm (Parallax, 2005).

- Two **Parallax's PING**^{TM} ultrasound sensors: these sensors are placed over the x-axis of the robot, one at the front and another one at the rear. Each sensor provides non-contact distance measurements in the range of 2 cm to 3 m (Parallax, 2006).

- Six **FSR400 series** force sensing resistors: these sensors are located on the tip of every leg. They can be used either as contact or pressure sensors, providing 0 or 1 reading or values in the unit interval respectively (Interlink, 2010).

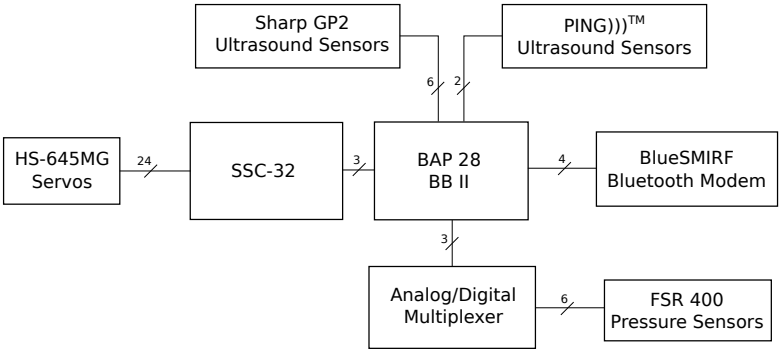

Figure 5.2: Block diagram of the fully equipped T-Hex robot.

Additionally, the robot is complemented with a 16 channel Analog/Digital MUX Breakout (Sparkfun, 2008) and a BlueSMIRF T9JRN-41-1 Bluetooth Modem (Sparkfun, 2009). The former overcomes the lack of digital input pins in the Bot Board II, while the latter equips the robot with a wireless communication system. The combination of the robot kit with these range of sensors turns the robot into an autonomous mobile system with the potential to interactively navigate around its surrounding environment. The block diagram in Figure 5.2 schematically specifies the relationships between the various hardware components. The T-Hex robot equipped with all the sensors can be seen in Figure 5.3.

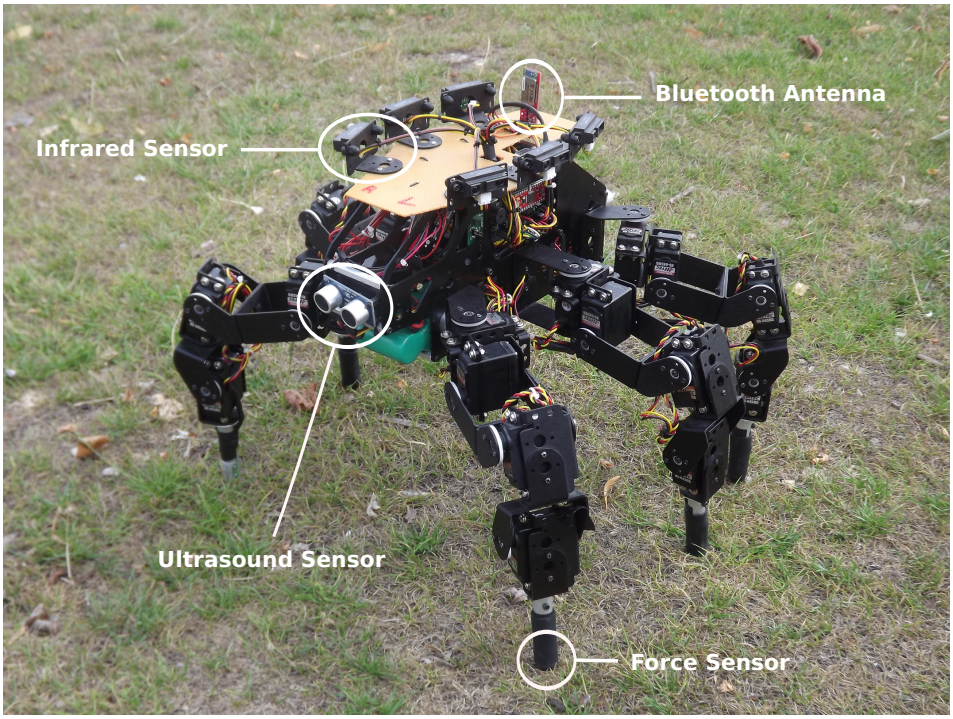

Figure 5.3: T-Hexapod robot equipped with six infrared sensors, two ultrasound sensors, six force sensors, and one bluetooth antenna.

Having described the robotic platform developed for the purpose in this thesis, the remaining of the chapter focuses on the kinematical analysis of the T-Hex robot.

5.3 Robot Kinematics

Kinematics is the study of the movement of robotic systems independently of what causes the motion. In a kinematical context, robotic systems are viewed as multi-degree of freedom manipulators, whose links are rigid bodies and joints engage the motion using pure rotations and translations. These transformations are the main elements in robot kinematics and permit the expression of link and joint parameters independently of the robotic configuration. They enable to translate link and joint parameters into different robotic configurations. A complete description of the mathematical principles underlying the kinematic problem is available in Appendix C.

The kinematic analysis of robotic systems can be divided into forward kinematics and inverse kinematics. The forward kinematic problem applies the joint parameters to describe the links' position and orientation. There always exists a forward kinematic solution for a robotic system. Inverse kinematic represents the opposite problem, which is more difficult to

solve. It considers a set of nonlinear positional equations and calculates the joint variables. For both problems, the kinematic expressions of the T-Hex problem will be derived. In order to do so, the 3R planar manipulator and the PUMA 560 commercial robot are also reviewed. The combination of the inverse kinematic solutions of these two general purpose robots makes it possible to overcome the singularities and nonlinearities of the T-Hex leg.

5.4 Forwards Kinematics

The *forward kinematic* problem can be stated as follows: given the geometrical relationships amongst the joint variables in a robotic system, determining the position and orientation of each link. A list of the mathematical symbols used along this section has been included in Appendix B.

5.4.1 The Denavit-Hartenberg Method

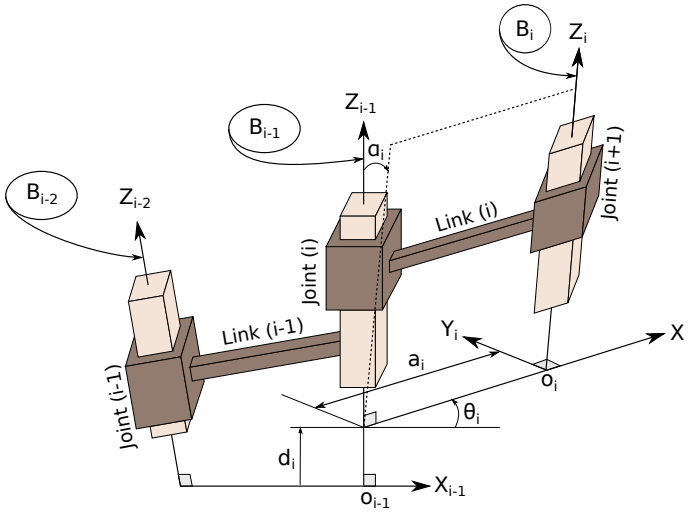

Figure 5.4: Description of a manipulator using the Denavit-Hatenberg method. The D-H parameters are defined for the *ith* joint and *ith* link. Adapted from Figure 5.2 in Jazar (2010).

The Denavit-Hartenberg (D-H) method is the systematic procedure that defines the orientation and position of two neighbouring links. It uses a minimal line representation to unambiguously define the characteristics of links and joints. The D-H notation is widely used to establish reference coordinate frames in real robot applications. Coordinate frames, and the notation used in this chapter, are introduced in Appendix C for anyone unfamiliar with this concept.

The method begins with the assumption that a manipulator with n joints has $n+1$ links. The first step is the numbering of the links. It starts from 0 and increases sequentially up to $n+1$. The link 0 is called the *fixed base link* and the link $n+1$ is called the *end-effector*. Likewise, joints are also numbered starting from 1 and increasing sequentially up to n. Therefore, the first joint connects the fixed base link with the first moving link. Following this notation the link (i) is connected to its lower link $(i-1)$ by the joint (i) and then, to its upper link $(i+1)$ by the joint $(i+1)$, as shown in Figure 5.4.

During the second step, a local coordinate frame B_i is attached to each link i at the joint $i+1$. Alternatively, it is also possible to assign the frame B_i to the joint i (Wolovich, 1987). A D-H coordinate frame, in both notations, is established as follows:

- The z_i-axis is chosen along the $i+1$ joint axis.
- The x_i-axis is aligned with the common normal from z_{i-1}- to z_i-axis and O_i is located at the intersection of x_i- with z_i-axis.
- The y_i-axis is determined from x_i- and z_i-axis using the right-hand rule.

Once all D-H frames are defined, the final step characterises each frame using the following four parameters:

- *Link length*, a_i, the distance between O_{i-1} and O_i.
- *Link twist*, α_i, the required rotation about x_i-axis that carries z_i-axis parallel to z_{i-1}-axis.
- *Joint distance*, d_i, the distance between x_{i-1}- and x_i-axis along the z_{i-1}-axis.
- *Joint angle*, θ_i, the required rotation about z_i-axis that carries x_i-axis parallel to x_{i-1}-axis.

An illustration of the four D-H parameters defining the coordinate frame i associated with the link i can be seen in Figure 5.4. Particularly, the parameters θ_i and d_i, known as *joint parameters*, determine the position of two consecutive links connected through the joint i. Likewise, the parameters a_i and α_i, termed *link parameters*, characterise the position of the joints $i-1$ and i on each end of the link i. For any manipulator, a_i and α_i are constant and defined by its physical configuration at the joint i for the link i.

The kinematical configuration of each coordinate frame is commonly summarised in a D-H table, as shown below in Table 5.1. Such a table has five columns showing the frame index and the four D-H parameters.

Table 5.1: D-H table for establishing link relationships

Frame No.	a_i	α_i	d_i	θ_i
1	a_1	α_1	d_1	θ_1
2	a_2	α_2	d_2	θ_2
...	...	...	...	...
n	a_n	α_n	d_n	θ_n

5.4.2 Transformation between Adjacent Frames

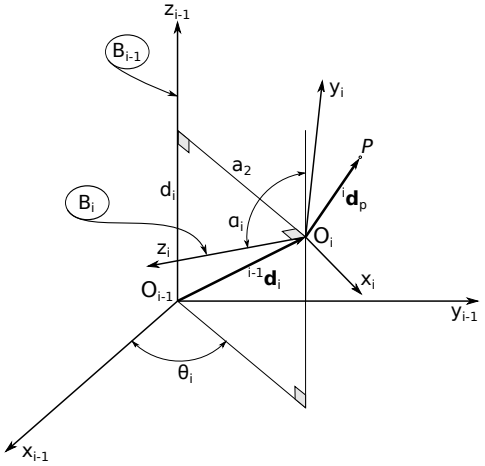

Figure 5.5: Two connected coordinate frames defined by the D-H parameters. Adapted from Figure 5.8 in Jazar (2010).

Considering the two coordinate frames B_{i-1} and B_i defined according to the D-H method in Figure 5.5. The representation of B_i in B_{i-1} is a transformation matrix ${}^{i-1}T_i$ resulting from the combination of four homogeneous transformations.

1. A translation about the z_i-axis by a distance d_i, D_{z_{i-1},d_i}.

2. A rotation of θ_i degrees about the translated z_i-axis, R_{z_{i-1},θ_i}.

3. A translation about the x_i-axis by a distance a_i, D_{x_{i-1},a_i}

4. A rotation of α_i degrees about the translated x_i-axis, R_{x_{i-1},α_i}.

The product of these transformations provides the Denavit-Hartenberg transformation ${}^{i-1}T_i$:

$$\begin{aligned} {}^{i-1}T &= D_{z_{i-1},d_i} R_{z_{i-1},\theta_i} D_{x_{i-1},a_i} R_{x_{i-1},\alpha_i} \\ &= \begin{bmatrix} \cos\theta_i & -\sin\theta_i \cos\alpha_i & \sin\theta_i \sin\alpha_i & a\cos\theta_i \\ \sin\theta_i & \cos\theta_i \cos\alpha_i & -\cos\theta_i \sin\alpha_i & a\sin\theta_i \\ 0 & \sin\alpha_i & \cos\alpha_i & d_i \\ 0 & 0 & 0 & 1 \end{bmatrix} \end{aligned} \tag{5.1}$$

where,

$$R_{x_{i-1},\alpha_i} = \begin{bmatrix} 1 & 0 & 0 & 0 \\ 0 & \cos\alpha_i & -\sin\alpha_i & 0 \\ 0 & \sin\alpha_i & \cos\alpha_i & 0 \\ 0 & 0 & 0 & 1 \end{bmatrix} \tag{5.2}$$

$$R_{z_{i-1},\theta_i} = \begin{bmatrix} \cos\theta_i & -\sin\theta_i & 0 & 0 \\ \sin\theta_i & \cos\theta_i & 0 & 0 \\ 0 & 0 & 1 & 0 \\ 0 & 0 & 0 & 1 \end{bmatrix} \tag{5.4}$$

$$D_{x_{i-1},a_i} = \begin{bmatrix} 1 & 0 & 0 & a_i \\ 0 & 1 & 0 & 0 \\ 0 & 0 & 1 & 0 \\ 0 & 0 & 0 & 1 \end{bmatrix} \tag{5.3}$$

$$D_{z_{i-1},d_i} = \begin{bmatrix} 1 & 0 & 0 & 0 \\ 0 & 1 & 0 & 0 \\ 0 & 0 & 1 & d_i \\ 0 & 0 & 0 & 1 \end{bmatrix} \tag{5.5}$$

The transformation equation that unambiguously describes a rigid body in relation to the coordinate frame B_i with respect to its previous coordinate frame B_{i-1} is

$$\begin{bmatrix} x_{i-1} \\ y_{i-1} \\ z_{i-1} \\ 1 \end{bmatrix} = {}^{i-1}T_i \begin{bmatrix} x_i \\ y_i \\ z_i \\ 1 \end{bmatrix} \tag{5.6}$$

The transformation matrix ${}^{i-1}T_i$ can also be seen as the combination of a unique rotation and a unique translation.

$${}^{i-1}T_i = \begin{bmatrix} {}^{i-1}R_i & {}^{i-1}\mathbf{d}_i \\ 0 & 1 \end{bmatrix} \tag{5.7}$$

Given the D-H transformation matrices between the successive frames of a multiple-link manipulator, the kinematic analysis is mathematically stated as,

$$ {}^{n}T_0 = {}^{0}T_1(q_1)\,{}^{1}T_2(q_2)\,{}^{2}T_3(q_3)\ldots{}^{n-1}T_n(q_n) \tag{5.8} $$

where non-linear joint variables are:

$$ \mathbf{q} = [q_1, q_2, q_3, \ldots, q_n] \tag{5.9} $$

Formally, the finding of a point P in the global coordinate frame given the joint variables is called *forward kinematics*. On the contrary, the determination of the joint variables given the links configuration is called *inverse kinematics*.

5.4.3 An Articulated 3R Planar Manipulator

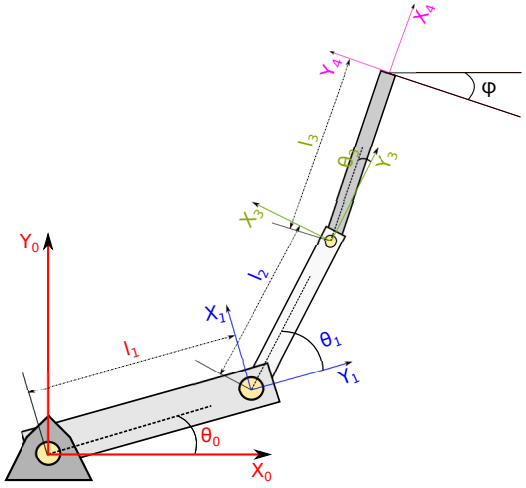

Figure 5.6: Illustration of a 3R planar manipulator. Adapted from Figure 5.15 in Jazar (2010)

Figure 5.6 shows a 3R planar manipulator ($R\,||R\,||R$) with three revolute joints (3-DOF), described using the D-H method. A manipulator is said to be planar when all the joint axes are parallel, then $\alpha_i = 0^o$ or 180^o.Table 5.2 summarises the D-H parameters associated with each link.

Table 5.2: D-H table of the 3R planar manipulator shown in Figure 5.6.

Frame No.	a_i	α_i	d_i	θ_i
1	l_1	0	0	θ_1
2	l_2	0	0	θ_2
3	l_3	0	0	θ_3

The direct substitution of the D-H parameters in Equation (5.1) leads to the individual transformation matrices (5.10) - (5.12) of the 3R planar manipulator.

$$ {}^{0}T_1 = \begin{bmatrix} \cos\theta_1 & -\sin\theta_1 & 0 & l_1\cos\theta_1 \\ \sin\theta_1 & \cos\theta 1 & 0 & l_1\sin\theta_1 \\ 0 & 0 & 1 & 0 \\ 0 & 0 & 0 & 1 \end{bmatrix} \tag{5.10} $$

$$ {}^{1}T_2 = \begin{bmatrix} \cos\theta_2 & -\sin\theta_2 & 0 & l_2\cos\theta_2 \\ \sin\theta_2 & \cos\theta 2 & 0 & l_2\sin\theta_2 \\ 0 & 0 & 1 & 0 \\ 0 & 0 & 0 & 1 \end{bmatrix} \tag{5.11} $$

$$ {}^{2}T_3 = \begin{bmatrix} \cos\theta_3 & -\sin\theta_3 & 0 & l_3\cos\theta_3 \\ \sin\theta_3 & \cos\theta 3 & 0 & l_3\sin\theta_3 \\ 0 & 0 & 1 & 0 \\ 0 & 0 & 0 & 1 \end{bmatrix} \tag{5.12} $$

The overall transformation matrix relating the position of the manipulator end-effector with respect to the global frame is,

$$ \begin{aligned} {}^{0}T_3 &= {}^{0}T_1\,{}^{1}T_2\,{}^{2}T_3 \equiv \\ &\equiv \begin{bmatrix} \cos(\theta_1+\theta_2+\theta_3) & -\sin(\theta_1+\theta_2+\theta_3) & 0 & r_{14} \\ \sin(\theta_1+\theta_2+\theta_3) & \cos(\theta_1+\theta_2+\theta_3) & 0 & r_{24} \\ 0 & 0 & 1 & 0 \\ 0 & 0 & 0 & 1 \end{bmatrix} \end{aligned} \tag{5.13} $$

where,

$$r_{14} = l_1 \cos\theta_1 + l_2 \cos(\theta_1 + \theta_2) + l_3 \cos(\theta_1 + \theta_2 + \theta_3) \tag{5.14}$$

$$r_{24} = l_1 \sin\theta_1 + l_2 \sin(\theta_1 + \theta_2) + l_3 \sin(\theta_1 + \theta_2 + \theta_3) \tag{5.15}$$

5.4.4 The Puma 560 Robot

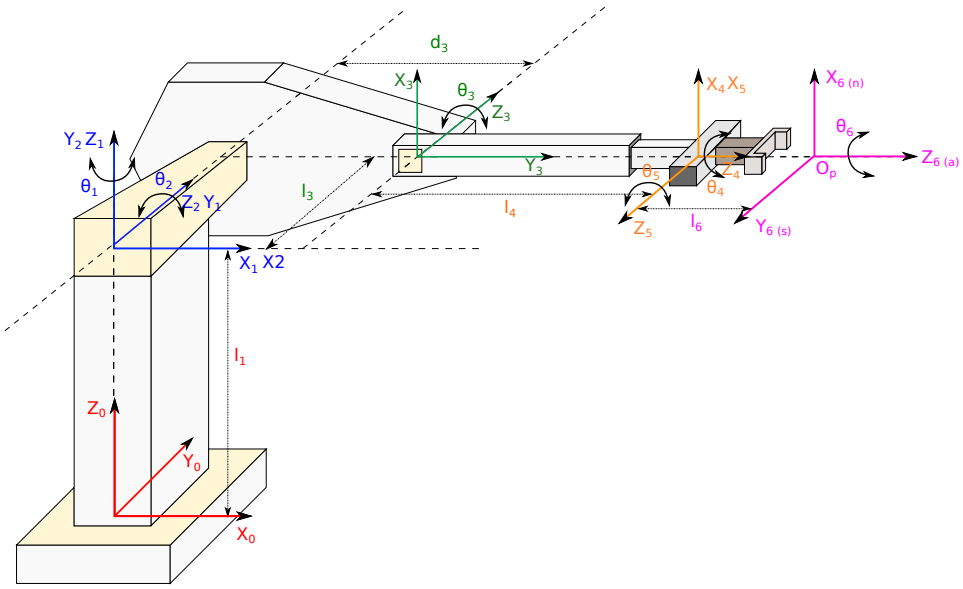

Figure 5.7: Illustration of the PUMA 560 robot with a spherical wrist. Adapted from Figure 2.4.29 in Wolovich (1987).

Figure 5.7 shows the Puma 560 robot. It consists of a robotic arm and spherical wrist with a gripper attached to its end-effector. In total, the robot has six degrees of freedom: three in the arm and another three at the wrist. Table 5.3 summaries the D-H parameters associated to each link.

Table 5.3: D-H table of the PUMA 560 robot with spherical wrist shown in Figure 5.7.

Frame No.	a_i	α_i	d_i	θ_i
1	0	0^o	l_1	θ_1
2	0	-90^o	0	θ_2
3	d_3	0^o	l_3	θ_3
4	0	-90^o	l_4	θ_4
5	0	-90^o	0	θ_5
6	0	$+90^o$	l_6	θ_6

The direct substitution of the D-H parameters in Equation (5.1) leads to the individual transformation matrices of the PUMA robot, whose multiplication provides the overall transformation matrix (5.16) and relates the manipulator gripper to the robot global frame. The approximation vectors $\hat{\mathbf{n}}$, $\hat{\mathbf{s}}$ and $\hat{\mathbf{a}}$ denote the gripper orientation while the vector $\hat{\mathbf{p}}$ captures its position. A detailed description of the transformation matrices of the PUMA 560 robot are can be found in Wolovich (1987).

$$ {}^{0}T_{6} = {}^{0}T_{1}\,{}^{1}T_{2}\,{}^{2}T_{3}\,{}^{3}T_{4}\,{}^{4}T_{5}\,{}^{5}T_{6} = \begin{bmatrix} & {}^{0}R_{6} & & {}^{0}D_{6} \\ 0 & 0 & 0 & 1 \end{bmatrix} \equiv \begin{bmatrix} n_x & s_x & a_x & p_x \\ n_y & s_y & a_y & p_y \\ n_z & s_z & a_z & p_z \\ 0 & 0 & 0 & 1 \end{bmatrix} \tag{5.16} $$

5.4.5 T-Hex Robot

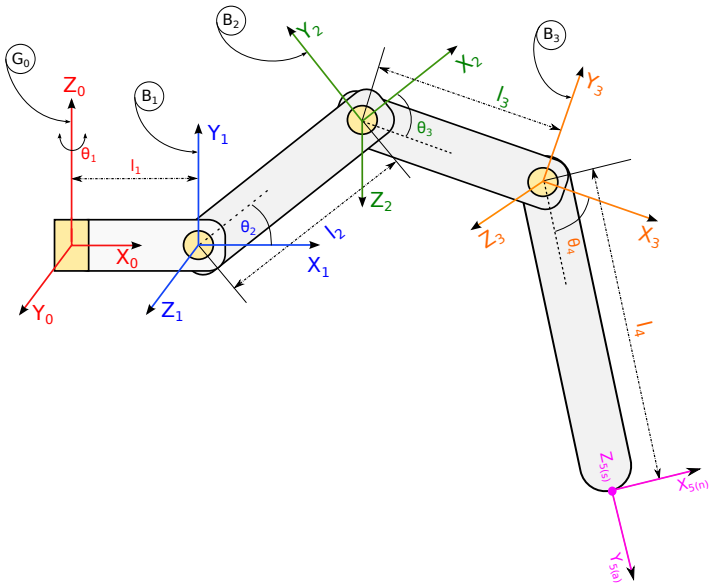

Figure 5.8: Illustration of a T-Hex robotic leg showing its kinematic configuration.

A schematic representation of a real T-Hex leg is illustrated above in Figure 5.8. The T-Hex robot comprises six legs. Each leg moves independently and has four degrees of freedom in the form of four revolute joints: one perpendicular followed by three disposed in parallel, $(R \perp R \,||\, R \,||\, R)$.

The forward kinematic of the T-Hex robot is produced through two steps. Firstly, the leg tip is described in relation to the point where each leg is attached to the body. Secondly,

the leg tip is defined with regard to the center of the robot. Some authors omit this first step and describe the leg tip directly from the center of the robot (Potts & da Cruz, 2011). Nevertheless, this requires the definition of a passive joint between the leg and the robot, which increases the complexity of the kinematic analysis.

In contrast to Mankegh et al. (2011), the forward kinematic analysis presented here assumes frames G and B_1 have a common x-axis, therefore $d_1 = 0$. In the real robot, d_1 is $\approx 4\,mm$. This means that the coordinate frames G_0 and B_1 become parallel along their x-axis, which entails a minimal loss of accuracy, but simplifies the kinematic problem in the T-Hex robot. The analysis starts by defining a global coordinate frame with its origin at the T-Hex leg base to locally describe the leg tip. Table 5.4 summarises the D-H parameters of each link in a T-Hex robotic leg.

Table 5.4: D-H table of a T-Hexapod robotic leg shown in Figure 5.8

Frame No	a_i	α_i	d_i	θ_i
1	l_1	90^o	0	θ_1
2	l_2	0	0	θ_2
3	l_3	0	0	θ_3
4	l_4	0	0	θ_4

The direct substitution of the D-H parameters in Equation (5.1) leads to the individual transformation matrices (5.17) - (5.20) of the T-Hex robot leg.

$$ {}^{0}T_1 = \begin{bmatrix} \cos\theta_1 & 0 & \sin\theta_1 & l_1\cos\theta_1 \\ \sin\theta_1 & 0 & -\cos\theta_1 & l_1\sin\theta_1 \\ 0 & 1 & 0 & 0 \\ 0 & 0 & 0 & 1 \end{bmatrix} \tag{5.17} $$

$$ {}^{2}T_3 = \begin{bmatrix} \cos\theta_3 & -\sin\theta_3 & 0 & l_3\cos\theta_3 \\ \sin\theta_3 & \cos\theta_3 & 0 & l_3\sin\theta_3 \\ 0 & 0 & 1 & 0 \\ 0 & 0 & 0 & 1 \end{bmatrix} \tag{5.18} $$

$$ {}^{1}T_{2} = \begin{bmatrix} \cos\theta_2 & -\sin\theta_2 & 0 & l_2\cos\theta_2 \\ \sin\theta_2 & \cos\theta_2 & 0 & l_2\sin\theta_2 \\ 0 & 0 & 1 & 0 \\ 0 & 0 & 0 & 1 \end{bmatrix} \tag{5.19} $$

$$ {}^{3}T_{4} = \begin{bmatrix} \cos\theta_4 & -\sin\theta_4 & 0 & l_4\cos\theta_4 \\ \sin\theta_4 & \cos\theta_4 & 0 & l_4\sin\theta_4 \\ 0 & 0 & 1 & 0 \\ 0 & 0 & 0 & 1 \end{bmatrix} \tag{5.20} $$

The overall transformation matrix relating the position of the leg tip with respect to the global frame is given by Equation 5.21.

$$ {}^{0}T_{6} = {}^{0}T_{1}\,{}^{1}T_{2}\,{}^{2}T_{3}\,{}^{3}T_{4} = \begin{bmatrix} & {}^{0}R_{4} & & {}^{0}D_{4} \\ 0 & 0 & 0 & 1 \end{bmatrix} \equiv \begin{bmatrix} n_x & s_x & a_x & p_x \\ n_y & s_y & a_y & p_y \\ n_z & s_z & a_z & p_z \\ 0 & 0 & 0 & 1 \end{bmatrix} \tag{5.21} $$

where the orientation of the manipulator tip is given by $\hat{\mathbf{n}}$, $\hat{\mathbf{s}}$ and $\hat{\mathbf{a}}$ in the form,

$$ n_x = \cos(\theta_2+\theta_3+\theta_3)\cos\theta_1 \tag{5.22} $$

$$ n_y = \cos(\theta_2+\theta_3+\theta_3)\sin\theta_1 \tag{5.23} $$

$$ n_z = \sin(\theta_2+\theta_3+\theta_3) $$

$$ o_x = -\sin(\theta_2+\theta_3+\theta_4)\cos\theta_1 \tag{5.24} $$

$$ o_y = -\cos(\theta_2+\theta_3+\theta_4)\sin\theta_1 \tag{5.25} $$

$$ o_z = \cos(\theta_2+\theta_3+\theta_4) \tag{5.26} $$

$$ \tag{5.27} $$

$$a_x = \sin\theta_1 \tag{5.28}$$

$$a_y = -\cos\theta_1 \tag{5.29}$$

$$a_z = 0 \tag{5.30}$$

and the position $\hat{\mathbf{p}}$ is given by,

$$p_x = \cos\theta_1(l_1 + l_2\cos\theta_2 + l_3\cos(\theta_2+\theta_3) + l_4\cos(\theta_2+\theta_3+\theta_4)) \tag{5.31}$$

$$p_y = \sin\theta_1(l_1 + l_2\cos\theta_2 + l_3\cos(\theta_2+\theta_3) + l_4\cos(\theta_2+\theta_3+\theta_4)) \tag{5.32}$$

$$p_z = l_2\cos\theta_2 + l_3\cos(\theta_2+\theta_3) + l_4\cos(\theta_2+\theta_3+\theta_4) \tag{5.33}$$

Figure 5.9 illustrates four different and randomly chosen valid configurations of a T-Hex robotic leg given the rotational angles θ_i of each joint. Particularly, Figure 5.9a represents the initial motionless position of each leg.

The second step of the forward kinematic analysis relates the global coordinate frame of the T-Hex leg G_0 with regard to the torso global coordinate frame G_R. For convenience, the X_{G_R}- and Y_{G_R}-axis refers to the forward and lateral motion of the robot respectively. Figure 5.10 schematically illustrates the relationship between G_0 and G_R where, P_0 indicates the position of the leg limb with respect to G_0, P_G defines the position of the leg limb with respect to G_R and θ is the rotation of the leg about the Z_0-axis. Therefore, the transformation matrix ${}^{R}T_0$ to relate the robot frame with the leg frame is:

$${}^{R}T_0 = \begin{bmatrix} \cos\theta & 0 & \sin\theta & p_{0_x} \\ 0 & 1 & 0 & p_{0_y} \\ -\sin\theta & 0 & \cos\theta & p_{0_z} \\ 0 & 0 & 0 & 1 \end{bmatrix} = \begin{bmatrix} R_{z_0,\theta} & {}^{G}\mathbf{d}_0 \\ 0 & 1 \end{bmatrix} \tag{5.34}$$

where $p_{0_x} = X_{offset}$, $p_{0_y} = Y_{offset}$ and $p_{0_z} = 0$. Attending to the robot dimensions summarised in Table 5.5, the leg angular configuration shown in Figure 5.9a, the initial lengthways leg rotations of 45^0, 0^0 and -45^0 from the front to the rear, the set of transformation matrices derived in Equations (5.17)-(5.20), the tip-leg transformation matrix (5.21) and the leg-robot transformation matrix (5.34), the kinematical representation of the T-Hex robot in its motionless position is shown in Figure 5.11.

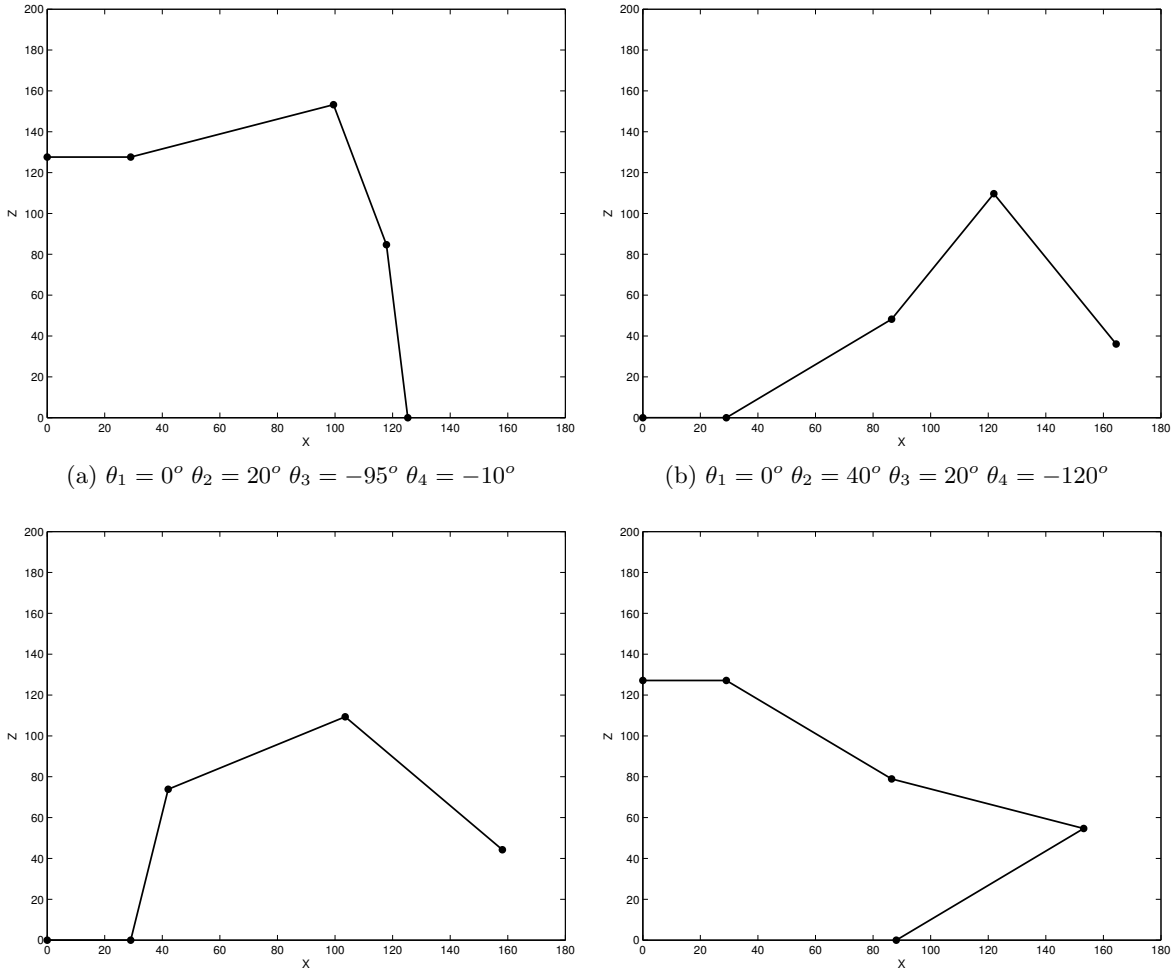

(a) $\theta_1 = 0^o\ \theta_2 = 20^o\ \theta_3 = -95^o\ \theta_4 = -10^o$

(b) $\theta_1 = 0^o\ \theta_2 = 40^o\ \theta_3 = 20^o\ \theta_4 = -120^o$

(c) $\theta_1 = 0^o\ \theta_2 = 80^o\ \theta_3 = -50^o\ \theta_4 = -80^o$

(d) $\theta_1 = 0^o\ \theta_2 = -40^o\ \theta_3 = 20^o\ \theta_4 = -120^o$

Figure 5.9: Samples of different configurations of a T-Hexapod leg using forward Kinematics.

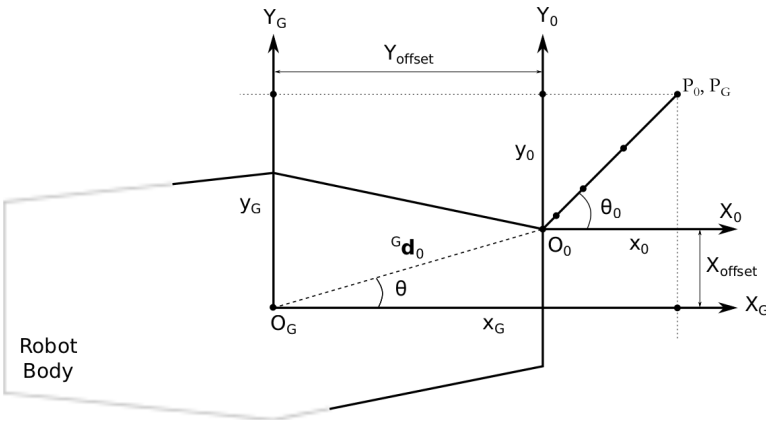

Figure 5.10: Relationship between leg G_0 and robot G_R coordinate frames. While the former frame describes link positions within the leg scope, the latter translates these positions to the center of the robot given the displacement ${}^{G}\mathbf{d}_0$ and the rotation θ_0.

5.5 Inverse Kinematics

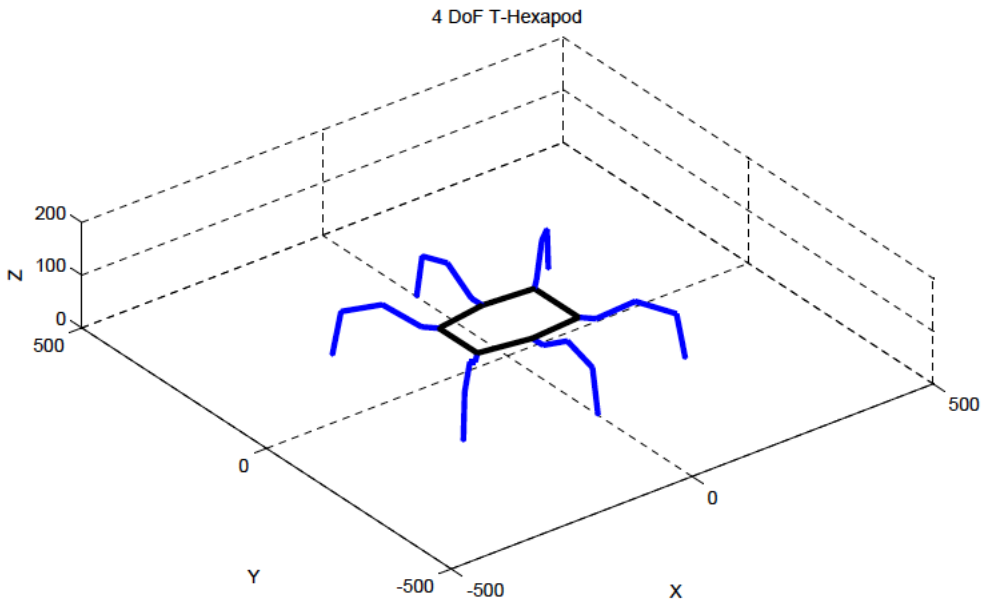

Figure 5.11: Kinematical model of the T-Hex robot using forward kinematics.

Inverse kinematic is a nonlinear problem in which finding a set of joint variables produces a specific end-effector position and orientation. There is no a general solution to solve the inverse kinematic problem. A manipulator is solvable when it is possible to calculate all its joint variables for a particular position and orientation. Considering the previous definition, inverse kinematic methods provide two types of solutions: numerical and analytical. While the former relies on computationally expensive approximation methods to iteratively converge to the solution and avoid joint redundancies (Craig, 1989), the latter is based on non-iterative analytical expressions to find the solutions of robotic manipulators with very few degrees of freedom by the direct resolution of polynomial equations (Paul, 1981). The computation of analytical solutions is also very fast, which has a great importance in real time applications (Baerlocher, 2001). However, analytical methods fail to find the solution for conventional robots with 6 or more degrees of freedom. This manuscript considers more appropriate the analytical approach to solve the inverse kinematic problem in the T-Hex robot because it does not have redundant solutions and these can be directly obtain using trigonometrical expressions which also increases the computation time. Likewise, it is possible to distinguish two types of analytical solutions: algebraic and geometric (Jazar, 2010).

The presence of coupled nonlinear equations in the inverse kinematic problem entails two

main problems: the existence of a kinematic solution and the existence of multiple solutions. Trigonometric equations aggravate these problems as they are inherently redundant. A kinematic solution exists if the desired point lies within the space the manipulator can reach in at least one direction. This space is known as the robot *workspace*. Joint mechanical limits often reduce drastically the robot workspace. The multiple solution problem is normally heuristically solved. The robotic system should decide in advance the posture to adopt. A general decision criteria is the proximity of the new desired position, which minimises the movement of each joint. However, the existence of obstacles in the robot workspace may force a change in the criteria to prevent collisions. Additionally, a list of the mathematical symbols used along this section has been also included in Appendix B.

Table 5.5: Summary of the T-Hex robot dimension in milimeters.

Robot Component	Dimension
Tar Link Length (l_4)	85 mm
Tibia Link Length (l_3)	71 mm
Femur Link Length (l_2)	75 mm
Coxa Link Length (l_1)	29 mm
Torso Length	204 mm
Torso Front Width	104 mm
Torso Middel Width	136 mm
Torso Rear Width	120 mm

5.5.1 An Articulated 3R Planar Manipulator

Figure 5.6 describes an articulated 3R planar manipulator according to its coordinate frames. The manipulator comprises three links connected thought three parallel revolute joints. Because the manipulator is planar, its orientation will only have one degree of freedom. Further, 3R planar manipulators are highly redundant. This means that such manipulators will equally attain any desired point in their workspace with one degree of freedom less. The main consequence of this is the existence of an infinite number of kinematic solution. However, redundancy may also be beneficial as it increases the manipulator maneuverability. To mitigate this situation, the orientation of the manipulator ϕ is determined in advance, so that the end-effector becomes totally described. ϕ reduces the number of valid kinematic solutions to a maximum of two configurations.

Considering the forward kinematics in Equation (5.13), the inverse kinematic problem

entails the solution of the following three nonlinear equations:

$$X = l_1 \cos\theta_1 + l_2 \cos(\theta_1 + \theta_2) + l_3 \cos(\theta_1 + \theta_2 + \theta_3) \tag{5.35}$$

$$Y = l_1 \sin\theta_1 + l_2 \sin(\theta_1 + \theta_2) + l_3 \sin(\theta_1 + \theta_2 + \theta_3) \tag{5.36}$$

$$\phi = \theta_1 + \theta_2 + \theta_3 \tag{5.37}$$

where Equations (5.35) and (5.36) refers to end-effector position and correspond to the elements r_{14} and r_{24} of the transformation matrix (5.13) and Equation (5.37) is the end-effector orientation and can be derived from,

$$\phi = \text{atan2}\,\frac{\sin(\theta_1 + \theta_2 + \theta_3)}{\cos(\theta_1 + \theta_2 + \theta_3)} = \frac{r_{12}}{r_{11}} \tag{5.38}$$

where r_{12} and r_{11} are also elements in Equation (5.13). Substituting Equation (5.37) into Equations (5.35) and (5.36), the number of nonlinear equations is reduced to two.

$$X - l_3 \cos\phi = l_1 \cos\theta_1 + l_2 \cos(\theta_1 + \theta_2) \tag{5.39}$$

$$Y - l_3 \sin\phi = l_1 \sin\theta_1 + l_2 \sin(\theta_1 + \theta_2) \tag{5.40}$$

These equations indirectly separate the position (right-hand side) and orientation (left-hand side) of the end-effector. Hence, the solution of the inverse kinematic problem will only depend on the end-effector position, which is known. Renaming, $X_\phi = X - l_3 \cos\phi$ and $Y_\phi = Y - l_3 \sin\phi$, squaring and adding Equations (5.39) and (5.40) gives,

$$X_\phi^2 + Y_\phi^2 = (l_1 \cos\theta_1 + l_2 \cos(\theta_1 + \theta_2))^2 + (l_1 \sin\theta_1 + l_2 \sin(\theta_1 + \theta_2))^2 \tag{5.41}$$

Simplifying this equation yields,

$$X_\phi^2 + Y_\phi^2 = l_1^2 + l_2^2 + 2l_1 l_2 \cos\theta_2 \tag{5.42}$$

Now, θ_2 can be obtained in the form,

$$\cos\theta_2 = \frac{X_\phi^2 + Y_\phi^2 - l_1^2 + l_2^2}{2l_1 l_2} \tag{5.43}$$

and,

$$\theta_2 = \arccos\frac{X_\phi^2 + Y_\phi^2 - l_1^2 + l_2^2}{2l_1 l_2} \tag{5.44}$$

For a solution to exist, the right-hand side of Equation (5.43) must be in the range $[-1, 1]$. Assuming it does exist, the half angle trigonometrical relationship is used to find θ_2, as it avoids the inaccuracy associated to the arccos expression.

$$\theta_2 = \pm 2\text{atan2}\sqrt{\frac{(l_1 + l_2)^2 - (X_\phi^2 + Y_\phi^2)^2}{(X_\phi^2 + Y_\phi^2)^2 - (l_1 + l_2)^2}} \tag{5.45}$$

The sign in this equation indicates the existence of multiple solutions. These two solutions are called *elbow-up* and *elbow-down*. They correspond to the triangle formed by the first two links as shown in Figure 5.12. In the case of the 3R planar robot, the validity of the solutions will depend of the position of the manipulator base. If it is parallel with respect to the ground, the *elbow-down* solution is unreachable.

Now, θ_1 can be found using θ_2 in the form,

$$\theta_1 = \text{atan2}\,\frac{Y}{X} \;\pm\; \text{atan2}\,\frac{l_2 \sin\theta_2}{l_1 + l_2\cos\theta_2} \tag{5.46}$$

where the negative and positive signs correspond to the *elbow-down* and *elbow-up* solutions respectively. Knowing θ_1 and θ_2, the solution for θ_3 is written as,

$$\theta_3 = \phi - \theta_1 - \theta 2 \tag{5.47}$$

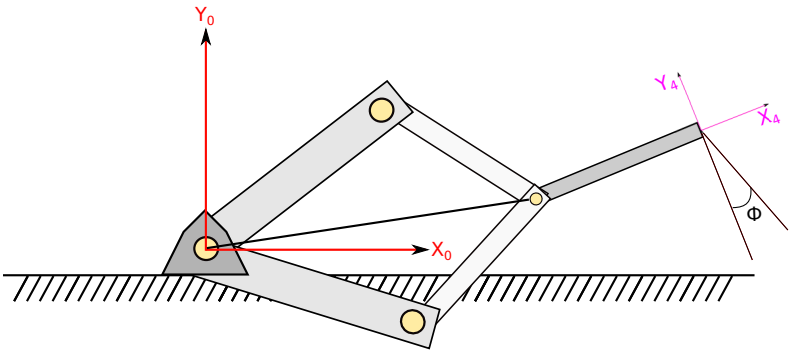

Figure 5.12: Elbow-up and elbow-down solutions in the 3R planar manipulator. Although, the inverse kinematic problem provides the elbow-down solution, this is unattainable. The first link of the 3R manipulator collides with the ground.

5.5.2 The Puma 560 Robot

In manipulators with more than three degrees of freedom, the inverse kinematic problem provides also the joint variables to attain a desired point within a desired orientation. The starting point is the decoupling of the inverse kinematic problem into two independent subtasks, known as *inverse position* and *inverse orientation*, each with a maximum of three unknown variables. This is a consequence of the high dependence between elements in the transformation matrix resulting from the direct kinematics (Jazar, 2010). Taking into account the decoupling principle, the overall transformation matrix can be decomposed into rotation and translation,

$$ {}^0T_n = \begin{bmatrix} {}^0R_n & {}^0\mathbf{d}_n \\ 0 & 1 \end{bmatrix} = {}^0D_n\,{}^0R_n = \begin{bmatrix} \mathbf{I} & {}^0\mathbf{d}_n \\ 0 & 1 \end{bmatrix} \begin{bmatrix} {}^0R_n & 0 \\ 0 & 1 \end{bmatrix} \tag{5.48} $$

where n indicates the number of degrees of freedom up to a maximum of six, ${}^0D_n$ is the translation matrix and encapsulates the three joint variables describing the position of the end-effector, and ${}^0R_n$ is the rotation matrix and comprises the additional joint variables, which describe the orientation of the end-effector.

$$ {}^0T_6 = T_{arm}T_{wrist} = {}^0T_3\,{}^3T_6 \tag{5.49} $$

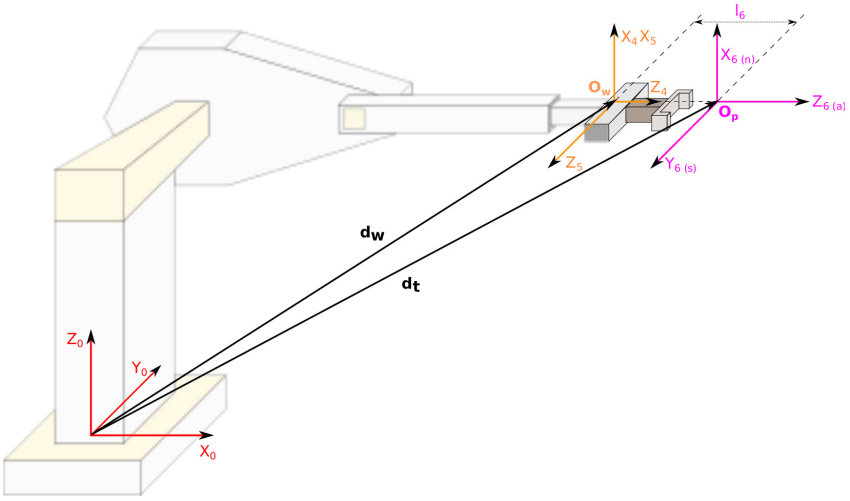

Figure 5.13: Application of the decoupling technique in the Puma 560 robot. Adapted from Figure 2.4.29 in Wolovich (1987). The inverse kinematic problem is divided into two independent subtasks: the calculation of the arm and wrist joints' angles. Each task computes three angles.

The PUMA 560 robot, illustrated in Figure 5.7 is a six degrees of freedom robot with a spherical wrist made of three revolute joints. The fact that all wrist axis converge to the same origin O_w enables the separation of the arm and wrist kinematics into two problems, the *arm position* and *wrist orientation*. Then, the overall transformation matrix of the PUMA 560 robot is decomposed in arm and wrist transformation matrices.

Following an algebraic approach, the inverse kinematic solution of the PUMA 560 starts with the description of robot wrist with regard to the robot tip. Figure 5.13 defines the robot end-effector in terms of two displacement vectors d_w and d_t from the global coordinate frame to the wrist and tip coordinate frames respectively. Considering the approximation vector $\hat{\mathbf{a}}$ and the length of the end-effector l_6, the position of the tip relative to the global coordinate frame is given by the addition of two vectors:

$$d^t = {}^0d_6 = \begin{bmatrix} p_x \\ p_y \\ p_z \end{bmatrix} = d^w + l_6 \cdot \mathbf{a} = d^w + \begin{bmatrix} l_6 a_x \\ l_6 a_y \\ l_6 a_z \end{bmatrix} \tag{5.50}$$

Thus, the position of the wrist can be unambiguously described in terms of the robot tip, which enables the solving of the arm position and rotation problems independently.

$$d_w \equiv \begin{bmatrix} p_{x_w} \\ p_{y_w} \\ p_{z_w} \end{bmatrix} = \begin{bmatrix} p_x - l_6 a_x \\ p_y - l_6 a_y \\ p_z - l_6 a_z \end{bmatrix} \tag{5.51}$$

d_w is the wrist position described from the robot tip. However, this position can also be defined relative to the PUMA 560 global coordinate frame using the positional column ${}^0d_4$ of the transformation matrix ${}^0T_4$. Therefore,

$$d_w = {}^0d_4 \equiv \begin{bmatrix} p_{x_w} \\ p_{y_w} \\ p_{z_w} \end{bmatrix} \tag{5.52}$$

Using the Pieper or inverse transformation technique (Jazar, 2010), the positional equation of the PUMA 560 robot can be derived from its individual transformation matrices. Such a technique relies on the fact that the multiplication of a transformation matrix by its inverse is equal to the identity matrix. This reduces the correlation between the kinematical nonlinear

equations. The joint variables can be found by the solution of the following equalities.

$$ {}^{0}T_{1}^{-1}\,{}^{0}T_{4} = {}^{0}T_{1}^{-1}({}^{0}T_{1}\,{}^{1}T_{2}\,{}^{2}T_{3}\,{}^{3}T_{4}) = {}^{1}T_{4} \tag{5.53} $$

$$ {}^{1}T_{2}^{-1}\,{}^{1}T_{4} = {}^{1}T_{2}^{-1}({}^{1}T_{2}\,{}^{2}T_{3}\,{}^{3}T_{4}) = {}^{2}T_{4} \tag{5.54} $$

$$ {}^{2}T_{3}^{-1}\,{}^{2}T_{4} = {}^{2}T_{3}^{-1}({}^{2}T_{3}\,{}^{3}T_{4}) = {}^{3}T_{4} \tag{5.55} $$

$$ {}^{3}T_{4}^{-1}\,{}^{3}T_{4} = {}^{3}T_{4}^{-1}\,{}^{3}T_{4} = \mathbf{I} \tag{5.56} $$

$$ \tag{5.57} $$

A detailed solution of the inverse kinematic problem in the PUMA 560 robot can be found in (Wolovich, 1987).

5.5.3 The T-Hex Robot

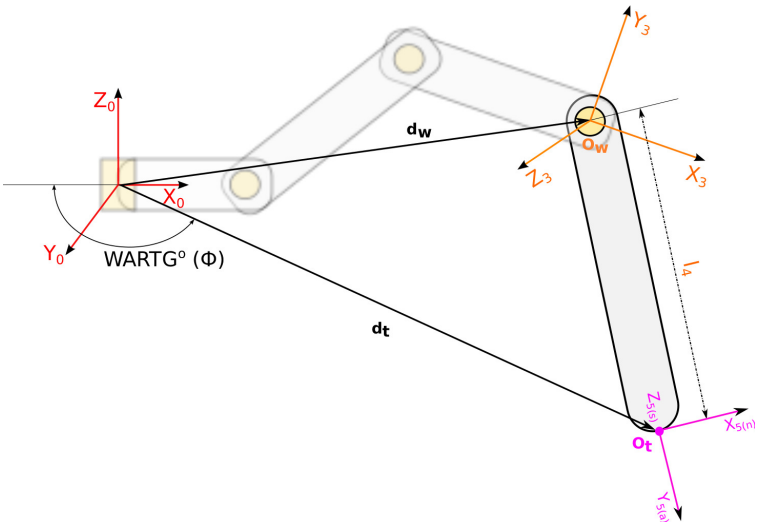

Figure 5.14: Application of the decoupling technique in the T-hexapod robot leg. The wrist has only one degree of freedom.

As mentioned at the beginning of this chapter, each of the six legs of the T-Hex robot has four degrees of freedom (see Figure 5.8). All legs are similarly disposed, starting with a perpendicular joint followed by another three joints disposed in parallel. This configuration presents two main consequences. Firstly, the leg workspace is not planar. Hence, the inverse kinematic problem is decoupled into leg position and leg orientation. Secondly, each leg is redundant. This implies the desired orientation of the leg tip should be specified in advance. In this context, the leg orientation is termed Wrist Angle Relative to Ground or WARG (Koyuncu & Güzel, 2008). In an attempt to simplify the inverse kinematic problem, the

WARG angle, illustrated in Figure 5.14, is always constant and here, it is established based on the T-Hex motionless joints angle configuration depicted in Figure 5.9a.

The solution of the T-Hex robot kinematic problem inputs the forward kinematic associated to the overall transformation matrix (5.21), which relates the leg tip to the global coordinate frame at the base of the leg. The solution outlined in this section is partially algebraic and partially geometric.

In order to obtain a solution, the inverse kinematic problem is divided into two subtasks, known as *leg position* and *leg orientation*. The former task has three unknown variables, while the latter task considers the $4th$ joint as a spherical wrist with only one rotational axis. Therefore, the T-Hex can be described by the displacement vectors d_w and d_t, which relate the T-Hex global frame with the wrist origin and the leg tip respectively (see Figure 5.14). Because of this decoupling the leg position and leg orientation now represent two unrelated problems.

Considering the situation depicted above in Figure 5.14, the first three positional equations of the T-Hex leg can be found from,

$$
{}^{0}T_{3_4} = {}^{0}T_1\,{}^{1}T_2\,{}^{2}T_{3_4} = \begin{bmatrix} d_w \\ 1 \end{bmatrix} \equiv
$$

$$
\begin{bmatrix} \cos\theta_1(l_1 + l_2\cos\theta_2 + l_3\cos(\theta_2+\theta_3)) \\ \sin\theta_1(l_1 + l_2\cos\theta_2 + l_3\cos(\theta_2+\theta_3)) \\ l_2\sin\theta_2 + l_3\sin(\theta_2+\theta_3) \\ 1 \end{bmatrix} = \begin{bmatrix} p_{x_w} \\ p_{y_w} \\ p_{z_w} \\ 1 \end{bmatrix} \equiv \begin{bmatrix} p_x - l_4 a_x \\ p_y - l_4 a_y \\ p_z - l_4 a_z \\ 1 \end{bmatrix} \tag{5.58}
$$

Using the Pieper technique, the multiplication of both sides by ${}^{0}T_1^{-1}$ provides:

$$
{}^{1}T_{3_4} = {}^{0}T_1^{-1}({}^{0}T_1\,{}^{1}T_2\,{}^{2}T_{3_4}) \equiv \begin{bmatrix} l_3\cos(\theta_2+\theta_3) + l_2\cos\theta_2 \\ l_3\sin(\theta_2+\theta_3) + l_2\sin\theta_2 \\ 0 \\ 1 \end{bmatrix} = \begin{bmatrix} p_{x_w}\cos\theta_1 - l_1 + p_{x_w}\sin\theta_1 \\ p_{z_w} \\ p_{x_w}\sin\theta_1 - p_{y_w}\cos\theta_1 \\ 1 \end{bmatrix} \tag{5.59}
$$

Multiplying once again both sides by ${}^1T_2^{-1}$ yields:

$$ {}^2T_{3_4} = {}^1T_2^{-1}({}^1T_2\,{}^2T_{3_4}) \equiv \begin{bmatrix} l_3\cos\theta_3 \\ l_3\sin\theta_3 \\ 0 \\ 1 \end{bmatrix} = \begin{bmatrix} \cos\theta_2(p_{x_w}\cos\theta_1 - l_1 + p_{y_w}\sin\theta_1) - l_2 + p_{z_w}\sin\theta_2 \\ p_{z_w}\cos\theta_2 - \sin\theta_2(p_{x_w} - l_1 + p_{y_w}\sin\theta_1) \\ p_{x_w}\sin\theta_1 - p_{y_w}\cos\theta_1 \\ 1 \end{bmatrix} \tag{5.60} $$

Finally, the last positional equation can be found by multiplying each side by ${}^2T_3^{-1}$:

$$ \begin{aligned} &T_{3_4} = {}^2T_3^{-1}({}^2T_{3_4}) \equiv \\ &\begin{bmatrix} l_3 \\ \\ 0 \\ \\ 0 \\ 1 \end{bmatrix} = \begin{bmatrix} \sin\theta_3(p_{z_w}\cos\theta_2 - \sin\theta_2(p_{x_w}\cos\theta_1 - l_1 + p_{y_w}\sin\theta_1)) - l_3 + \\ \qquad + \cos\theta_3(\cos\theta_2(p_{x_w}\cos\theta_1 - l_1 + p_{y_w}\sin\theta_1) - l_2 + p_{z_w}\sin\theta_2) \\ \cos\theta_3(p_{z_w}\cos\theta_2 - \sin\theta_2(p_{x_w}\cos\theta_1 - l_1 + p_{y_w}\sin\theta_1)) - \\ \qquad - \sin\theta_3(\cos\theta_2(p_{x_w}\cos\theta_1 - l_1 + p_{y_w}\sin\theta_1) - l_2 + p_{z_w}\sin\theta_2) \\ p_{x_w}\sin\theta_1 - p_{y_w}\cos\theta_1 \\ 1 \end{bmatrix} \end{aligned} \tag{5.61} $$

In view of Equations (5.58), (5.59), (5.60) and (5.61) the positional relationship relative to the wrist of the T-Hex leg are in the form,

$$ \cos\theta_1(l_1 + l_2\cos\theta_2 + l_3\cos(\theta_2+\theta_3)) = p_{x_w} \tag{5.62} $$

$$ \sin\theta_1(l_1 + l_2\cos\theta_2 + l_3\cos(\theta_2+\theta_3)) = p_{y_w} \tag{5.63} $$

$$ l_2\sin\theta_2 + l_3\sin(\theta_2+\theta_3) = p_{z_w} \tag{5.64} $$

$$ l_3\cos(\theta_2+\theta_3) + l_2\cos\theta_2 = p_{x_w}\cos\theta_1 - l_1 + p_{x_w}\sin\theta_1 \tag{5.65} $$

$$ p_{x_w}\sin\theta_1 - p_{y_w}\cos\theta_1 = 0 \tag{5.66} $$

$$ \cos\theta_2(p_{x_w}\cos\theta_1 - l_1 + p_{y_w}\sin\theta_1) - l_2 + p_{z_w}\sin\theta_2 = l_3\cos\theta_3 \tag{5.67} $$

$$ p_{z_w}\cos\theta_2 - \sin\theta_2(p_{x_w} - l_1 + p_{y_w}\sin\theta_1) = l_3\sin\theta_3 \tag{5.68} $$

$$ \begin{aligned} &\sin\theta_3(p_{z_w}\cos\theta_2 - \sin\theta_2(p_{x_w}\cos\theta_1 - l_1 + p_{y_w}\sin\theta_1)) - l_3 + \\ &\cos\theta_3(\cos\theta_2(p_{x_w}\cos\theta_1 - l_1 + p_{y_w}\sin\theta_1 = l_3 \end{aligned} \tag{5.69} $$

$$ \begin{aligned} &\cos\theta_3(p_{z_w}\cos\theta_2 - \sin\theta_2(p_{x_w}\cos\theta_1 - l_1 + p_{y_w}\sin\theta_1)) - \\ &\sin\theta_3(\cos\theta_2(p_{x_w}\cos\theta_1 - l_1 + p_{y_w}\sin\theta_1) - l_2 + p_{z_w}\sin\theta_2) \end{aligned} \tag{5.70} $$

The first joint variable θ_1 can be derived from the trigonometric equation (5.66).

$$\theta_1 = \text{atan2}\,\frac{p_{y_w}}{p_{x_w}} \tag{5.71}$$

Since P_w and P_t are both in the plane defined by θ_1, this equation can be rewritten as,

$$\theta_1 = \text{atan2}\,\frac{p_y}{p_x} \tag{5.72}$$

In order to obtain θ_2 the first step is the combination of Equations (5.62) and (5.63).

$$p_{x_w}\cos\theta_1 + p_{y_w}\sin\theta_1 = l_1 + l_2\cos\theta_2 + l_3\cos(\theta_2+\theta_3) \tag{5.73}$$

The rearranging of Equation (5.73) and combining with Equation (5.64), and their squaring yields,

$$((p_{x_w}\cos\theta_1 + p_{y_w}\sin\theta_1) - l_1 - l_2\cos\theta_2)^2 + (p_{z_w} - l_2\sin\theta_2)^2 = l_3^2 \tag{5.74}$$

By solving the algebraic equalities on the left-hand side this equation can be rewritten in the form,

$$\begin{aligned} l_3^2 - ((p_{x_w}\cos\theta_1 + p_{y_w}\sin\theta_1)^2 + l_1^2 + p_{z_w}^2 + l_2^2 - 2((p_{x_w}\cos\theta_1 + p_{y_w}\sin\theta_1)l_1 = \\ \cos\theta_2 2l_2(l_1 - (p_{x_w}\cos\theta_1 + p_{y_w}\sin\theta_1)) - 2p_{z_w}l_2\sin\theta_2 \end{aligned} \tag{5.75}$$

which is in the from of the following trigonometric equation

$$a\cos\theta_2 + b\sin\theta_2 = c \tag{5.76}$$

Thus, θ_2 can be found from

$$a = 2l_2\,(l_1 - (p_{x_w}\cos\theta_1 + p_{y_w}\sin\theta_1)) \tag{5.77}$$

$$b = -2p_{z_w}l_2 \tag{5.78}$$

$$c = l_3^2 - \left((p_{x_w}\cos\theta_1 + p_{y_w}\sin\theta_1)^2 + l_1^2 + p_{z_w}^2 + l_2^2 - 2l_1(p_{x_w}\cos\theta_1 + p_{y_w}\sin\theta_1)\right) \tag{5.79}$$

then,

$$\theta_2 = \text{atan2}\,\frac{b}{a} + \text{atan2}\,\frac{\pm\sqrt{a^2+b^2+c^2}}{c} \tag{5.80}$$

where the two solutions again correspond to an *elbow-up* and *elbow-down* configuration.

Now, the determination of θ_3 offers two different approaches. While one approach combines the positional equations (5.67) and (5.68), the other approach, which is considered here, divides Equation (5.64) by Equation (5.73).

$$\tan(\theta_2 + \theta_3) = \frac{p_{y_w} - l_2 \sin\theta_2}{(p_{x_w} \cos\theta_1 + p_{y_w} \sin\theta_1) - l_1 - l_2 \cos\theta_2} \tag{5.81}$$

Therefore,

$$\theta_3 = \text{atan2}\left(\frac{p_{y_w} - l_2 \sin\theta_2}{(p_{x_w} \cos\theta_1 + p_{y_w} \sin\theta_1) - l_1 - l_2 \cos\theta_2}\right) - \theta_2 \tag{5.82}$$

Likewise, the solution of θ_4 yields to two different alternatives: algebraic and geometric. The algebraic approach applies the Pieper technique to the leg wrist to determine its two orientation equations. On the contrary, the geometrical approach relies on the procedure previously used to determine the orientation of the 3R planar manipulator (see Section 5.5.1). Thus, θ_4 can be expressed according the value of the WARG angle (ϕ). Here, the geometrical solution is considered, since it is fast and simpler to compute. To geometrically define θ_4, ϕ needs to be firstly determined. Considering these three elements of the transformation matrix (5.21)

$$r_{21} = -\sin(\theta_2 - \theta_3 - \theta_4)\cos\theta_1 \tag{5.83}$$

$$r_{22} = -\sin(\theta_2 - \theta_3 - \theta_4)\sin\theta_1 \tag{5.84}$$

$$r_{23} = \cos(\theta_2 - \theta_3 - \theta_4) \tag{5.85}$$

It is possible to obtain the solution for θ_{234} or ϕ by equating these equations above.

$$-\sin(\theta_2 + \theta_3 + \theta_4)(\cos\theta_1 + \sin\theta_1) + \cos(\theta_2 + \theta_3 + \theta_4) = 0 \tag{5.86}$$

Consequently

$$\tan(\theta_2 + \theta_3 + \theta_4) = \frac{1}{\cos\theta_1 + \sin\theta_1} = \tan\phi \tag{5.87}$$

and,

$$\phi = \theta_2 + \theta_3 + \theta_4 = \frac{1}{\cos\theta_1 + \sin\theta_1} \tag{5.88}$$

Now, the leg orientation θ_4 is given by,

$$\theta_4 = \phi - \theta_2 - \theta_3 \tag{5.89}$$

Finally, the inverse kinematic is solved by finding the origin of the leg wrist P_w.

$$p_{x_w} = p_x - l_4 \cos\theta_1 \sin\phi \tag{5.90}$$

$$p_{y_w} = p_y - l_4 \sin\theta_1 \sin\phi \tag{5.91}$$

$$p_{z_w} = p_z - l_4 \cos\phi \tag{5.92}$$

As shown earlier, the solution of the inverse kinematic problem for the T-Hex has two valid solutions, which correspond to the negative and positive value of θ_2. In order to discriminate between these solutions, the angular proximity criteria is chosen here. Therefore, solutions are selected based on the absolute difference between the calculated joints angle with respect to the previously chosen joint angles. The objective is to minimize such difference. Since the motionless leg position corresponds to the elbow-up solution, it is expected this selection criteria continues providing elbow-up solutions.

5.6 Real Time T-Hex Simulator

An important milestone in the process of developing an adaptive, multi-layer, self-organising and decentralised robot control system is the demonstration of its validity. As such, a robotic simulator of the T-Hex robot was implemented to analyse the different components of the controller and support the development of the walking algorithms. In the particular context of this thesis, it is not also safe to perform test on the real system as the locomotive solutions obtained through an evolutionary process are not always ideal and may not be achievable by the real robot. Using a simulator is then possible to avoid damages while safely testing different behaviours with independence of the physical limitations of the real robot. A model of the T-Hex robot equipped with all its sensors was developed in Java using ODE (Open Dynamical Engine) (Smith, 2000) through the ode4j library (Zäschke, 2009), so that the control of the system can be coupled with the evolutionary part and also evaluated in real time. ODE is an open source physical engine for the simulation of rigid body dynamics. It offers an advanced joint design integrated with a collision detection engine, which enables the interaction between bodies in the simulation space. ODE is licensed under both BSD (Berkeley Software Distribution) and LGPL (Lesser General Public License) licenses.

ODE is configured with a step size of $\Delta_t = 0.01$, friction of 100N, CFN (Constraint Force Mixing, an ODE parameter) of 10^{-5}, and standard gravity. Actuators have a maximum

angular velocity of $4ms^{-1}$ and a maximum torque of $45Nm$. Their movements are limited in both the z-axis plane for the coxa joint and the x-axis plane for the femur, tibia and tar joints, to a maximum rotation of 90^o and a minimum of -90^o. Force sensing resistors are modelled in a manner they can act either as contact or pressure sensors. The simulated robotic model is a 20 times smaller and scaled representation of the real T-Hex with a density of $20\,Kgm^{-3}$. These values are sufficient to mimic the characteristics of the real T-Hex robot while reducing the rendering const of the simulator. Initial results have shown that a real-scale simulated T-Hex robot approximately duplicates the computation time. Interestingly, the simulator also emulates the hardware procedure to engage motion in the servos of the T-Hex robot. Hence, the robot controller can be directly transferred to the real robot without any additional modification. The simulated T-Hex can be seen in Figure 5.15.

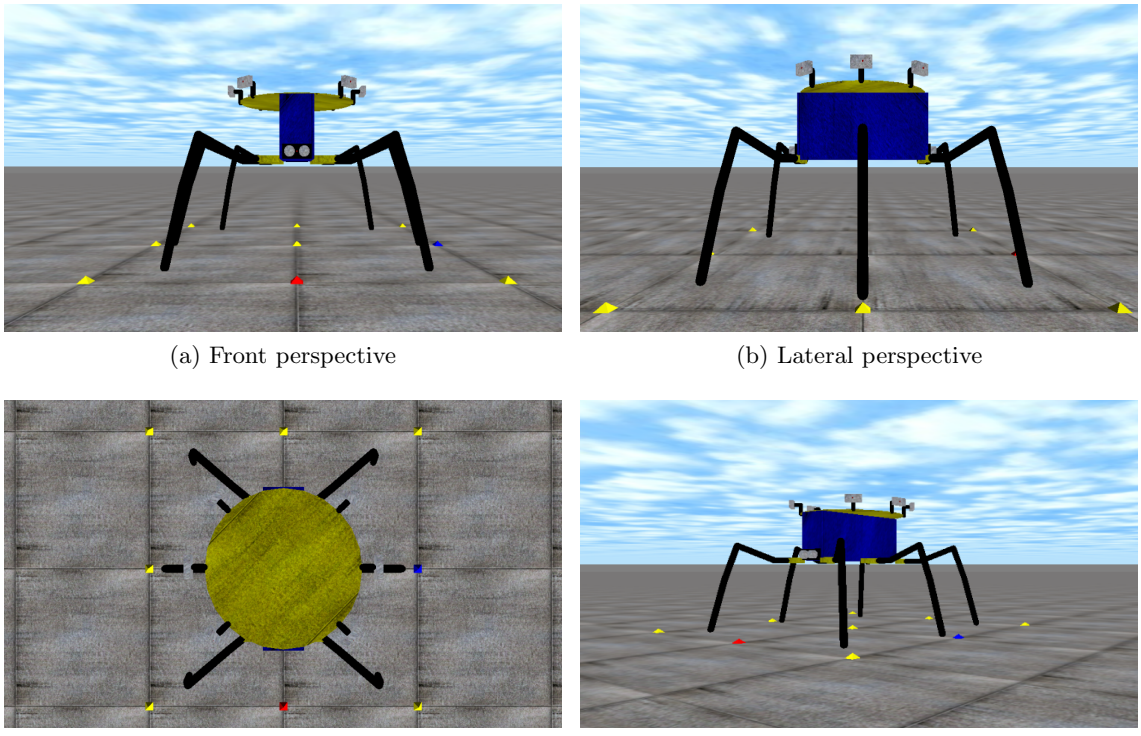

(a) Front perspective

(b) Lateral perspective

(c) Top perspective

(d) Diagonal

Figure 5.15: Simulated model in ODE of the T-Hex robot

Transferring simulations of evolved controllers onto real systems is a critical issue in evolutionary robotics (ER). This is mainly because the existing gap between effective and controlled simulated environments, and noisy-contaminated environments. This phenomena, typically known as reality gap (Jakobi, 1998; Nolfi & Floreano, 2001), states that a simulated behaviour cannot be transferred to a physical domain unless the simulation and reality are qualitatively similar. In an attempt to reduce the reality gap, the proposed simulation of

the T-Hex robot includes two mechanisms to add environmental noise into the simulated behaviours. Firstly, ultrasound and infrared sensors distort distance readings by adding a randomly selected noise component in the interval [0,0.1]. Secondly, the contact sensor readings are produced by the ODE are not completely accurate. This mostly occurs when the leg of the simulated robot steps on the edge of the simulated obstacles and it is due to the collision detection mechanism implemented in ODE considers capsule geometries as boxes geometries. Both features are considered in the simulation process as a source of desired noise to increase the robustness of the ASN-based controllers when applied to the physical robot.

5.7 Summary

This chapter has presented a kinematic analysis of the T-Hex walking robot. The analysis was divided into the forward kinematic and the inverse kinematic problems. The former attempts to describe the position and orientation of every link given the joints variables, while the latter resolves the joint variables to locate the end-effector tip at a desired position with a desired orientation.

Forward kinematics uses the Denavit-Hartemberg method, a frame-based procedure, to unambiguously define links and joints, and therefore, determine the homogenous transformation matrices relating the motion of each link with regard to a global coordinate frame. Inverse kinematics is a nonlinear problem that requires numerical or analytic approaches for solution(s). Since numerical approximations are not always accurate and hard to compute, only analytical approaches have been considered. There are two types of analytical solutions: geometric and algebraic. Both provide all the solutions for the inverse kinematic problem and can be equally applied to any robotic system. Nevertheless, the approachability of the inverse kinematic solution may vary in difficulty depending on the type of analytical technique chosen. Additionally, not all the inverse kinematic solutions are attainable. They might lie outside of the robot workspace boundaries, which could severely compromise the validity of the solution. Therefore, the kinematic solution needs to be selected in advance, making the selection criteria mostly ambiguous.

The T-Hex robot comprises six similar legs, each with four active revolute joints: one perpendicular followed by three in parallel. This kinematic configuration presents two main problems: high redundancy and non-planar workspace. In order to solve these problems,

the kinematic analysis of the T-Hex is complemented with the study of two general purpose robots. The 3R planar manipulator and the commercial PUMA 560 robot. This is because the 3R planar robot is redundant and the PUMA 560 robot has a non-planar workspace, which enables the usage of the decoupling principle. Such a principle eases the solution of complex inverse kinematic problems by dividing them into two independent subproblems: robot translation and robot orientation.

The solution proposed here for the kinematic problem in the T-Hex robot is partially algebraic and partially geometric. Firstly, the position of each link, each leg and the robot is established using transformation matrices (forward kinematic problem). Secondly, the Pieper technique, the decoupling principle and the wrist angle relative to ground are used to describe the T-Hex robot in terms of the position of its links and the orientation of its joints (inverse kinematic problem). This completely parametrises the motion of the T-Hex robot. Thus, the forward kinematic corresponds to the transformation matrices (5.17) - (5.10) and the four inverse kinematics expression are listed in Equations (5.72), (5.80), (5.82) and (5.89). The next chapter rests on this kinematic analysis in order to propose a decentralised bio-inspired control architecture for the T-Hex robotic platform. This is a hierarchical three-layered system made of a CASN to translate sensory feedback into modulative pulses, a CPG to generate locomotive trajectories and a kinematic layer to translate these trajectories in joint angles. Overall, this architecture allows the robotic system to regulate its internal architecture based on sensory feedback in order to produce adaptive locomotion movements.

Chapter 6

Evolved Adaptive Locomotion Controllers for a Hexapod Robot

Contents

The problem of locomotion control within legged robots can also be tackled by taking inspiration from biology and applying to generation of locomotion methodologies and control structures the principles of walking in living systems. The main idea underneath this type of computation is called *bio-inspired robotics* (Floreano & Mattiussi, 2008).

This work focuses on bio-inspired locomotion control in a hexapod robot (Fuente et al., 2013*a*). This includes high-level control to integrate sensory information and low-level control

to determine the robot's posture and gait. Three different biological concepts are considered to achieve high-level locomotion: *cellular signalling*, *decentralised control* and *central pattern generators*. Their combination with the inverse kinematics technique for low-level control results in a layered decentralised architecture for bio-inspired legged locomotion. The core of this approach is that a system of nonlinear Hopf oscillators is efficiently optimised by an evolved coupled signalling network, which, in turns is coupled with the mechanical body of the robot. The proposed topology comprises three hierarchical layers: a top layer of sensory integration and behaviour modulation, an intermediate layer of gait generation and a bottom layer of posture formation. In this context, the term decentralised refers to the capacity of Artificial Signalling Networks to solve complex problems wherein there is a high correlation amongst their underlying variables. In comparison to Chapter 4 where effective controllers were found for chaos control in two idealised dynamical systems, the control of legged locomotion is a clear example of complex behaviour in the real world.

This chapter outlines the proposed bio-inspired control strategy to generate locomotion in the T-Hex robot. In order to do so, the initial section describes the principal concepts of locomotion in legged robots and highlights its mathematical principles. Prior to the introduction of the proposed architecture, the chapter unravels the algorithm which describes how periodically stable trajectories can lead to motion patterns based on the wave rule. Then, the next section presents the design approach behind the proposed architecture and describes the manner by which each layer interacts with each other. The validation of the design is done by testing the bio-inspired controller over a set of uneven terrains in the ODE robot simulator. The chapter concludes with final remarks about the proposed methodology.

6.1 Locomotion in Legged Robots

The necessity to survive causes living organisms to develop distinctive abilities to interactively adapt to their surrounding environment. Locomotion is an example of this type of behaviour, permitting actions such as chasing prey, evading predators or exploring the environment. Locomotion in robots is only achievable using wheeled, legged or metachronal (i.e wave and undulating) mechanisms. Each has its benefits, nevertheless legged systems are apparently beneficial for increasing robots' stability when tranversing uneven terrains.

A *gait* is a pattern of locomotion in legged robots. It is commonly defined as the sequence

of limb and body movements, enabling the transportation of a body from one point to another. There exists two main types of gaits: *nonperiodic* or irregular, and *periodic* or regular. While the former does not exhibit rhythmical motion when dealing with terrain inconsistencies, the latter emerges from simple control rules and generates smooth and synchronous trajectories. Despite nonperiodic gaits showing a higher adaptability to real world environments, biological systems rarely use them. Instead, they make use of adjustable periodic gaits which vary with regard to the locomotion speed. Although changes in the walking speed do not affect the innate stability of periodic gaits, they are the criteria to switch between different gait patterns. In this work, only periodic gaits are considered.

In a mathematical context, a periodic gait is fully characterised by its duty factor, β and its cycle time, T. The duty factor, $\beta \in [0, 1]$, is the fraction of time a leg is on the ground with respect to the cycle time. The cycle time is the time interval between the repetition of exactly the same walking event. Likewise, the movement of each leg during a cycle time can be partitioned into the *stance phase* or the time the leg is in direct contact with the ground, and the *swing phase* or the time the same leg is swinging in the air. The relationship between the duty factor and the cycle time is given by:

$$\beta = \frac{T_{st}}{T} = \frac{T_{st}}{T_{st} + T_{sw}} \tag{6.1}$$

where T_{st} is the stance period and T_{sw} is the swing period. This separation of the cycle time into swing and stance phase allows to independently modulate the duration of each phase (Santos & Matos, 2011). Thus, the cycle time can also be expressed as the sum of the swing and stance frequencies as follows,

$$T = \frac{\pi}{w_{st}} + \frac{\pi}{w_{sw}} \tag{6.2}$$

where ω_{st} is the stance frequency and ω_{sw} is the swing frequency. Amongst the numerous periodic gaits, *wave gaits* are extensively used to model locomotion in living creatures. Characteristic of this gait are its high stability and its capacity to produce effortless transitions between different gait patterns (Inagaki & Kobayashi, 1994). Wave gaits are commonly denoted by the following two rules:

- *Lengthwise legs*: In lengthwise series of legs, each leg motion has $1 - \beta$ phase shift increment with respect to its fore side leg[1].

[1] Given a leg in a multi-legged system, its fore side leg is the leg located in front of it at the opposite side.

- *Bilateral legs*: Bilateral legs display the same motion alternatively with half cycle phase shift.

According to these indications the phase relationship between two legs i, j can be mathematically defined by:

$$\theta_i^j = \begin{cases} (1-\beta)2\pi & \text{lengthwise legs} \\ \pi/2 & \text{bilateral legs} \end{cases} \tag{6.3}$$

Therefore, it is possible to generate locomotive trajectories by uniquely specifying the duty factor. In addition, gaits with a desired duty factor can also be obtained by keeping the swing frequency constant and adjusting the stance frequency as illustrated below in Equation 6.4. Nevertheless, this may also lead to gait sequences which do not necessarily meet the wave rule. In hexapod robots, duty factors over 0.5 are considered a "walk", while those less than 0.5 are considered a "run".

$$\omega_{st} = \frac{1-\beta}{\beta}\omega_{sw} \tag{6.4}$$

Having reviewed the fundamentals of locomotion in legged systems, the rest of this section provides an overview of the main types of periodically stable wave gaits. In the context of this thesis, they are analysed attending to their applicability to a six-legged robotic system.

6.1.1 Periodically Stable Wave Gaits

Wave gaits can be classified based on the number of legs in contact with the ground during the stance phase. The tripod, ripple and metachronal patterns of motion are the most common wave gaits. They exemplify the movements of insects at high, medium and low speeds respectively. Following the limb convention to describe gait symmetries, limbs on the left (L) and right (R) sides of the hexapod are numbered from the front to the rear starting at one (Collins & Stewart, 1993).

Tripod gait

This gait mimics insect motion at high velocities. It is characterised by having three legs off the ground swinging while the other three legs are in contact with the ground supporting and propelling forward the robot body. In terms of its symmetry, the tripod gait is given by:

$$(R_3L_2R_1),(L_3R_2L_1) \tag{6.5}$$

In the tripod gait, locomotion consists of two stepping actions. The ipsilateral[2] front and back legs and the contralateral middle leg move together and in phase. On each segment, contralateral legs are 180^o out of phase. Adjacent limbs on each side are also 180^o out of phase. The tripod gait has a duty factor β of 1/2. The tripod gait is illustrated in Figure 6.1(a).

Ripple gait

This gait describes insects' medium-speed locomotion patterns. It is characterised by having four legs in contact with the ground while the other two legs simultaneously swing forward. In terms of its symmetry, the ripple gait is given by:

$$L_2,(R_3L_1),R_2,(R_1L_3) \tag{6.6}$$

In the ripple gait, locomotion consists of four stepping actions. The contralateral front and back legs move together in phase. On each segment, contralateral limbs are 180^o out of phase. Consecutive movements of the limbs are 90^o out of phase. The ripple gait has a duty factor β of 5/8. The ripple gait is depicted in Figure 6.1(b).

Metachronal gait

This gait imitates slow insects displacements. It is described as a wave propagating forward from the rear of the hexapod, first on the right side and then on the left side. The adjacent limbs on each half of the robot are 60^o out of phase. Contralateral limbs are 180^o out of phase. The metachronal gait has a duty factor β of 3/4. The metachronal gait is illustrated in Figure 6.1(c). In terms of its symmetry, the metachronal is given by:

$$R_3, R_2, R_1, L_3, L_2, L_1 \ldots \tag{6.7}$$

[2] Ipsilateral legs refers to the legs than are in the same side of the body.

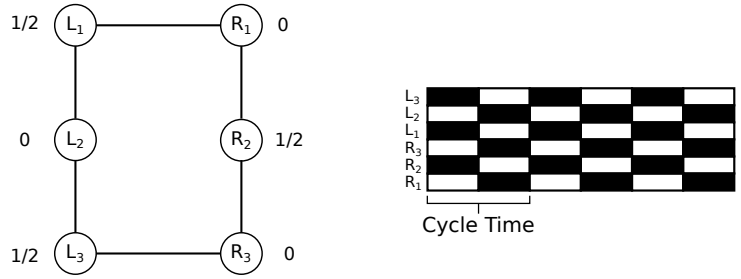

(a) Tripod gait

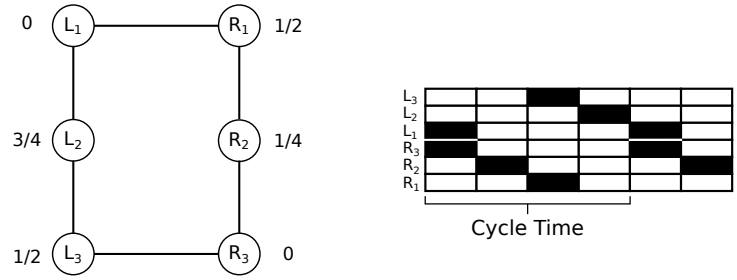

(b) Ripple gait

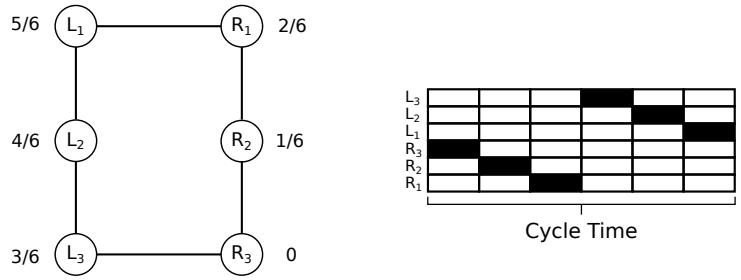

(c) Metachronal gait

Figure 6.1: The most common gaits in hexapod robots and their relative phases. Limbs on the left (L) and right (R) sides of the hexapod are numbered from the front to the back starting at 1. Black and white blocks on the right-hand side figures stand for the swing and stance phases respectively. (a) Tripod gait (high speed) with $\beta = 1/2$. (b) Ripple gait (medium speed) with $\beta = 5/8$. (c) Metachronal gait (low speed) with $\beta = 3/4$.

6.2 Trajectory Planning in the T-Hex Robot

This section describes the path planning algorithm through which locomotion can be produced using a wave-motivated gait pattern and a sigmoid curve. Path planning is the process that converts high-level locomotion specifications into low level descriptions of how to move. In this respect, it relates the kinematics and dynamics of a robot.

The process to generate locomotion is twofold. First, it is necessary to determine a group

of desirable setpoints in the motion path. Second, the inverse kinematic technique inputs them in order to calculate the location and orientation of each joint to reach the desired position. The validity of the algorithm is initially tested using the cycloid function, which is extensively used to model locomotion in legged robots since it shows a high resemblance with the walking patterns in living systems (Kim, 2006). The cycloid function is a sinusoid curve that describes the circular trajectory generated by a point on the rim of a circular wheel when it rolls forward in a straight line over a flat surface (see Figure 6.2).

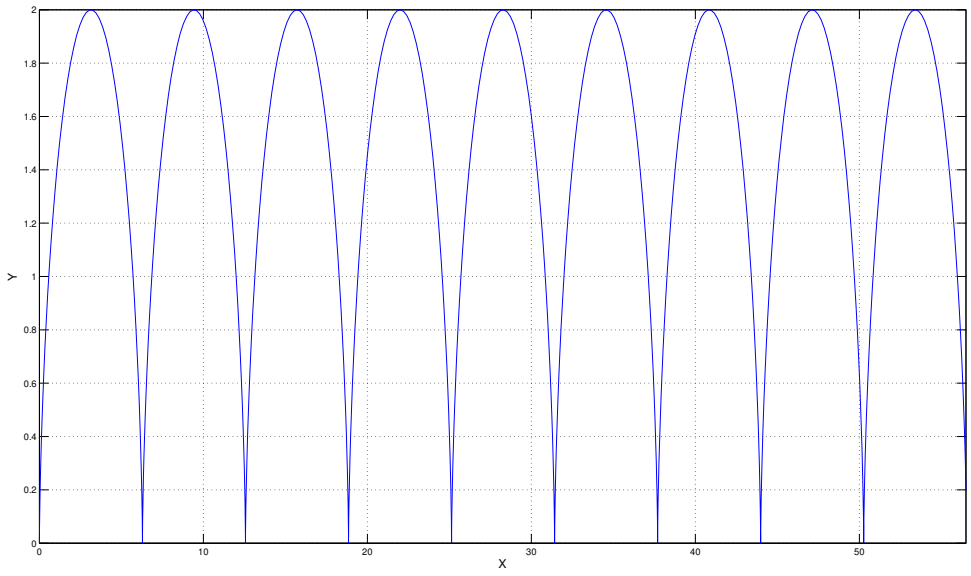

Figure 6.2: The cycloid function.

The cycloid path relies on the cycloid function to define the trajectory followed by each leg during a planned time frame in a three dimensional space. Note that the cycloid path does not account for each leg's phase relationships. The path planning algorithm inputs the characteristics of the cycloid path between two points in the Cartesian space and a wave-motivated pattern of motion. Its outputs are the aimed position of the setpoints in the leg workspace. In contrast to other robot controllers, which consider the centre of the robot as a benchmark, the cycloid path is here calculated with respect to the point where each leg attaches to the body of the robot. Although this increases the computation time, it allows to independently determine the motion of each leg. Then, inverse kinematics translates these setpoints into the joint space to specify the time evolution of the joint variables. The time-

dependent cycloid path considered in this work is given by:

$$x_1(t) = x_0 - x_f \cos\left(\pi \frac{t - t_0}{t_f - t_0}\right) \tag{6.8}$$

$$y_1(t) = y_0 - y_f \cos\left(\pi \frac{t - t_0}{t_f - t_0}\right) \tag{6.9}$$

$$z_1(t) = \frac{1}{2}\left(1 - \cos\left(\pi \frac{t - t_0}{t_f - t_0}\right) + (z_0 - z_f)\left(\frac{t - t_0}{t_f - t_0}\right)\right) \tag{6.10}$$

where t_0 is the initial time, t_t is the final time, x_0 and x_f are the initial and final points along the x-axis, y_0 and y_f are the initial and final points along the y-axis, and z_0 and z_f are the initial and final points along the z-axis. In an attempt to simplify the control problem, equations (6.8) - (6.10) define the motion path regardless of the acceleration and velocity. For alternative expressions of the cycloid path taking into consideration these two variables see (Wolovich, 1987; Jazar, 2010). Finally, the multiplication of the x- and y-trajectories of the cycloidal path by a unit vector normal to the surface of the XY plane defines the direction of motion. Figure 6.3 illustrates the cycloid path in the joint domain of the leg L5 when the robot displaces forward along a straight line.

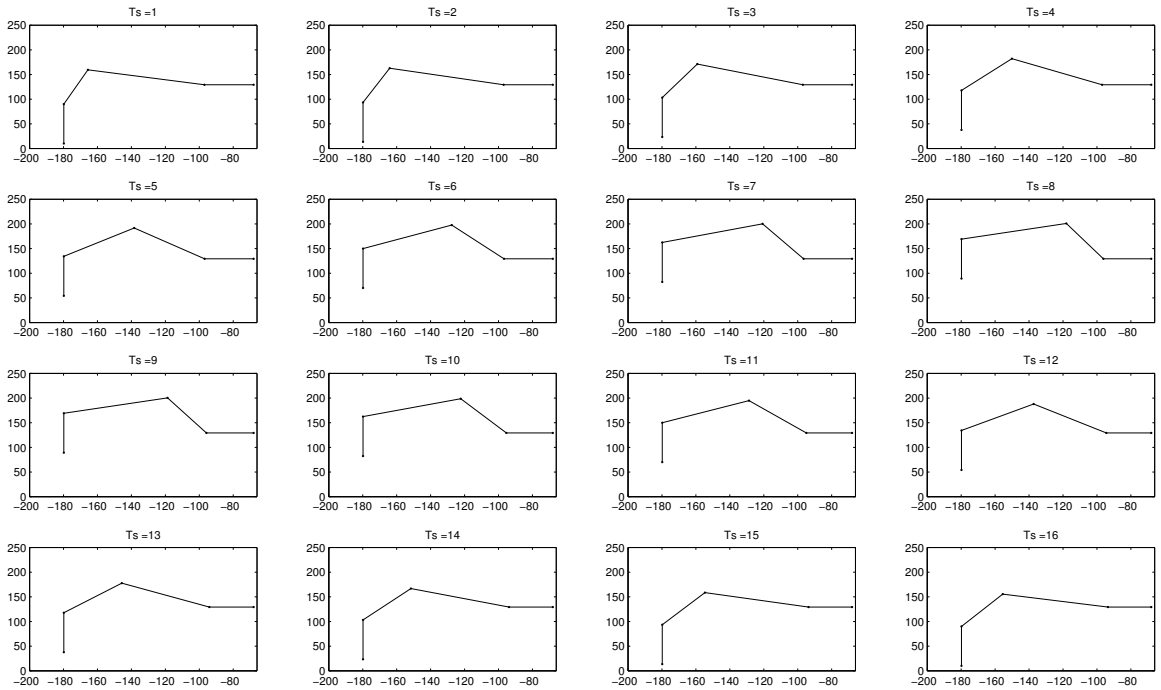

(a) Leg movement in the YZ plane

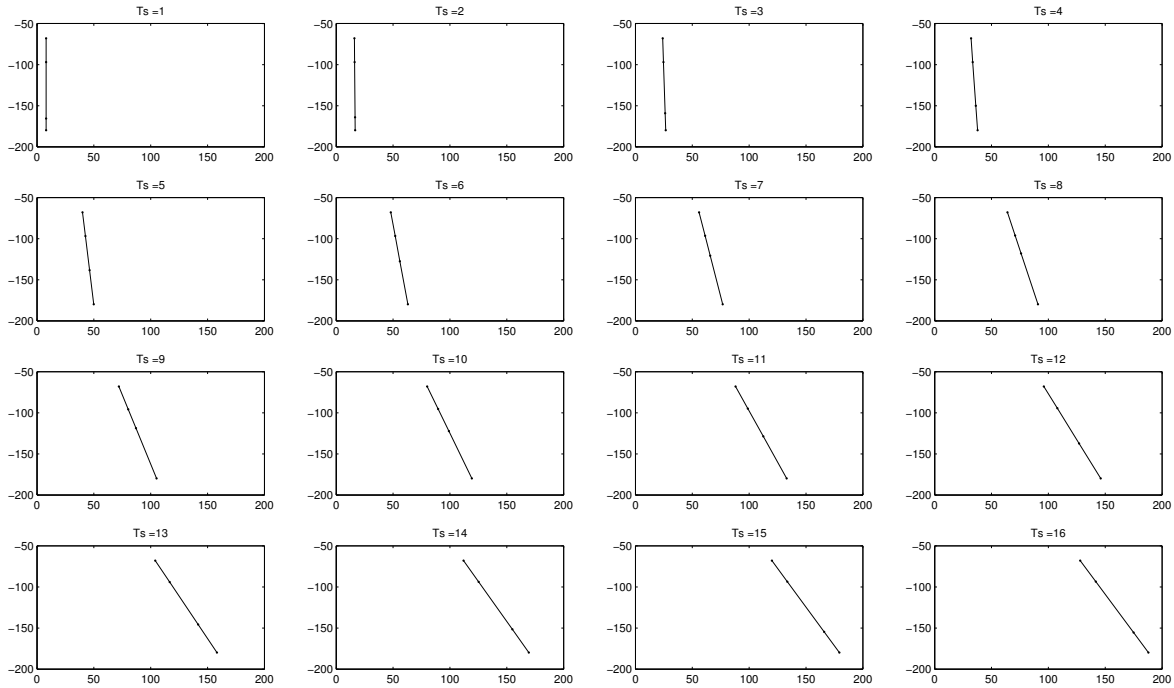

(b) Leg movement in the XY plane

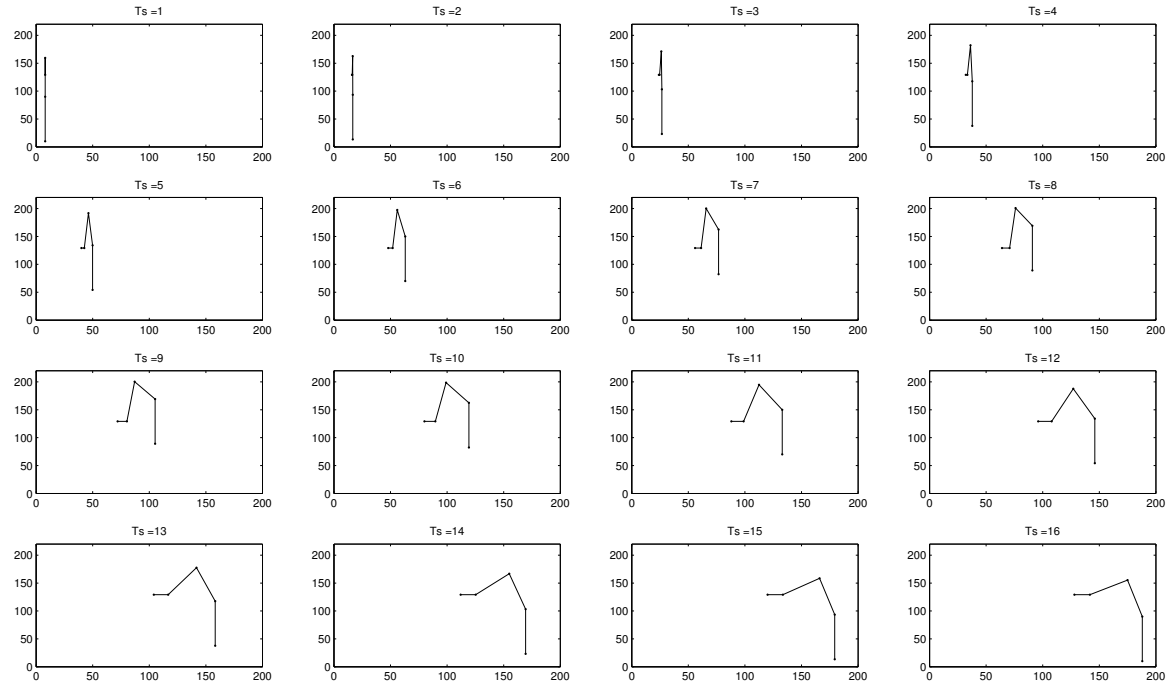

(c) Leg movement in the XZ plane

Figure 6.3: Example of motion in the joint domain of the leg L2 when the robot displaces forward along a straight line. Each diagram plots the position of the leg at each set point on (a) the YZ plane, (b) the XY plane and (c) the XZ plane using $S_r = 16$.

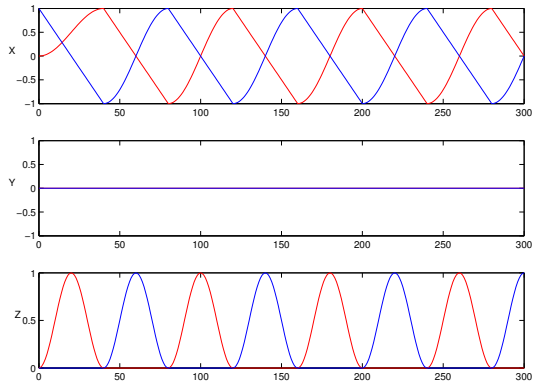

(a) $X_{\text{dir}} = 90^o$ and $Y_{\text{dir}} = 0^o$

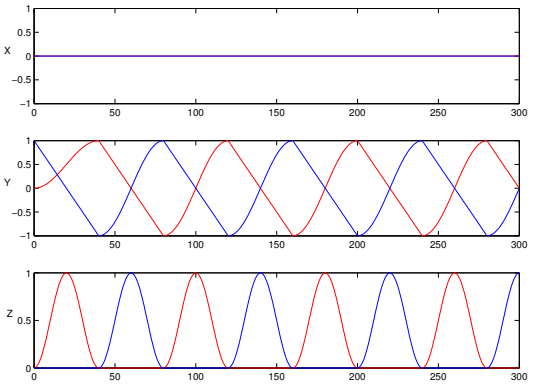

(b) $X_{\text{dir}} = 0^o$ and $Y_{dir} = 90^o$

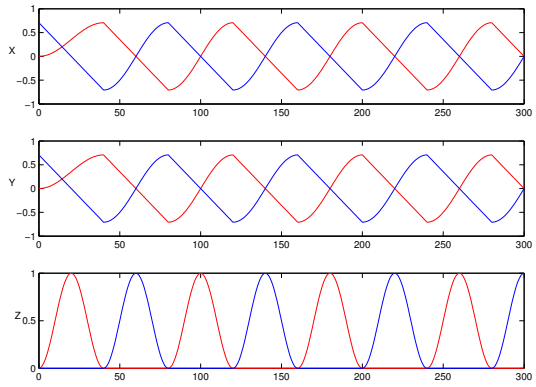

(c) $X_{\text{dir}} = 45^o$ and $Y_{\text{dir}} = 45^o$

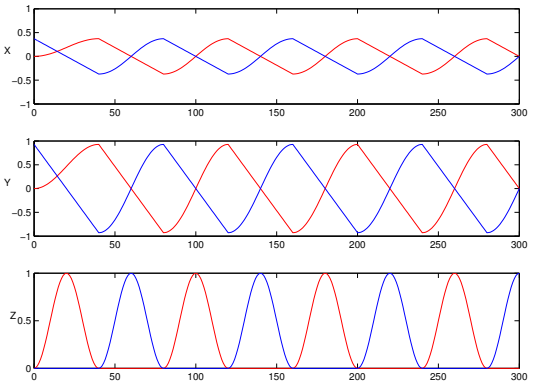

(d) $X_{\text{dir}} = 20^o$ and $Y_{\text{dir}} = 45^o$

Figure 6.4: Illustration of different directions of the T-Hex robot in the Cartesian space. The x, y and z components of the cycloidal trajectory are plotted for each direction. The direction of the T-Hex is illustrated using the tripod gait (see Figure 6.3(a)).

Figure 6.4 illustrates four different directions of the generated cycloid path for the tripod gait in the three dimensional Cartesian space. For each representation, the x-, y- and z-trajectories of the cycloid path are considered. Forward motion along a straight line is illustrated in Figure 6.4(a). The absence of lateral displacements is denoted by an oscillatory x-trajectory and a constant y-trajectory fixed to 0. On the other hand, an absolute lateral locomotion as in Figure 6.4(b) outlines a plain x-trajectory fixed to 0 and an oscillatory y-trajectory. The generation of diagonal displacements (see Figure 6.4(c) - (d)) requires the combination of the oscillatory x- and y-trajectories. In contrast, the shape of the z-trajectory of the cycloid path remains constant with respect to the robot's direction. Interestingly, this separation enables to scale the cycloid path according to the step variables. This is done by multiplying the x- and y-trajectories by the desired step length S_L and the z-trajectory by

the desired step height S_H (see Algorithm 6.1).

Figure 6.4 also shows that the x- and y-trajectories of the cycloid path results from the combination of a linear and a cosine-like function. This is not an unknown phenomenon as it was also observed in Muecke (2009). The reason for this duality is the manner in which the trajectory is calculated during the stance and swing phase. As can be seen in Algorithm 6.1, the cycloid function is uniquely considered to produce the motion during the swing phase, while the linear function is only responsible for the stance phase. During the stance phase, the inverse kinematic solver only generates new values for the coxa joints, which displace the leg horizontally. This guarantees the leg stands on the ground for supporting and pushing the robot body forward. Algorithm 6.1 describes the pseudocode of the path planning algorithm.

Algorithm 6.1 Plath planning algorithm

Require: $t_f \geq 0 \wedge S_r \geq 3$
Ensure: $\mathrm{X}_{dir} \in (0, 1)$
Ensure: $\mathrm{Y}_{dir} \in (0, 1)$
  while $time \leq t_f$ **do**
    Normalise X_{dir} and Y_{dir}
    $T_{frame} = T_s/(S_r \cdot T_g)$
    for $i = 0$ to Legs **do**
      if $T_i \leq S_r$ **then**
        if Stance equals to False **then**
          $P_{\text{old}} \leftarrow$ old setpoint
          $P_{\text{new}} \leftarrow (S_L \cdot \hat{\mathrm{X}}_{dir}, S_L \cdot \hat{\mathrm{Y}}_{dir}, 0)$
          Stance $\leftarrow$ True
        end if
        Calculate new cyloidal setpoint
        $P_{\text{new}} \leftarrow (x_{new}, y_{new}, S_H \cdot z_{new})$
      else
        $x_{new} \leftarrow x_{old} - T_{frame} \cdot 2 \cdot \hat{\mathrm{X}_{dir}}$
        $y_{new} \leftarrow y_{old} - T_{frame} \cdot 2 \cdot \hat{\mathrm{Y}_{dir}}$
        $z_{new} \leftarrow 0$
        Stance $\leftarrow$ False
      end if
    end for
  end while

Another interesting feature when modelling robot locomotion is the sampling rate S_r. It defines the number of setpoints per cycle time and tailors the shape of the cycloid path. The smaller the number of setpoints is, the lesser the number of leg displacements per cycle is but the more imprecise the cycloid path is outlined. On the other hand, an increment in the number of setpoints better describes the cycloid function but also decreases the walking speed. Figure 6.5 illustrates the effect of the sample rate over the x-trajectory of a cycloid

path configured using the tripod gait.

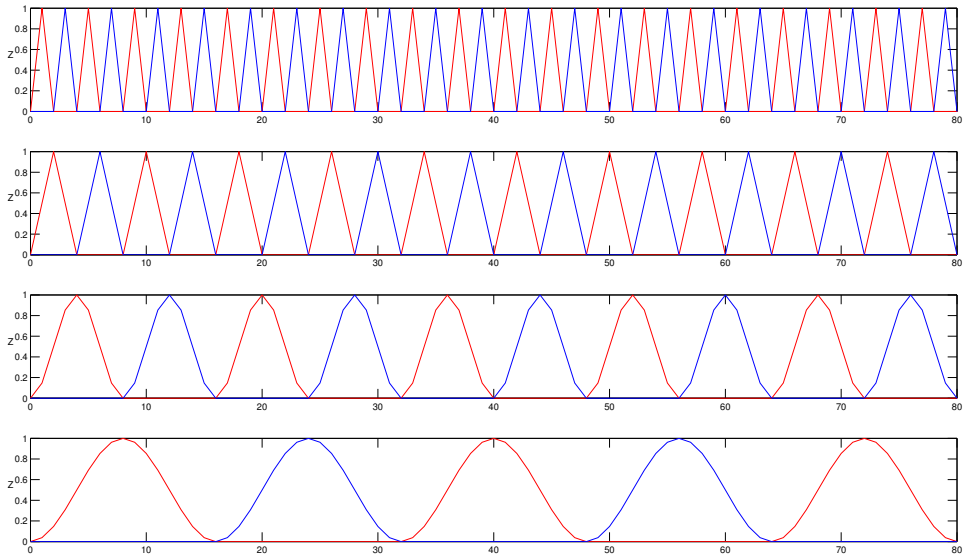

Figure 6.5: Example of the z component of the cycloidal trajectory with sampling rates of $S_r = 2$, 4, 8 and 16 respectively from the top to the bottom plot. The illustrated trajectory is obtained using a tripod gait configuration (see Figure 6.1(b)).

The sequence of a video still in Figure 6.6 exemplifies the walking of the T-Hex robot using the tripod gait. Sequences of the metachronal and ripple gaits can also be found Appendix D. Further, sequences of a video still showing the walking of the physical T-Hex using several gaits can be found in Appendix E.

6.3 Adaptive Locomotion Architectures

Locomotion is an example of a widespread adaptive response used by living organisms to interactively handle environmental stimuli. It is adaptive in the sense that it is able to accordingly adapt itself based on the terrain irregularities (*adaptivity*) rather than forcing living organims to change their activity and function in order to adapt their behaviour accordingly (*adaptability*) (Oppermann & Rasher, 1997). Locomotion typically stems from the combination of a set of rhythmical actions by which biological or synthetic systems displace from one point to another within the environment. In living creatures, locomotion is conceived as the reflex generated by an specific neural circuit, which activates the structures and effectors of locomotion. From a robotic perspective, locomotion attempts to imitate biological

morphologies and models of locomotion and their control mechanisms (Ijspeert, 2008).

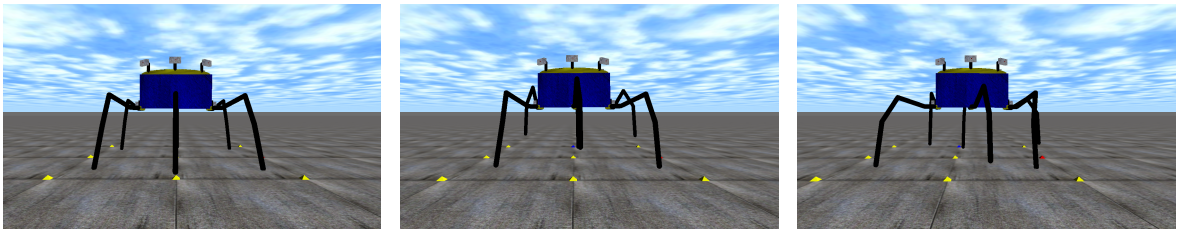

(a) $t = 0$ (b) $t = 5$ (c) $t = 8$

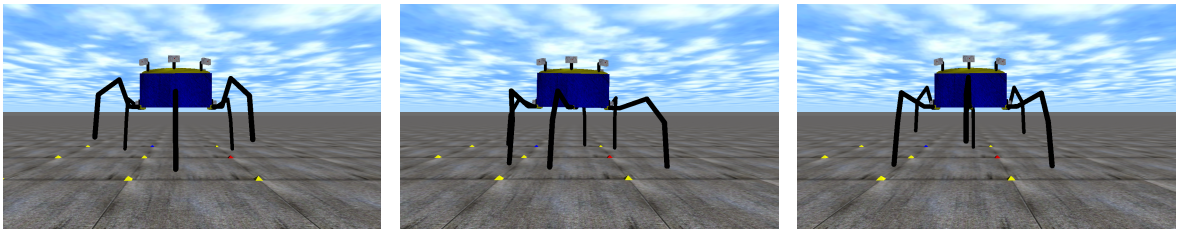

(d) $t = 12$ (e) $t = 15$ (f) $t = 18$

Figure 6.6: An example sequence of the tripod gait within the ODE simulated T-Hex.

6.3.1 Adaptive Locomotion in Multi-legged Robots

Although legged locomotion is the most common displacement mechanism in the natural world, legged robots are not yet able to mimic the complexity found in legged creatures to move across rough terrains. Compared with wheeled mobile robots, multi-legged robots can easily step over obstacles and walk through irregular surfaces. This is because they have a bending body and therefore, can efficiently deal with complex environments. Nevertheless, there are other aspects in the locomotion process which make locomotion control in multi-legged robots a more complicated task (Wu, Liu, Zhang & Chen, 2009), such as redundant degree of freedom in legs, balance keeping and the lack of adequate actuators. Bio-inspired control architectures offer a natural possibility to overcome these limitations increasing the robot's mobility (Quinn et al., 2002). Generally speaking there are three main bio-inspired control strategies to produce adaptive locomotive movements in multi-legged robotic systems: model-based, reflexive and pattern-based controllers (Chen et al., 2014).

Model-based control architectures consider multi-legged robots as parallel robots, meaning that the supporting legs are computed together with the robotic body and the environmental surface. These controllers normally require kinematics and motion dynamics to

calculate the control parameters for every step (de Lasa et al., 2010). Examples of this control paradigm include the big dog (Buehler et al., 2005), the little dog (Kalakrishnan et al., 2010) and the Case Western Hexapod Robot II (Quinn et al., 2001). Characteristic of these approaches is not only their capacity to produce precise patterns of motion, but also their limited ability to generate gait diversity and switch amongst gaits, and their high computational cost.

Reflexive controllers emerge from the observation of the movement of real insects (Dickinson et al., 2000). These controllers follow a reactive design in order to produce leg motion, gait coordination and respond to incoming stimuli. The maximal exponent is the Walknet robot (Cruse et al., 1998). This stick-insect approach comprises a decentralised structure made of locally coupled nonlinear dynamical systems which are able to organise themselves based on a set of local reflexes acting on two kinematic parameters (Cruse et al., 1997). Each leg controller has only two control signals that alternate between low and high excitation. This ensures the correct movement of the leg in stance and in swing, generating a biological behaviour (Cruse, 1990). Alternative legged robots using a reflexive controllers are the lamprey proposed by Grillner et al. (1991) that swims by rhythmical undulations of its body and the 12-DOF MTA hexbot (Frasca et al., 2004) that implements a decentralised architecture governed by six second-order dynamical systems.

Pattern-based controllers group the set of architectures inspired by the modulatory properties found in the vertebrate's spinal cord or invertebrate's ganglions (Delcomyn, 1999). Likewise, pattern-based controllers can be divided into analytical and intelligent solutions (Wright & Jordanov, 2012). Analytical approaches are task-dependent and require extensive *a priori* knowledge of the task to be solved. Although appropriate solutions can be found using analytical approaches, their scope is very specific and generally restricted to the behaviours of the observed task. On the other hand, intelligent solutions favour the parameterisation of motion patterns, which reduces the limitation exhibited by the analytical techniques. Central Pattern Generators (CPGs) stand out amongst other intelligent solutions because of their capacity to generate simple locomotion patterns based on oscillatory primitives. These entrain the limbs to oscillate offhand at a continuous frequency. This mechanism has been successfully applied to different types of legged robots, including bipedal locomotion (Miyakoshimi et al., 2000; Aoi et al., 2012), quadrupedal locomotion (Kimura et al., 2007; Zhang & Zheng, 2008) and hexapedal locomotion (Arena et al., 2004; Inagaki et al., 2006). Other types of bio-inspired robots using CPGs are the amphibious robot by Ijspeert et al.

(2007), the snake-like robot proposed in Crespi & Ijspeert (2008) and the robot fish by Yu & Wei (2013). In this work, central pattern oscillators are also considered to control the locomotion of an autonomous hexapod robot.

6.3.2 Central Pattern Generators

A Central Pattern Generator is a common approach to modelling and, in turn, generating locomotive patterns (Frasca et al., 2004). It is biologically inspired by the neural circuits within living organisms that when activated, produce rhythmical patterns of neural activity without requiring sensory feedback (Ijspeert, 2008).

Whilst CPGs are often implemented using biologically-motivated models, such as feed-forward neural networks (Capi et al., 2001) or artificial homeostatic networks (Moioli et al., 2009), they can also be considered as systems of specialised nonlinear coupled oscillators. Examples of this approach in robotic systems include the dynamical modulation of periodic gait in a quadruped robot (Liu et al., 2009), the modelling of the oscillatory patterns in the crawling of a baby (Righetti & Ijspeert, 2006) or the stabilisation of a bipedal robot (Aoi & Tsuchiya, 2004).

CPGs based on systems of oscillators are mathematical models of the locomotion patterns found in biological CPGs. Attending to the phenomena under study, these models can be categorised as biophysical models, connectionist models, neuromechanical oscillatory models or abstract systems of coupled oscillators (Ijspeert, 2008). While the first three approaches emulate in isolation the activity of a single neuron or small circuit, systems of coupled oscillators represent the locomotion activity as an oscillatory working unit, where each oscillator is an oscillatory centre. In this respect, these models analyse the capacity of the inter-oscillator couplings to affect the dynamics of the entire system and the synchronisation of each oscillator within the working unit. Within systems of coupled oscillators, the dynamics of the entire system arise mainly from the topology and the type of coupling instead of the mathematical terminology describing the trajectories. Because of this, CPG models simplify the validation of oscillatory robotic architectures as they can be coupled with mechanical robotic bodies (i.e salamander robot (Ijspeert et al., 2007)).

The majority of CPGs are denoted by a set of coupled differential equations that when numerically integrated exhibit a periodically stable trajectory. Alternatively, there also exist

CPG models whose solutions result from the addition of a sinusoidal component to the differential expression. In this case the resultant pattern of motion, which depends exclusively on the sinusoidal term, can be directly applied to locomotion (Mehta et al., 2008; Lachat et al., 2006). Other CPG representations include hardware implementations or the application of chaotic maps to generate more expressive patterns of motion (Lones et al., 2011). Independently of its representation, a CPG based on systems of oscillators exhibits several benefits in the generation of locomotion in robotic systems. These include:

- *A high robustness to external perturbations.* This is a consequence of the limit cycle property of nonlinear oscillators, which offer resilience to the perturbation of their state variables.

- *Smooth gait transitions.* This refers to the capacity of nonlinear oscillators to produce rhythmical behaviours after their state variables or their coupling weights are drastically modified.

- *A well defined parametric structure* denoted by its governing parameters. Their modulation outlines the shape of the oscillatory trajectory.

- *The ability to produce distributed control methodologies.* This contributes to reduce the dimensionality of the locomotion problem.

- *A high capacity for integrating sensory information*, which increases the adaptability of the generated trajectories.

- *Its capacity to be optimised.*

Despite all these advantages, CPGs based on a system of coupled oscillators also show some inconveniences. These are commonly related with the limit cycle property, which reduces their capacity to express complex behaviours. Nonetheless, there is a growing interest in using oscillators in the modeling of CPGs. Examples of this include Rayleigh (de Pina Filho et al., 2005), Matsuoka (Habib et al., 2007), Kuramoto (Moioli et al., 2010) and Armari-Hopfield (Nakada et al., 2003) oscillators. Most of these models take advantage of the limit cycle and synchronisation properties to produce effective locomotion in robotic systems.

Amongst other models, the CPG system based on Hopf oscillators initially introduced in Righetti & Ijspeert (2006) and endorsed lately in Campos et al. (2010) is of special relevance in this work. The Hopf oscillator is considered in this research due to four main considerations.

First, it exhibits a smooth harmonic oscillatory trajectory which is highly dependent of its parameters which eases the modulation of the output pattern by changing the corresponding parameter. Second, it allows the independent modulation of the ascending (swing) and descending (stance) phases. Third, it is well suited for integrating sensory information in the sense it can rapidly change the phase space of the CPG. Four, it is easier to develop coupling terms in an analytical form for multiple coupled Hopf oscillators.

Campos et al. (2010) exemplifies the usage a CPG based on Hopf oscillators in the generation of gait transitions in a hexapod robot. Interlimb coordination was achieved by coupling the Hopf oscillators in a predefined manner, which ensures the limbs remain synchronised. The relevance of this work is the capacity for controlling the oscillatory phase relationships given an unsteady coupling, which leads to effortless transitions amongst gait trajectories. The trajectory switching is sheerly governed by a bespoke and piecewise linear function of a modulatory parameter.

Using Hopf oscillators, the work described in this thesis presents a CPG consisting of six oscillators, which are coupled in a diffusive manner. As a consequence, it is possible to explore the existing damping in the coupling of complex biochemical networks and apply it to locomotion. The aim of this model is to assess the capacity of a periodically stable system to adaptively generate locomotion patterns. Instead of manually specifying the oscillator constants and coupling weights, an evolutionary algorithm is used to calibrate these values.

6.3.3 Evolutionary Strategies in CPGs

Evolutionary algorithms have been extensively used to optimise CPGs. This is because of their capacity to widely explore the state space of CPGs and precisely exploit those regions where the optima are more likely to be. In this respect, evolutionary algorithms do not need to know the underlying objective function that is being optimised in the CPG domain to successfully evaluate the overall behaviour of the CPG. Instead, robotic systems are assessed by measuring their performance in a high-level task. Forward speed locomotion, following a line or avoiding obstacles are examples of these measurements.

The applicability of evolutionary algorithms is restricted to CPGs where there exists an evident separation between their state variables. Such variables are usually the period and amplitude of oscillation and the coupling weights. The Hopf oscillator belongs to this group

of oscillators. Its generated trajectory can be uniquely modulated by performing changes on its amplitude and frequency, while preserving unaltered the additional parameters (see Figure 6.7). Parametric optimisation of a CPG based on coupled Hopf oscillators using evolutionary algorithms has been summarily explored in Nicolas (2005) to produce locomotion in a bipedal robot. The authors use a floating point representation to encode each governing parameter in the genome. The CPG is then optimised using a standard generational genetic algorithm.

This work also considers parametric optimisation using evolutionary algorithms on a CPG based on coupled Hopf oscillators. Instead of directly optimising the state variables of the CPG, the evolutionary algorithm aims to find an appropriate CASN that, over the course of time, modulates them. Furthermore, the inclusion of the CASN favours the coupling of the CPG with the robot's external environment. This provokes the entrainment between the CPG and the mechanical robotic body, and increases the adaptability of the generated trajectory.

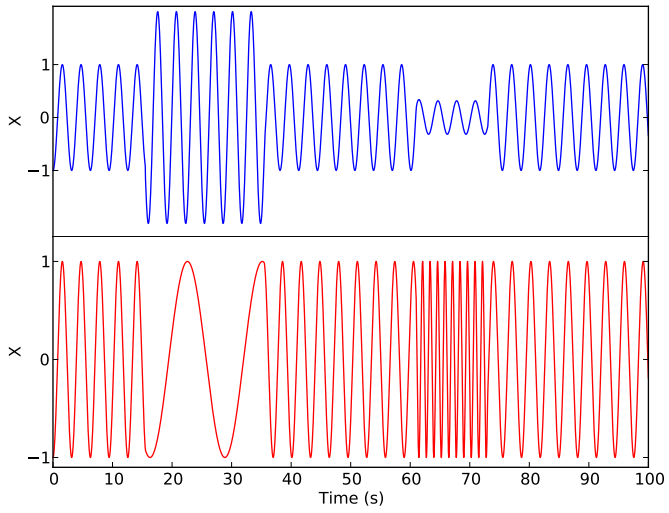

Figure 6.7: A example trajectory showing the capacity of the Hopf oscillator to independently modulate the frequency ω (bottom graph) and the amplitude A (upper graph).

6.4 A Decentralised Locomotion Controller

This section describes the decentralised bio-inspired controller used for locomotion in the T-Hex robot. The control paradigm is based on a layered topology, in which an evolved and distributed network of signalling pathways modulates the state variables of an (also distributed) network of nonlinear oscillators. The generation of locomotion patterns is the

result of the local influences amongst individual oscillators. In this sense this scheme differs completely from the traditional CPG models as they do not consider sensory feedback in the generation of adaptive and synchronous trajectories. A schematical representation of the proposed architecture is presented in Figure 6.8.

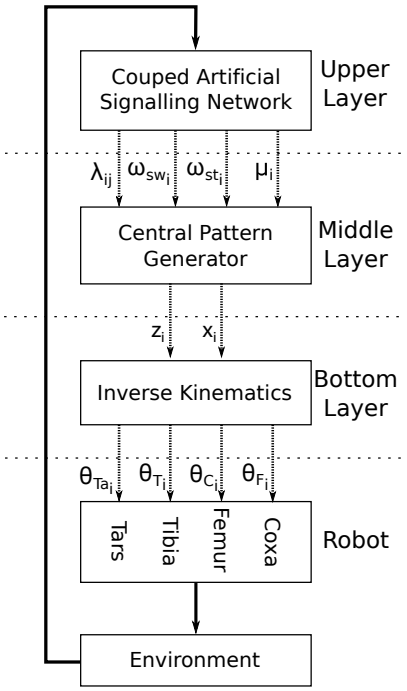

Figure 6.8: Functional division of the T-Hex controller in terms of its structures. The upper layer receives the environment excitatory signals. A network of ASNs accordingly modulates them. The CASN outputs are directly connected with the medium layer inputs and modulate the parameters of a network of CPGs. These generate gait trajectories, which are translated into robotic motion using the inverse kinematic technique encapsulated in the lower layer.

In more detail, the upper layer comprises a CASN, which groups together numerous ASNs coupled in a specific manner. This layer retrieves environmental signals from the robot's external sensors and modulates the state variables of a CPG. Locomotion patterns are produced within the middle layer, which is defined by a CPG based on a system of nonlinear coupled Hopf oscillators. The coupling connections within the CPG mirrors the crosstalk relationships in the CASN. After inputing the modulatory values from the outputs of the CASN, this layer delivers a set of adaptive and oscillatory trajectories. Finally, the bottom layer transforms these trajectories into robot movements using a trajectory planning algorithm. Overall, this computational model aims to emulates how the hierarchical control and locomotion pattern generation system taking place at the neural level emerges from the local influences amongst the network of neuron in change of the control of each leg and the generation of locomotive movements. Unlike artificial neural networks, signalling networks

are computational models inspired by the biochemical structures related to the regulation of cells activity via the processing of external stimuli rather producing control commands. In this respect, they offer a natural possibility to develop large processing units able to simultaneously process multiple environmental signals and collectively generate modulatory commands. This is perhaps the main difference between artificial neutral networks and ASNs. The former describes the signalling process amongst several interconnected neurons (simplest processing units) while the latter is biologically designed to cooperate with another signalling networks (a pathway is its simplest processing unit and is made of several interconnected enzymes).

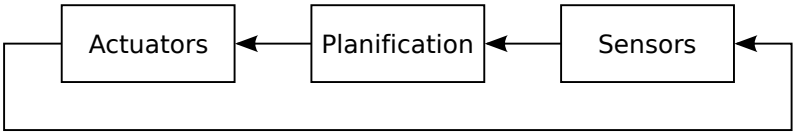

(a) Deliberative Paradigm

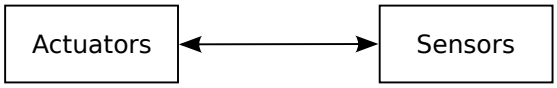

(b) Reactive Paradigm

Figure 6.9: Schematic representation of deliberative (a) and reactive (b) robotic paradigms. In a deliberative paradigm robots follow a top-down architecture, meaning that they first sense their surrounding, then plan the the next action and finally act. This process is iteratively repeated on each move. The hierarchical architecture is an action-selection technique, which computes the next action instantly based on the current environment. Actions are represented by hand-designed concurrent behaviours.

Conventional robots have typically followed a deliberative paradigm (see Figure 6.9(a)). These robots operated in a linear manner which includes sensing word, planning the next action and acting. Nevertheless, this architecture produced rigid and deterministic control mechanisms as they were mostly based on advance symbolic representations of the robot's surrounding, making the robot vulnerable to changes on its context. Brooks (1991) introduced a new control paradigm closely related to behavioural-based robotics, which aimed to develop autonomous robots able to operate with independence of their environment. Brooks' *subsumption architecture* decomposes the overall behaviour of a robotic system into sub-behaviours hierarchically organised (see Figure 6.10). Each layer is responsible only for a single behaviour. Layers are executed in parallel and outputs inhibit and suppress signals passing from a higher layer to a lower layer.

The subsumption architecture is reactive and advocates a bio-inspired design (Harvey et al., 1992). It is reactive in the sense that robotic systems respond to their environment based on their sensors values, rather just producing anticipatory behaviours in advance of future situations (see Figure 6.9(b)). However, every individual behaviour is designed by hand and subsumes to the additional behaviours. This reduces the capacity of the robot to operate in changing environments. Unlike the subsumption architecture, the proposed CASN controller is able to operate in real-time generating memoryless reactive behaviours in response to changing and unpredictable environments (see Chapter 4). The proposed control architecture inputs abstract sensory information in every instant based on the robot's current context and internal dynamics, rather using predefined behavioural descriptions. This smooths the outputted behaviour and increases the adaptivity of the coupled signalling networks.

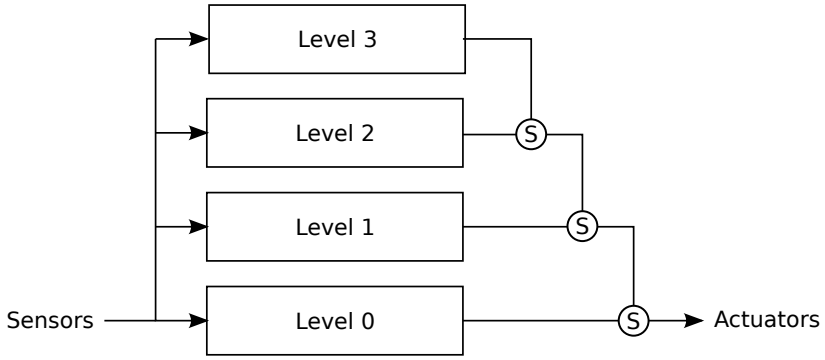

Figure 6.10: Schematic representation of the Subsumption architecture. Each later is responsible only for the execution of a single behaviour. Layer are computed in parallel and output suppression signals passing from the higher layer to the lower one.

Brooks' s subsumption architecture also follows an incremental design (Vargas et al., 2014). It aims to build entire robots from simple behaviours, and then adding additional mechanisms to orchestrate these behaviours and increasing the level of sophistication of the robot controller. This permits to break down a large design problem into smaller ones, which are more tractable and can be independently solved. Following this principle, a 24 degrees-of-freedom kinematic model of the T-Hex robot was created in a first stage. In the second stage a central pattern generator was hand-design and coupled with the morphology of the robot. In the final stage a CASN was mounted on top of the central pattern generator and sensory sensory input was added to the network. Overall, this topology shows that efficient locomotion can be generated to several surfaces by adding biological signalling networks.

6.4.1 Coupled Artificial Signalling Networks

Initial interpretations of biological CPGs considered them as autonomous nervous centres able to oscillate at a constant frequency and provide motor directives to overcome the dissipation usually associated with friction, gravity or other circumstances (Brown, 1914). However, locomotion also relies on limb dynamics and signalling pathways are also involved in locomotion. Although the consideration of environmental information is not a requirement to produce effective locomotion, feedback is essential to preserve the synchronisation amongst limb movements, increasing the adaptability and stability of control systems in real time (Frasca et al., 2004).

In fact, the combination of limb dynamics and feedback information promotes the usage of decentralised robot controllers (Kuo, 2002). Despite CPGs naturally sustaining oscillatory behaviours, biological organisms do not exhibit periodically stable movements. In this sense, the feedback signals retrieved from different oscillatory centres can independently compensate unexpected disturbances and account for the physical properties of the terrain. This broadens the controller's robustness and increases its performance upon drastic changes in the sensory information.

In a biological context, there exists enough evidence to demonstrate that signalling pathways affect the performance of CPGs (Grillner et al., 1981). However, integrating environmental information is a hard task in control theory, particularly when these sensory signals come from multiple, diverse and potentially noisy sources, such as the sensors mounted in a robot. This lack of accuracy entails that sensory signals imprecisely monitor the state of the system, which results in fuzzy control commands. Nevertheless, this is a task that cellular signalling networks are evidently good at solving within a biological context.

The first layer of the proposed architecture encapsulates a CASN. In this respect, the work on this thesis explores whether computational analogues to cellular signalling networks and their self-emergent and dynamical interactions can solve an analogous task within a robotic system. As mentioned previously in Chapter 3, these networks are computationally interesting for a number of reasons. This includes their capacity to express complex behaviors, their robustness, their capacity to adapt to changing environments, their ability to reduce environmental noise when individual ASN are loosely coupled (low levels of crosstalk) and their evolvability. From the perspective of robotic locomotion, CASNs have the capacity to

solve problems with a strong dependence amongst their inputs using a set of weakly interconnected networks, producing a joint response. This pattern of behaviour seems particularly appropriate for locomotion control, in which there are often many, potentially dependent, inputs.

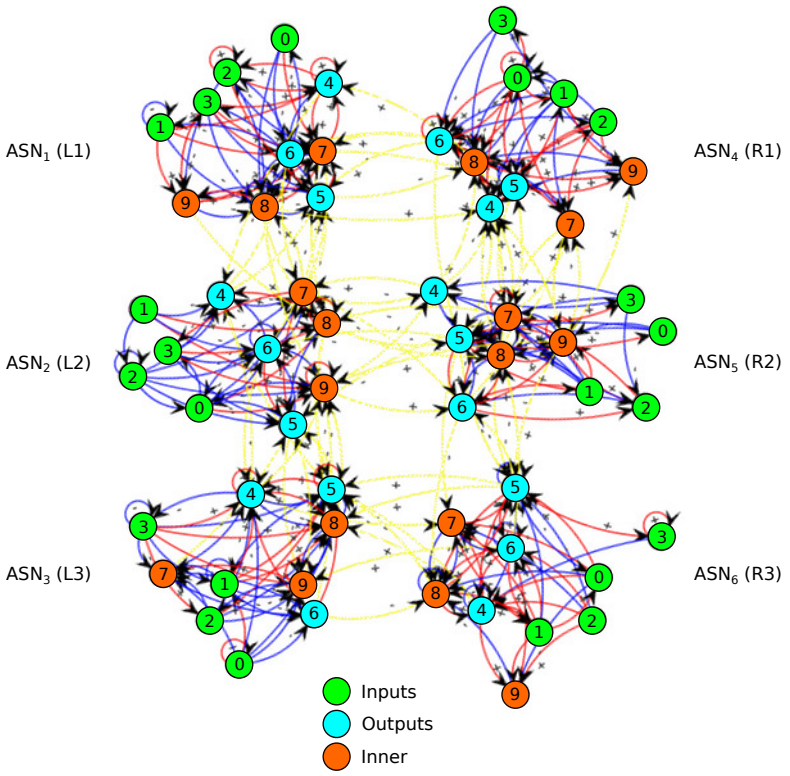

Figure 6.11: A coupled artificial signalling network evolved to provide an adaptive gait within uneven environments. The inputs, for each component network, are from the contact sensor on the corresponding leg, and the three infrared sensors on the corresponding side of the robot. The outputs are CPG control parameters. Crosstalk edges are shown in yellow.

An evolutionary algorithm is used to design a CASN that, when stimulated with environmental information, produces reactive behaviours which modulate the governing parameters of a set of CPGs in order to effectively propel a legged robot. The global dynamics of the CASN are the results of the crosstalk interactions between the different ASNs. Figure 6.11 shows an example of a CASN evolved to provide an adaptive gait in an uneven environment. It illustrates how local inputs are delivered to different ASNs and also the patterns of crosstalk connections between ASNs.

6.4.2 Central Pattern Generation Model

The middle layer of the proposed topology builds the CPG in charge of the generation of the rhythmic motion patterns needed for locomotion in a six legged robot. Locomotion patterns are modulated by simple commands coming from the outputs of the upper-layer. The CPG is modelled by a set of dynamical oscillators, one per limb. In particular, the movement of each limb is independently controlled by the x and z variables of a single nonlinear Hopf oscillator (Righetti & Ijspeert, 2006) as follows:

$$\dot{x_i} = \alpha(\mu - r_i^2)x_i - \omega_i z_i \tag{6.11}$$

$$\dot{z_i} = \gamma(\mu - r_i^2)z_i + \omega_i x_i \tag{6.12}$$

where x_i and z_i are state variables, $r_i = \sqrt{x_i^2 + z_i^2}$, the amplitude of the oscillator is given by $A = \sqrt{\mu}$ for $\mu > 0$ and the frequency of the oscillator (in $rad \cdot s^{-1}$) is governed by ω_i. α and γ are positive constants that determine the velocity of convergence to the limited cycle. The relaxation to the limit cycle is given by $(2\alpha\mu)^{-1}$ and $(2\gamma\mu)^{-1}$. The usage of different convergence speeds for the x and z variables allows a higher degree of control over the generated trajectory (Righetti & Ijspeert, 2008). Figure 6.12 shows an example of a trajectory generated by a Hopf oscillator.

The Hopf oscillator in equations (6.11) and (6.12) encodes an oscillatory behaviour where the ascending (swing) part and the descending (stance) part have equal frequencies. In order to independently modulate the frequency of these parts the following expression is considered (Righetti & Ijspeert, 2006):

$$\omega = \frac{\omega_{st}}{e^{-sz_i} + 1} + \frac{\omega_{sw}}{e^{sz_i} + 1} \tag{6.13}$$

where ω switches between two different values, the stance frequency, ω_{st}, and the swing frequency, ω_{sw}, based on the sign of z_i. The switching velocity is determined by the value of s. In general, it is possible to obtain a desired gait by independently modulating both frequencies.

In contrast to Campos et al. (2010), where the trajectory of each 3-DOF limb in a six-legged robot is uniquely controlled by the $\dot{x}_i$ generated solution of a Hopf oscillator, this work considers both trajectories, $\dot{x}$ and $\dot{z}$, to control the position and orientation of the tip of each 4-DOF limb within the T-Hex workspace. The x variable represents the movement of the coxa joint, while the z variable defines the angles of the tar, tibia and femur joints.

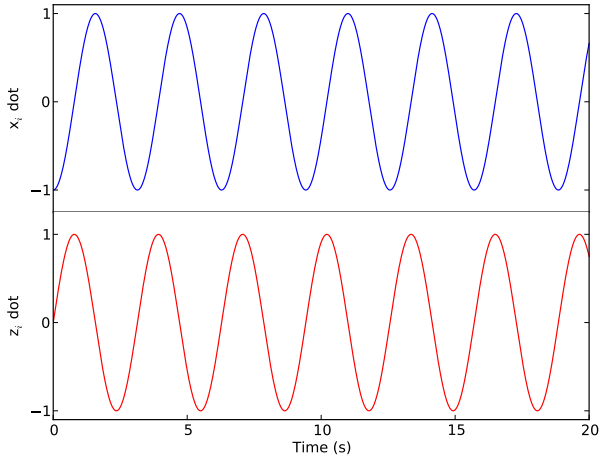

Figure 6.12: Generated $\dot{x}_i$ (upper graph) and $\dot{z}_i$ (bottom graph) outputs of a Hopf oscillator, where $\omega = 4\,\mathrm{rad} \cdot \mathrm{s}^{-1}$, $\mu = 1$, $\alpha = 5$ and $\beta = 50$. The ascending and descending phases have the same frequency.

In terms of robotic locomotion, this oscillator has three prominent benefits. First, the system enables the generation of periodic locomotion patterns without sensory information or rhythmical feedback. Second, it is able to preserve smooth, stable and cyclic trajectories in the presence of small perturbations (Santos & Matos, 2011). Third, the generated trajectory can be exclusively modulated by performing changes to its amplitude μ, and its frequency ω, whilst preserving unaltered the additional parameters. This parameter separation also eases optimisation using evolutionary algorithms and makes possible the integration of feedback information. The benefits of evolutionary techniques in controlling robotic system are reviewed in Section (6.3.3).

Interlimb Coordination

Interlimb coordination is achieved by non-diffusive coupling of the nonlinear Hopf oscillators. Despite being a type of weak connection, non-diffusive coupling has a positive impact on the stability of the CPG as it increases the coupling robustness upon the presence of noise (Hale, 1997) and ensures that each oscillator stays synchronised. Hopf oscillators are coupled as follows:

$$\begin{bmatrix} \dot{x}_i \\ \dot{z}_i \end{bmatrix} = \begin{bmatrix} \alpha(\mu_i - r_i^2) & -\omega \\ \omega & \gamma(\mu_i - r_i^2) \end{bmatrix} \begin{bmatrix} x_i \\ z_i \end{bmatrix} + \begin{bmatrix} 0 \\ \sum k_{ij}(z_i + \lambda_{ij} z_j) \end{bmatrix} \tag{6.14}$$

where $i, j \in \{L_1, L_2, L_3, R_1, R_2, R_3\}$, $k_{ij} \in [0, 1]$ is the diffusive coupling term and λ_{ij} is the coupling coefficient that defines the effect of the ith oscillator on the jth oscillator, which establishes phase relationships between them. The value of λ_{ij} is set to 1 if the oscillators excite each other and to -1 if the oscillators inhibit each other (Liu et al., 2009). Note that this distribution of the λ values corresponds to the tripod gait. Figure 6.13 illustrates the generated $\dot{x}_i$ and $\dot{z}_i$ trajectories of such an oscillator-based network.

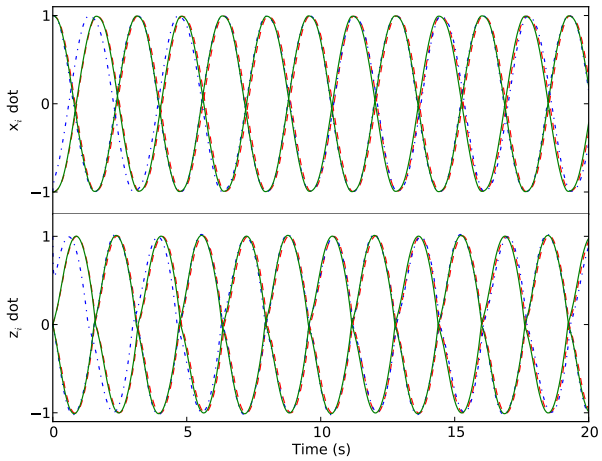

Figure 6.13: Generated $\dot{x}_i$ (upper graph) and $\dot{z}_i$ (bottom graph) trajectories of an oscillator-based network. The network is composed of six non-diffusive coupled oscillators. Trajectories obtained for aleatory k_{ij} and constant $\omega_{st} = 2\,\text{rad} \cdot \text{s}^{-1}$, $\omega_{sw} = 2\,\text{rad} \cdot \text{s}^{-1}$, $\mu = 1$, $\alpha = 5$ and $\beta = 50$. Notice that non-diffusive coupling favours entrainment between oscillators.

In accordance with the previous CASN topology, the decentralised CPG also consists of six different CPG-units, one per robotic leg. Each is immediately connected with its corresponding upper-level ASN, whose outputs represent the amplitude of the oscillator μ, the swinging frequency, ω_{sw}, and the stance frequency, ω_{st}. The CPG mimics the coupling between ASNs and the crosstalk probability, C_p, between the ASN_i and ASN_j becomes the diffusive coupling term k_{ij}. Using this approach the behaviours arising in the CASN are directly translated into gait trajectories, which are individually generated based on the limb's dynamics and sensory feedback information. Figure 6.14 illustrates the bio-inspired controller associated with each leg.

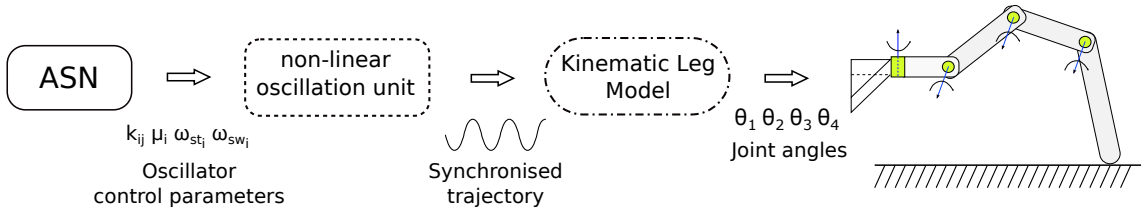

Figure 6.14: Each ASN takes sensory information and outputs a set of parameters that modulate the generated trajectory of each nonlinear oscillator unit. Likewise, the kinematic layer samples each trajectory to obtain every joint angle and thereby controls the hexapedal locomotion.

6.5 Inverse Kinematics

This section describes the bottom layer of the proposed architecture. This layer relies on a trajectory planning algorithm to translate the CPG generated trajectories into limb movements. The kinematic layer inputs the $\dot{x}$ and $\dot{z}$ generated solutions of each Hopf oscillator. Its outputs are the joint angles of each 4-DOF leg of the T-Hex robot. As described in section 6.2, oscillatory trajectories are initially sampled at a constant rate. Then, the selected points are fed to an inverse kinematic algorithm to calculate the joint angles, which describe the position and orientation of the limb's tip in the robot workspace.

In contrast to section 6.2, where a path planning algorithm is applied directly over a cycloid function, the transformation of CPG trajectories into joint angles must consider a number of factors:

- The height of the robot leg remains constant during the stance (supporting) phase.
- The y-axis orientation of the T-Hex robot when the CPG generates synchronised trajectories in which the duration of the stance and swing phase is constant and equals to 0. This means the robot displaces in a straight line and each limb during the supporting phase is in direct contact with the ground.
- The oscillation frequency and amplitude exclusively modulate the gait's height and length respectively.

Taking into account these three considerations, the global orientation of the T-Hex robot in its workspace stems uniquely from the oscillatory amplitude, and the relationship between the stance and swing phases. While the former is representative of step length, the latter controls the direction of the robot. Therefore, oscillatory trajectories with an equal duration

of the stance and swing phase produce forward motion along a straight line. Oscillatory trajectories with uneven distribution between the stance and swing phases are characteristic of circular motion. This is because the stance phase (time where limbs push the robot forward) is bigger that the swing phase. Figure 6.15 illustrates the effect of different values of the swing and stance phase in an oscillatory trajectory.

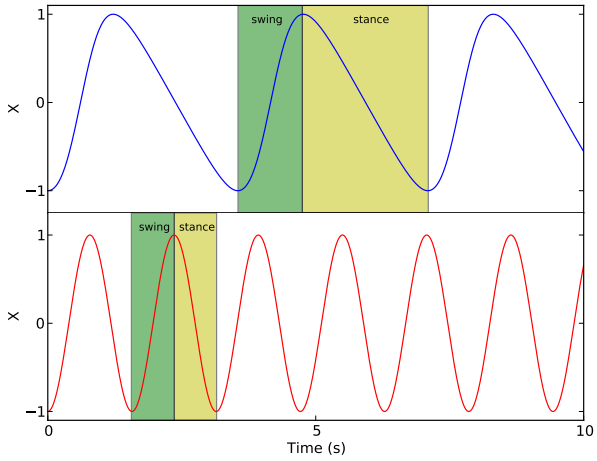

Figure 6.15: Effect of different uneven values of the swing and stance phase in an oscillatory trajectory. The upper diagram represents an example trajectory with $\omega_{sw} = 4$ and $\omega_{st} = 1$. The lower diagram plots an example trajectory with even swing and stance frequency $\omega_{st} = \omega_{sw} = 4$.

In order to achieve independence between the step's length and height, the trajectory of the coxa joint (gait length) is controlled using the generated $\hat{x}$ solution and the trajectory of the femur, tibia and tar joints (gait height) is driven using the generated $\hat{z}$ solution. Therefore, setpoints inputed by the inverse kinematic technique are denoted by $(x_i, 0, z_i)$. Figure 6.16 exemplifies the rhythmic gait trajectories used in the kinematic layer to generate motion in the T-Hex robot.

The path planning algorithm used to translate the trajectories of the CPG into locomotive movements is similar to the algorithm exposed in Section 6.2. Unlike the cycloid function where a unit vector determined the x- and y-direction of the robot, the oscillator period and amplitude now define the direction of the robot.

6.6 Evolving a Decentralised Robot Controller

All the experiments and results presented in this chapter are initially verified in the ODE robot simulator. However, they could not be replicated in the physical robot mostly due to the lack of consistency of the force sensor readings and the difficulty to replicate the simulated environment in a real context. A more rationale explanation about the inability to validate the results exposed along this chapter in the real T-Hex robot can be found in Appendix E for further information). The robot is initially configured using the tripod gait as its limited adaptability is advantageous to determine the capacity of the decentralised approach to adaptively modulate locomotion patterns using environmental feedback.

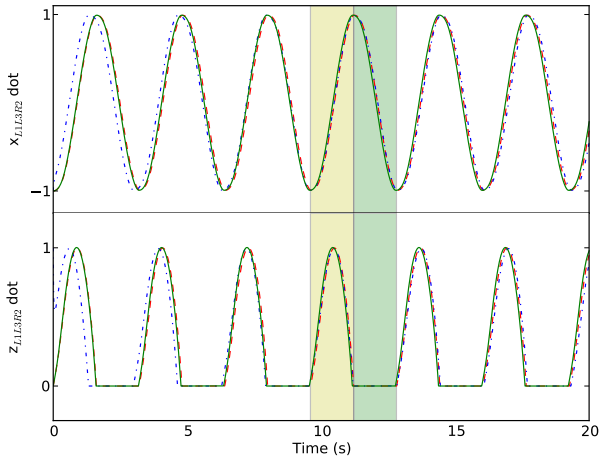

Figure 6.16: Modulated $\dot{x}$ and $\dot{z}$ solution of the L1, L3 and R2 nonlinear oscillators. Trajectories obtained for aleatory k_{ij} and constant $\omega_{st} = 2\text{rad}\cdot\text{s}^{-1}$, $\omega_{sw} = 2\text{rad}\cdot\text{s}^{-1}$, $\mu = 1$, $\alpha = 5$ and $\beta = 50$. The green and yellow coloured areas are the swing and stance phases respectively. During the swing phase the robotic limbs move forward (upper graph) while describing an elliptical arc (bottom graph), which starts at $\dot{x} = -1$ and reaches its peak at $\dot{x} = 0$. Likewise, the limb returns to the stance phase when $\dot{x} = 1$. On the contrary, the robotic limbs collide with the ground ($\dot{z} = 0$) while moving backwards along the stance phase.

Within the CASN, each sub-ASN has four inputs, corresponding to the leg contact sensor and the three lateral sensors on the same side, and three outputs which modulate the stance frequency, swing frequency and oscillatory amplitude. The signal coming from each contact sensor is not completely accurate and sometimes (i.e when the leg is sliding) it does not indicate the correct status of the leg. Although this is sufficient for the purpose of these experiments in the simulator and demonstrates the ability of the proposed architecture to sensory faults, it also compromises the validation of the simulation-based results in the phys-

ical robot. The existing noise of real environments is simulated by the lateral ultrasound sensors readings, which input noise to each ASN in the interval [0.9, 1.0]. Frequency outputs are linearly scaled in the range [0, 8] while the amplitude output is mapped in the interval [0, 2]. These values have been selected based on previous experimentation and are sufficient to guarantee locomotion. Higher values lead to undesired Hopf bifurcations, the lost of periodic oscillations and the appearance of neutral landscapes during the evolutionary process in which the generated patterns of motion are unable to propel the robot forwards. Evolved robots remains at the initial point with their legs moving arbitrarily in an asynchronous maner. The inputs of each ASN are delivered to the substrate concentration of the lower-indexed enzymes and the outputs of each ASN are deduced from the product concentration of the high-indexed enzymes. Finally, the CASN is uniquely regulated using the Probabilistic Michaelis-Menten equation and fixed crosstalk rates of 0.25 and 0.5 since these parametrisations produce the best solutions when controlling chaos in the Chirikov's map and Lorenz system (see Chapter 4).

The CPG is randomly initialised and numerically integrated using the fifth-order Dormand-Prince method with a step size of $\Delta_t = 0.01$. The generated trajectories are scaled with a maximum step height of $S_H = 70\ mm$, and maximum length of $S_L = 60\ mm$. The sampling rate, S_r is equal to $\pi/2$, or 80 integration time steps. Using this sampling rate, the generated trajectories are mapped four times per gait cycle time. These values were chosen based on experience and to prevent leg collisions. The CASN is executed every 22 simulation steps, the time the simulated robot needs to complete each movement. For each mapped point in the oscillator, the kinematic layer calculates the rotational angle for every actuator.

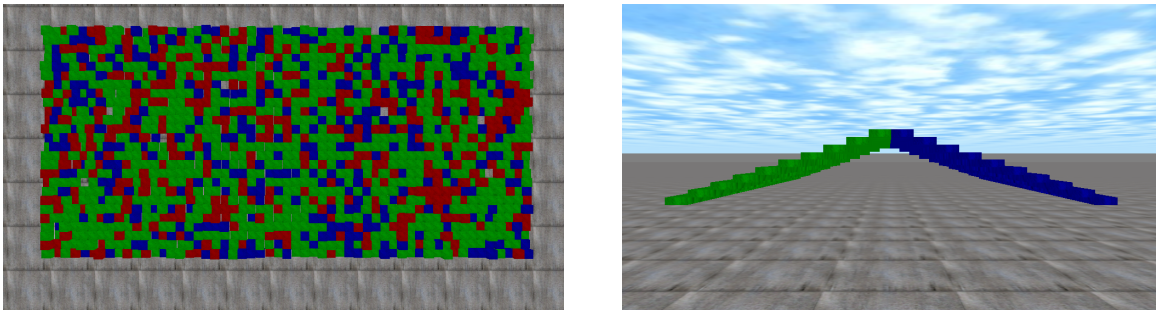

(a) Rough terrain (b) Up-and-down stairs terrain

Figure 6.17: Terrains considered to evaluate the capacity of CASN-based controllers to produce adaptive locomotion. (a) is a rectangular surface composed of 1430 boxes, each of which is randomly crease with a side of 0.2 ODE units, a maximum rotation of 20^o and a randomly selected height. (b) up-and-down staircase made of 40 rectangular steps of a height of 0.4 ODE units and a length of 1 ODE unit. The staircase width is sufficient to ensure the robot does not fall down.

The performance of the bio-inspired controller is tested upon two different types of terrains: a set of box-like shapes and a staircase-motivated surface (see Figure 6.17). The former is a rectangular surface made of 1430 boxes, each randomly created with a side of 0.2 ODE units and maximum rotation of 20^o. The height of these boxes is also selected randomly between 0 and the maximum roughness of the terrain t_r. The upper-limit roughness considered in this work is 0.6 ODE units, values over this threshold prevent the robot from moving forwards. The latter is an up-and-down staircase made of rectangular steps with a fixed height of 0.4 ODE units and a fixed length of 0.8 ODE unit. The width of the staircase is sufficiently large to prevent the simulated robot from falling off. Additionally, the staircase contains 40 steps, of which 20 are to ascend and 20 to descend. Both terrains are placed at a distance of 2.5 ODE units away from the robot center position and 1.25 ODE units for the front legs, meaning that controllers are required to move forwards, which establishes the dynamics of the CASN, before dealing with the terrain's properties.

Table 6.1: Evolution/model parameters in the evolution of locomotive gaits using the T-Hex robot

Variable	Type	Range
ω	Double	[0.0 – 8.0]
μ	Double	[0.0 - 2.0]
Mapping equation	–	Prb. Michaelis-Menten
Crosstalk Rate	Double	0.25, 0.50
Infrared readings	Double	[0.9 – 1.0]
Step Length Avg. (S_L)	Double	60 mm
Step Height Avg. (S_H)	Double	70 mm
Sample Rate (S_r)	Double	$\pi/2$
Δ_t	Double	0.01
CASN execution	–	22 steps
Terrain Roughness (t_r)	Double	[0.1 – 0.6]
Elitism	–	0.2
Mutation	–	0.015
Crossover	–	0.3
Population	–	500
Generations	–	200

The task is to evolve an CASN able to perceive environmental properties and accordingly modulate each Hopf oscillator inside the CPG to produce locomotive movements. The main objective of the set of experiments proposed in this chapter is to examine the capacity of the CASNs to express differential behaviours per leg in the form of adaptive gait trajectories. A standard generational evolutionary algorithm with elitism (rate 0.2), tournament selection

(size = 4), single point crossover (rate = 0.3) and point mutation (rate = 0.015/element). Evolutionary operators were chosen based on previous experience, and have not been optimised for individual problems. A multi-chromosomal representation is used to evolve CASNs. The population size is 500, with a generation limit of 200. Evolved CASN controllers are required to generate hexapedal gait patterns to move the robot as fast as possible in a given direction. Assuming locomotion in a straight line and no stopping, fitness is equivalent to the walked distance during a period of 2000 ODE time steps, which corresponds to ~ 15 s in real time. In order to avoid solutions showing horizontal displacements, lateral walking distances are deducted from final walked distance. Solutions causing the robot to displace backwards are penalised with a negative fitness. The process starts with the generation of a random initial population. Table 6.1 summarises the parameters of the proposed architecture and evolutionary process used to evolve locomotive gaits in a six-legged robot.

6.7 Evolution of Adaptive Gaits

When the CASN layer is not considered and the oscillator parameters are kept constant ($\omega_{st} = 2\,\mathrm{rad} \cdot \mathrm{s}^{-1}$, $\omega_{st} = 2\,\mathrm{rad} \cdot \mathrm{s}^{-1}$, and $\mu = 1$) the furthest average distance walked by the simulated robot in the evaluation period was 5.83, 5.22, 4.42, 4.16 and 3.15 ODE units using the CPG over irregular terrains with roughness of $t_r = 0.10$, 0.15, 0.2, 0.25 and 0.3 respectively. Likewise, the furthest average walked distance in the evaluation period when motion is exclusively delivered by the cycloid function was 5.56, 4.31, 3.8, 2,9, and 2.9 ODE units using the same terrain configurations with a step length and height of $60\,mm$ and $70\,mm$ respectively. In the case of the staircase terrain, the furthest average walked distances are 2.8 ODE units (third stair) using the CPG and 2.93 ODE units (third stair) before falling backward using the cycloid function. These distances correspond to the x-position of the centre of the robot. Figure 6.18 shows the fitness distribution of evolved controllers when propelling the robot forward using the the probabilistic Michaelis-Menten regulatory function and crosstalk rates of 0.25 and 0.5. For both terrain surfaces, signalling networks are able to find valid solutions, even considering CASNs must stabilise CPG trajectories before walking forward as they are randomly initialised. While there is little difference amongst averaged fitnesses for different terrains and parameterisations (when $t_r > 0.1$), the fitness distributions vary markedly. However, it is observable that evolved controllers are able to move significantly further on uneven terrains than non-adaptive controllers, meaning this

increment in performance does not come about through the use of modulation alone, but rather through evolved patterns of modulation.

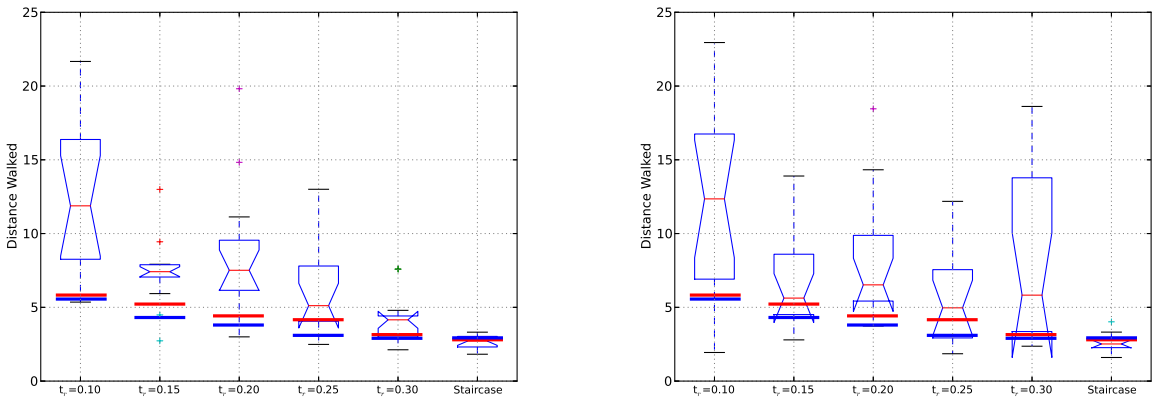

(a) Crosstalk = 0.25

(b) Crosstalk = 0.5

Figure 6.18: Fitness distribution for the proposed robotic architecture using the probabilistic Michaelis-Menten equations with crosstalk rates of (a) 0.25 and (b) 0.5 over uneven terrains with incremental roughness. Distributions towards the top of the figures are better. Thick horizontal red and blue lines indicate the furthest walking distance using the CPG and the cycloid function respectively.

Tables 6.2 and 6.3 summarise the p-values associated to the hypothesis that the controllers using the proposed CASN-based architecture shows higher walking distances on uneven terrains that non-adaptive controllers. The p-value is an estimated probability used in the context of the null hypothesis H_0 to assess the statistical significance of a result dataset. A result is said to be statistically significative if it can reject the null hypothesis, meaning that the alternative hypothesis is more plausible. In the context of this chapter, the p-value indicates the probability of observing that the distances walked using the CASN-based controller comes from a result dataset with a mean equal or smaller than the walked distance measured using non-adaptive controllers (null hypothesis), against the alternative that the mean is higher that such walked distance. Since the the result data is not uniformly distributed[3], the *Pearson's chi-squared test* was used to determined the p-values. The test returns the p-value and H, which is equal to 1 if the test rejects the null hypothesis at 5% significance level, and 0 otherwise. The smaller the p-value the larger the significance, meaning that the hypothesis under consideration may not consistently explain the observation.

The returned H values in Tables 6.2 and 6.3 (all equal to one) indicates that the Pearson's

[3] The distribution of a dataset determines the type of test used to calculate the p-values. The Kolmogorov-Smirnov Goodness-of-Fit Test (Chakravarty et al., 1967) was considered to determine if the results obtained comes from an uniform distribution.

Table 6.2: P-values of the observation that the null hypothesis, the distances walked using CASN-based controllers coupled with a crosstalk rate of 0.25, comes from a result dataset with a mean equal or smaller than the walked distance measured when using non-adaptive controllers H_0, against the alternative that the mean is higher that such walked distance.

Terrain	H_0	H	p-value
Squares $t_r = 0.1$	5.83	1	1.9239×10^{-4}
	5.56	1	1.4059×10^{-4}
Squares $t_r = 0.15$	5.22	1	0.0713
	4.31	1	0.094
Squares $t_r = 0.20$	4.42	1	0.0016
	3.8	1	5.2317×10^{-4}
Squares $t_r = 0.25$	4.16	1	0.0447
	2.9	1	0.0044
Squares $t_r = 0.3$	3.15	1	0.0022
	2.9	1	0.0016
Staircase	2.8	1	0.8554
	2.93	1	0.9640

Table 6.3: P-values of the observation that the null hypothesis, the distances walked using CASN-based controllers coupled with a crosstalk rate of 0.5 comes from a result data set with a mean equal or smaller than the walked distance measured when using non-adaptive controllers H_0, against the alternative that the mean is higher that such walked distance.

Terrain	H_0	H	p-value
Squares $t_r = 0.1$	5.83	1	2.8944×10^{-4}
	5.56	1	2.0387×10^{-4}
Squares $t_r = 0.15$	5.22	1	0.0011
	4.31	1	5.2218×10^{-5}
Squares $t_r = 0.20$	4.42	1	0.0011
	3.8	1	3.7451×10^{-4}
Squares $t_r = 0.25$	4.16	1	0.0188
	2.9	1	0.0011
Squares $t_r = 0.3$	3.15	1	0.0272
	2.9	1	0.0091
Staircase	2.8	1	0.8482
	2.93	1	0.9778

chi-squared test rejects the null hypothesis at the 5% significance level, in favour of the alternate hypothesis that the data comes from a data with a mean greater than the waked distance using non-adaptive controller. This reinforces the original perception that CASN-based controllers improve the adaptivity of the hexapod robot on uneven terrains. The CASNs layer then provides the robot controller with a variety of local leg reflexes which enhances it capacity to negotiate irregular terrains. As with Figure 6.18, the Pearson's chi-

squared test produces relatively low p-values with the notably exception of the staircase terrain. This indicates that CASN-based controllers output effective and robust locomotive patterns on irregular terrains, but they minimally enhance the locomotive properties of non-adaptive controllers in the case of the staircase terrain.

Figure 6.18 also highlights that stand-alone signalling networks can be coupled to carry out locomotion using low levels of crosstalk. This finding correlates with the results in Chapter 4, allowing the speculation that a weak linkage amongst ASNs promotes extended processing structures with tuneable behaviours. While crosstalk rates of 0.25 produced the best averaged distances, crosstalk rates of 0.5 produced the overall furthest walked distances. This is especially evident when comparing the fitness distributions associated to $t_r = 0.3$ and suggests that the level of crosstalk has a remarkable impact on both the dynamics of coupled signalling networks (even more than in Chirikov's map and Lorenz system) and the behaviour of the robot. A possible interpretation of these results is that low fitness distributions in plot 6.18(a) promotes straightforward locomotive movements, so the robot mostly walk over the uneven part of the terrain. Conversely, the fitness distributions slightly shifted toward the upper area in plot 6.18(b) indicate the robot often, but not always, steeply rotates when counteracting the uneven part of the terrain, causing the robot laterally to exit the uneven terrain onto the flat surface. Figures 6.19(d)-(e) compare the robotic trajectories of the evolved controllers when $t_r = 0.3$. A crosstalk rate of 0.25 shows the robot is able to initially locomote over the uneven terrain before floundering. The terrain's irregularities then induce severe changes in the locomotion direction. A crosstalk rate of 0.5 illustrates the robot is occasionally unable to step over the uneven terrain, so that it diverges, marginally going along the terrain's edge and then, walks apart from it. An interesting observation is that most of the trajectories, when $t_r = 0.3$, rotate to the left side. This is due to the robot initially stepping over the uneven terrain using the front left leg. The similarity between the fitness distributions associated to $t_r = 0.1$ reveals that the terrain characteristics do not prevent locomotion when reaching the uneven terrain, but are sufficient to deliver noticeable perturbations in the sense of changes in the robot direction (see Figure 6.19(a)-(b)). In the case of the staircase, it is difficult to measure the impact different crosstalk rates have on the dynamics of the controller. Unlike non-adaptive controllers, the evolved controllers prevents the simulated robot from flipping over. However, it seems the robot experiences some difficulties stepping over the first stair of the staircase. Overall, CASN controllers appear to dynamically express different behaviours when faced with changing environments

(i.e. moving form the flat part of the terrain to the uneven section and vice versa) so that the simulated robot can move over different terrain surfaces. This shows controllers have the ability to adjust their dynamics in the presence of strong perturbations, increasing their adaptability. These robotic behaviours also reflect the capacity of sub-ASNs to produce coordinated and robust responses based not only on their internal states but also on their local environment.

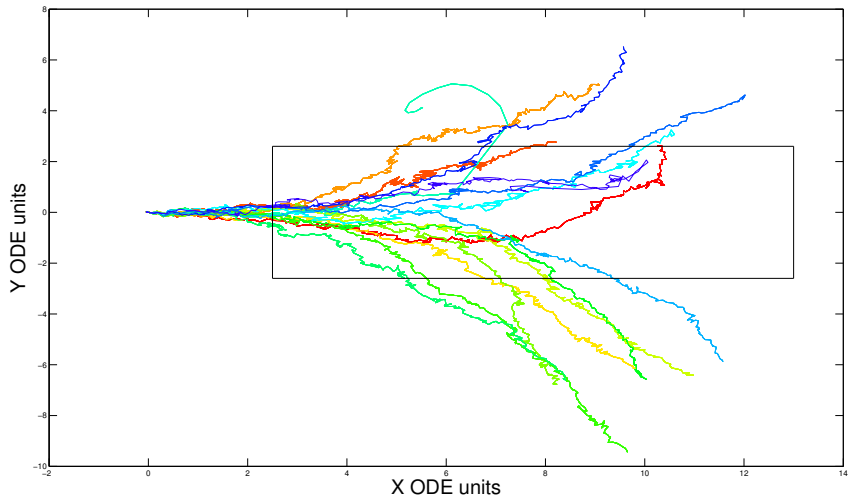

(a) $t_r = 0.1$, crosstalk $= 0.25$

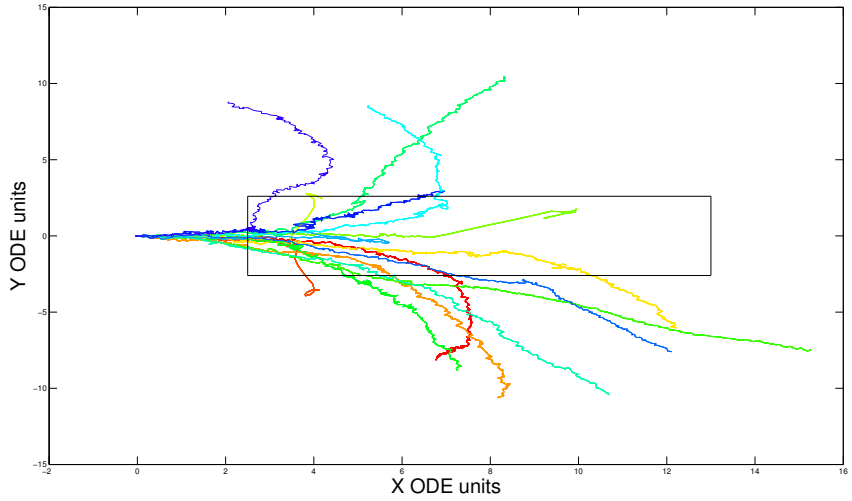

(b) $t_r = 0.1$, crosstalk $= 0.5$

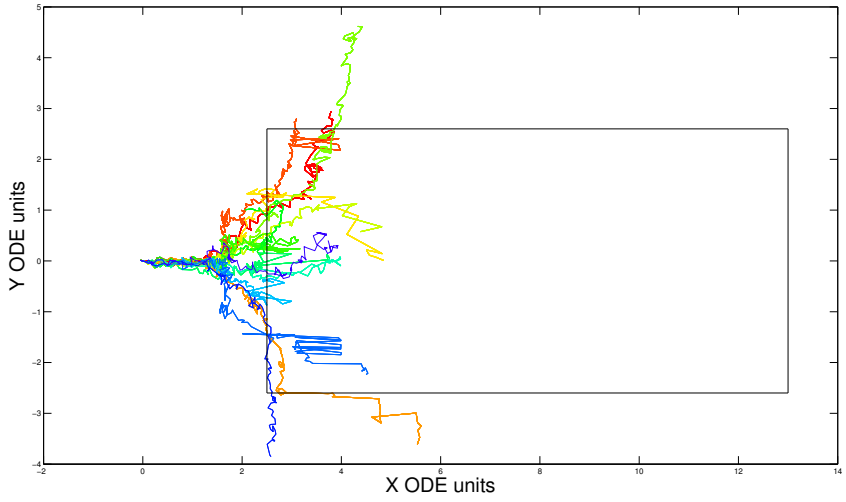

(c) Staircase, crosstalk = 0.25

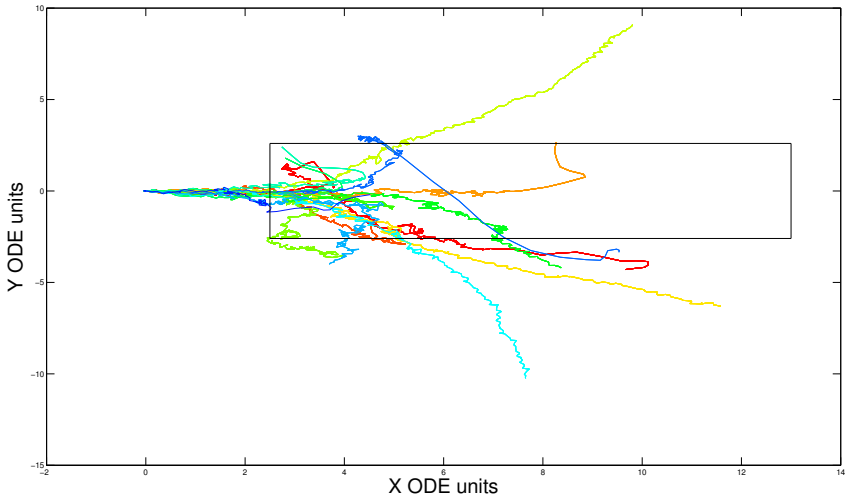

(d) $t_r = 0.3$, crosstalk = 0.25

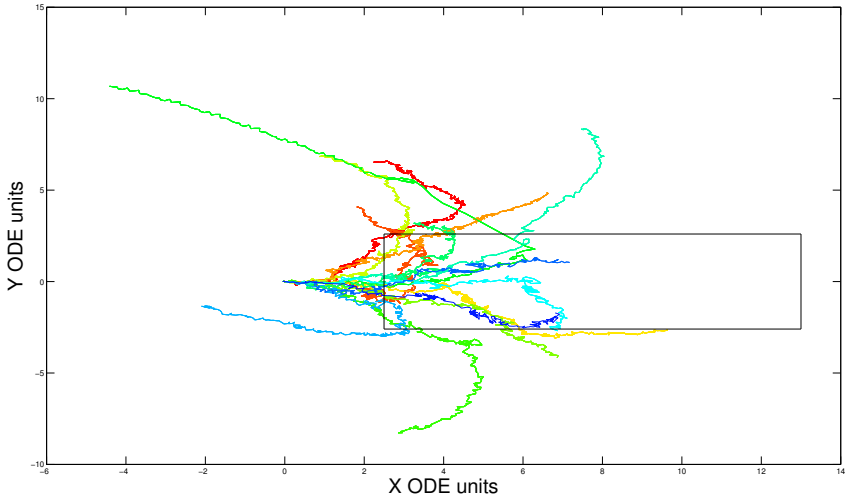

(e) $t_r = 0.3$, crosstalk = 0.5

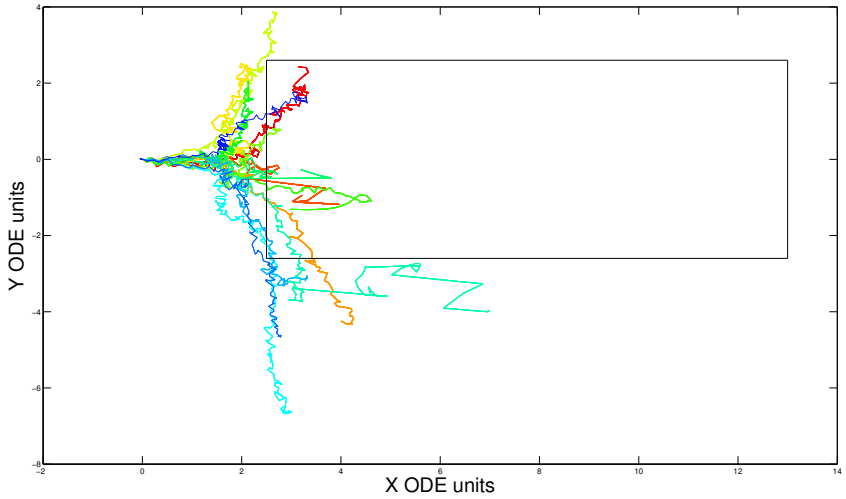

(f) Staircase, crosstalk = 0.5

Figure 6.19: Comparison of the evolved controllers' trajectories when locomoting over a range of uneven terrains when CASNs and CPGs are coupled with different crosstalk rates.

Unlike the Chirikov's map and Lorenz system the crosstalk rate in the CPG also specifies the coupling strength amongst Hopf oscillators. This also contributes to explaining the difference in performance and behaviours of controllers illustrated in Figure 6.19 when coupled with different crosstalk rates. Within the CASN, lower rates minimises local influences raising the responsiveness of the network to abrupt environmental perturbations. Within CPGs, the role of the crosstalk rate is opposite. This means that lower rates increase the capacity of individual oscillators to independently modulate their trajectory, raising the sensitivity of CPGs to changes to their governing parameters. Thus, a crosstalk rate of 0.25 induces robust patterns of locomotion which permit the robot to step over the uneven terrain but have difficulties in walking over it. Conversely, a crosstalk rate of 0.5 increases inter limb coordination but produces static and crude locomotive trajectories which make it difficult for the robot to step over the uneven terrain and induce a left rotation in the robot trajectories. Nevertheless, these results are indicative that the self-organised dynamics regulating multi-legged locomotion depend mainly on the connections amongst legs and individual controllers rather than on a single centralised controller. Similar arguments are also stated in (Frasca et al., 2004). It also hints that a trade-off between expressiveness and modularity appears to be essential to increase the overall performance of the controller and also suggests that the crosstalk rate and coupling strength should not be represented with the same variable. The effect of coupling strength in the CPG is observable in figure 6.20.

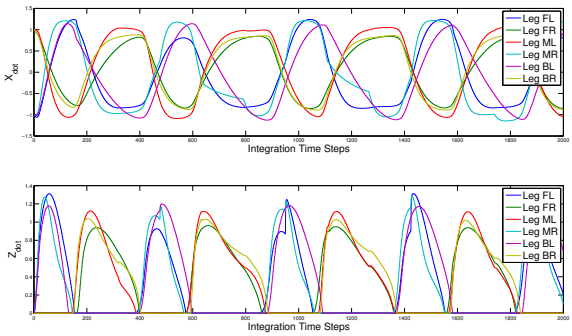

(a) GPG waveforms, $t_r = 0.5$, crosstalk = 0.5

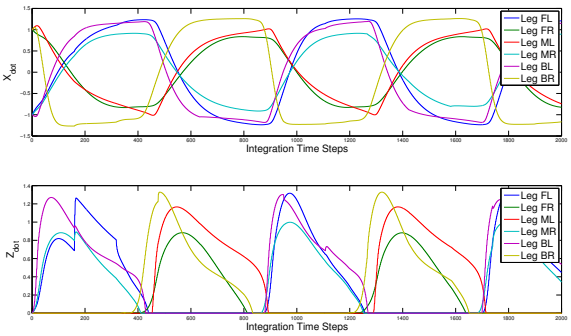

(b) GPG waveforms, $t_r = 0.25$, crosstalk = 0.25

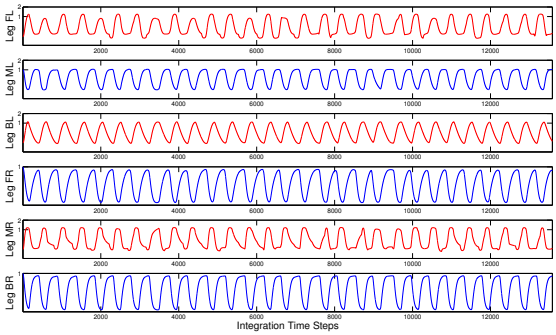

(c) $\dot{x}$ Hopf trajectory, $t_r = 0.5$, crosstalk = 0.5

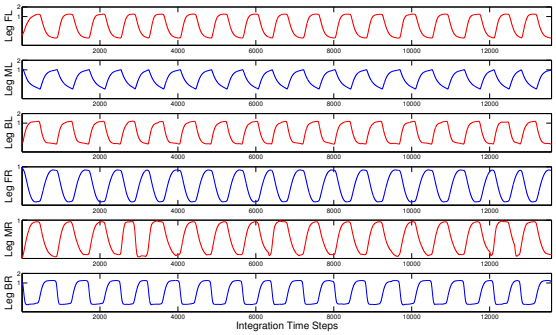

(d) $\dot{x}$ Hopf trajectory, $t_r = 0.25$, crosstalk = 0.25

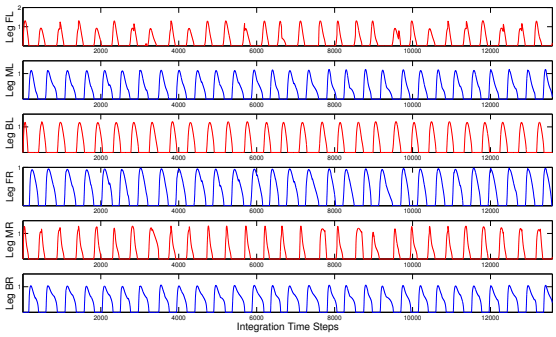

(e) $\dot{z}$ Hopf trajectory, $t_r = 0.5$, crosstalk = 0.5

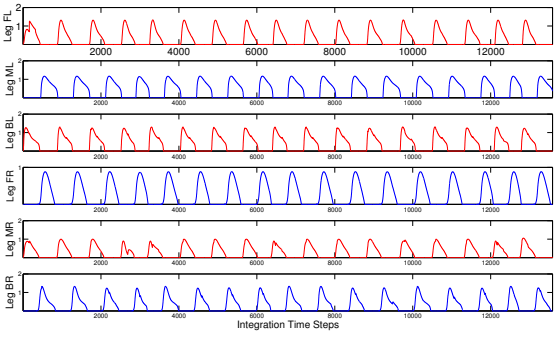

(f) $\dot{z}$ Hopf trajectory, $t_r = 0.25$, crosstalk = 0.25

Figure 6.20: Example of the CPG trajectories modulated by an evolved CASN. (a) and (b) illustrates the global output of two CPGs when regulated with crosstalk rates of 0.5 and 0.25 respectively. (c) and (d) show the $\dot{x}$ trajectory of each Hopf oscillator. (e) and (f) displays the $\dot{z}$ components of each Hopf oscillator. The top three patterns on each plot corresponds to the left leg, while the three bottom trajectories denote right leg trajectories. Red-plotted trajectories are 180^o out-of-phase with respect to blue-plotted trajectories.

Figure 6.20 shows the trajectories of evolved controllers when moving forward on an uneven terrain with $t_r = 0.25$. The front leg of the robot makes contact with the uneven part of the terrain at $\Delta_t \sim 2000$ and $\Delta_t \sim 2100$ when the crosstalk rates are 0.25 and 0.5 respectively. A pertinent observation is that trajectories maintain their periodicity and synchronisation during the evaluation time despite stand-alone ASNs being quasi-independently modulated. Individual trajectories alter their amplitude and frequency showing a distinctive structure. This highlights the role of CASNs in producing adaptive trajectories. It is perhaps surprising that controllers regulated with a crosstalk rate of 0.25 require a lesser number of step during evaluation time. However low crosstalk rates increase the behavioural expressiveness of CPGs, easing the robot's ability to counteract terrain characteristics. Figure 6.20 also reflects that oscillator modulations are not related only with the amount of exchanged information amongst sub-ASNs but also amongst the coupling structure amongst CPG-units. It can be observed that perturbations in the front legs are mainly propagated between legs that are in-phase. An example of this phenomenon can be seen in the trajectory labelled as Leg FL (front left) in plots 6.20(c)-(d) at $t_s = 2000$.

In general, it can be noted that although the ratio between the swing phase and stance phase steadily changes, trajectories are mainly modulated during the swing phase whilst the stance phase is practically constant. It is convenient to note that there was not any limitation in the capacity of CASNs to modulate CPG trajectories during the evolution time. This property is the main characteristic of wave gaits and suggests that CASNs can be effectively considered to evolve irregular patterns of motion which lead to locomotive gaits. However, it is also arguable that the intrinsic features of Hopf oscillators biases the capacity of evolved controllers to deliver gait diversity and preserves the tripod-gait. Recent work shows that locomotive approaches using these oscillators require low convergence rates to exhibit gait diversity (Campos et al., 2010; Santos & Matos, 2011).

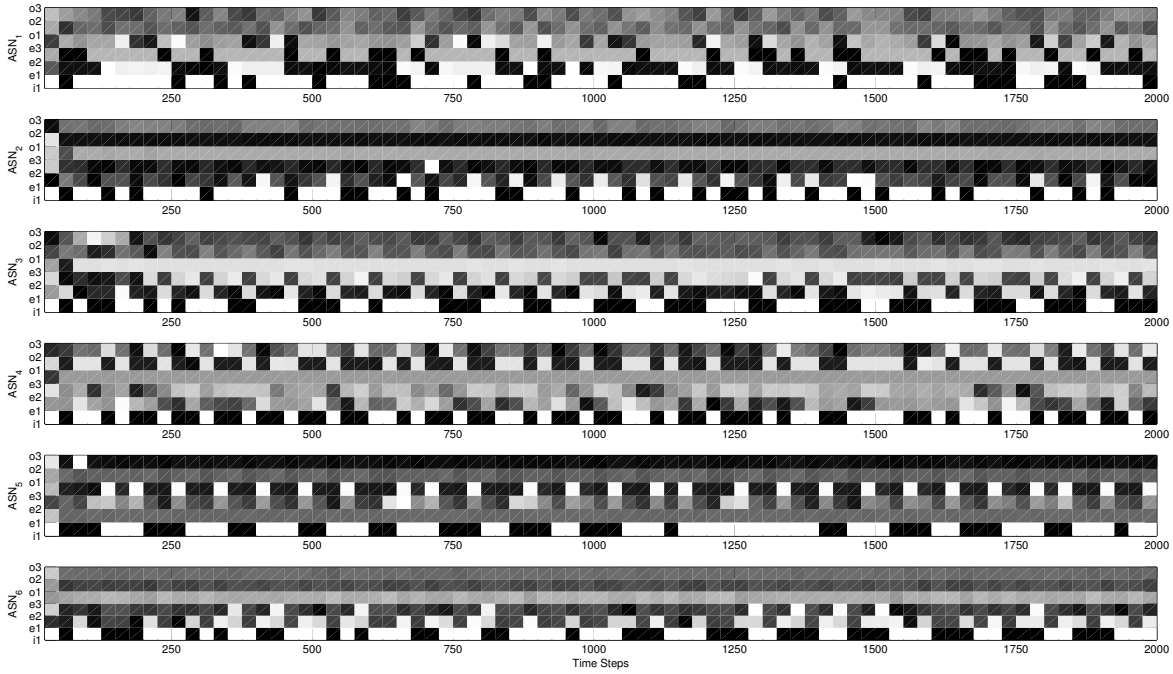

(a) Uneven terrain with $t_r = 0.2$ and crosstalk rate = 0.25

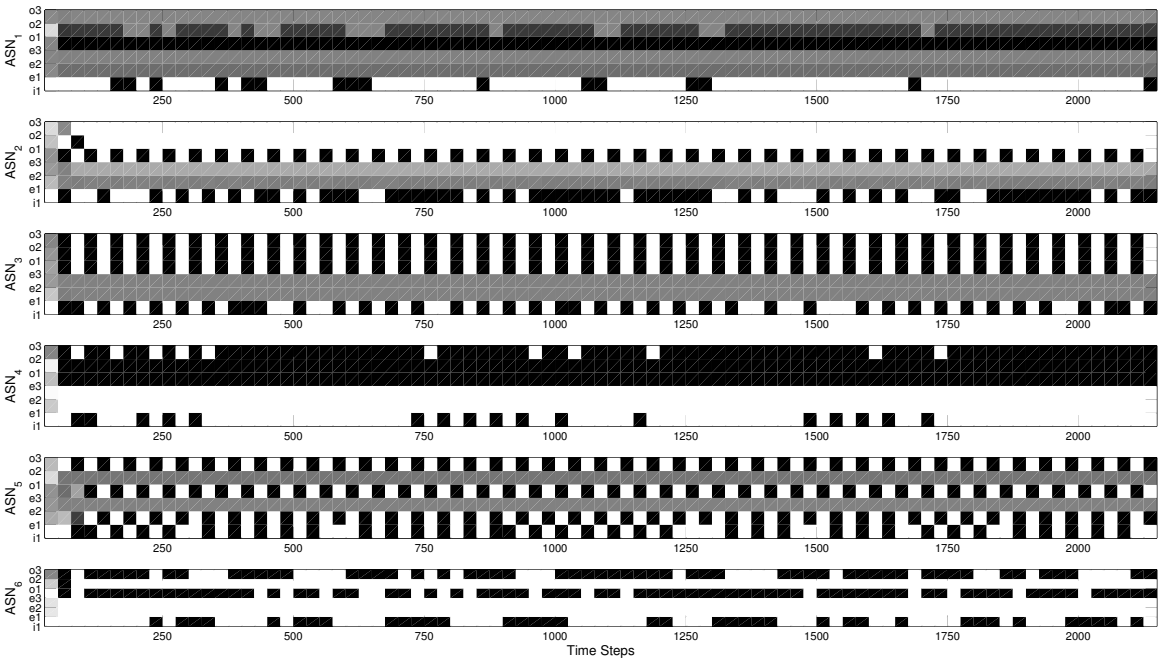

(b) Staircase and crosstalk rate = 0.25

Figure 6.21: Example of the internal state of evolved CASNs controlling the gait modulation of the hexapod robot.

Figure 6.21 shows the internal state of two evolved CASNs carrying out locomotion on the uneven terrains and staircase. To ease visualisation, the noise inputs corresponding to the lateral infrared sensors (inputs $\{i_2, i_3, i_4\}$ in the CASN) are not shown. It can be seen that sensory feedback plays an important role in the dynamics of coupled signalling networks to regulatory CPG trajectories. Similar conclusions have also been noted by the authors in Frasca et al. (2004). In the case of figure 6.21(a), it is rather difficult to extract any clear conclusion. Contact sensors exhibit a markedly irregular sensing pattern, which lead to unstable behaviours in the coupled signalling networks. Although these imbalances prevent CASNs from expressing ordered dynamics, it is possible to suggest that they induce the essential irregular perturbations across the network that allow the robot to locomote in stochastic terrains. On the contrary, locomotion over the staircase shows more ordered dynamics (see Figure 6.21(b)), which to a certain extent match the sensory patterns. Simulations have revealed that this sort of dynamics promote short steps which permit the robot to overcome the first step of the staircase and prevent it from falling backwards.

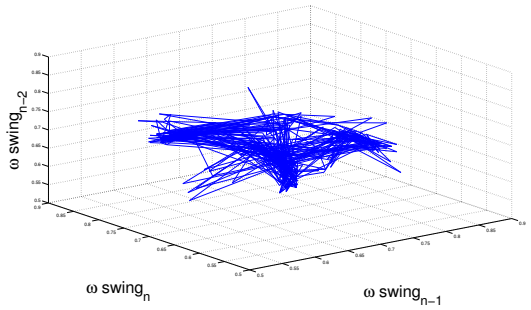

(a) Right front leg

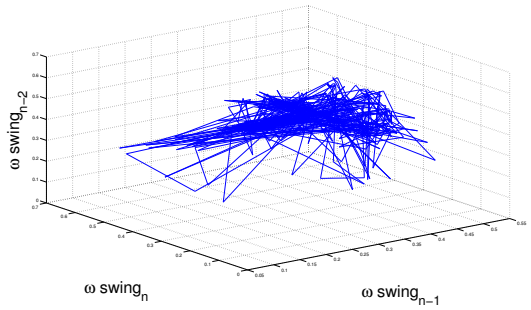

(b) Left front leg

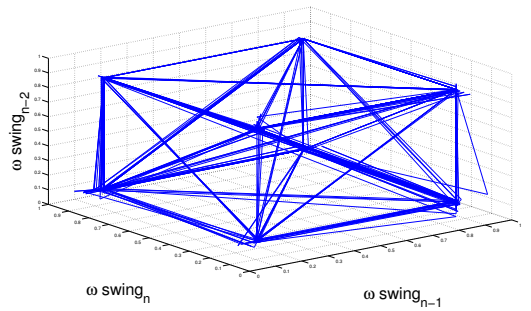

(c) Right middle leg

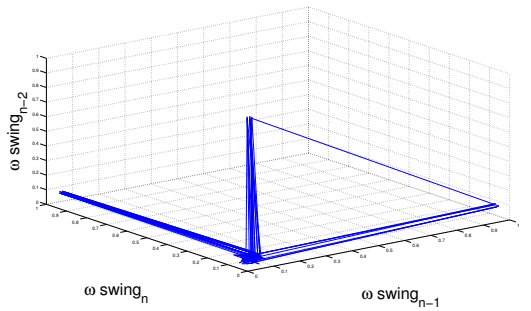

(d) Left middle leg

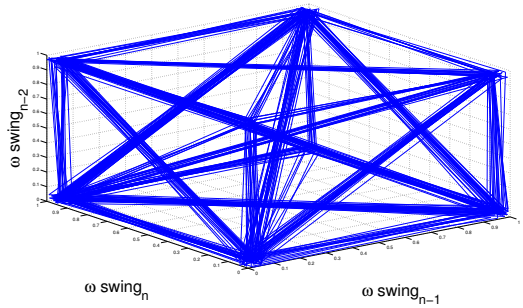

(e) Right rear leg

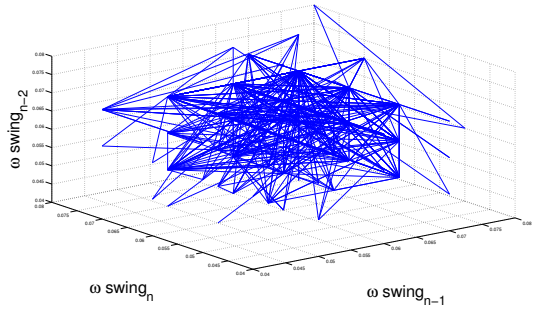

(f) Left rear leg

Figure 6.22: Swing frequency phase space of a robot whilst moving forward over a staircase.

Figures 6.22 and 6.23 display the reconstructed phase spaces of the swing frequency of two robots when locomotion is governed by the CASNs in figure 6.21. While locomotion over an uneven terrain with $t_r = 0.25$ shows irregular phase spaces that are independent of leg, the phase spaces associated to locomotion over the staircase is ordered and depends on the leg's position in the robot. Particularly, the left side of the robot depicts somewhat atypical phase spaces without a clear structure and the right side exhibits entirely stable attractors in legs located toward the rear of the robot. These attractors have a box-shaped structure with diagonal paths between vertices, corresponding to changes in the swing phase whilst the robot is in different states on the staircase. In part this reflects the complexity of the problem, since the network needs to handle different step lengths corresponding to the terrain properties in order to maximise fitness. Further, this evolution of the attractor structure may also suggest that legs have different roles according to their position in the robot. While the front legs are used to sense the terrain characteristics, the back legs propel the robot forward with the notable exception of the back right leg. As a consequence this leg reaches the terrain the last, it steadily stalls behind the initial stair, preventing the robot from moving over the staircase. In this sense the imbalances in the right rear contact pattern distort the attractor shape in order to cope with non-flipping transitions between the flat terrain and the staircase.

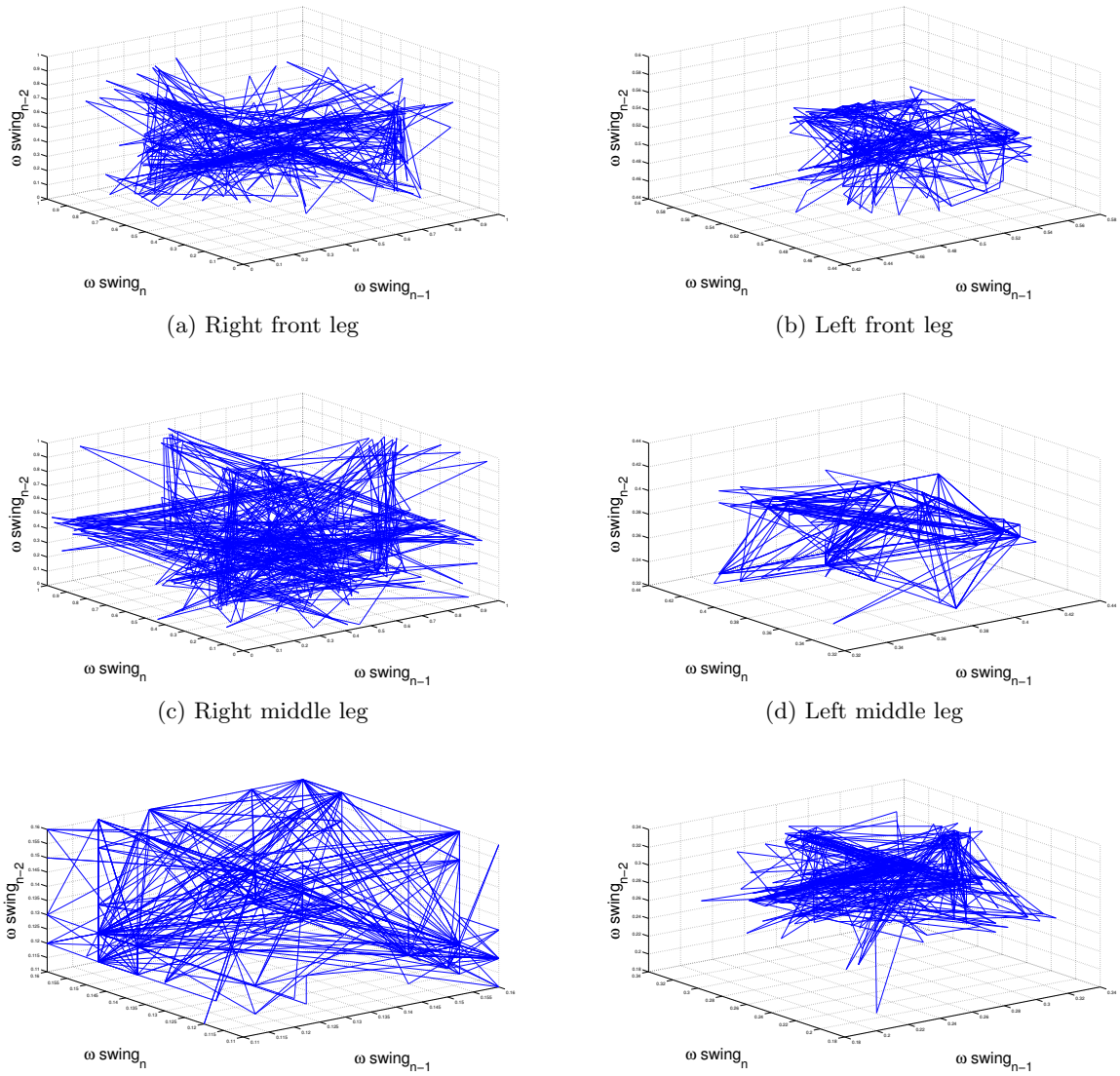

(a) Right front leg

(b) Left front leg

(c) Right middle leg

(d) Left middle leg

(e) Right rear leg

(f) Left rear leg

Figure 6.23: Swing frequency phase space of a robot whilst moving forward over an uneven terrain with $t_r = 0.25$.

Figure 6.24 and 6.25 illustrate the sequence of video stills of adaptive locomotion using the proposed architecture on an uneven terrain with $t_r = 0.25$ and the staircase respectively.

6.8 Summary

This chapter has introduced an evolvable bio-inspired architecture for the controlling of a six-legged robotic system. This architecture comprises three layers and is responsible for the generation of adaptive trajectories using sensory information. The upper layer is a CASN

made of six coupled ASNs (one per leg). This layer retrieves environmental information and outputs control directives which modulate the governing parameters of a CPG. Locomotive patterns are produced in the middle layer, which is defined by a CPG of six coupled Hopf oscillators. Finally, a kinematic layer transforms the oscillatory trajectories into robotic movements using a path planning algorithm. Overall, this architecture aims to imitate the hierarchical control and locomotion pattern generation that take place at the neural level and emerges from the local influences amongst the network of neurons in charge of the control of each leg.

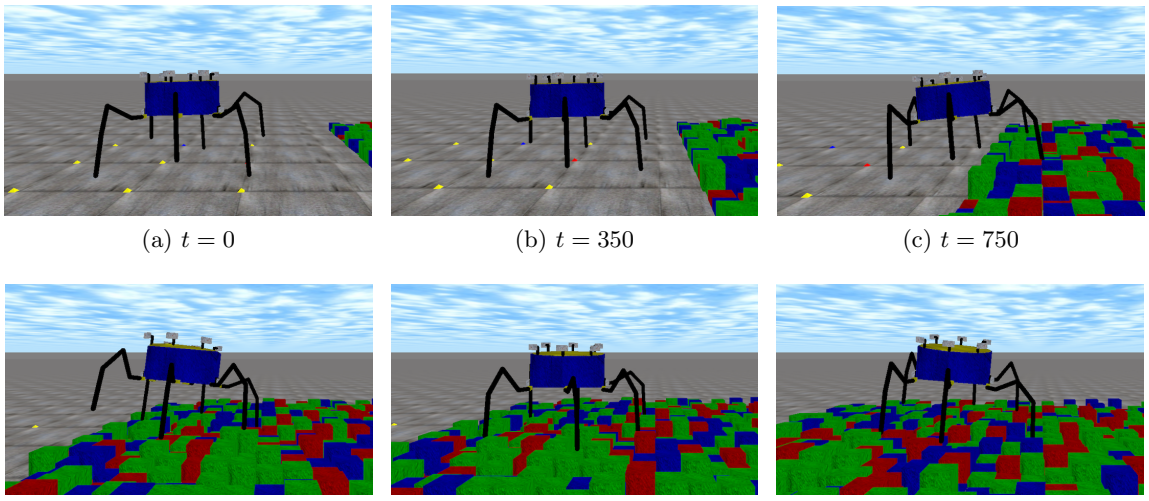

(a) $t = 0$ (b) $t = 350$ (c) $t = 750$

(d) $t = 1100$ (e) $t = 1450$ (f) $t = 1900$

Figure 6.24: Example of adaptive locomotion on uneven terrain with $t_r = 0.2$.

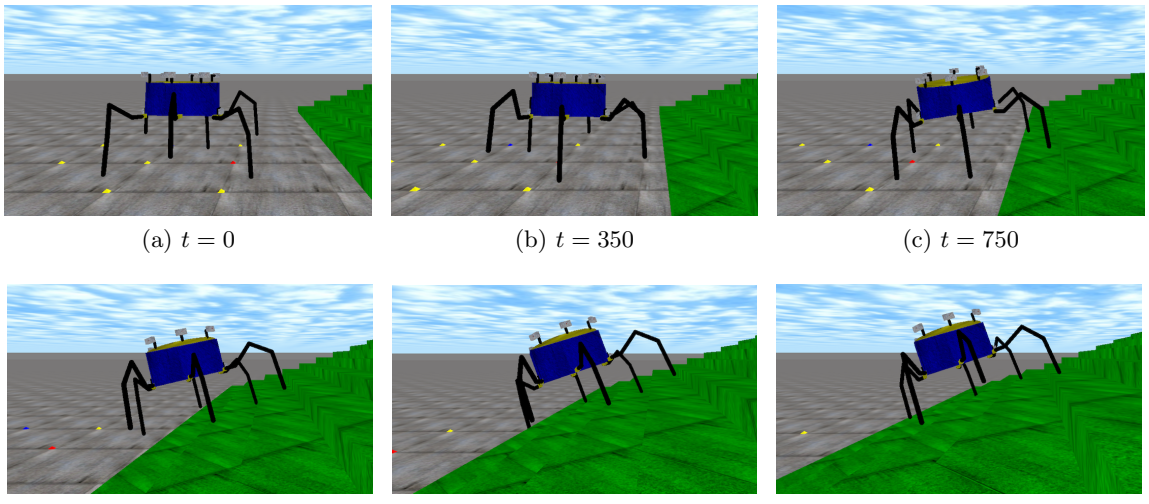

(a) $t = 0$ (b) $t = 350$ (c) $t = 750$

(d) $t = 1100$ (e) $t = 1450$ (f) $t = 1900$

Figure 6.25: Example of adaptive locomotion on a staircase.

The proposed topology has been evaluated using two types of terrains: an uneven terrain with incremental roughness and a staircase. While the former is mainly stochastic and was used to evaluate the capacity of controllers to generate adaptive trajectories, the latter explores the generation of stable locomotive behaviours. In both cases, results have indicated that crosstalked ASNs were able to effectively modulate the CPG trajectory in order to produce locomotive behaviours. It suggests that local influences amongst ASNs are beneficial to propagate environmental information amongst neighbouring ASNs and generate adaptive gaits, even when the dynamics of each leg change completely. This self-organising capacity hints that CASNs can be a suitable way to model insect locomotion, which depends on the linkage amongst ASNs more than on a centralised architecture. The results also highlight the capacity of CASNs to express different behaviours when faced with changing environments while assuring an overall organisation of the spatio-temporal dynamics of the CPG in the form of locomotive motion patterns. In particular, locomotion mostly depends on the phase lag between consecutive steps. Interestingly, the network was able to regularly preserve the stability of the stance phase while mainly modulating the swing phase without manually specifying this during evolution time. Further, sensory feedback appears to play an important role in the generation of coordination amongst legs. It has also been noted that the proposed decentralised architecture shows some sort of recovery capability that makes it robust to imbalanced sensory readings.

The next chapter concludes this manuscript by presenting the main conclusions, discussing the objectives, revising the initial hypothesis and presenting future areas of research.

Chapter 7

Conclusions

Contents

This chapter summarises the work documented in this thesis, presents conclusions, validates the initial hypothesis, highlights limitations and speculates about future work.

7.1 Summary

This manuscript begun by hypothesising that "*evolvable computational abstractions of signalling networks can be used as bio-inspired control architectures for multi-legged robotic systems*". Biological systems show social complexity in the form of constant cooperations whilst accomplishing particular tasks. Typically these require behavioural diversity and robust interactions with the environment to assure the survival of the biological system. A similar level of interaction is found at a cellular level, which begins at the cell surface and terminates with a biochemical response. The complex molecular interactions taking place inside cells lead to a set of biochemical networks whose activities and functions determine the cellular behaviour.

Signalling networks are the biochemical networks responsible for perceiving and decoding environmental stimuli. They comprise a set of enzyme-mediated interactions located in the

cytoplasm, between the cellular membrane and the cytosol. Signalling pathways are the simplest working units. They communicate cells with their outside by means of the transduction of concrete extracellular stimuli. Cells also exhibit a more sophisticated signalling mechanism that allow them the simultaneous transduction of multiple stimuli and the collaboration with other cells in order to produce more robust cellular responses. Two of the main tools involved in this process are crosstalk and compartmentalisation. While the former promotes the interaction amongst pathways, the exchange of extracellular information, and the formation of extended processing structures, the latter limits the spreading of intracellular messengers, giving rise to highly specialised processing units.

This thesis has presented two computational abstractions that aim to capture the processing abilities of biological cells: a stand-alone artificial signalling network (ASN) and a coupled artificial signalling network (CASN). While the former mimics the catalytic relationships amongst enzymes in a signalling pathway, the latter replicates the connectionism amongst pathways. Formally, an ASN has been defined as an indexed set of enzyme-based nodes and a set of directed connections representing the participants of a catalytic reaction and their type. Two classes of enzymes have been considered based on their connectivity: receptor enzymes (zero inputs and multiple outputs) and regulatory enzymes (multiple inputs and outputs). The interaction amongst ASNs has been modelled by the probability of crosstalk and represented by a set of crosstalk enzyme-based nodes linking two neighboring ASNs. This thesis has also examined the regulatory capacity of the main catalytic functions in biological systems: Hill, Michaelis-Menten, probabilistic Michaelis-Menten and Phosphorylation equations.

The dynamical properties of both stand-alone and coupled signalling networks have been initially analysed upon controlling the Chirikov's map and Lorenz systems. Despite lying at opposite ends of the dynamical spectrum, their chaotic behaviors can both be controlled by applying time-dependent perturbations to their governing parameters. Unlike the conventional chaos control methods, this thesis has considered the use of evolutionary algorithms to infer the structure of the controllers from the interaction between the signalling network and its environment. The results have indicated that stand-alone and coupled ASNs can be evolved to carry out chaos targeting in both dynamical systems. While CASN controllers led to the best controllers in the Lorenz system, ASN controllers often, but not always, perform better in Chirikov's standard map. Furthermore, it has been observed that high-ordered regulatory functions constantly led to the evolved controllers with the best performance.

Perhaps the most significative observation raised from these initial results is the capacity of crosstalk to first support extended computational models that mimic the spatial relationships in biological signalling networks and second solve highly correlated problems in a decentralised manner. It has been speculated that low crosstalk rates are beneficial to obtain collaborative solutions since they are sufficient to induce a dynamical change in the coupled networks, but also to maintain unaltered the intrinsic dynamics of each sub-ASN. Conversely, high crosstalk rates distort sensory information adding uncorrelated noise. Further, the results have also highlighted the importance of the global output of a CASN has on finding valid controllers. It has been demonstrated that the calculation of the global output of a CASN as the standard mean of all contributing sub-ASNs penalises the performance of evolved controllers.

Having evaluated the processing properties of signalling networks, this thesis has presented a novel bio-inspired architecture for controlling a six-legged robot. The evolvable architecture comprises three layers and generates adaptive leg trajectories using sensory information. The upper layer is a CASN made of six coupled ASNs (one per leg). It retrieves environmental information and outputs control directives which modulate the governing parameters of a CPG. Locomotive patterns are produced in the middle layer, which is defined by a CPG of six coupled Hopf oscillators. Finally, the bottom layer relies on a complete kinematic analysis of the robotic system to transform oscillatory trajectories into robotic movements using an innovative path planning algorithm. It uses both trajectories of a two-dimensional oscillator to achieve independence between the step length and height.

The proposed architecture has been examined using two types of surfaces: an uneven terrain with incremental roughness and a staircase. While the former is mainly stochastic and was used to determine the capacity of evolved controllers to engage adaptive trajectories, the latter explores the generation of stable patterns of locomotion. Upon both terrains, the results have shown that coupled ASNs can individually modulate trajectories of a CPG and deliver adaptive locomotion on irregular terrains. Further, it has also been noted the capacity of CASNs to express different behaviours when faced with changing environments. Interestingly, the proposed architecture was able to regularly preserve the stability of the stance phase while mainly modulating the swing phase without manually specifying this during evolution time. In this sense, it has been observed that sensory feedback plays an important role in order to achieve inter-limb coordination.

7.2 Conclusions

Artificial Signalling Networks have been applied to a range of complex control problems. The analysis of their performance and behaviour has led to a number of conclusions.

Highly correlated problems can be solved in a decentralised manner

Coupled signalling networks represent a collection of connected pathways, each with its own inputs and outputs. This allows the formation of extended abstractions in which each signalling pathway is responsible for the processing of individual variables. Therefore, non-linear problems with a high dependence amongst variables can be decomposed into smaller sub-tasks, which are totally or partially independently solved by each sub-ASN in the coupled signalling network. This is evidenced by the fact that coupled signalling networks can be evolved to carry out control tasks in various kind of complex dynamical systems using a range of crosstalk rates.

Weak crosstalk promotes the emergence of collaborative behaviours

The level of crosstalk defines the intensity of the local influences amongst ASNs. Low levels of crosstalk limit the interaction amongst ASNs, preserving the nature of their dynamics. This decreases the sensitivity of CASNs to environmental noise but elicits a gradual dynamical change in the coupled network as abrupt alterations in the sensory feedback propagate across ASNs. This is supported by a significant amount of experimental evidence showing that an ASN modifies its behaviour based on the dynamical state of adjacent ASNs and the overall behaviour of CASNs cannot be deducted from the dynamics of individual ASNs.

High-ordered catalytic equations lead to more effective regulation

This is suggested by the positive effect of multi-substrate reactions. When signalling networks are regulated by catalytic reactions that explicitly take into account the existence of several binding sites in an enzyme the performance of evolved controllers considerably increases. The effect of this is to strengthen the internal connectivity of signalling networks. Broadcast signals rapidly flow amongst enzymes, increasing the network's capacity to regulate the intensity of its output.

Distributed architectures promote adaptive locomotion

The main experimental evidence is that the robotic system displaces further when the control architecture is adaptive. In this sense, local influences amongst ASNs are suitable to ensure forward locomotion, even when the dynamics of the coupled network changes completely. The self-organised dynamics regulating locomotion depend on the connections amongst sub-ASNs more than on the coupled network. This is supported by the capacity of CASNs to express different dynamics and maintain inter limb coordination upon changes in the terrain's surface.

Hopf oscillators constrain coupled network expressiveness

With no limitations of modulation during evolution time, coupled signalling networks were able to preserve stable the duration of the stance phase while modulating the swing phase and oscillation amplitude. Thus, the robot displaces at a relatively constant speed delivering steps with variable length and height and promoting adaptation. However, it is difficult to make general conclusions about the impact of Hopf oscillators upon the proposed controller, since CPG dynamics appear to be significantly biased by the properties of the oscillator. It can be speculatively suggested that the initial coupling amongst Hopf oscillators defines their dynamics and limits the capacity of CPGs to promote gait diversity. This argument is somewhat supported by the observation that CPGs do not vary their initial coupling upon changes to the terrain surface. This supports the view of other researches (Righetti & Ijspeert, 2006; Campos et al., 2010; Santos & Matos, 2011; Zhou & Low, 2012) that gait diversity in Hopf oscillators does not directly arise from the terrain's features but from analytical modulation.

If Hopf oscillators are not suitable to generate efficient locomotive patterns on irregular terrains, which will be the ideal type of oscillator? Firstly, the type of oscillator depends to the the control architecture. This thesis proposes a decentralised control architecture in which the movement of the robot is governed uniquely by six coupled oscillators. This contradicts other conventional locomotive architectures that achieve forward motion using on oscillator per joint. Despite this coupling producing robust locomotive patterns, these architectures also require additional mechanisms to preserve the synchronisation amongst oscillators (i.e. coupling oscillator using their phase difference). Unless these topologies in which the pattern

of motion of each leg emerges from the internal dynamics of a network of oscillators, this thesis just requires two-dimensional oscillators to independently model the step's length and height of each leg.

Having said that, the Hopf oscillator outputs two harmonic and periodic sinusoidal waves whose characteristics are tightly coupled to its governing parameters (μ and ω). This facilities the shaping of the oscillator's trajectories by modulating the corresponding parameter and eases the development of robust coupling terms which can be solved in an analytical way. As a consequence, Hopf oscillators also produce rigid coupling terms, which increase the robot stability under flat surfaces but lead to coarse patterns of motion on irregular terrains. Authors have attempted to overcome this inconvenience by either rotating the oscillator's output to a desired phase or appending an alternative sinusoidal term to the oscillator to modulate their dynamics. In the first case, Campos et al. (2010) are also able to shift the phase of the oscillator by decreasing the oscillator's converge rate, which lightens its coupling but also increase its instability.

Whilst it is arguable the necessity of sensory feedback to produce conventional locomotive patterns, sensory information is a requirement to generate gait diversity. Thus, dynamical gait diversity can only be achieved via external perturbations and gait switching arises as the natural response to the CPG to such perturbations. Likewise, the stability of a locomotive approach in multi-legged robotic systems can only be guaranteed if sensory feedback modifies the locomotive pattern without a severe change in the intrinsic behaviour of each oscillator. This means that if a perturbation is exerted on a particular oscillator its trajectory and the trajectories of its neighbouring oscillators will describe a characteristic period and amplitude before coming automatically back to their normal behaviour.

Unless harmonic oscillators whose shape remains constant during propagation and reflection, and interference does not take place, *chaotic* oscillators display different dynamical states while preserving their synchronisation. These not only allow trajectories to show periodic and chaotic dynamics but also constitute a more reliable abstraction of the activities and function of biological oscillators. The application of external periodical forces to a chaotic oscillator presents two major advantages: synchronisation of the phase of the chaotic oscillator to that of the applied stimulus and the suppression of chaos (Chen, 1999). *Chaos controlled* oscillators show stable and periodical trajectories via reducing its chaotic nature but maintaining is chaotic properties. Likewise, these oscillators typically rely on their governing

parameters to regulate their internal dynamics and shift their phase when coupled. In this case, a small external perturbation suffices to produce a qualitative change of the oscillator's dynamical behaviour. In harmonic oscillators, the magnitude of an external perturbation need to be enhanced to show a noticeable effect in the trajectory pattern. Initial results about the applicability of chaos controlled oscillators in robotic locomotion are discussed in Section 7.4.

These conclusions support the hypothesis that evolvable computational abstractions of signalling networks can be used as bio-inspired control architectures for multi-legged robotic systems.

7.3 Limitations of this Research

Whilst considerable effort has been made to verify these conclusions documented throughout this thesis, there are several limitations of the theoretical understanding and experimental method which might reduce their generality. Likewise, these constitute the principal venues for future work. From a theoretical context, the main limitations are the regulation of all enzymes in a signalling network by the same catalytic equation and the method used to determine the global output of coupled signalling networks. Partially, they are a consequence of the comparison of the capacity the main biological regulatory function have to express complex dynamics. Suggestions as to how these might be overcome are described in the future work section. Further, the expressiveness of the proposed robotic architecture has not been rigorously analysed upon a wider range of robotic gaits. Whist the tripod gait was selected due to its stability and active coupling, it is not representative of all locomotive patterns in legged systems. This limitation shows the necessity to generalise the manner in which the proposed CPG operates so environmental features may elicit different oscillatory behaviours and switch amongst them. However, it is closely related to the computational properties of the CPG-units. Particularly, the Hopf oscillators used in this research require fast convergence rates to express different gaits, but they also lead to unstable couplings. Finally, there has been little direct comparison between the experimental results and the behaviour of the real T-Hex in a physical environment. This is due to the lack of capacity to physically recreate some of the environments used in the simulator. Nevertheless, it is expected these limitations can be addressed in future research.

7.4 Future Work

There are several issues raised by this research which merit further attention. These encompass three research directions: improving the proposed ASN model, the development of a bio-inspired control system able to dynamically switch amongst gaits and the reconstruction of biological signalling networks using ASNs.

Chapter 3 defines the computational structure of a signalling network and considers four different biological regulatory functions, which are separately used to regulate both standalone and coupled ASNs. An important aspect for future work will be the usage of multiple regulatory functions simultaneously in an ASN. This might introduce two benefits. First, ASN models will more closely represent biological signalling networks. Current signalling approaches depend on the amount and quality of information available. Typically, this has originated computational expensive mathematical abstractions and, perhaps, it is the reason why there is not unanimity amongst the proposed models of concrete pathways. The usage of different regulatory functions with different reactions rates in an ASN might, in the short term, overcome the complexity of existing mathematical models and bring on more realistic computationally representations. Second, enzymes may differentiate attending to their connectivity. The proposed ASN model uniquely distinguishes between receptor enzymes (zero inputs and multiple outputs) and other enzymes (multiple inputs and outputs). The consideration of multiple regulatory functions may have a greater impact in the network's topology, making it possible to cluster groups of enzymes attending to the reaction order of their regulatory function and the number of catalytic reactions in which they are involved. Thus, first-order reactions may act as receptors and be mainly involved in the transduction of extracellular information. Nonetheless, this might also require to redefine the chemical rules used in this thesis to mutate chemical reactions during evolution time.

The process to calculate the global output of CASNs is unsophisticated. In a biological context, the output of a signalling network reacts to certain genes and modulates their expression level which in turn, provokes a change in the cell's activity. The number of active genes and their expression levels are always constant and are called a *genetic program*. A detailed abstraction would include the coupling of a signaling network with a regulatory network, so that the number of active genes at each time would vary according to the state of each sub-ASN. Although the idea of coupling different cellular networks has been successfully evaluated in (Lones et al., 2014) and would be feasible for the Chirikov's map and Lorenz

system, it would entail a major change in the proposed robotic architecture as a centralised CPG would be necessary. A more plausible approach might be the calculation of the CASN's overall output as the weighted average of all contributing outputs. Thus, the degree of participation of each sub-ASN in the global output would depend on its importance in the solution of the control problem. Therefore, it might be possible to reduce the unfavourable impact the values of the y-coordinate have in the evolved controllers for Chirikov's map, increasing the evolved controller performance.

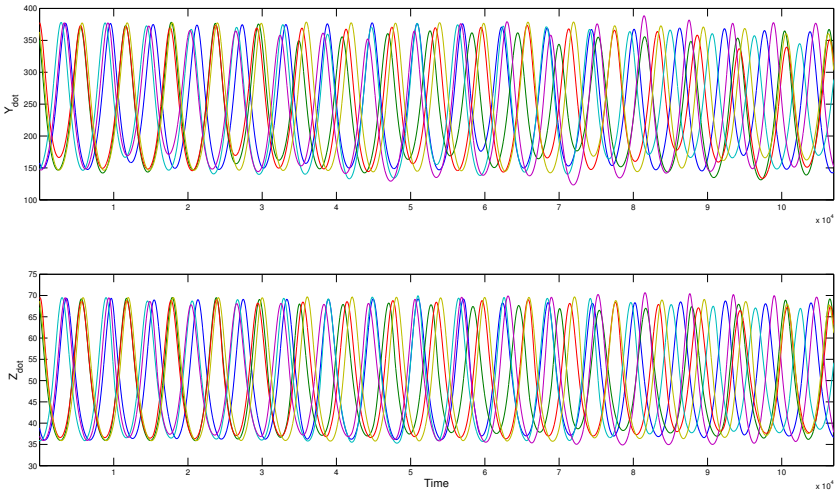

Figure 7.1: $\dot{y}$ and $\dot{z}$ trajectories of a CPG comprising six Wu oscillators. Initially oscillators are coupled imitating the tripod gait. When the CPG is perturbed at $t = 5$, each Wu oscillator independently modifies its initial oscillatory phase and amplitude. At $t = 8$ the CPG shows a coupling which to a certain extend resembles the metachronal gait.

Chapter 6 introduces a layered architecture to translate sensory information into reactive robotic movements. Particularly, this thesis considers a CPG made of six Hopf oscillators as the engine to produce locomotive patterns. The ability to transverse a wide range of terrains is a fundamental requirement to accomplish useful tasks and, in the case of legged system, it also involves behavioural diversity. This is perhaps the main limitation of the Hopf oscillator, whose harmonic trajectory is rather constant upon changes on its governing parameters. Although it eases the shaping of the oscillatory output, it substantially reduces the oscillator's capacity to show a noticeable modulation of its trajectory when perturbed. Authors have attempted to overcome this by appending an alternative sinusoid term (Zhou & Low, 2012) or by reducing the oscillator's convergence rate so that it is possible to change the oscillation phase using algebraic rotation matrices (Santos & Matos, 2011; Campos et al., 2010). In both solutions, oscillation phases are typically defined in advance and do not correlate with

the terrain features. An interesting avenue for this research will be to look at alternative oscillatory systems able to show richer dynamical behaviors and a higher sensitivity to external perturbations. The Wu oscillator (Wu, Chen & Yuan, 2009) is a four-dimensional autonomous dynamical system able to exhibit a large variety of dynamical states, including a periodic attractor. Its four nonlinearity points help to rapidly propagate small alterations across the system and, when coupled, throughout neighbouring systems. Further, it is also easy to develop time-delay coupling terms in an analytical way. However, the main advantages of the Wu system are that the oscillator self-regulates adjusting each inter limb phase and oscillatory amplitude upon parameter fluctuations in order to maintain its periodic dynamical state. When coupled, the system's overall state can uniquely be deduced from the interactions amongst individual oscillators. Thus, a CPG made of six Wu oscillators might be able to induce different dynamical states and naturally switch amongst them based on the control directives provided by a CASN. Initial results show that time-dependent alterations in the system's governing parameters successfully express noticeable changes in each generated trajectory (see Figure 7.1).

A final thought is that ASNs can be used to validate biological ideas on how pathways are organised and their application to solve engineering problems. The reconstruction of the functional context of cellular genes and the inference of their underlaying signalling networks from the available date is currently a challenging task. One of the main issues in network inference is the large amount of possible network topologies for a given number of genes. Further there is a limited ability to reconstruct biological networks experimentally, since their temporal and spatial organisation is lost when attempting to measure kinase concentrations. Without this information, identifying what does and does not interact is certainly impossible. ASNs models could provide an alternative source of information to discover signalling structures and components and, therefore, guide biologists to infer signalling networks.

Appendix A

Acronyms

ABN – Artificial Biochemical Network

ADP – Adenosine Diphosphate

AGN – Artificial Genetic Network

ASN – Artificial Signalling Network

AMN – Artificial Metabolic Network

ATP – Adenosine Triphosphate

BSD – Berkeley Software Distribution

CASN – Coupled Artificial Signalling Network

CFN – Constraint Force Mixing

CPG – Central Pattern Generator

CST – Cell Signalling Technology

D-H – Denavit-Hartenberg

DNA – Deoxyribonucleic Acid

DOF – Degree of Freedom

EA – Evolutionary Algorithm

EC – Evolutionary Computation

GA – Genetic Algorithm

GTP – guanosine triphosphate

JAK/STAT – Janus kinase/Signal Transducer and Activator of Transcription

LGPL – Less General Public License

MAPK – Mitogen-Activated Protein Kinases

ODE – Open Dynamical Engine

OGY – Ott-Grebogi-Yorke

PMM – Probabilistic Michealis-Menten

WARG – Wrist Angle Relative to Ground

Appendix B

Mathematical Symbols

List of mathematical symbols used in Chapter 5:

a	link length
a, b, c	additional trigonometric variables
$\hat{\mathbf{a}}$, $\hat{\mathbf{n}}$, $\hat{\mathbf{s}}$	orientation approximation vector
d	joint distance
B	body coordinate frame
D	translation transformation matrix
$\mathbf{d}$	displacement vector between coordinate frames
G	global coordinate frame
$\mathbf{I}$	identity matrix
l	length
$\hat{\mathbf{p}}$	position approximation vector
q	joint variable
r_{ij}	matrix element in row i and column j
t	robot tip position
T	homogeneous transformation matrix between coordinate frames
T_j	vector representing column j of T
x, y, z	local coordinate frame axes
X, Y, Z	global coordinate frame axes
w	robot wrist position
θ	joint rotational angle

α	link twist
ϕ	manipulator orientation angle, WARG angle

List of mathematical symbols used in Appendix C:

A, B, C	local coordinate frames, body frame (B)
c	cosine
$\mathbf{d}$	displacement vector between coordinate frames
G	global coordinate frame
$\hat{i}$, $\hat{j}$, $\hat{k}$	coordinate frame axes unit vectors
$\mathbf{p}$	positional vector between a coordinate frame and P, translation vector
P	fixed point in B
r_{ij}	matrix element in row i and column j
R	rotation transformation matrix
s	sine
T	homogeneous transformation matrix between coordinate frames
$\mathbf{v}$	general purpose vector
X, Y, Z	global coordinate frame axes
γ, β, α	rotational angles about coordinate system axes

Appendix C

Mathematical Preliminaries

Contents

Kinematics deals with the relationships between the different robot components, which are assumed to provide motion. These are typically rotations and translations of rigid bodies. Positioning displaces a rigid body to a new position, while orientation alters the direction of such a body at the new position. Although the kinematic problem can be interpreted as the addition of a translation and a rotation, both vectors must be previously transformed and expressed in relation to the same frame. This appendix introduces the mathematical preliminaries and reviews the notation underlying the kinematic problem.

C.1 Cartesian Coordinate System

A coordinate system is defined by a triad, which is the combination of four non-coplanar points O, A, B, C. Such combination produces three lines OA, OB and OC with a common origin. A triad also comprises three unit vectors $\hat{i}$, $\hat{j}$, $\hat{k}$. If each vector is orthogonal to each other, then they constitute an orthogonal triad or a *Cartesian coordinate system*. The lines OA, OB and OC are its *coordinate axis*. Since each vector is of unit length the coordinate

systems is said to be orthonormal and therefore,

$$\hat{i} \cdot \hat{j} = 0 \quad \hat{j} \cdot \hat{k} = 0 \quad \hat{k} \cdot \hat{i} = 0 \tag{C.1}$$

and,

$$|\,\hat{i}\,| = |\,\hat{j}\,| = |\,\hat{k}\,| = 1 \tag{C.2}$$

Whenever the unit vectors of an orthonormal coordinate system follow the direction of the main axes, and a rotation of 90^o about OA transforms OB into OC, then they constitute a right-handed Cartesian coordinate system. Likewise, an opposite orthonormal coordinate system or left-handed coordinate system can also be obtained by moving OA to the other side of O. Hereafter, right-handed Cartesian coordinate systems will be the only system used and they will be referred to as coordinate frames, or just frames.

By standard notation, any vector $\mathbf{v}$ in the Cartesian coordinate system B is represented based on its orthogonality condition and labelled indicating the system in which it is expressed.

$$\mathbf{v} = (\mathbf{v} \cdot \hat{i})\hat{i} + (\mathbf{v} \cdot \hat{j})\hat{j} + (\mathbf{v} \cdot \hat{k})\hat{k} \tag{C.3}$$

$$\hat{i} = \begin{bmatrix} 1 \\ 0 \\ 0 \end{bmatrix} \quad \hat{j} = \begin{bmatrix} 0 \\ 1 \\ 0 \end{bmatrix} \quad \hat{k} = \begin{bmatrix} 0 \\ 0 \\ 1 \end{bmatrix} \tag{C.4}$$

The manner in which two frames are related defines the kinematic behaviour of a robotic system. Three frames are identified when considering robotic motion:

- A *fixed frame*, a motionless frame attached to the ground. It represents the origin of the robot.

- A *global frame*, the Cartesian space in which the robot moves.

- A *local frame*, the Cartesian space where each links moves. It is also named *body frame*.

Therefore, the position and orientation of each robot component with respect to the fixed frame is described by the position and orientation of its local reference frame in a global reference frame as shown in Figure C.1.

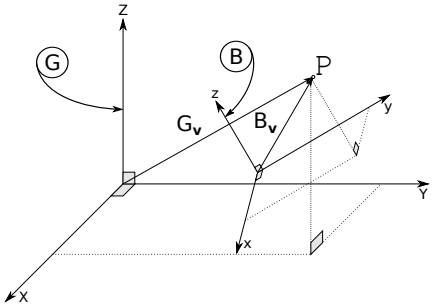

Figure C.1: Decomposition of the position of a point P into its Body frame B and its Global frame G. In this case the fixed frame matches the global frame. Adapted from (Jazar, 2010)

C.2 Transformation Matrices

Links in robotic systems are modelled as rigid bodies, each able to rotate or displace independently. When this happens, a local frame defined along the joint axis is used to describe the new position and orientation with respect to a global frame. Considering two coordinate frames G and B, there exists a *transformation matrix* that describes completely the relative configuration of B in G.

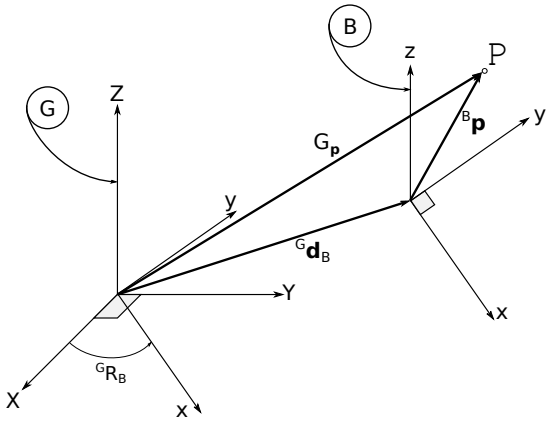

Figure C.2: Rotation and translation of a point P in a local coordinate frame with regard to the global frame.

A transformation from a local frame B to a global frame G encapsulates two individual operations which define the motion of a rigid body defined in B with respect to a global frame G: a *rotation* θ and *translation* $\mathbf{d}$. In kinematical terms, a transformation is seen as the sum of the translation of a rigid body plus its rotation at the new position (see Figure C.2).

$$G_{\mathbf{p}} = {}^{G}R_{B}\,{}^{B}\mathbf{p} + {}^{G}\,\mathbf{d}_{B} \tag{C.5}$$

where ${}^{B}\mathbf{p}$ is the position vector of a point in the coordinate frame B, $G_{\mathbf{v}}$ is the position

vector of the same point in the coordinate frame G, ${}^{G}\mathbf{d}_{B}$ is the displacement vector linking the origins of the frames B and G and ${}^{G}R_{B}$ is a rotation matrix which superimposes the axis of B onto the axis of G. In geometry, a transformation uniquely comprising rotations and translations is termed *rigid motion*.

C.2.1 Rotation

A rotation R between two coordinate frames G and B attached to the same fixed point is a 3×3 transformation matrix that describes the directions of B in G (see Equation C.6). In kinematics, this is used to establish the orientation of a point P relative to B in G (see Figure C.2).

$$ {}^{G}\mathbf{p} = {}^{G}R_{B}\,{}^{B}\mathbf{p} = \begin{bmatrix} r_{11} & r_{12} & r_{13} \\ r_{21} & r_{22} & r_{23} \\ r_{31} & r_{32} & r_{33} \end{bmatrix} \cdot {}^{B}\mathbf{p} \tag{C.6} $$

Any coordinate frame can be rotated in three different directions. A rotation about the X-axis is named *roll*, a rotation about the Y-axis is named *pitch* and a rotation about the Z axis is named *yaw*. The global rotation matrix between two neighbouring coordinate frames is as follows,

$$ {}^{G}R_{B} = R_{Z,\gamma}, R_{Y,\beta}, R_{X,\alpha} = \begin{bmatrix} c\beta c\gamma & -c\alpha s\gamma + c\gamma s\alpha s\beta & s\alpha s\gamma + c\gamma c\alpha s\beta \\ c\beta s\gamma & c\alpha s\gamma + s\gamma s\alpha s\beta & -c\alpha s\gamma + c\gamma s\alpha s\beta \\ -s\beta & c\beta s\alpha & c\alpha c\beta \end{bmatrix} \tag{C.7} $$

C.2.2 Translation

A translation $\mathbf{d}$ is the isometric displacement of a rigid body in a coordinate frame B to a new reference position. This means that all points must preserve their relative position and maintain a constant displacement distance independently of the new position and orientation. Any translation is unambiguously described in a coordinate frame by a 3×1 position vector.

Considering the point P in Figure C.2, the translation vector can be expressed in the form,

$$ {}^{B}\mathbf{p} = \begin{bmatrix} X_o \\ Y_o \\ Z_o \end{bmatrix} \tag{C.8} $$

C.2.3 Homogeneous Transformation Matrix

As shown in Figure C.2, the description of a rigid body with respect to a reference global coordinate frame is the sum of a translation plus a rotation. However, it can also be expressed using *homogeneous transformation matrices*. They encapsulate affine transformations as well as easing the description of rigid motion in robotic systems using a matrix notation. Therefore, Equation C.5 can be rewritten and simplified as follows,

$$ G_{\mathbf{p}} = {}^{G}T_{B}\,{}^{B}\mathbf{p} \tag{C.9} $$

where ${}^{G}T_{B}$ is the 4×4 homogeneous transformation matrix from coordinate system B to the coordinate system G. ${}^{G}T_{B}$ encloses two different transformation: a rotation ${}^{G}R_{B}$, and a translation ${}^{G}\mathbf{d}_{B}$.

$$ {}^{G}T_{B} = \begin{bmatrix} r_{11} & r_{12} & r_{13} & X_o \\ r_{21} & r_{22} & r_{23} & Y_o \\ r_{31} & r_{32} & r_{33} & Z_o \\ 0 & 0 & 0 & 1 \end{bmatrix} \equiv \left[\begin{array}{ccc|c} & {}^{G}R_{B} & & {}^{G}\mathbf{d}_{B} \\ \hline 0 & 0 & 0 & 1 \end{array}\right] \equiv \begin{bmatrix} {}^{G}R_{B} & {}^{G}\mathbf{d}_{B} \\ 0 & 1 \end{bmatrix} \tag{C.10} $$

and

$$ {}^{G}\mathbf{p} = \begin{bmatrix} X_P \\ Y_P \\ Z_P \end{bmatrix} \quad {}^{B}\mathbf{p} = \begin{bmatrix} x_P \\ y_P \\ z_P \end{bmatrix} \quad {}^{G}\mathbf{d}_{B} = \begin{bmatrix} X_o \\ Y_o \\ Z_o \end{bmatrix} \tag{C.11} $$

Additionally, considering the ${}^{G}T_{B}$ transformation matrix, it is possible to define an inverse homogeneous transformation matrix, ${}^{B}T_{G}$, of a point P relative to the coordinate system G

with respect to the coordinate system B as follows,

$$ {}^{B}T_{G} = \begin{bmatrix} {}^{B}R_{G} & -{}^{B}\mathbf{d}_{G} \\ 0 & 1 \end{bmatrix} = {}^{G}T_{B}^{-1} \tag{C.12} $$

For the sake of notational simplicity, homogeneous transformation matrices will be referred to as transformation matrices.

C.3 Compound Transformations

Figure C.3 shows three coordinate frames A, B and C and a point P relative to C. Upon this situation, the position and orientation of each frame is only known with regard to its previous frame. Likewise, the point P is only known relative to the frame C. The compound transformation is the kinematic operation by which a rigid object in a coordinate frame can be described in another non-neighbouring coordinate frame. This ability is fundamental in robotics since it relates mathematical descriptions with graphical representations.

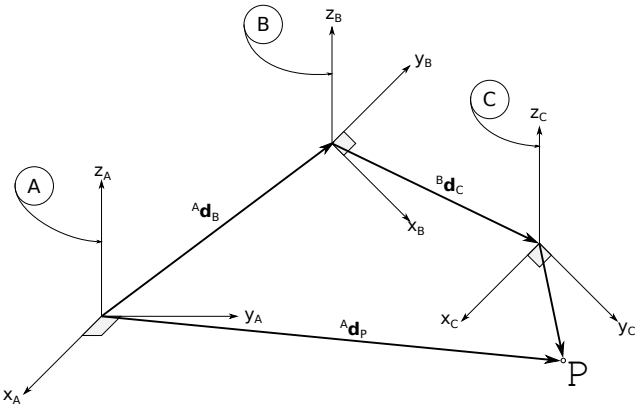

Figure C.3: Three coordinate frames A, B and C in an example of compound frames. The direction of the arrow connecting two frames indicates the manner in which the frames are defined. Adapted from (Craig, 1989).

Considering the three frames in Figure C.3, the *composed transformation matrix* from the coordinate frame A to the point P, ${}^{A}T_{P}$, is as follows,

$$ {}^{A}T_{P} = {}^{A}T_{B}\,{}^{B}T_{C}\,{}^{C}T_{P} \tag{C.13} $$

where,

$$ {}^{A}T_{B} = \begin{bmatrix} {}^{A}R_{B} & {}^{A}\mathbf{d}_{B} \\ 0 & 1 \end{bmatrix} \quad {}^{B}T_{C} = \begin{bmatrix} {}^{B}R_{C} & {}^{B}\mathbf{d}_{C} \\ 0 & 1 \end{bmatrix} \quad {}^{C}T_{P} = \begin{bmatrix} {}^{C}R_{P} & {}^{C}\mathbf{d}_{P} \\ 0 & 1 \end{bmatrix} \tag{C.14} $$

Multiplying these three matrices yields,

$$ {}^{A}T_{P} = \begin{bmatrix} {}^{A}R_{P} & {}^{A}\mathbf{d}_{P} \\ 0 & 1 \end{bmatrix} \tag{C.15} $$

Appendix D

Robotic Gaits

Contents

D.1 Ripple Gait

The sequence of a video still showing the walking of the simulated T-Hex robot using the ripple gait.

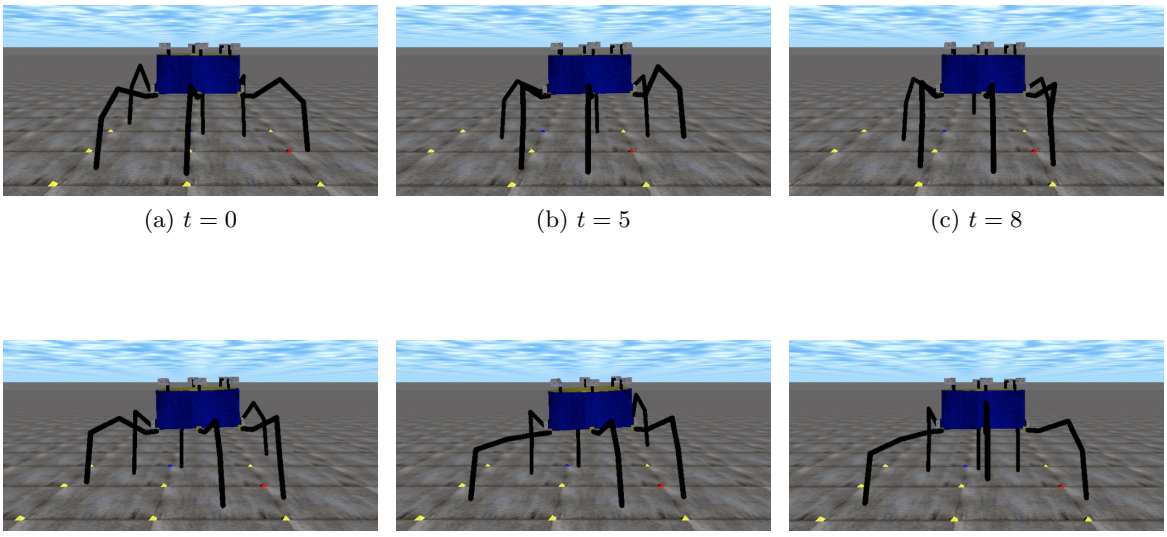

(a) $t = 0$ (b) $t = 5$ (c) $t = 8$

(d) $t = 12$ (e) $t = 15$ (f) $t = 18$

Figure D.1: An example sequence of the ripple gait in the ODE simulated T-Hex

D.2 Metachronal Gait

The sequence of a video still showing the walking of the simulated T-Hex robot using the metachronal gait.

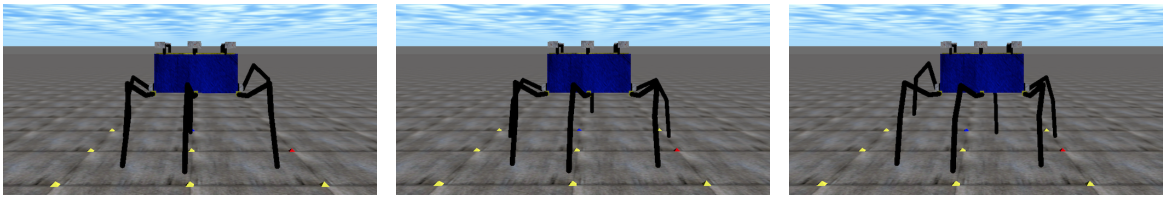

(a) $t = 0$ (b) $t = 5$ (c) $t = 8$

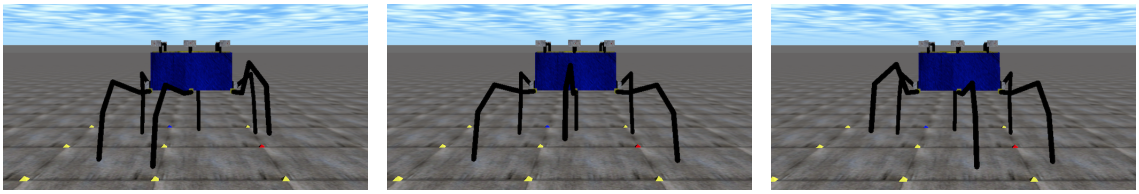

(d) $t = 12$ (e) $t = 15$ (f) $t = 18$

Figure D.2: An example sequence of the metachronal gait in the ODE simulated T-Hex

Appendix E

The T-Hex Robot

Contents

This thesis relies on a simulated representation of the T-Hex robot to validate both the experiments and the results. However, some work has also been done in the physical T-Hex robot to validate the results obtained in the ODE simulator. The T-Hex is a six-legged robotic system with 24-DOF manufactured by Lynxmotion (Lynxmotion, 2003). Each leg has four joints connected by actuators at the corners. Likewise, legs are lengthwise connected to a rectangular-shaped body. The basic T-Hex robot was also equipped with 6 infrared sensors located in a spherical base on top of the robot body, 2 ultrasound sensors placed at the front and the rear of the robot's body and 6 force sensors located at the tip of every leg.

E.1 Interfacing the T-Hex

The T-Hex standard serial connectivity was extended with the BlueSMIRF T9JRN-41-1 Bluetooth Modem (Sparkfun, 2009). It directly interfaces the BAP-28 embedded micro-controller and grants the robot with a wireless communication system. The working range of

the bluetooth modem is 20 meters, which is sufficient to evaluate the capacity of CASNs to produce adaptive locomotive patterns.

In oder to reduce to a minimum the workload on the robot and maximise its operability, the computation of each leg's trajectory is carried out on a remote computer. Therefore, the T-Hex is only responsible for the gathering of sensor information and the processing of the received actuator pulses. The remote computer is a MacBook Pro 2.8 GHz Intel Core i7 with 4 GB of RAM memory and 1333 MHz DDR3. A wireless communication protocol was developed in JAVA using the RXTXComm library and allows a bidirectional connection between the computer and the T-Hex robot. Such protocol begins by identifying the T-Hex robot and verifying both its correct working and the correct working of all sensor before reseting each leg to its resting position. Then, the T-Hex sends to the computer the force sensor and infrared readings, which are fed into the CASN using the low-numbered enzymes in each stand-alone ASN. The proposed bio-inspired control system outputs the angles of each joint that permit each leg to describe the trajectory generated by the CPG. Note that the shape of the trajectory showed by each leg depends on the sampling rate. Finally, these angles are sent to the robot which delivers them to the corresponding actuator. This process is continuously repeated for either a certain number of time steps in the case of the simulated robot or a predefined number of steps in the case of the T-Hex robot. When the CASN controller is not active and the movement of the robot exclusively depends on either the cycloid function of the CPG and sensory information is not sent from the robot to the computer.

Unlike the ODE simulation environment, the communication with the T-Hex robot presents two main disadvantages. First, there is data loss amongst consecutive sendings between the computer and the T-Hex. Surprisingly, there is no delays or data loss between the T-Hex to the remote computer. Second, the size of the packages of the bluetooth modem is 8 bits, meaning that only natural numbers between 0 and 256 can be sent. In this sense, larger numbers need to be broken into several packages, which might not be received. A conventional solution for the first issue would entail the implementation of an ack-based communication protocol, however it would be computational expensive and is out of the scope of this research. In this work, a small delay of 140 mm is applied between two consecutive sendings so the clocks of the computer and the T-Hex robot can resynchronise. The initial experiments have shown that 140 mm is the minimum delay that guarantees an effective communication between the computer and the robot. However, this also causes that a time

window of 3360 mm is required to sent to the T-Hex robot the 24 actuator pulses. The second issue can be solved by considering the actuators resting position equivalent to angular initial position. Therefore, it is possible to calculate the angular displacement of each joint and obtain the proportional actuator pulse of the integer part of the angle. The actuator pulses are then divided by 10 to fit them uniquely in one package. When received, they are multiplied by 10 to recover the original pulse. Considering that the ratio between pulses and angles is 10:1, the accuracy of the pulses sent to the robot is $\pm\ 2^o$ (joints angles are considered in degrees).

E.2 Wave gaits

This section exemplifies locomotion in the physical T-Hex robot when the proposed adaptive controller is not active. In this sense, locomotion is uniquely generated using a CPG of six Hopf oscillators for the tripod gait and the cycloid function for the ripple and metachronal gaits. In both cases, the kinematic layer is responsible for the translation of locomotive trajectories into joint angles.

E.2.1 Tripod Gait

The sequence of a video still showing the walking of the T-Hex robot using the tripod gait.

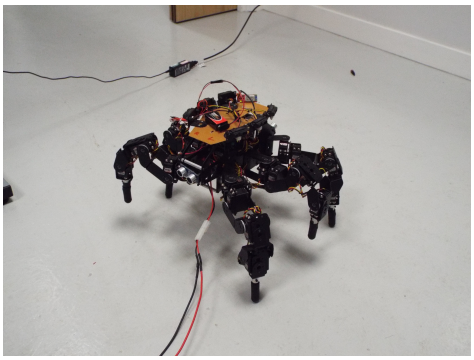

(a) $t = 0$

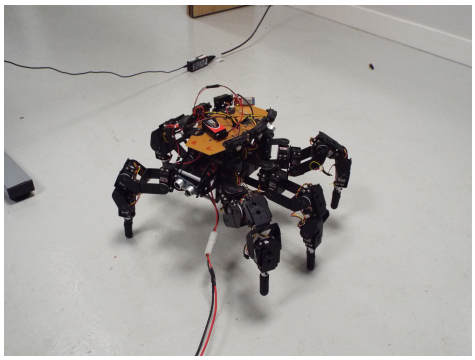

(b) $t = 3$

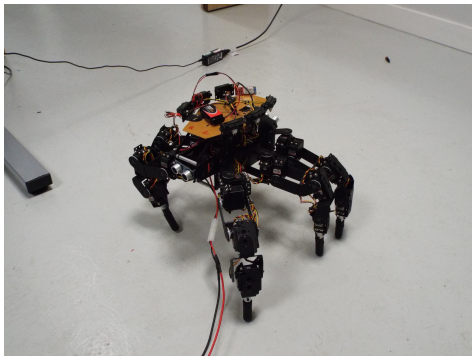

(c) $t = 6$

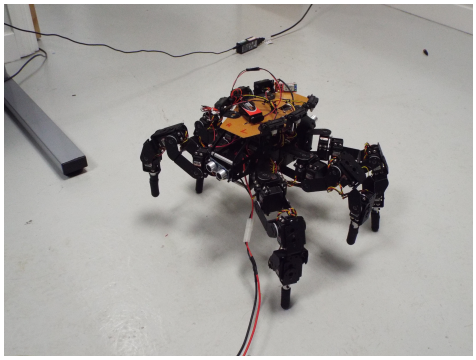

(d) $t = 9$

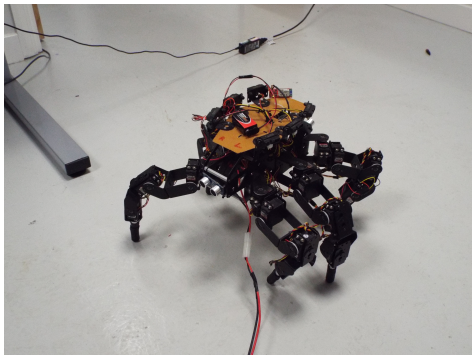

(e) $t = 12$

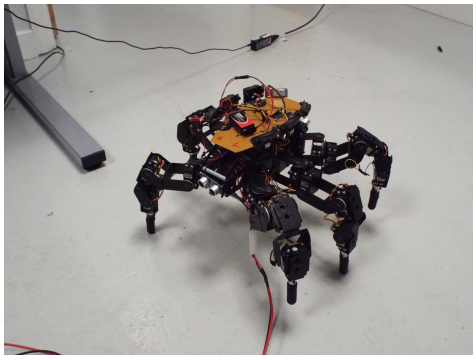

(f) $t = 15$

Figure E.1: An example sequence of the tripod gait T-Hex robot.

E.2.2 Ripple Gait

The sequence of a video still showing the walking of the T-Hex robot using the ripple gait.

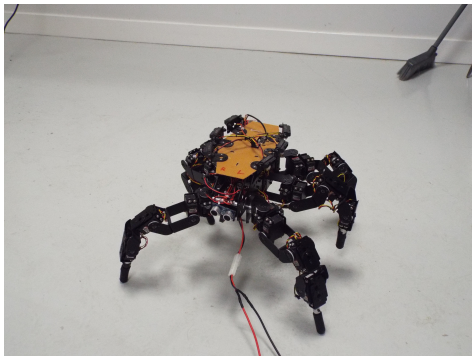

(a) $t = 0$

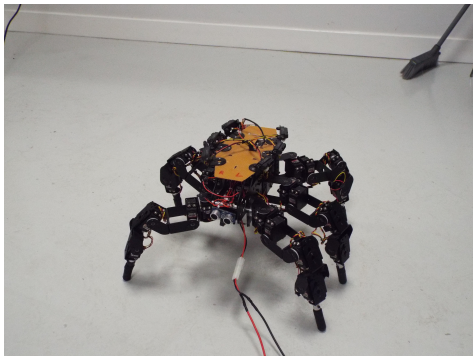

(b) $t = 3$

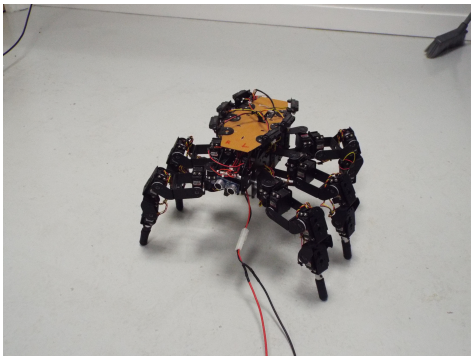

(c) $t = 6$

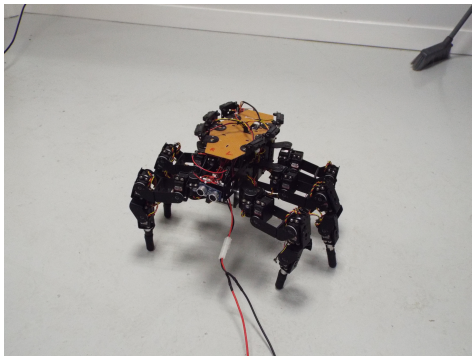

(d) $t = 9$

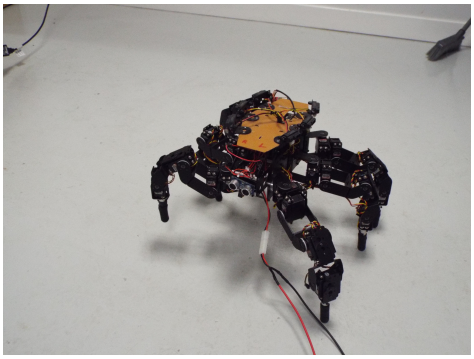

(e) $t = 12$

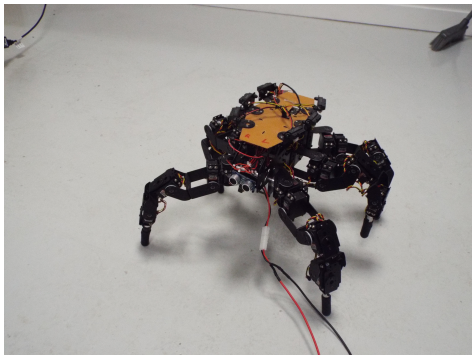

(f) $t = 15$

Figure E.2: An example sequence of the ripple gait in T-Hex robot.

E.2.3 Metachronal Gait

The sequence of a video still showing the walking of the T-Hex robot using the metachronal gait.

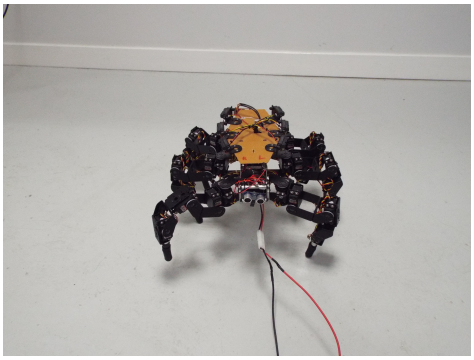

(a) $t = 0$

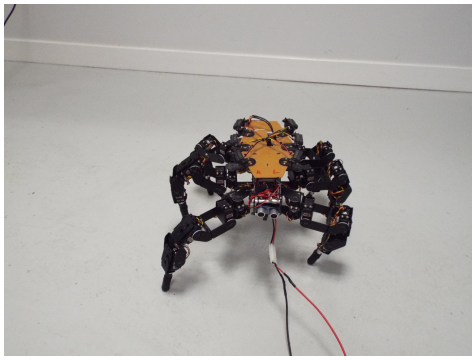

(b) $t = 3$

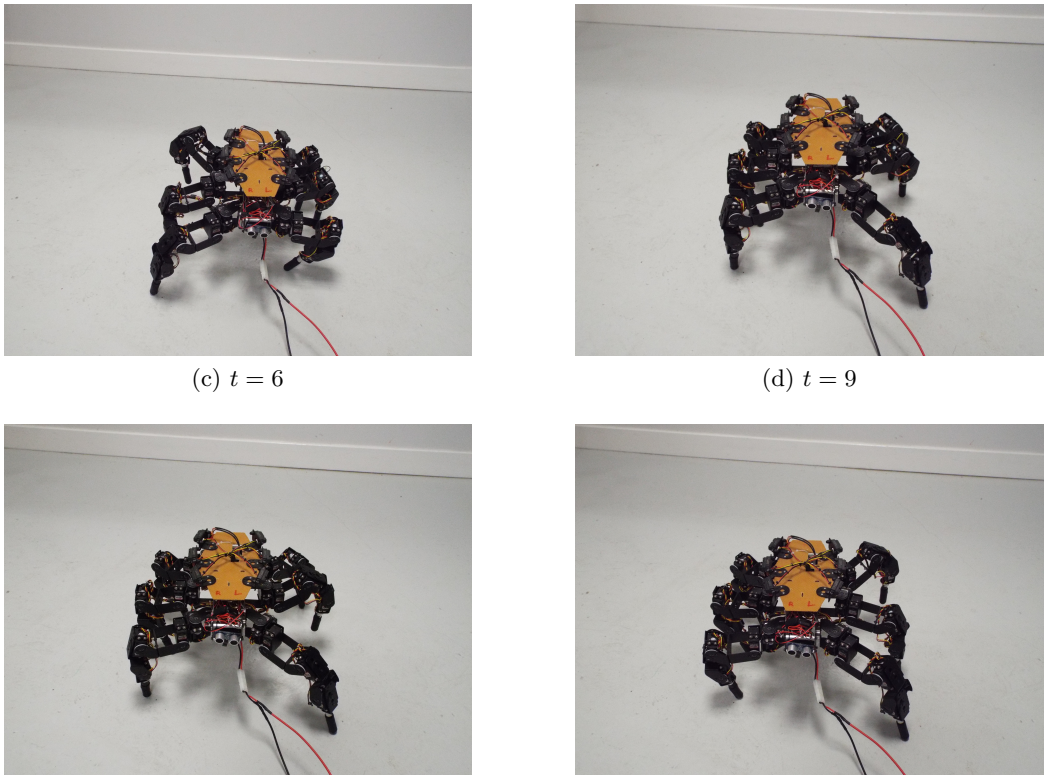

(c) $t = 6$ (d) $t = 9$

(e) $t = 12$ (f) $t = 15$

Figure E.3: An example sequence of the metachronal gait in the T-Hex robot.

E.3 Bio-Inspired Decentralised Controller

Although it was possible to port an evolved controller to the T-Hex and it was able to move forward, it was not possible to both achieve proper adaptive control and validate the data obtained from the simulated robot when governed by proposed three-layered architecture. This is mainly due to the lack of consistency in the force sensors readings, which prevents CASNs to express reactive dynamics relative to the terrain characteristics. The force sensors are placed at the end of an aluminum tube in the tip of each leg and are protected with a plastic cap (see Figure E.4). The entire leg's tip is also covered by a back plastic hood. This configuration causes that the force sensors still perceive some sort of force when the robot leg is swinging in the air. As a consequence the force sensors readings remain mostly constant during most of the evaluation time. Several attempts have been made to overcome this inconvenience by (*i*) adding a small space between the plastic cap and hood, however the plastic cap itself applies a force over the sensor when the leg is in the air; (*ii*) removing the plastic cap, however it is not possible to hold firmly the sensor to the end of the aluminum tube; and (*iii*) taking several consecutive reading of the force sensors, however their states remain stable.

(a) Plastic cap over the force sensor (b) Final leg configuration with the force sensor

Figure E.4: Force sensor assembly configuration in the T-Hex robot. (a) shows the position of the plastic cap over the force sensor. (b) illustrates the final configuration of the leg's tip when the plastic hood is on. Taken from (Lynxmotion, 2003).

Figure E.5 shows the sequence of force sensor readings measured from the T-Hex robot during the evaluation time whist the robot locomotes using the CASN adaptive controller over the staircase.

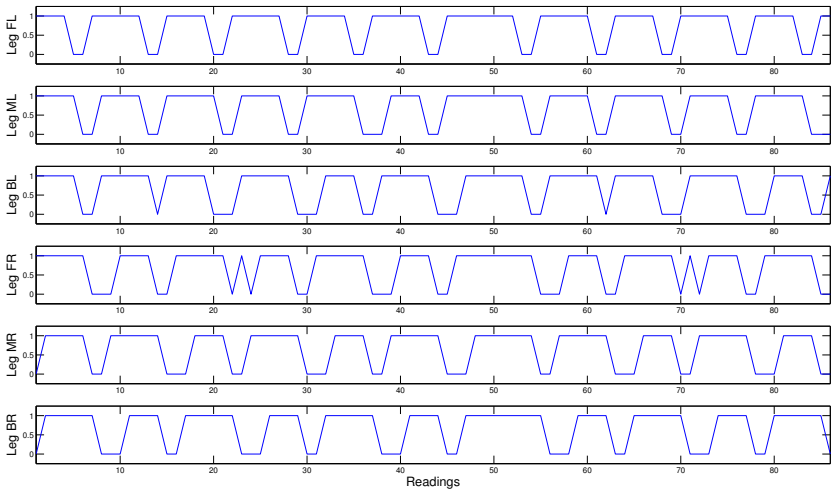

Figure E.5: Force sensor readings in the T-Hex robot.

Figure E.6 shows the internal state of the coupled network. It can be observed that ASN_{1-4} are unable to express any concrete behaviour, while $ASN_{5,6}$ exhibits periodic behaviours which do not match with the force sensors readings. This causes that the T-Hex robot slowly moves forward showing an unstructured locomotive gait pattern.

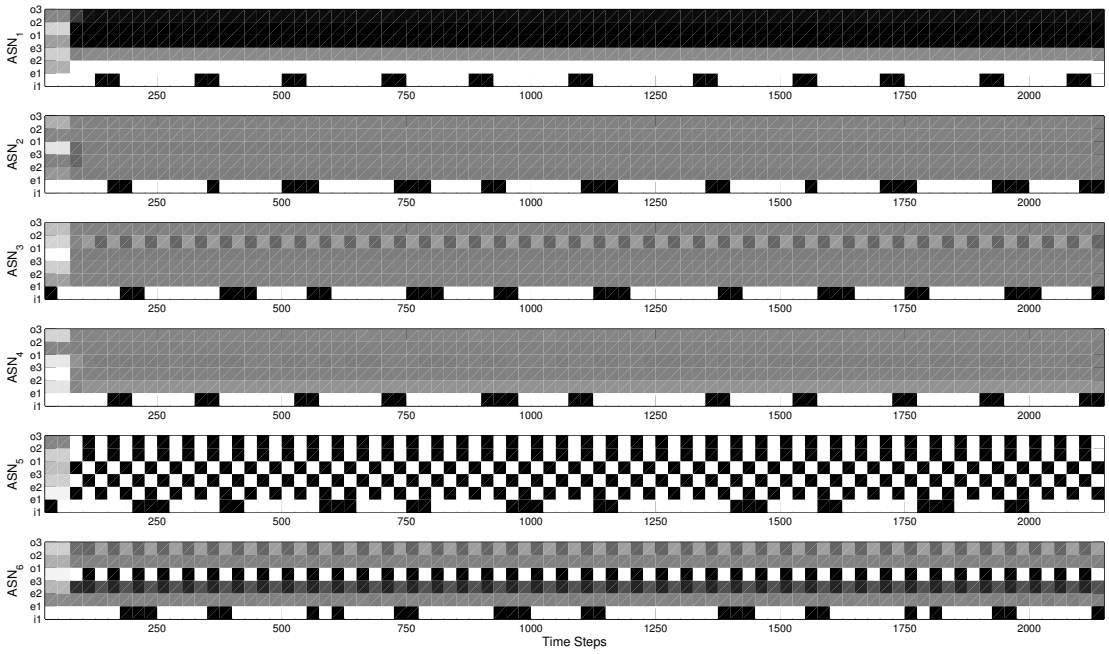

Figure E.6: Internal state of an evolved CASN controlling the T-Hex robot.

Bibliography

Agarwal, P. K. (2005), 'Role of protein dynamics in reaction rate enhancement by enzymes', *Journal of the American Chemical Society* **127**(43), 15248–15256.

Alon, U. (2007), *An Introduction to System Biology, Design Principles of biological Circuits*, Chapman & Hall/CRC.

Aoi, S., Egi, Y., Sugimoto, R., Yamashita, T., Fujiki, S. & Tsuchiya, K. (2012), 'Functional roles of phase resetting in the gait transition of a biped robot from quadrupedal to bipedal locomotion', *Robotics, IEEE Transactions on* **28**(6), 1244–1259.

Aoi, S. & Tsuchiya, K. (2004), Stability analysis of a simple walking model driven by a rhythmic signal, *in* 'Intelligent Robots and Systems, 2004.(IROS 2004). Proceedings. 2004 IEEE/RSJ International Conference on', Vol. 2, IEEE, pp. 1365–1370.

Arena, P., Fortuna, L., Frasca, M. & Sicurella, G. (2004), 'An adaptive, self-organizing dynamical system for hierarchical control of bio-inspired locomotion', *Systems, Man, and Cybernetics, Part B: Cybernetics, IEEE Transactions on* **34**(4), 1823–1837.

Arias, A. M. & Hayward, P. (2006), 'Filtering transcriptional noise during development: concepts and mechanisms', *Nature Reviews Genetics* **7**(1), 34–44.

Arkin, A. & Ross, J. (1994), 'Computational functions in biochemical reaction networks', *Biophysical Journal* **67**(2), 560–578.

Asthagiri, A. R. & Lauffenburger, D. A. (2000), 'Bioengineering models of cell signaling', *Annual Review of Biomedical Engineering* **2**(1), 31–53.

Baerlocher, P. (2001), Inverse Kinematics Techniques for the Interactive Posture Control of Articulated Figures, PhD thesis, Ecole Polytechnique Federale de Lausanne.

Barnett, L. (2001), Netcrawling-optimal evolutionary search with neutral networks, *in* 'Evolutionary Computation, 2001. Proceedings of the 2001 Congress on', Vol. 1, IEEE, pp. 30–37.

Berg, J. M., Tymoczko, J. L. & Stryer, L. (2002), *Biochemistry*, fifth edition edn, W H Freeman.

Bhalla, U. S. & Iyengar, R. (1999), 'Emergent properties of networks of biological signaling pathways', *Science* **283**(5400), 381–387.

Bishop, A. & Hall, A. (2000), 'Rho gtpases and their effector proteins', *Biochem. j* **348**, 241–255.

Bisswanger, H. (2002), *Enzyme Kinetics, Principle and Methods*, Chapman & Hall/CRC.

Bleich, M. & Socolar, J. E. S. (1996), 'Stability of periodic orbits controlled by time-delay feedback', *Physics Letters A* **210**(1-2), 87 – 94.

Bollt, E. M. (1995), Controlling Chaos, Targeting, and Transport, PhD thesis, University of Colorado.

Bray, D. (1990), 'Intracellular signalling as a parallel distributed process', *Journal of theoretical biology* **143**(2), 215–231.

Bray, D. (1995), 'Protein molecules as computational elements in living cells', *Nature* **376**(6538), 307–312.

Bray, D. & Lay, S. (1994), 'Computer simulated evolution of a network of cell signalling molecules', *Biophysical Journal* **66**(4), 972–977.

Bray, S. J. (2006), 'Notch signalling: a simple pathway becomes complex', *Nature Reviews Molecular Cell Biology* **9**, 678689.

Brooks, R. A. (1991), 'Intelligence without representation', *Artificial intelligence* **47**(1), 139–159.

Brown, T. G. (1914), 'On the nature of the fundamental activity of the nervous centres; together with an analysis of the conditioning of rhythmic activity in progression, and a theory of the evolution of function in the nervous system', *The Journal of Physiology* **48**(1), 18–46.

Buehler, M., Playter, R. & Raibert, M. (2005), Robots step outside, *in* 'Int. Symp. Adaptive Motion of Animals and Machines (AMAM), Ilmenau, Germany', pp. 1–4.

Calvo, O. & Cartwright, J. H. E. (1998), 'Fuzzy control of chaos', *International Journal of Bifurcation and Chaos* **8**(8), 1743–1747.

Cammack, M. (2003), Control of a chaotic double pendulum using the OGY method, Technical report, Georgia Institute of Technology.

Campos, R., Matos, V. & Santos, C. (2010), Hexapod locomotion: A nonlinear dynamical systems approach, *in* 'IECON 2010-36th Annual Conference on IEEE Industrial Electronics Society', IEEE, pp. 1546–1551.

Capi, G., Nasu, Y., Barolli, L., Mitobe, K. & Takeda, K. (2001), 'Application of genetic algorithms for biped robot gait synthesis optimization during walking and going up-stairs', *Advanced Robotics* **15**(6), 675–694.

Cavill, R., Smith, S. & Tyrrell, A. (2005), Multi-chromosomal genetic programming, *in* 'Proceedings of the 2005 conference on Genetic and evolutionary computation', ACM, pp. 1753–1759.

Celso, G. & Lai, Y.-C. (1997), 'Controlling chaos in high dimensions', *Circuits and Systems I: Fundamental Theory and Applications, IEEE Transactions on* **44**(10), 971–975.

Chakravarty, I., Roy, J. & Laha, R. (1967), 'Handbook of methods of applied statistics'.

Chen, G. (1999), *Controlling chaos and bifurcations in engineering systems*, CRC press.

Chen, G. & Dong, X. (1998), *From Chaos To Order Methodologies, Perspectives and Applications*, World Scientific Publishing Company.

Chen, W., Ren, G., Wang, J. & Liu, D. (2014), 'An adaptive locomotion controller for a hexapod robot: Cpg, kinematics and force feedback', *Science China Information Sciences* **57**(11), 1–18.

Chirikov, B. V. (1962), Research concerning the theory of nonlinear resonance and stochasticity, Technical report, Institute of Nuclear Physics, Novosibirsk.

Collins, J. J. & Stewart, I. (1993), 'Hexapodal gaits and coupled nonlinear oscillator models', *Biological Cybernetics* **68**(4), 287–298.

Conrad, M. (1990), 'The geometry of evolution', *BioSystems* **24**(1), 61–81.

Cooper, G. M. (2000), *The Cell - A Molecular Approach 2nd Edition*, Sunderland (MA): Sinauer Associates.

Craig, J. J. (1989), *Introduction to Robotics: Mechanics and Control*, second edition edn, Addison Wesley Longman.

Crespi, A. & Ijspeert, A. J. (2008), 'Online optimization of swimming and crawling in an amphibious snake robot', *Robotics, IEEE Transactions on* **24**(1), 75–87.

Cruse, H. (1990), 'What mechanisms coordinate leg movement in walking arthropods?', *Trends in neurosciences* **13**(1), 15–21.

Cruse, H., Dean, J., Kindermann, T., Schmitz, J. & Schumm, M. (1997), 'Simulation of complex movements using artificial neural networks.', *Zeitschrift fur Naturforschung. C, Journal of biosciences* **53**(7-8), 628–638.

Cruse, H., Kindermann, T., Schumm, M., Dean, J. & Schmitz, J. (1998), 'Walkneta biologically inspired network to control six-legged walking', *Neural networks* **11**(7), 1435–1447.

CST (1999), 'Cell signalling technology', Available from http://www.cellsignal.com/about/index.html.

Danos, V., Feret, J., Fontana, W. & Krivine, J. (2008), Abstract interpretation of cellular signalling networks, *in* 'Verification, Model Checking, and Abstract Interpretation', Springer, pp. 83–97.

Darwin, C. & Bynum, W. F. (1859), *The origin of species by means of natural selection: or, the preservation of favored races in the struggle for life*, AL Burt.

de Lasa, M., Mordatch, I. & Hertzmann, A. (2010), 'Feature-based locomotion controllers', *ACM Transactions on Graphics (TOG)* **29**(4), 131.

de Paula, A. S. & Savi, M. A. (2011), 'Comparative analysis of chaos control methods: A mechanical system case study', *International Journal of Non-Linear Mechanics* **46**(8), 1076 – 1089.

de Pina Filho, A. C., Dutra, M. S. & Raptopoulos, L. S. (2005), 'Modeling of a bipedal robot using mutually coupled rayleigh oscillators', *Biological cybernetics* **92**(1), 1–7.

Deckard, A. & Sauro, H. M. (2004), 'Preliminary studies on the in silico evolution of biochemical networks', *ChemBioChem* **5**(10), 1423–1431.

Decraene, J., Mitchell, G. G. & McMullin, B. (2007), Evolving artificial cell signaling networks: Perspectives and methods, *in* 'Advances in Biologically Inspired Information Systems', Springer, pp. 165–184.

Delcomyn, F. (1999), 'Walking robots and the central and peripheral control of locomotion in insects', *Autonomous Robots* **7**(3), 259–270.

Dickinson, M. H., Farley, C. T., Full, R. J., Koehl, M., Kram, R. & Lehman, S. (2000), 'How animals move: an integrative view', *Science* **288**(5463), 100–106.

Dressler, U. & Nitsche, G. (1992), 'Controlling chaos using time delay coordinates', *Phys. Rev. Lett.* **68**, 1–4.

Ehrlich, P. (1897), 'Die wertbemessung des diphtherieheilserums und deren theoretische grundlagen', *Himmelweit* **2**, 107–125.

Eungdamrong, N. J. & Iyengar, R. (2004), 'Modeling cell signaling networks', *Biology of the Cell* **96**(5), 355–362.

Fersht, A. (1999), *Structure and mechanism in protein science: a guide to enzyme catalysis and protein folding*, Macmillan.

Fisher, M. J., Paton, R. C. & Matsuno, K. (1999), 'Intracellular signalling proteins as smart-agents in parallel distributed processes', *Biosystems* **50**(3), 159–171.

Fisher, M., Malcolm, G. & Paton, R. C. (2000), 'Spatio-logical processes in intracellular signalling', *Biosystems* **55**(1-3), 83–92.

Floreano, D. & Mattiussi, C. (2008), *Bio-Inspired Artificial Intelligence: Theories, Methods, and Technologies*, The MIT Press.

Flynn, D. C. (2001), 'Adaptor proteins', *Oncogene* **20**, 6270–6272.

Fogel, L., Owens, A. & Walsh, M. (1966), *Articial intelligence through simulated evolution*, wiley.

Frasca, M., Arena, P. & Fortuna, L. (2004), *Bio-inspired emergent control of locomotion systems*, Vol. 48, World scientific.

Fuente, L. A., Lones, M. A., Turner, A. P., Caves, L. S., Stepney, S. & Tyrrell, A. M. (2012), Evolved artificial signalling networks for the control of a conservative complex dynamical system, *in* '9th International Conference on Information Processing in Cells and Tissues (IPCAT 2012) Cambridge, UK', Vol. 7223 of *LNCS*, Springer, pp. 38–49.

Fuente, L. A., Lones, M. A., Turner, A. P., Caves, L. S., Stepney, S. & Tyrrell, A. M. (2013*a*), Adaptive robotic gait control using coupled artificial signalling networks, hopf oscillators and inverse kinematics, *in* 'Evolutionary Computation (CEC), 2013 IEEE Congress on', IEEE, pp. 1435–1442.

Fuente, L. A., Lones, M. A., Turner, A. P., Caves, L. S., Stepney, S. & Tyrrell, A. M. (2013*b*), 'Computational models of signalling networks for non-linear control', *Biosystems* **112**(2), 122 – 130.

Galván-López, E., Poli, R., Kattan, A., ONeill, M. & Brabazon, A. (2011), 'Neutrality in evolutionary algorithms what do we know?', *Evolving Systems* **2**(3), 145–163.

Gazi, B. & Ghassemlooy, Z. (2004), Sigmoid function based dynamic threshold scheme for shared-buffer switches, *in* 'International symposium, Communication systems, networks and digital signal processing; CSNDSP 2004', IEEE, pp. 412–415.

Graham, L. D., Haggett, K. D., Jennings, P. A., Brocque, D. S. L., Whittaker, R. G. & Schober, P. A. (1993), 'Random mutagenesis of the substrate-binding site of a serine protease can generate enzymes with increased activities and altered primary specificities', *Biochemistry* **32**(24), 6250–6258.

Grillner, S., McClellan, A. & Perret, C. (1981), 'Entrainment of the spinal pattern generators for swimming by mechano-sensitive elements in the lamprey spinal cord in vitro', *Brain research* **217**(2), 380–386.

Grillner, S., Wallen, P., Brodin, L. & Lansner, A. (1991), 'Neuronal network generating locomotor behavior in lamprey: circuitry, transmitters, membrane properties, and simulation', *Annual review of neuroscience* **14**(1), 169–199.

Guillot, A. (2008), Biologically inspired robots, *in* 'Springer Handbook of Robotics', Springer, pp. 1395–1422.

Habib, M. K., Liu, G. L., Watanabe, K. & Izumi, K. (2007), Bipedal locomotion control via cpgs with coupled nonlinear oscillators, *in* 'Mechatronics, ICM2007 4th IEEE International Conference on', IEEE, pp. 1–6.

Hale, J. K. (1997), 'Diffusive coupling, dissipation, and synchronization', *Journal of Dynamics and Differential Equations* **9**(1), 1–52.

Hartwell, L. H., Hopfield, J. J., Leibler, S. & Murray, A. W. (1999), 'From molecular to modular cell biology', *Nature* **402**, C47–C52.

Harvey, I., Husbands, P., Cliff, D. et al. (1992), *Issues in evolutionary robotics*, School of Cognitive and Computing Sciences, University of Sussex.

Heinrich, R., Neel, B. G. & Rapoport, T. A. (2002), 'Mathematical models of protein kinase signal transduction', *Molecular cell* **9**(5), 957–970.

Hepler, J. R. & Gilman, A. G. (1992), 'G proteins', *Trends in biochemical sciences* **17**(10), 383–387.

Hickman, A. B., Namboodiri, M. A. A., Klein, D. C. & Dyda, F. (1999), 'The structural basis of ordered substrate binding by serotonin n-acetyltransferase: Enzyme complex at 1.8 resolution with a bisubstrate analog', *Cell* **97**(3), 361 – 369.

Hill, A. V. (1910), 'The possible effects of the aggregation of the molecules of hemoglobin on its dissociation curves', *The Journal of Physiology* **40**(Suppl), iv–vii.

Holland, J. H. (1975), *Adaptation in natural and artificial systems: An introductory analysis with applications to biology, control, and artificial intelligence.*, U Michigan Press.

Huang, Z. & Hahn, J. (2009), 'Fuzzy modeling of signal transduction networks', *Chemical Engineering Science* **64**(9), 2044–2056.

Ijspeert, A. J. (2008), 'Central pattern generators for locomotion control in animals and robots: a review', *Neural Networks* **21**(4), 642–653.

Ijspeert, A. J., Crespi, A., Ryczko, D. & Cabelguen, J.-M. (2007), 'From swimming to walking with a salamander robot driven by a spinal cord model', *science* **315**(5817), 1416–1420.

Inagaki, K. & Kobayashi, H. (1994), Adaptive wave gait for hexapod synchronized walking, *in* 'IEEE International Conference on Robotics and Automation', Vol. 2, pp. 1326–1331.

Inagaki, N., Ito, M., Nakano, T. & Inagaki, M. (1994), 'Spatiotemporal distribution of protein kinase and phosphatase activities', *Trends in biochemical sciences* **19**(11), 448–452.

Inagaki, S., Yuasa, H., Suzuki, T. & Arai, T. (2006), 'Wave cpg model for autonomous decentralized multi-legged robot: Gait generation and walking speed control', *Robotics and Autonomous Systems* **54**(2), 118–126.

Interlink (2010), Fsr 400 data sheet, Technical report, Interlink Electronics - Sensor Technologies.

Jakobi, N. (1998), Running across the reality gap: Octopod locomotion evolved in a minimal simulation, *in* 'Proceedings of the First European Workshop on Evolutionary Robotics: EvoRobot98', Springer-Verlag, pp. 39–58.

Jazar, R. N. (2010), *Theory of Applied Robotics. Kinematics, Dynamics and Control*, second edition edn, Springer.

Kalakrishnan, M., Buchli, J., Pastor, P., Mistry, M. & Schaal, S. (2010), Fast, robust quadruped locomotion over challenging terrain, *in* 'Robotics and Automation (ICRA), 2010 IEEE International Conference on', IEEE, pp. 2665–2670.

Kampmann, C. E. (1996), Feedback loop gains and system behavior, *in* 'Proceedings of the 1996 International System Dynamics Conference', pp. 260–263.

Kantz, H. & Schreiber, T. (2004), *Nonlinear time series analysis*, Vol. 7, Cambridge university press.

Katada, Y., Ohkura, K. & Ueda, K. (2004), An approach to evolutionary robotics using a genetic algorithm with a variable mutation rate strategy, *in* 'Parallel Problem Solving from Nature-PPSN VIII', Springer, pp. 952–961.

Katz, B.-Z., Zamir, E., Bershadsky, A., Kam, Z., Yamada, K. M. & Geiger, B. (2000), 'Physical state of the extracellular matrix regulates the structure and molecular composition of cell-matrix adhesions', *Molecular Biology of the Cell* **11**(3), 1047–1060.

Kestler, H. A., Wawra, C., Kracher, B. & Kühl, M. (2008), 'Network modeling of signal transduction: establishing the global view', *Bioessays* **30**(11-12), 1110–1125.

Kholodenko, B. N., Hoek, J. B., Westerhoff, H. V. & Brown, G. C. (1997), 'Quantification of information transfer via cellular signal transduction pathways', *FEBS letters* **414**(2), 430–434.

Kim, J. (2006), On the Stable Dynamic Walking of Biped Humanoid Robots, PhD thesis, Advanced Institute of Science and Technology, Daejeon, South Korea.

Kimura, H., Fukuoka, Y. & Cohen, A. H. (2007), 'Adaptive dynamic walking of a quadruped robot on natural ground based on biological concepts', *The International Journal of Robotics Research* **26**(5), 475–490.

Klamt, S., Saez-Rodriguez, J., Lindquist, J. A., Simeoni, L. & Gilles, E. D. (2006), 'A methodology for the structural and functional analysis of signaling and regulatory networks', *BMC bioinformatics* **7**(1), 56.

Koshland, D. E. (1995), 'The key–lock theory and the induced fit theory', *Angewandte Chemie International Edition in English* **33**(23-24), 2375–2378.

Kostelich, E. J. & Barreto, E. (1996), Targeting and control of chaos, *in* 'Control and Chaos', Vol. 8 of *Mathematical Modelling*, Birkh'auser Boston, pp. 158–169.

Koyuncu, B. & Güzel, M. (2008), 'Software development for the kinematic analysis of a lynx 6 robot arm'.

Koza, J. R. (1992), *Genetic Programming: vol. 1, On the programming of computers by means of natural selection*, Vol. 1, MIT press.

Krauss, G. (2001), *Biochemistry of Signal transduction and Regulation*, second edn, Wiley-VCH Verlag GmbH.

Kunkel, B. & Brooks, D. (2002), 'Cross talk between signaling pathways in pathogen defense.', *Curr Opin Plant Biol* **5**(4), 325–31.

Kuo, A. D. (2002), 'The relative roles of feedforward and feedback in the control of rhythmic movements', *MOTOR CONTROL-CHAMPAIGN-* **6**(2), 129–145.

Kwon, Y.-K. & Cho, K.-H. (2008), 'Coherent coupling of feedback loops: a design principle of cell signaling networks', *Bioinformatics* **24**(17), 1926–1932.

Lachat, D., Crespi, A. & Ijspeert, A. J. (2006), Boxybot: a swimming and crawling fish robot controlled by a central pattern generator, *in* 'Biomedical Robotics and Biomechatronics, 2006. BioRob 2006. The First IEEE/RAS-EMBS International Conference on', IEEE, pp. 643–648.

Lai, Y.-C., Ding, M. & Grebogi, C. (1993), 'Controlling Hamiltonian chaos', *Physical Review E* **47**(1), 86.

Langton, C. G. (1990), 'Computation at the edge of chaos: phase transitions and emergent computation', *Physica D: Nonlinear Phenomena* **42**(1), 12–37.

Lee, A. I., Fugmann, S. D., Cowell, L. G., Ptaszek, L. M., Kelsoe, G. & Schatz, D. G. (2003), 'A functional analysis of the spacer of v (d) j recombination signal sequences', *PLoS biology* **1**(1), e1.

Liu, C., Chen, Q. & Zhang, J. (2009), Coupled van der pol oscillators utilised as central pattern generators for quadruped locomotion, *in* 'Control and Decision Conference, 2009. CCDC'09. Chinese', IEEE, pp. 3677–3682.

Locasale, J. W., Shaw, A. S. & Chakraborty, A. K. (2007), 'Scaffold proteins confer diverse regulatory properties to protein kinase cascades', *Proceedings of the National Academy of Sciences* **104**(33), 13307–13312.

Lones, M. A. (2004), Enzyme Genetic Programming: Modelling Biological Evolvability in Genetic Programming, PhD thesis, Department of Electronics, University of York.

Lones, M. A., Tyrrell, A. M., Stepney, S. & Caves, L. S. (2010), Controlling complex dynamics with artificial biochemical networks, *in* 'Genetic Programming, Proc. EuroGP, 2010', Springer, pp. 159–170.

Lones, M. A., Tyrrell, A. M., Stepney, S. & Caves, L. S. (2011), Controlling legged robots with coupled artificial biochemical networks, *in* 'Proc. ECAL 2011, Paris, France, August 2011', MIT Press, pp. 465–472.

Lones, M., Fuente, L., Turner, A., Caves, L., Stepney, S., Smith, S. & Tyrrell, A. (2014), 'Artificial biochemical networks: Evolving dynamical systems to control dynamical systems', *Evolutionary Computation, IEEE Transactions on* **18**(2), 145–166.

Lorenz, E. N. (1963), 'Deterministic nonperiodic flow', *Journal of the Atmospheric Science* **20**(2), 130–141.

Lynxmotion (2003), 'Lynxmotion robotic toolkit', Available from http://www.lynxmotion.com/.

Lynxmotion (2010), '4dof t-hex combo kit for bot board/ssc-32/bap28', Available from http://www.lynxmotion.com/c-151-t-hex-4-dof.aspx.

Mankegh, T., Hindash, A. & Al-Jarabi, M. (2011), Hexapod robot: Robot design, model and control, Master's thesis, German Jordanian University.

Marijuán, P. C. (1995), 'Enzymes, artificial cells and the nature of biological information', *BioSystems* **35**(2), 167–170.

Marijuán, P. C., del Moral, R. & Navarro, J. (2013), 'On eukaryotic intelligence: Signalling system's guidance in the evolution of multicellular organization', *Biosystems* **114**(1), 8–24.

Mayer, H. A. & Spitzlinger, M. (2003), Multi-chromosomal representations and chromosome shuffling in evolutionary algorithms, *in* 'Evolutionary Computation, 2003. CEC '03. The 2003 Congress on', Vol. 2, pp. 1145–1149.

McCarthy, N. (2010), 'Cell signalling: regulation and crosstalk', *Nature Reviews Molecular Cell Biology* **11**(6), 390–390.

Mehta, V., Brennan, S. & Gandhi, F. (2008), 'Experimentally verified optimal serpentine gait and hyperredundancy of a rigid-link snake robot', *Robotics, IEEE Transactions on* **24**(2), 348–360.

Michaelis, L. & Menten, M. L. (1913), 'Die kinetik der invertinwirkung', *Biochem* **Z**(49), 333–369.

Milo, R., Shen-Orr, S., Itzkovitz, S., Kashtan, N., Chklovskii, D. & Alon, U. (2002), 'Network motifs: simple building blocks of complex networks', *Science* **298**(5594), 824–827.

Mitsubori, K. & Aihara, K. (2002), 'Delayed–feedback control of chaotic roll motion of a flooded ship in waves', *Proceedings of the Royal Society of London. Series A: Mathematical, Physical and Engineering Sciences* **458**(2027), 2801–2813.

Miyakoshimi, S., Taga, G. & KUNIYOSHI, Y. (2000), Stabilization of periodic motions - from juggling to bipedal walking, *in* 'In Proceedings of the International Symposium on Adaptive Motion of Animals and Machines (AMAM2000', p. 2431.

Moioli, R. C., Vargas, P. A. & Husbands, P. (2009), A multiple hormone approach to the homeostatic control of conflicting behaviours in an autonomous mobile robot, *in* 'Evolutionary Computation, 2009. CEC'09. IEEE Congress on', IEEE, pp. 47–54.

Moioli, R. C., Vargas, P. A. & Husbands, P. (2010), Exploring the kuramoto model of coupled oscillators in minimally cognitive evolutionary robotics tasks, *in* 'Evolutionary Computation (CEC), 2010 IEEE Congress on', IEEE, pp. 1–8.

Mor, A. & Philips, M. R. (2006), 'Compartmentalized ras/mapk signaling', *Annu. Rev. Immunol.* **24**, 771–800.

Morgan, N. G. (1989), *Cell Signalling*, first edition edn, Open University Press.

Morris, M. K., Saez-Rodriguez, J., Sorger, P. K. & Lauffenburger, D. A. (2010), 'Logic-based models for the analysis of cell signaling networks', *Biochemistry* **49**(15), 3216–3224.

Muecke, K. J. (2009), An Analytical Motion Filter for Humanoid Robots, PhD thesis, Faculty of the Virginia Polytechnic Institute.

Nakada, K., Asai, T. & Amemiya, Y. (2003), 'An analog cmos central pattern generator for interlimb coordination in quadruped locomotion', *Neural Networks, IEEE Transactions on* **14**(5), 1356–1365.

Neves, S. R. & Iyengar, R. (2002), 'Modeling of signaling networks', *Bioessays* **24**(12), 1110–1117.

Nicolas, J. (2005), 'Artificial evolution of controllers based on non-linear oscillators for bipedal locomotion'.

Nolfi, S. & Floreano, D. (2001), Evolutionary robotics. the biology, intelligence, and technology of self-organizing machines, Technical report, MIT press.

Oppermann, R. & Rasher, R. (1997), 'Adaptability and adaptivity in learning systems', *Knowledge transfer* **2**, 173–179.

Ott, E. (2002), *Chaos in dynamical systems*, Cambridge university press.

Ott, E., Grebogi, C. & Yorke, J. A. (1990), 'Controlling chaos', *Phys. Rev. Lett.* **64**, 1196–1199.

Parallax (2005), Sharp gp2d12 analog distance sensor (605-00003), Technical report, Parallax TM.

Parallax (2006), Ping)))tm ultrasonic distance sensor (28015), Technical report, Parallax TM.

Paul, R. P. (1981), *Robot Manipulators: Mathematics, Programming and Control*, MIT Press.

Pierrot, H. J. & Hinterding, R. (1997), Using multi-chromosomes to solve a simple mixed integer problem, *in* 'Advanced Topics in Artificial Intelligence', Springer, pp. 137–146.

Potts, A. S. & da Cruz, J. J. (2011), *A Kinematical and Dynamical Analysis of a Quadruped Robot*, InTech.

Prehoda, K. E. & Lim, W. A. (2002), 'How signaling proteins integrate multiple inputs: a comparison of n-wasp and cdk2', *Current Opinion in Cell Biology* **14**(2), 149–154.

Pyragas, K. (1992), 'Continuous control of chaos by self-controlling feedback', *Physics Letters A* **170**(6), 421 – 428.

Quinn, R. D., Nelson, G. M., Bachmann, R. J., Kingsley, D. A., Offi, J. & Ritzmann, R. E. (2001), 'Insect designs for improved robot mobility', *Climbing and Walking Robots: From Biology to Industrial Applications* p. 59.

Quinn, R. D., Offi, J. T., Kingsley, D. A. & Ritzmann, R. E. (2002), Improved mobility through abstracted biological principles, *in* 'Intelligent Robots and Systems, 2002. IEEE/RSJ International Conference on', Vol. 3, IEEE, pp. 2652–2657.

Rhee, S. G. (2006), 'Cell signaling', *H2O2, a necessary evil for cell signaling. Science* **312**, 1882–1883.

Righetti, L. & Ijspeert, A. J. (2006), Design methodologies for central pattern generators: An application to crawling humanoids., *in* 'Robotics: Science and Systems'.

Righetti, L. & Ijspeert, A. J. (2008), Pattern generators with sensory feedback for the control of quadruped locomotion, *in* 'Robotics and Automation, 2008. ICRA 2008. IEEE International Conference on', IEEE, pp. 819–824.

Robotics-Institute (1984), Cmu-ri-tr-84-04, Technical report, Carnegie Mellon University, Pittsburgh, PA.

Rogers, A. & Gibon, Y. (2009), *Enzyme kinetics: Theory and Practice*, Plant Metabolic Networks, Springer Science+Business Media.

Roozemond, D. (1996), 'Intelligent traffic management and urban traffic control based on autonomous objects'.

Rosemberg, R. (1967), Simulation of Genetic Populations with Biochemical Properties, PhD thesis, University of Grenoble, France.

Rosenstein, M. T., Collins, J. J. & De Luca, C. J. (1993), 'A practical method for calculating largest Lyapunov exponents from small data sets', *Physica D: Nonlinear Phenomena* **65**(1), 117–134.

Sachs, K., Gifford, D., Jaakkola, T., Sorger, P. & Lauffenburger, D. A. (2002), 'Bayesian network approach to cell signaling pathway modeling', *Science Signaling* **2002**(148), pe38.

Sachs, K., Perez, O., Pe'er, D., Lauffenburger, D. A. & Nolan, G. P. (2005), 'Causal protein-signaling networks derived from multiparameter single-cell data', *Science* **308**(5721), 523–529.

Sackmann, A., Heiner, M. & Koch, I. (2006), 'Application of petri net based analysis techniques to signal transduction pathways', *BMC bioinformatics* **7**(1), 1–17.

Said, M. R., Oppenheim, A. V. & Lauffenburger, D. A. (2003), Modeling cellular signal processing using interacting markov chains, *in* 'Acoustics, Speech, and Signal Processing, 2003. Proceedings.(ICASSP'03). 2003 IEEE International Conference on', Vol. 6, IEEE, pp. VI–41.

Salazar, C. & Hofer, T. (2003), 'Allosteric regulation of the transcription factor nfat1 by multiple phosphorylation sites: A mathematical analysis', *Journal of Molecular Biology* **327**(1), 31 – 45.

Santos, C. P. & Matos, V. (2011), 'Gait transition and modulation in a quadruped robot: A brainstem-like modulation approach', *Robotics and Autonomous Systems* **59**(9), 620–634.

Schroer, C. G. & Ott, E. (1997), 'Targeting in Hamiltonian systems that have mixed regular/chaotic phase spaces', *Chaos* **7**, 512–519.

Sengupta, N., Vinod, P. K. & Venkatesh, K. V. (2007), 'Crosstalk between cAMP-PKA and MAP kinase pathways is a key regulatory design necessary to regulate FLO11 expression.', *Biophysical chemistry* **125**(1), 59–71.

Senkerik, R., Zelinka, I. & Davendra, D. (2007), Comparison of evolutionary algorithms in the task of chaos control optimization, *in* 'Evolutionary Computation, 2007. CEC 2007. IEEE Congress on', IEEE, pp. 3952–3958.

Setti, G., Rovatti, R. & Mazzini, G. (2003), Control of chaos statistics for optimization of DS-CDMA systems, *in* 'Chaos Control', Springer, pp. 295–320.

Shaham, S. (2005), *Methods in Cell Biology*, The C. elegans Research Community, WormBook Ed.

Shea, L. D., Omann, G. M. & Linderman, J. J. (1997), 'Calculation of diffusion-limited kinetics for the reactions in collision coupling and receptor cross-linking', *Biophysical journal* **73**(6), 2949–2959.

Silverthorn, D. U. (2009), *Human Physiology: An Integrated Approach*, first edition edn, Addison Wesley.

Siso-Nadal, F., Fox, J. J., Laporte, S. A., Hébert, T. E. & Swain, P. S. (2009), 'Cross-Talk between Signaling Pathways Can Generate Robust Oscillations in Calcium and cAMP', *PLoS ONE* **10**, e7189+.

Smith, R. (2000), 'Open dynamic environment', Available from http://www.ode.org/.

Somogyi, R., Fuhrman, S., Askenazi, M. & Wuensche, A. (1997), 'The gene expression matrix: towards the extraction of genetic network architectures', *Nonlinear Analysis, Theory, Methods & Applications* **30**(3), 1815–1824.

Somsen, O. J., Siderius, M., Bauer, F. F., Snoep, J. L. & Westerhoff, H. V. (2002), 'Selectivity in overlapping map kinase cascades', *Journal of theoretical biology* **218**(3), 343–354.

Soong, C., Huang, W., Lin, F. & Tzeng, P. (2004), 'Controlling chaos with weak periodic signals optimized by a genetic algorithm', *Physical Review E* **70**(1), 016211.

Sparkfun (2008), 'Analog/digital mux breakout', Available from https://www.sparkfun.com/products/9056.

Sparkfun (2009), 'Bluetooth modem - bluesmirf gold', Available from https://www.sparkfun.com/products/10268.

Sprinzl, M. (1994), 'Elongation factor tu: a regulatory gtpase with an integrated effector', *Trends in biochemical sciences* **19**(6), 245–250.

Stepney, S. (2012), Nonclassical computation: a dynamical systems perspective, *in* G. Rozenberg, T. Bäck & J. N. Kok, eds, 'Handbook of Natural Computing, volume 4', Springer, chapter 59, pp. 1979–2025.

Taniguchi, C. M., Emanuelli, B. & Kahn, R. C. (2006), 'Critical nodes in signalling pathways: insights into insulin action', *Nat Rev Mol Cell Biol* **7**(2), 85–96.

Tu, X., Joeng, K. S., Nakayama, K. I., Nakayama, K., Rajagopal, J., Carroll, T. J., McMahon, A. P. & Long, F. (2007), 'Noncanonical wnt signaling through g protein-linked pkcδ activation promotes bone formation', *Developmental cell* **12**(1), 113–127.

Tulupyev, A. L. & Nikolenko, S. I. (2005), Directed cycles in bayesian belief networks: probabilistic semantics and consistency checking complexity, *in* 'MICAI 2005: Advances in Artificial Intelligence', Springer, pp. 214–223.

Turner, A. P., Lones, M. A., Fuente, L. A., Stepney, S., Caves, L. S. & Tyrrell, A. M. (2012), Using artificial epigenetic regulatory networks to control complex tasks within chaotic systems, *in* '9th International Conference on Information Processing in Cells and Tissues (IPCAT 2012) Cambridge, UK', Vol. 7223 of *LNCS*, Springer, pp. 1–11.

Turner, A. P., Lones, M. A., Stepney, S., Caves, L. S., Tyrrell, A. et al. (2013), The artificial epigenetic network, *in* 'Evolvable Systems (ICES), 2013 IEEE International Conference on', IEEE, pp. 66–72.

Uhlik, M. T., Abell, A. N., Cuevas, B. D., Nakamura, K. & Nakamura, G. L. (2004), 'Wiring diagrams of mapk regulation by mekk1, 2, and 3', *Biochemistry and Cell Biology* **82**(6), 658–663.

Vargas, P. A., Di Paolo, E. A., Harvey, I. & Husbands, P. (2014), *The Horizons of Evolutionary Robotics*, MIT Press.

Weeks, E. R. & Burgess, J. M. (1997), 'Evolving artificial neural networks to control chaotic systems', *Phys. Rev. E* **56**, 1531–1540.

Weiss, J. N. (1997), 'The hill equation revisited: uses and misuses.', *The FASEB journal* **11**(11), 835–841.

Weng, G., Bhalla, U. S. & Iyengar, R. (1999), 'Complexity in biological signaling systems', *Science* **284**(5411), 92–96.

Widgerow, A. D. (2011), 'Cellular/extracellular matrix cross-talk in scar evolution and control.', *Wound repair and regeneration* **19**(2), 117–133.

Wolovich, W. A. (1987), *Robotics: Basic Analysis and Design*, Series in Electrical and Computer Engineering, Holt, Rinehart and Winston.

Wright, J. & Jordanov, I. (2012), Intelligent approaches in locomotion, *in* 'Neural Networks (IJCNN), The 2012 International Joint Conference on', IEEE, pp. 1–8.

Wu, Q., Liu, C., Zhang, J. & Chen, Q. (2009), 'Survey of locomotion control of legged robots inspired by biological concept', *Science in China Series F: Information Sciences* **52**(10), 1715–1729.

Wu, W., Chen, Z. & Yuan, Z. (2009), 'The evolution of a novel four-dimensional autonomous system: among 3-torus, limit cycle, 2-torus, chaos and hyperchaos', *Chaos, Solitons & Fractals* **39**(5), 2340–2356.

Yamada, S., Shiono, S., Joo, A. & Yoshimura, A. (2003), 'Control mechanism of jak/stat signal transduction pathway', *FEBS letters* **534**(1), 190–196.

Yu, J. & Wei, C. (2013), 'Towards development of a slider-crank centered self-propelled dolphin robot', *Advanced Robotics* **27**(12), 971–977.

Zäschke, T. (2009), 'ode4j: A java 3d physics engine and library', Available from http://ode4j.sourceforge.net/ode4j-contact.html.

Zhang, X. & Zheng, H. (2008), 'Walking up and down hill with a biologically-inspired postural reflex in a quadrupedal robot', *Autonomous Robots* **25**(1-2), 15–24.

Zhou, C. & Low, K. (2012), 'Design and locomotion control of a biomimetic underwater vehicle with fin propulsion', *Mechatronics, IEEE/ASME Transactions on* **17**(1), 25–35.

Ziegler, J. & Banzhaf, W. (2001), 'Evolving control metabolisms for a robot', *Artificial Life* **7**(2), 171–190.